

# **Unsymmetrical Squaraine Based NIR-active Dyes for Dye-sensitized Solar Cells: Controlling the Aggregation and Orientation of Dyes on the TiO<sub>2</sub> Surface**

**Thesis Submitted to AcSIR**  
*For the Award of the Degree of*  
**DOCTOR OF PHILOSOPHY**  
*In*  
**CHEMICAL SCIENCES**



By  
**Punitharasu Vellimalai**  
(AcSIR Reg. No: 10CC13A26027)

Under the Guidance of  
**Dr. Jayaraj Nithyanandhan (Supervisor)**

Physical and Material Chemistry Division,  
CSIR-National Chemical Laboratory,  
Pune-411008, India

**May 2018**

# सीएसआईआर - राष्ट्रीय रासायनिक प्रयोगशाला

(वैज्ञानिक तथा औद्योगिक अनुसंधान परिषद)

डॉ. होमी भाभा मार्ग, पुणे - 411 008, भारत



## CSIR - NATIONAL CHEMICAL LABORATORY

(Council of Scientific & Industrial Research)

Dr. Homi Bhabha Road, Pune - 411 008, India

### CERTIFICATE

This is to certify that the work incorporated in this Ph.D. thesis entitled “**Unsymmetrical Squaraine Based NIR-active Dyes for Dye-sensitized Solar Cells: Controlling the Aggregation and Orientation of Dyes on the TiO<sub>2</sub> Surface**” submitted by **Mr. Punitharasu Vellimalai** to Academy of Scientific and Innovative Research (AcSIR) in fulfilment of the requirements for the award of the Degree of Doctor of Philosophy in Chemical Sciences, embodies original research work under my supervision. I further certify that this work has not been submitted to any other University or Institution in part or full for the award of any degree or diploma. Research material obtained from other sources has been duly acknowledged in the thesis. Any text, illustration, table etc., used in the thesis from other sources, have been duly cited and acknowledged.

V. Punitharasu  
1015118

Research Student

**Punitharasu Vellimalai**

J. Nithyanandhan  
May 10, 2018

Research guide

**Dr. Jayaraj Nithyanandhan**

Senior Scientist

#### Communication Channels

NCL Level DID : 2590  
NCL Board No. : +91-20-25902000  
EPABX : +91-20-25893300  
: +91-20-25893400



#### FAX

Director's Office : +91-20-25902601  
COA's Office : +91-20-25902660  
SPO's Office : +91-20-25902664

#### WEBSITE

[www.ncl-india.org](http://www.ncl-india.org)

## DECLARATION

I hereby declare that the original research work embodied in the thesis entitled, "**Unsymmetrical Squaraine Based NIR-active Dyes for Dye-sensitized Solar Cells: Controlling the Aggregation and Orientation of Dyes on the TiO<sub>2</sub> Surface**" submitted to Academy of Scientific and Innovative Research (AcSIR) for the award of degree of Doctor of Philosophy (Ph.D.) is the outcome of experimental investigations carried out by me under the supervision of Dr. Jayaraj Nithyanandhan at CSIR-National Chemical Laboratory, Pune. I further affirm that to the best of my knowledge, the work incorporated is original and has not been submitted any other Academy, Institute and University for the award of any degree.

May, 2018

CSIR-National chemical Laboratory

Pune-411008

*V. Punitharasu*  
10/5/18

**Punitharasu Vellimalai**

(Research Student)



*Dedicated*

*To*

*My Beloved Parents*

*For their Love, Support and Encouragement....*

---

## **Acknowledgements**

First of all, my heartily praises and thanks to the God, the almighty for his great blessing throughout my difficult research period and gave the capability to complete research successfully.

I would like to express my sincere thanks to my research supervisor Dr. Jayaraj Nithyanandhan for his invaluable guidance, understanding and patience which helped very much to my research carrier. I wish to express my sincere appreciation to him for sharing his scientific information and experience with me. He is a thoughtful and very energetic person and my sincere regards and respect for him, everlastingly. Moreover, I would also like to thank Dr. Kothandam Krishnamoorthy for his kind help, great discussion and invaluable suggestion with respect to scientific problems through our research review meetings. Furthermore a warm thank to my Doctoral Advisory Committee (DAC) members, Dr Kiran Kulkarni and Dr. Arup Rath who gave confidence to me with their important suggestions, guidance and useful criticism during my work presentations.

I sincerely thank the Council of Scientific and Industrial Research (CSIR) for my ph.d fellowship. I would also like to express my gratitude to Director, CSIR –National Chemical Laboratory and Head of Physical and Material Chemistry Division, for providing the great infrastructure and sophisticated facilities for the research purpose and also gave a chance to work at CSIR-NCL.

I would like to acknowledge the great support of all the members of the CSIR-NCL instrumental facilities of NMR and Mass. I sincerely admire and appreciate Student Academic Office (SAO) staff, library staff, Workshop, members of Glass blowing, Accounts and Bill section and other office staffs for their appropriate help.

I would like to give very special thanks to Dr. Ponrathanam Sir, Dr. Mayadevi Mam, Dr Karthikeyan Sir, Dr. Muthukrishnan Sir, and Dr. Vincent Paul Sir who supported in my difficult time like a family members.

I wish to thank my fellow labmates, MK Munavvar Fairoos, Kubendiran Kolanji, Alagumalai Ananthan, Ashwath , Saranya , Ranjit, Ambarish Kumar singh, Amrita singh, Supriya, Dhanushree, Neeta Karjule, Rajesh Bhisht, Indrajeet, Manik sil, Jessy Anna Benny, Jenny Rose Benny and Bhavisha. I am also thankful to Dr. Krishnamoorthy group members, Kumar Subramanayan, sudhakar, Anup singh, Gunuvant Deshmukh, chitravel, geethanjali for providing their valuable support.

---

I owe deeply to my true friends, Saranya Thangachi, Deepika Thangachi, EswerKumar, Pirabhu, Raja, John Aruldoss, Mohan Anna, Wasif Sir, Sam Anna, Haggai, John, Esther, Asir Anna, Munavvar Fairoos, Syam, Nikhil, Sinju, Layana, Nivedhitha, Nasreen, Gatha, Shifana, Shreya, Anu, Milda, Sruthy, Kavya, Anusree, Joonaa (Devathai), Haritha, Amrutha, Anju, Ragimma, Manod, Akhil, Rahul, Syam(MG), Vipin, Jishnu, Monika, Subhara Jyotsna, Roopasree, Rajsree, Chaya Patil, and Jithin for all their affection, friendship, helping tendency and constant support. Their constant support and help that encouraged me throughout my Ph.d carriers and also urther extend my thankfulness to all my friends of CSIR Tamil group of CSIRNCL, Sridhar Anna, Sangeetha, Rani, Vinoth, Saravanan, Chitravel, Rajagopal Anna, Deepak, Arivazhakan, Vasu, Mokka Mohan, Ashok, Loganathan, Pandi, Dr. Murugesan, Manikandan, Periyasamy, Kutta Prabhu, Netti Prabhu, Raja, Suresh, jumbo, Devaraj, Rupa, Vinothini, Kalai, for their help and beautiful moments.

I would like to express my deep sense of gratitude to my family for the constant support and affection. I have no word to express my feeling especially for my AMMA Mrs. Nagavalli, APPA Mr. M. Vellimalai for their unconditional love, affection, blessing and support throughout my Ph.d life. With their all sacrifice, adjustment, constant support and patience that made me achieve my dreams. My sincere thanks to them for their countless and very caring love and affection. They are the one who became my motivation and strength in my difficult situations. Very sincere thanks for their patience, love, support and for believing in my dreams.

Thank you for everything

Punitharasu Vellimalai

CSIR-NCL, Pune

---

---

## Table Contents

Abbreviations	i
Synopsis	iv

### Chapter 1

#### Introduction of Dye Sensitized Solar Cells

1.1 General Introduction	2
1.1.1 Global Energy Demand	2
1.1.2 Renewable Energies	2
1.2 Overview of Photovoltaics	3
1.2.1 History of Solar Cells	3
1.3 Dye Sensitized Solar Cells	4
1.3.1 Advantages and Disadvantages of DSSCs	5
1.3.2 Dye-sensitized Solar Cell Architecture	6
1.3.3 Operating Principle of DSSCs	7
1.4 Solar Cell Measurements	8
1.4.1 Short-circuit Current	9
1.4.2 Open-circuit Voltage	9
1.4.3 Fill-factor	10
1.4.4 Power Conversion Efficiency	10
1.4.5 Incident Photon to Current Conversion Efficiency	11
1.4.6 Electrochemical Impedance Spectroscopy	11
1.5 Key Components of DSSCs	13
1.5.1 Nanostructured Metal Oxide Electrodes	13
1.5.2 Different Redox Mediators	13
1.5.3 Counter Electrode	14
1.6 Dye Design	15
1.6.1 Ruthenium Complexes	16
1.6.2 Porphyrin and Phthalocyanine Dyes	18
1.6.3 Metal-free Organic Dyes	20
1.7 Challenges and Perspectives	25
1.7.1 Dye Aggregation on the Surface of Semiconductor Metal Oxide	25

---

1.7.2 Charge Recombination	26
1.7.3 Position of Alkyl Groups and Importance on the Photovoltaic Cell	27
1.7.4 Optical Response towards Photovoltaic Cells	28
1.7.5 The Role of $\pi$ -bridges and Anchoring Groups on Solar Cell Performance	28
1.8 References	29

## Chapter 2

### **Interplay between $\pi$ -bridge and position of branched –alkyl groups of unsymmetrical D-A-D- $\pi$ -A squaraine in Dye–sensitized Solar Cells: Mode of Dye Anchoring and Charge Transfer Process at TiO<sub>2</sub>-Dye/Electrolyte Interface**

2.1 Introduction	47
2.2 Results and Discussion	49
2.2.1 Synthesis of PSQ Sensitizers	49
2.2.2 Photophysical Properties	51
2.2.3 Mode of adsorption on TiO <sub>2</sub> and Structure of PSQ Dyes	56
2.2.4 Electrochemical Characterizations	58
2.2.5 Density Functional Theory (DFT) Calculations and Energy Levels	59
2.2.6 Photovoltaic Studies of PSQ1-5	63
2.2.7 Electrochemical Impedance Analysis	68
2.3 Summary	71
2.4 Experimental Section	72
2.4.1 Materials and Characterization	72
2.4.2 Device Fabrication Procedure	73
2.4.3 Relative Method	74
2.4.4 Synthetic Procedure and Characterization data	74



---

2.5 References	83
----------------	----

### Chapter 3

#### **Self-assembly of Cis-configured Squaraine Dyes at TiO<sub>2</sub>-Dye Interface: Far-Red Active Dyes for Dye-Sensitized Solar Cells**

3.1 Introduction	93
3.2 Results and Discussions	95
3.2.1 Syntheses of cis-configured squaraine sensitizers	95
3.2.2 Photophysical Properties	96
3.2.3 Photophysical Characterization on the Surface	101
3.2.4 Electrochemical Characterization	104
3.2.5 Density Functional Theory (DFT) Calculations	106
3.2.6 Photovoltaic Studies of PSQ11-15	110
3.2.7 Electrochemical Impedance Analysis	115
3.3 Summary	118
3.4 Experimental Section	118
3.4.1 Materials and Characterization	119
3.4.2 Device Fabrication Procedure	119
3.4.3 Synthetic Procedures and Characterization Data	120
3.5 References	124

### Chapter 4

#### **$\pi$ -Extended *cis*-Configured Unsymmetrical Squaraine Dyes for Dye-sensitized Solar Cells: Panchromatic Light Absorption**

4.1 Introduction	131
4.2 Results and Discussions	132
4.2.1 Syntheses of cis-configured squaraine sensitizers	133
4.2.2 Photophysical Properties	134
4.2.3 Electrochemical Characterization	138

---

4.2.4 Density Functional Theory (DFT) Calculations	140
4.2.5 Photovoltaic Studies of PSQ21-22	142
4.2.6 Electrochemical Impedance Analysis	144
4.3 Summary	146
4.4 Experimental Section	146
4.4.1 Materials and Characterization	146
4.4.2 Device Fabrication Procedure	147
4.4.3 Synthetic Procedures and Characterization Data	148
4.5 References	151

## **Chapter 5**

### **Effect of $\pi$ -Spacer and Anchoring Groups in Squaraine Based Dyes in the Dye Sensitized Solar Cells**

5.1 Introduction	155
5.2 Results and Discussions	157
5.2.1 Synthesis of PSQ sensitizers	157
5.2.2 Photophysical Properties	159
5.2.3 Electrochemical Characterization	161
5.2.4 Density Functional Theory (DFT) Calculations and Energy Levels	163
5.2.5 Photovoltaic Studies of PSQ31-33	165
5.2.6 Electrochemical Impedance Analysis	168
5.3 Summary	171
5.4 Experimental Section	171
5.4.1 Materials and Characterization	171
5.4.1 Device Fabrication Procedure	173
5.4.2 Synthetic Procedures and Characterization Data	173
5.5 References	175

---

## Chapter 6

### Summary and Future Perspective

6.1 Summary	179
6.2 Future Perspective	181
Erratum	182

---

## Abbreviations

Å	Angstrom
ACN	Acetonitrile
Ag	Silver
Ar	Argon
Au	Gold
br	Broad
°C	Degree Celsius
CB	Conduction band
CDCA	Chenodeoxycholic acid
CE	Counter Electrode
CV	Cyclic Voltammetry
CT	Charge Transfer
D- $\pi$ -A	Donor- $\pi$ -Acceptor
D-A- $\pi$ -A	Donor-Acceptor- $\pi$ -Acceptor
DCM	Dichloro Methane
DFT	Density Functional Theory
DMF	N,N,-dimethylformamide
DMSO	Dimethyl Sulfoxide
DPV	Differential Pulse Voltammetry
DSSC	Dye Sensitized Solar Cell
EtOAc	Ethyl acetate
Eg	Band Gap
EIS	Electrochemical Impedance Spectroscopy
eV	Electron Volt
FF	Fill Factor
FTIR	Fourier transform infrared spectroscopy
FTO	Fluorine Doped Tin Oxide
h	Hour(s)


---

HOMO	Highest Occupied Molecular Orbital
HRMS	High Resolution Mass Spectrometry
H <sub>2</sub> SO <sub>4</sub>	Sulfuric acid
IPCE	Incident Photon to Current Conversion Efficiency
ICT	Intramolecular Charge Transfer
I-V	Current-Voltage
J <sub>sc</sub>	Short circuit current density
LHE	Light Harvesting Efficiency
LUMO	Lowest Unoccupied Molecular Orbital
MALDI-TOF	Matrix-assisted laser desorption ionization-time of flight
min	Minutes
mmol	Millimole
MHz	Megahertz
NMR	Nuclear Magnetic Resonance
ppm	Parts Per Million
OPV	Organic Photovoltaic
PCE	Power Conversion Efficiency
Pt	Platinum
PV	Photovoltaics
RE	Reference Electrode
Redox	Reduction-Oxidation
SC	Solar Cells
<i>t</i> -BP	Tert-butylpyridine
TFA	Trifluoroacetic Acid
THF	Tetrahydrofuran
TMS	Tetramethyl Silane
TBAP	Tetra Butyl Ammonium Perchlorate
UV/Vis/NIR	Ultraviolet/Visible/Near-infrared
VB	Valence Band

---

$V_{OC}$	Open Circuit Voltage
WE	Working Electrode
$\lambda$	Wavelength
$\eta_{coll}$	Electron Collection Efficiency
$\phi_{inj}$	Electron Injection Efficiency

# Synopsis

 Synopsis of the Thesis Submitted to the Academy of Scientific and Innovative Research for the Award of the Degree of Doctor of Philosophy in Chemistry	
<b>Name of the Candidate</b>	Mr. Punitharasu Vellimalai
<b>Degree Enrolment No. &amp; Date</b>	Enrollment No: 10CC13A26027, 29-8-2013
<b>Title of the Thesis</b>	Unsymmetrical Squaraine Based NIR-active Dyes for Dye-sensitized Solar Cells: Controlling the Aggregation and Orientation of Dyes on the TiO <sub>2</sub> Surface
<b>Research Supervisor</b>	Dr. Jayaraj Nithyanandhan

## I) Introduction

Harvesting solar energy is one of the potential strategies to address the energy requirement for the future. Dye-sensitized solar cells (DSSCs), one of the third generation photovoltaic technologies, utilizes organic or organometallic sensitizers as light harvesting component for photon-to-current conversion.<sup>1</sup> Ruthenium(II) polypyridyl complexes have been highly studied since the beginning as sensitizer and PCE of 11.5% was achieved using I<sup>-</sup>/I<sub>3</sub><sup>-</sup> redox couple.<sup>2</sup> Highest device efficiency of 13% for organometallic dyes were reported for Zn (II)-porphyrin complex (SM-315) in the presence of Co(II/III) redox couple.<sup>3</sup>

Although these metal complexes showed broad spectral coverage and high efficiency, low molar extinction coefficient at higher wavelength, and difficulty in synthesis led toward metal-free organic dyes. Organic dyes have flexibility in terms of structural design and tuning of the molecular orbital energy levels, and their feasibility in synthesis makes them low cost alternative to metallated dyes.<sup>4</sup> Among metal-free dyes, N-annulated indoperylene based dye produced the efficiency of 12.5% with Co(II/III) based electrolyte.<sup>5</sup> Even though D- $\pi$ -A dyes exhibited good photon to current conversion efficiency in the visible region, their photo response in far-red and NIR region is limited. To utilize far red and NIR regions of solar spectrum, there are limited dyes available, which includes porphyrin,<sup>6</sup> phthalocyanine<sup>7</sup> and polymethine<sup>8</sup> chromophores. Squaraine (SQ) dyes are subclass of polymethine dyes, which owing to its low band gap and strong absorption ( $\epsilon > 10^5 \text{ M}^{-1} \text{ cm}^{-1}$ ) in the visible and NIR region, have found application in various areas like photovoltaics, sensor and xerography.

## II) Statement of Problem

Among the various interfaces formed by the DSSC components such as an anode, dye, electrolyte and cathode; TiO<sub>2</sub>-dye/electrolyte interface plays an important role in achieving high device efficiency. Apart from photophysical and electrochemical properties,

SQ dyes undergoes molecular aggregation due to the alignment of intrinsic molecular dipole.<sup>9</sup> Such aggregated structure may have either blue shifted (H-aggregate) or red-shifted absorption (J-aggregate) with respect to that of the monomer. Aggregation of SQ dyes on TiO<sub>2</sub> surface hampers the device efficiency due to the aggregation-induced self-quenching of photoexcited state. To minimize aggregation, incorporation of bulky substituent to the dye structure and the non-chromophoric adsorbate, such as chenodeoxycholic acid (CDCA), were used. Though squaraine dyes are exploited in dye-sensitized solar cells, controlling self-assembly of dyes on the TiO<sub>2</sub> surface that helps in achieving high device efficiency has remained unexplored.

## Results

### 1) Interplay Between $\pi$ -Bridge and Position of Branched-Alkyl Groups of Unsymmetrical D-A-D- $\pi$ -A Squaraine in Dye-Sensitized Solar Cells: Mode of Dye Anchoring and Charge Transfer Process at TiO<sub>2</sub>-Dye/Electrolyte Interface

To understand the effect of  $\pi$ -spacer and position of in-plane and out-of-plane alkyl groups in a SQ based D-A-D- $\pi$ -A dye, a series of unsymmetrical squaraine dyes **PSQ1-5** (Figure 1) were synthesised and tested the DSSC device performance. These dyes showed good

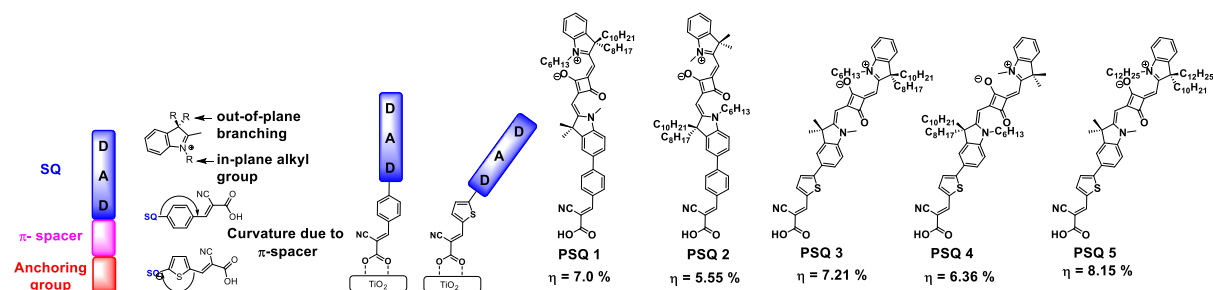


**Figure 1** D-A-D- $\pi$ -A dye based on unsymmetrical squaraines, **PSQ 1-5** dyes for DSSCs.

absorption in 680-690 nm regions with the extinction coefficient of  $2.2 \times 10^5 \text{ M}^{-1} \text{ cm}^{-1}$ . Selective alkyl functionalisation of indoline donors of D-A-D part of the sensitizer becomes a crucial part to control the nature of self-assembled monolayers on TiO<sub>2</sub>. Two positional isomers with phenyl or thiophene  $\pi$ -spacer were utilized to fabricate the DSSC devices. The photovoltaic device performance found to be increased, when the alkyl groups are placed far away from the TiO<sub>2</sub>. Thiophene-based **PSQ3** showed an efficiency of 7.21% and comparatively high  $J_{sc}$  than phenyl counterpart **PSQ1**. Length of the out-of-plane branching of **PSQ3** is increased in case of **PSQ5** to keep the dyes away from each other and which



showed a significant improvement in  $J_{sc}$  and  $V_{oc}$  in absence of optically transparent co-adsorbent. **PSQ5** exhibited PCE of 8.15% with a corresponding  $J_{sc}$  and  $V_{oc}$  of 19.73 mAcm<sup>-2</sup> and 630 mV, respectively. In addition, EIS studies on the DSSC device made out of **PSQ5** dye showed that the charge recombination process is effectively suppressed in compared to other dyes in this series.

## 2) Self-assembly of *Cis*-configured Squaraine Dyes at TiO<sub>2</sub>-Dye Interface: Far-Red Active Dyes for Dye-Sensitized Solar Cells

To understand the effect of *cis*-squaraine dyes with suitably functionalized alkyl groups which helps to control the self-assembly of dyes on the TiO<sub>2</sub> surface, a series of *cis*-configured unsymmetrical PSQ dye (**PSQ11-15**) dyes were designed and synthesised. These dyes possess following features, (i) in-plane and out-of-plane alkyl groups, which helped to control the self-assembly of the dyes on the TiO<sub>2</sub> surface (ii) electron withdrawing alkyl groups such as dicyano and cyano-ester which modulates the HOMO and LUMO energy level and further the extending the absorption in NIR as well as visible regions and (iii) number of anchoring group which helps strengthening the interaction between dye and TiO<sub>2</sub> surface (**Figure 2**) and orientation of dyes on the TiO<sub>2</sub> surface.

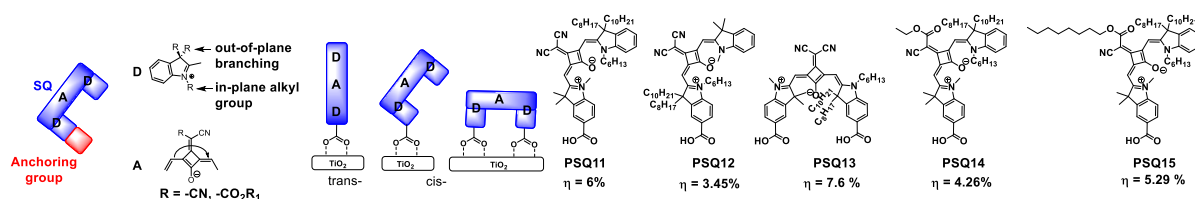


**Figure 2** D-A-D-Anchoring group dye based on *cis*-configured unsymmetrical squaraine dyes, **PSQ11-PSQ15** for DSSCs.

Photophysical studies were carried out in solution, TiO<sub>2</sub> and Al<sub>2</sub>O<sub>3</sub> to gain insight into the aggregation tendency of **PSQ11-15** dyes on surface. **PSQ13** dye exhibited DSSC performance of 7.6% with  $J_{sc}$  and  $V_{oc}$  of 17.18 mA cm<sup>-2</sup> and 618 mV, respectively. EIS studies showed that high charge transfer resistance for **PSQ13** than **PSQ11** and **PSQ12**. **PSQ11** and **PSQ12** showed the device efficiency of 6% and 3.45%, respectively. The insertion of an additional anchoring unit of **PSQ13** dye shows significant influence on the solar cells performance leading to higher DSSC device efficiency ( $\eta = 7.6\%$ ). Two positional isomers of **PSQ11** and **PSQ12** dye were examined to elucidate the importance of position of in-plane and out-of-plane branching with the *cis*-SQ units, and found that dyes with out of plane alkyl groups far away from the TiO<sub>2</sub> performed better.

### 3) $\pi$ -Extended *cis*-Configured Unsymmetrical Squaraine Dyes for Dye-sensitized Solar Cells: Panchromatic Light Absorption

As investigated in the previous sections that extending the absorption towards NIR regions can be effected by (i) introducing  $\pi$ -spacer with *trans*-SQ with appropriate acceptor units and (ii) introducing electron deficient units in the squaric acid unit which also helps to maintain the *cis*-configuration of the SQ dye unit. To understand the effect of  $\pi$ -spacer, *cis*-SQ units integrated with in-plane and out-of-plane alkyl groups, unsymmetrical SQ dyes **PSQ21** and **PSQ22** were designed to achieve a dye with panchromatic absorption property (**Figure 3**).

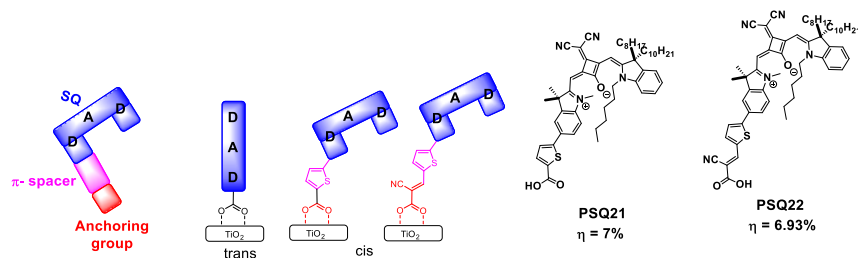


**Figure 3** D-A-D- $\pi$ -Anchoring group dye based on *cis*-configured unsymmetrical squaraine dyes, PSQ 21-22 for DSSCs.

Here the  $\pi$ -spacer, *cis*-SQ unit, different anchoring groups help to extend the absorption in NIR as well as visible region. Photophysical studies were carried out to gain insight into the extending the absorption of aggregation tendency of PSQ dyes on the surface. In terms of device **PSQ22** exhibited good photovoltaic performance on PCE of 7% with a corresponding  $J_{sc}$  and  $V_{oc}$  of  $17.22 \text{ mAcm}^{-2}$  and 579 mV, respectively. EIS studies showed that **PSQ21** dyes showed more  $R_{CT}$  enhanced charge transfer resistance across  $\text{TiO}_2$ -dye/electrolyte interface.

### 4) Effect of $\pi$ -Spacer and Anchoring Groups in Squaraine Based Dyes in the Dye Sensitized Solar Cells

To understand the effect of anchoring groups such as carboxylic acid vs cyano acetic acid groups on unsymmetrical D-A-D- $\pi$ -A squaraine dyes, we have designed and synthesized **PSQ31-33** (**Figure 4**). The DSSC devices were fabricated using **PSQ31-33** respectively as the sensitizers and the photovoltaic behavior was investigated. The overall power conversion efficiencies lie in the order of **PSQ31** > **PSQ32** > **PSQ33**. The **PSQ31**-based DSSCs exhibit the highest power conversion efficiency of 2.14% as well as EIS studies showed that **PSQ31** showed high recombination resistance. In contrast, the efficiency of **PSQ33**-based DSSC was only 0.92%. To further improve the cell performance, **PSQ5** was used as the co-sensitizer

for **PSQ31**, which showed a moderate efficiency of 2.10% with the  $J_{sc}$  and  $V_{oc}$  of 5.1 mA cm<sup>-2</sup> and 566 mV, respectively. This detailed study provides the importance of cyano acetic acid over carboxylic acid as a good anchoring group for this class of NIR active dyes.

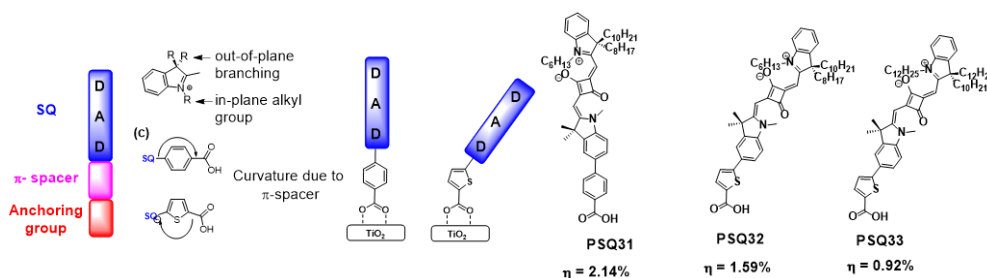


**Figure 4** D-A-D- $\pi$ -A based on unsymmetrical squaraine dyes, **PSQ31-33** for DSSCs.

### III) List of publications

1. **Punitharasu, V.;** Kavungathodi, M. F. M.; and Nithyanandhan, J. Self-Assembly of *Cis*-configured Squaraine Dyes at the TiO<sub>2</sub>-dye Interface: Far-Red Active Dyes for Dye-Sensitized Solar Cells. *ACS Appl. Mater. Interfaces* **2018**, *10*, Article ASAP, DOI: 10.1021/acsami.8b03106.
2. **Punitharasu, V.;** Kavungathodi, M. F. M.; and Nithyanandhan, J. Interplay between  $\pi$ -bridge and position of branched-alkyl groups of unsymmetrical D-A-D- $\pi$ -A squaraine in dye-sensitized solar cells: Mode of Dye Anchoring and Charge Transfer Process at TiO<sub>2</sub>-Dye/Electrolyte Interface, *ACS Appl. Mater. Interfaces*, **2017**, *9*, 32698–32712.
3. Sil, M. C.; Vediappan, S.; Kavungathodi, M. F. M.; **Punitharasu, V.;** Nithyanandhan, J. Orthogonally Functionalized Donor/Acceptor Homo- and Heterodimeric Dyes for Dye-Sensitized Solar Cells: An Approach to Introduce Panchromaticity and Control the Charge Recombination, *ACS Appl. Mater. Interfaces*, **2017** *9*, 34875–34890.
4. Alagumalai, A.; Kavungathodi, M. F. M.; **Punitharasu, V.;** Sil, M. C.; Nithyanandhan, J. Effect of Out-of-Plane Alkyl Group's Position in Dye-Sensitized Solar Cell Efficiency: A Structure-Property Relationship Utilizing Indoline Based Unsymmetrical Squaraine Dyes, *ACS Appl. Mater. Interfaces*, **2016**, *8*, 35353–35367.
5. **Punitharasu, V.;** Kavungathodi, M. F. M.; and Nithyanandhan, J.  $\pi$ -Extended *cis*-Configured Unsymmetrical Squaraine Dyes for Dye-sensitized Solar Cells: Panchromatic Light Absorption (manuscript under preparation).

6. **Punitharasu, V.**; Kavungathodi, M. F. M.; and Nithyanandhan, J. Effect of  $\pi$ -Spacer and Anchoring Groups in Squaraine Based Dyes in the Dye-sensitized Solar Cells (manuscript under preparation).

### III) Patents

1. Unsymmetrical Squaraine Dyes with Anchoring Group and Application thereof *Indian Pat. Appl.* (2018), IN201611025821 A 20180309.

### References

1. O'Regan, B.; Grätzel, M. *Nature* **1991**, 353, 737-740.
2. Chen, C.Y.; Wang, M.; Li, J.Y.; Pootrakulchote, N.; Alibabaei, L.; Ngoc-le, C.; Decoppet, J. D.; Tsai, J. H.; Grätzel, M.; Wu, C. G.; Zakeeruddin, S. M.; Grätzel, M. *ACS Nano* **2009**, 3, 3103–3109.
3. Mathew, S.; Yella, A.; Gao, P.; Humphry-Baker, R.; Curchod, B. F. E.; Ashari-Astani, N.; Tavernelli, I.; Rothlisberger, U.; Nazeeruddin, M. K.; Grätzel, M. *Nat. Chem.* **2014**, 6, 242–247.
4. Mishra, A.; Fischer, M. K. R.; Bäuerle, P. *Angew. Chem., Int. Ed.* **2009**, 48, 2474–2499.
5. Yao, Z.; Zhang, M.; Wu, H.; Yang, L.; Li, R.; Wang, P. *J. Am. Chem. Soc.* **2015**, 137, 3799–3802.
6. Urbani, M.; Grätzel, M.; Nazeeruddin, M. K.; Torres, T. *Chem. Rev.* **2014**, 114, 12330–12396.
7. Martín, -G, L.; Fernández, -L, F.; Sastre, -S, A'. *J. Mater. Chem. A* **2014**, 2, 15672–15682.
8. Saccone, D.; Galliano, S.; Barbero, N.; Quagliotto, P.; Viscardi, G.; Barolo, C. *Eur. J. Org. Chem.* **2016**, 2016, 2244–2259.
9. Kasha, M.; Rawls, H. R.; Ashraf, E. -B, M. *Pure Appl. Chem.* **1965**, 11, 371– 392.

# Chapter 1



**Introduction of Dye-Sensitized Solar Cells**

## 1.1 General Introduction

### 1.1.1 Global Energy Demand

One of the most important and challenge that we face today is the steady increase in energy consumption and global warming due to the unrestricted population growth and rampant urbanization. In 2001, the global energy consumption for the entire year was estimated to be 13.5 TW. Whereas fossil fuel such as coal, oil and natural gas is the significant main source.<sup>1</sup> Basically, the burning of fossil fuels creates more concerns about increase of carbon dioxide in the atmosphere of earth, has revealed public discussion. However the world can reduce the emissions because it causes geopolitical tension, irreversible environment damage and tragically climate changes.<sup>2</sup> On the other hand, the worldwide energy consumption is expected to set more than double which is estimated 30 TW by 2050 due to the large part involved towards the industrialisation globally.<sup>3</sup> In contrast there is a real urge for the development and initiation of additional sustainable power sources. Comparing the two main issues of increasing power production and reducing the carbon emissions which is a major challenge for the coming near future. For this purpose a number of research is being carried out on different ways for the production of clean sustainable energy in the 21<sup>st</sup> century.<sup>1</sup>

### 1.1.2 Renewable Energies

The next prime energy sources which are established for long term usage should be renewable due to their limited environmental impact and loss of resources. One of the promising opportunity is solar energy because of solar energy is renewable and it does not produce carbon dioxide, and can stay away from utilising hazardous chemicals.<sup>4</sup> The ultimate leading renewable energy sources are wind, wave, hydroelectric, biomass and solar energy. There are significant interest present in the merits, demerits and cost of energy from those renewable sources, and which are briefly summarized in **Table 1.1**.<sup>5</sup> However, renewable energy is recognized as an ideal solution towards the increasing energy demand with the possibility of carbon neutrality. The worldwide availability of an unlimited fuel source with no political consequences.<sup>6,7</sup> In addition, there is a hope that solar energy can contribute in future energy production. There were few reports proposed that photovoltaics (PV) could provide a significant energy proportion from 2025 onwards. The growth continues at a similar speed to recent years (an average annual growth of 35 % since 1998).<sup>8</sup>

**Table 1.1** Summary of various attributes of renewable energy sources<sup>5</sup>

Energy Source	Advantages	Disadvantages
Solar	Unlimited energy source; publically accepted technology.	Fluctuation of energy production due to daylight hours and cloudy weather.
Hydropower	No fuel-extracting infrastructure and no fuel transport; Cheap and mature technology.	Can have considerable environmental costs; not available in areas with low water reserves.
Biomass	Possibility of carbon negativity; mature and efficient technologies available.	Availability of land for fuel growth; changing climate may result in less land suitable for agriculture.
Wind	No fuel required.	Intermittent nature of wind; windiest places tend to be less populated; wind unequally distributed globally; public acceptance of wind farms is varied.
Wave	Tidal patterns predictable.	Coastline not available to every country; environmental impacts of large installations.

## 1.2 Overview of Photovoltaics

### 1.2.1 History of Solar Cells

The generation of electrical current upon light exposure was first ascertained in 1839 by Alexandre-Edmond Becquerel.<sup>9</sup> Becquerel created the primary photovoltaic cell, using plates coated in silver salts. Charles Fritts created the primary solar cell. This electrical cell was achieved an efficiency of more than 1%.<sup>10</sup> It was made using selenium based metal conductor and the top side layer coated with gold. The first generation semiconducting material primarily based silicon solar cell devices were developed in 1953 by the Bell Telephone Lab, USA. They have achieved the efficiency of 4.5% at that time, and further augmented to PCE of 6% in 1954.<sup>11</sup> The research of silicon-based photovoltaic cells have been followed by several research community due to the larger abundance of silicon on earth. These crystalline inorganic

photovoltaic cells are called the first generation solar cells. Silicon based solar cells are extremely expensive owing to the utilisation of pure silicon. Another fascinating part is that the efficiency of those forms of solar cell is near to their theoretical most efficiency (33%).<sup>12</sup> But, the best research power conversion efficiency is reported up to 20%. However, the PCE was limited to 15 to 18% for the industrial standard. The drawback of these photovoltaic cells are due to the urge of high pure silicon and high-temperature processability. More specifically, the purification of silicon is a difficult task and this makes the manufacture of such devices expensive.<sup>13</sup>

In order to reduce the cost of solar cells, the second generation solar cell was introduced the thin film technologies which incorporating less expensive materials such as CdTe, copper indium gallium diselenide, CdSe and amorphous silicon. The second generation solar cells are very less efficient in comparison to the crystalline silicon solar cells. This trade-off is one of the key driving forces for research into these technologies and make use of low cost materials within the manufacturing process.<sup>14</sup> CIGS and CdTe devices are attractive because of the high efficiencies (9–15%). There is a concern whether these technologies will support or not for large scale production because of the shortage of indium, selenium and tellurium. However these demand will massive increase in cost of these materials.<sup>15</sup> The toxicity of cadmium can also become a difficulty within the commercialisation of device cells with European legislation baned the sale of few CdTe modules. In addition there is an existing problem with the disposal of NiCd batteries once their period of time is over.<sup>14</sup>

Third-generation solar cells (SCs) are solution processable solar cells with outstanding potential for large-scale solar electricity generation. The third-generation solar cells show less expensive and compatible to several important applications than conventional silicon solar cells. These types of solar cells are mainly focused and fabricated through multiple layers of active materials to generate a lot of excitons and to get the high power conversion efficiency. It is one of the alternative resources for replacement of 1<sup>st</sup> and 2<sup>nd</sup> generation solar cells. The third generation solar cells cover all new techniques, including Quantum dots (QD) solar cells<sup>16–20</sup>, polymer solar cell<sup>21–24</sup>, perovskite cells<sup>25–28</sup>, organic tandem cells<sup>12,29–31</sup> and dye sensitized solar cells.<sup>32–39</sup> The use of cheap materials with high performance make third-generation dye-sensitized solar cells a bright candidate as a future photovoltaic technology. This thesis however is focused on the synthesis of dyes suitable for use in DSSCs.

### 1.3 Dye Sensitized Solar Cells



DSSC is an exciting class of photovoltaic technology in the emerging third generation solar cells. It has the potential to become a third generation technology utilizing the nanoscale properties of the device. This technology is receiving attention from scientists with different backgrounds due to the possibility of low-cost production and fabrication on flexible substrate. The DSSC is the only photovoltaic device that mimicking the natural process of photosynthesis which separates the process of light-harvesting and charge carrier transport. This separation means that there is no longer requirement for the high purity materials with controlled defect levels. Hence the cost of device cells can be foreseen to be substantially lower than those described above.

### 1.3.1 Advantages and Disadvantages of DSSCs

DSSCs have gained important recognition owing to their low cost, ease of production, and tunable optical properties.<sup>40,41</sup>

The advantages<sup>36</sup> of DSSC include:

- Light weighted device materials
- Modulated dye design for better light harvesting property
- Low manufacturing cost
- Possessing better suited to covering all type of applications
- Showing better performance in diffuse light even at higher temperatures
- Flexible in nature
- Shorter energy payback time

Generally, there are two types of tasks in DSSCs<sup>42</sup> in which the organic dye absorbs the light and then converts into a charge separated state. It was transported through both electrolyte and semiconductor. Therefore, the main focus can be completely on the organic material's capability to capture sunlight.<sup>4</sup> There were number of significant benefits for separating light absorption and charge transport.<sup>43</sup> These include:

- Doping treatments can be avoided
- Depending on the properties of sensitizers
- No need costly purification method
- Availability of charge transport materials

There is one main drawback proposing in DSSCs, which is more related to traditional inorganic solar cells, is large over potentials. This is more essential for dye regeneration and

electron injection into the semiconductor and provides a major loss of potential ( $>700$  mV).<sup>44</sup> In addition, over periods of sensitisation (more than 12 hours) of the  $\text{TiO}_2$  semiconducting electrode which showed increased quenching. Further, it varies in the geometry of adsorption, and giving an induced aggregation which decreased the device performance.<sup>45</sup>

### 1.3.2 Dye-sensitized Solar Cell Architecture

A conventional DSSC configuration<sup>46</sup> is basically a thin-layer solar cell which made by sandwich arrangements of two electrode on a glass substrate. The low cost and ease fabrication of DSSCs have been gained much interest since 2000. The basic device configuration of DSSC is given in **Figure 1.1**. The key components of DSSCs are photoanode, sensitizer, redox electrolyte, and the counter electrode.

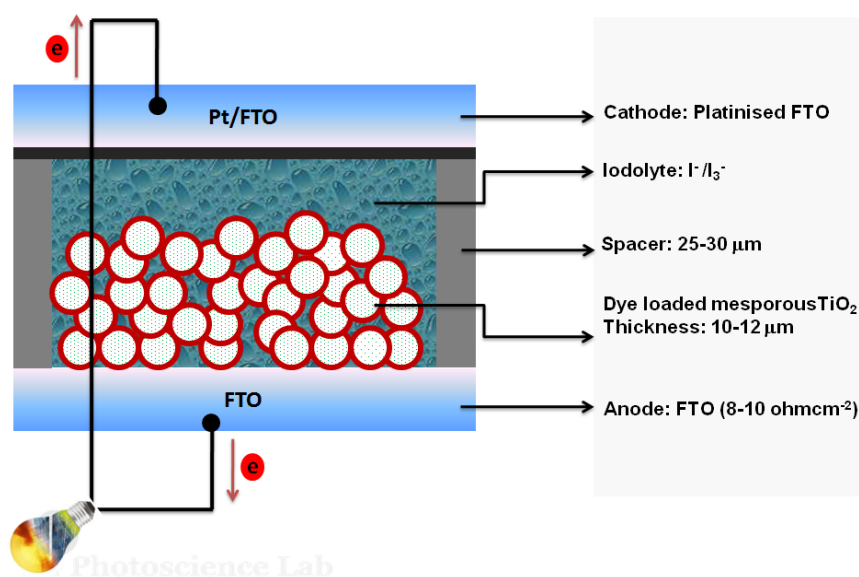


**Figure 1.1** Schematic diagrams of dye-sensitized solar cells.

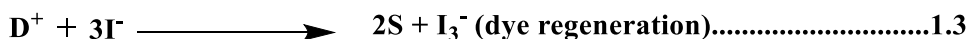
1. A thin, compact layer of  $\text{TiO}_2$  which is casted on FTO substrates is utilised as a blocking layer at the interface of FTO and photoanode.
2. The mesoporous  $\text{TiO}_2$  made of 20 nm particle size titanium dioxide is coated on blocking layer. These layers were sintered to construct a better-interconnected charge percolation network among the particles.
3. The surface of  $\text{TiO}_2$  is coated with dye via adsorption through chemical bonding. Upon photo-excitation, the LUMO state of the dye injects an electron to conduction band of  $\text{TiO}_2$ . After this process dye becomes its oxidized form. These oxidized sensitizers can be

reformed to its original ground state via an electron regeneration from redox couple in the electrolyte (iodide/triiodide)

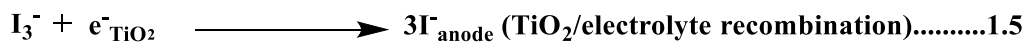
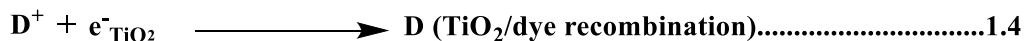
4. The redox couple in the electrolyte generally contains ionic salts dissolved in organic solvents
5. The oxidation and reduction reactions of  $I/I_3^-$  which direct the flow of electrons through the external circuit

### 1.3.3 Operating Principle of DSSCs

In this part, it will briefly discuss about the operating principle as well as electron transfer at various interfaces of DSSCs. The basic electron transfer reactions take place at various interfaces of DSSC is presented in **Figure 1.2** and pointed out below. Firstly, the dye (D) is excited by absorption of a photon to form its excited state ( $D^*$ ) (eqn 1.1) and then, excited state of dye ( $D^*$ ) can be injected an electron into the conduction band of the  $TiO_2$  (eqn 1.2). The injected electron moves through the mesoporous network of semiconductor electrode to reach the back electron collector electrode (counter electrode) through the external circuit. The oxidized dye ( $D^+$ ) is regenerated rapidly back to the ground state by the redox electrolyte (eqn 1.3). The ground state and excited state redox potentials must be positioned correctly for both electron injection and dye regeneration. For example, HOMO of sensitizers should be more positive potentials than the electrochemical potential of redox electrolyte couple (0.4 V vs NHE) that ensure the feasible regeneration of oxidised dye. Further, the LUMO of the dyes should be more negative potential than conduction band edge of  $TiO_2$  (-0.5 V vs NHE) which may result in a larger driving force for electron injection from the excited state of the sensitizer to the  $TiO_2$  conduction band



The recombination of the injected electron of the  $TiO_2$  active layer takes place either with the oxidized sensitizer (**eqn 1.4**) or with the oxidized redox couple at the  $TiO_2$  surface (**eqn 1.5**).



The dye in the excited state can decay back to the ground state when there is competition between the electron injection into the metal oxide and the radiative and non-radiative decay of the excited state dye (eq 1.6).

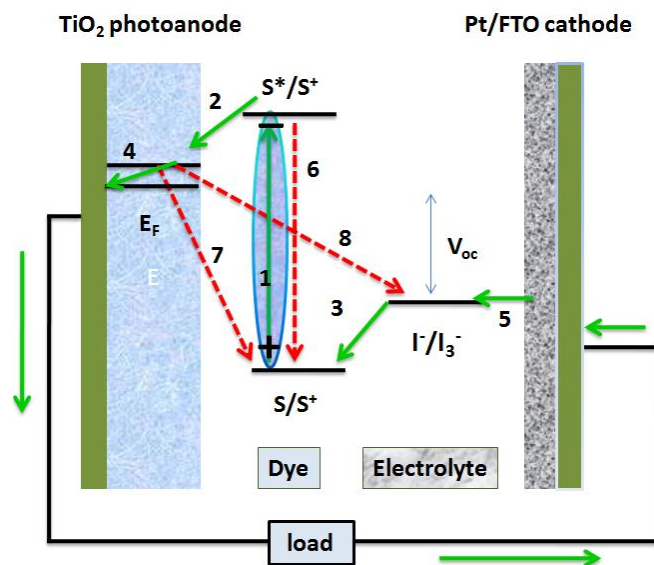


**Figure 1.2** Operating principle of Dye-sensitized solar cells.

### 1.4 Solar Cell Measurements

During the cell measurements in the dark condition, the current-density vs. voltage ( $J$ - $V$ ) characteristics of both organic and inorganic solar cells were be similar to with the response of a diode device. Upon illuminating a light on the device cell, that generates the photocurrent in a device cell as well as the diode characteristic features. In general, the  $J$ - $V$  characteristics of an ideal solar cell device can be illustrated as Shockley eq 1.7 with photocurrent term,

$$J = J_0 \left[ \exp \left( \frac{eV}{nKT} \right) - 1 \right] - J_{ph} \dots \dots \dots (1.7)$$

where  $J$  is the current density,  $V$  is voltage,  $J_0$  is the reverse bias current density of the solar cells,  $e$  is the elementary charge,  $n$  is the ideality factor,  $k$  is the Boltzmann constant, and  $T$  is temperature.

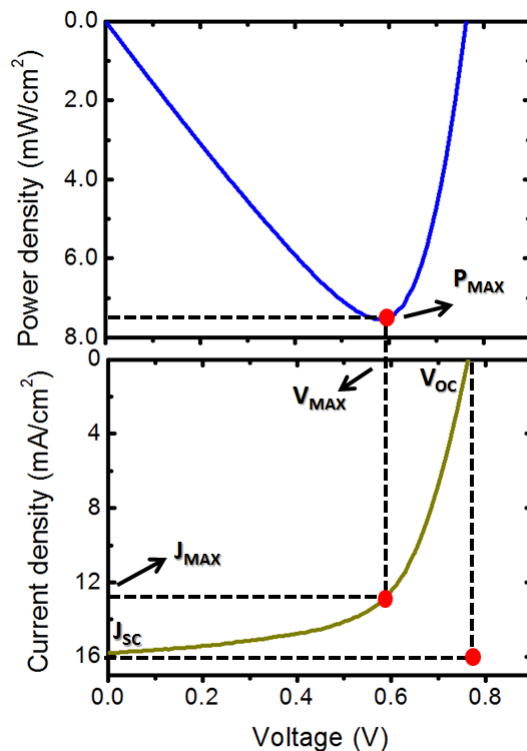


**Figure 1.3** J-V Characteristics of solar cells with all parameters

**Figure 1.3** depicts the  $J$ - $V$  plot for an ideal solar cell in the power generation region. The power density, the product of voltage and current density, versus voltage is also plotted, and negative power axes show the power generation upon illumination. The parameters which can be found from the  $J$ - $V$  characteristics curve of a device under illumination are short circuited current density ( $J_{sc}$ ), open-circuit voltage ( $V_{oc}$ ), fill factor ( $FF$ ), and power conversion efficiency ( $\eta$ ).

#### 1.4.1 Short-circuit Current

The short circuit current density  $J_{sc}$  can be illustrated as the current density when the voltage across the devices is zero ( $V = 0$ ), which is close to the two electrodes of the cells being short-circuited. Again, there is no power generated at this point since the  $V = 0$ , but the  $J_{sc}$  does mark the onset of power generation. In ideal devices, the  $J_{sc}$  will be the similar as that of the photocurrent density ( $J_{ph}$ ) produced in devices. On the other hand, it will lower than the  $J_{sc}$  from this ideal value owing to the loss process taking place at the devices. However  $J_{sc}$  is technically a negative number with the conventions used here during the power generation from the cells.

#### 1.4.2 Open-circuit Voltage

The open-circuit voltage ( $V_{oc}$ ) is the voltage across the solar cell while the current density is

Zero ( $J = 0$ ), which is resembling to the device being open-circuited. The  $V_{oc}$  can be expressed by the eq 1.8.

$$V_{oc} = \frac{E_{cb}}{e} + \frac{k_B T}{e} \ln \left( \frac{n}{N_{cb}} \right) - E_{redox} \dots\dots\dots(1.8)$$

where  $e$  is the elementary charge,  $n$  is the number of the electrons in  $TiO_2$ ,  $k_B$  is the Boltzmann constant,  $T$  is the absolute temperature,  $N_{cb}$  is the effective density of states, and  $E_{redox}$  is the redox potential of the redox couple. Thus, the maximum  $V_{oc}$  corresponds to the difference between the energy level ( $E_{cb}$ ) of the CB of  $TiO_2$  and the redox potential of the electrolyte. On the other hand, the actual  $V_{oc}$  is always lower than the expected theoretical value because of the recombination of injected electrons with electrolyte and oxidised dye cations.

**1.4.3 Fill-factor**

When  $V_{oc}$  and  $J_{sc}$  are the critical factors which decide the power generation in solar cells, the maximum power density generated at point  $P_{max}$  take place at the voltage  $V_{max}$  and current-density  $J_{max}$  where the product of  $J$  and  $V$  is at a minimum as shown in **Figure 1.3**. Owing to the diode behaviour an additional resistance and recombination losses in solar cells produced, which makes the  $J_{max}$  and  $V_{max}$  always lower than  $J_{sc}$  and  $V_{oc}$ , respectively. The fill factor  $FF$  illustrates the differences in the ratio of these parameters and can be given by the following eq 1.9,

$$FF = \frac{J_{max} V_{max}}{J_{sc} V_{oc}} \dots\dots\dots(1.9)$$

$FF$  which indicates that how close  $J_{max}$  and  $V_{max}$  to the  $J_{sc}$  and  $V_{oc}$  and also the sharpness of the bend in the exponential  $J$ - $V$  curve. Since higher  $FF$  which corresponds to higher maximum power, high  $FF$  is desired and however, the diode-like behaviour of solar cells resulting  $FF$  always lower than one. Devices with high  $J_{sc}$  and  $V_{oc}$  can still have low  $FF$ , suggesting that something must be done to improve device quality.

**1.4.4 Power Conversion Efficiency**

The most discussed significant parameter of a solar cell is the power conversion efficiency ( $\eta$ ). It is defined as the percentage of incident irradiance that is converted into output power. The maximum output power  $P_{max}$  is used for calculating power conversion efficiency. The cell efficiency can be written as follows,

$$\eta = \frac{J_{sc} V_{oc}}{I_L} \times FF \dots\dots\dots(1.10)$$

This clearly indicates that  $FF$ ,  $J_{sc}$ , and  $V_{oc}$  have direct effects on  $\eta$ . Power conversion efficiency is very important because it determines how effectively the space occupied by a solar cell is being utilised to generate a given amount of power. Because larger areas require more resources to cover the solar cells, higher  $\eta$  is often desirable. Power conversion efficiency is also very dependent on the power and spectrum of the light source since solar cells do not absorb and convert photons to electrons at all wavelengths with the same efficiency.

#### 1.4.5 Incident Photon to Current Conversion Efficiency (IPCE)

Monochromatic incident photon-to-current conversion efficiency (IPCE) can be defined as the percentage of photons that are converted to electric current when the cell is operated under short circuit conditions. The value corresponds to the photocurrent density produced in the external circuit under monochromatic illumination of the cell divided by the photon flux that strikes the solar cell.

$$IPCE(\lambda) = N_e / N_p \times 100\% = 1240 \times J_{sc} / (\lambda \times P_{in}) \dots\dots\dots 1.11$$

Here,  $N_e$  is the number of electrons generated in the external circuit,  $N_p$  is the number of incident monochromatic photons,  $J_{sc}$  is the short circuit current density,  $\lambda$  is the wavelength,  $P_{in}$  is the intensity of the incident light.

The factors determining the IPCE can be expressed as:

$$IPCE(\lambda) = LHE(\lambda) \cdot \phi_{inj} \cdot \eta_{coll} \dots\dots\dots 1.12$$

Here,  $LHE(\lambda)$  is the light-harvesting efficiency for photons of wavelength  $\lambda$ ,  $\phi_{inj}$  is the quantum yield for electron injection from the excited state dye in the conduction band of the semiconductor oxide.  $\eta_{coll}$  is the electron collection efficiency on the back contact of semiconductor oxide and the conducting glass.

#### 1.4.6 Electrochemical Impedance Spectroscopy (EIS)

Electrochemical impedance spectroscopy is one of the most important methods for evaluating the charge transfer dynamics at the interfaces, when it is applied to an electrochemical process called as electrochemical impedance spectroscopy (EIS). Furthermore, EIS measurements afford insights into the important variations in  $J_{sc}$  and  $V_{oc}$  for DSSCs to study the charge recombination

of interfacial dynamics between the injected electrons in  $\text{TiO}_2$  conduction band ( $\text{CB}_{\text{TiO}_2}$ ) and  $\text{I}_3^-$  in electrolyte at interfaces of  $\text{TiO}_2$ -dye/electrolyte under dark condition. In general for DSSC,  $V_{\text{oc}}$  is measured from the potential difference between shift of quasi- Fermi level of electron in the  $\text{TiO}_2$  ( $E_{\text{Fn}}$ ) and the fermi level of redox potential of electrolyte ( $E_{\text{F, redox}}$ ) in the electrolyte in eq 1.13.

$$V_{\text{oc}} = E_{(\text{F,redox})} - E_{(\text{F,n})} \quad (1.13)$$

The Nyquist plot **Figure 1.4** shows the current response to the application of an ac voltage as a function of the frequency, in the dark condition. The Nyquist plots were acquired in

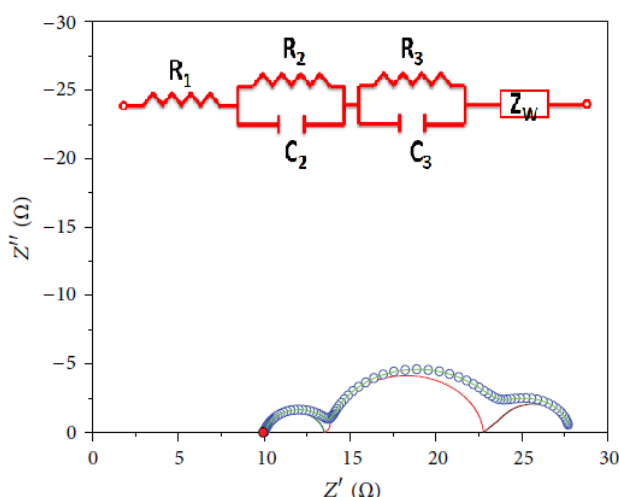


**Figure 1.4** Impedance analysis with Nyquist plot (inset shows the equivalent circuit)

the dark conditions at different applied bias in which the smaller semicircle at high frequency represents the impedance because of electron transfer occurs at the interface of Pt/electrolyte interface, whereas the larger semicircle at mid frequency range with respect to charge recombination resistance ( $R_{\text{ct}}$ ) because of charge transfer occurs at the interface of  $\text{TiO}_2$ -dye/electrolyte. The third semicircle at low frequency range represents the diffusion of electrolyte species in redox couples.

Several research groups have been established systematic approach efficiently to evaluate the EIS parameters for DSSCs. Determination of physical parameters from electrochemical impedance spectra of DSSCs is afforded by fitting the spectra to an equivalent circuit which showed in **Figure 1.4**, whereas  $R_1$ ,  $R_2$  and  $R_3$  is the resistance of the charge recombination process at the  $\text{TiO}_2$ -dye/electrolyte interface;  $C_2$ ,  $C_3$  is the chemical capacitance of the  $\text{TiO}_2$  film;



$Z_w$  is the Warburg element showing the Nernst diffusion of  $I_3^-$  in electrolyte; Herein, the high impedance at the interface of  $TiO_2$ -dye/electrolyte represents the minimum recombination reactions.

### 1.5 Key Components of DSSCs

The general configuration of DSSCs consists of four main components: a transparent photoanode, sensitizers adsorbed on mesoporous nanocrystalline metal oxide, an inorganic liquid electrolyte or solid organic hole-transporter, and a counter electrode.

#### 1.5.1 Nanostructured Metal Oxide Electrodes

Researchers reported very important breakthrough for DSSCs in 1991,<sup>36,42,47</sup> was usage of mesoporous  $TiO_2$  electrode, with a high internal surface area to support the monolayer of dyes. Furthermore, the nanostructured metal oxide which plays highly significant part in DSSC for dye adsorption and transport of the photogenerated electrons. Currently  $TiO_2$  has been broadly used for DSSCs purpose owing to its significant properties including a high refraction index, a good chemical stability, an amphoteric surface and a low manufacturing cost.<sup>36</sup>  $TiO_2$  contains a wide band gap of 3.2 eV which can be found in nature as anatase, rutile or brookite. Anatase is the most common structure used in high performance solar cells. Here, there are many other metal oxide<sup>4</sup> systems available such as  $ZnO$ <sup>42,48,49</sup>,  $SnO_2$ ,<sup>50</sup> and  $Nb_2O_5$ <sup>36,48</sup> have been tested and  $TiO_2$  provides the highest efficiencies.

In general, DSSC device, the size of  $TiO_2$  particles is around 20 nm and normally colloidal  $TiO_2$  dispersions are allowed to deposit nanocrystalline  $TiO_2$  films on FTO substrate. There are some techniques such as screen-printing and doctor-blading which are broadly used for the deposition of the  $TiO_2$  layer.<sup>51</sup> The key to the breakthrough for DSSCs technology was due to the  $TiO_2$  film, which contains a mesoporous semiconductor structure compared to a flat electrode. The mesoporous  $TiO_2$  films contains more surface area nearly 1000-times greater than a flat electrode. Furthermore, the porosity of these films which leads to the electrolyte to fill and cause better contact with the dye molecules and electrolyte.

#### 1.5.2 Different Redox Mediators

The redox mediator can lead the completion of the cell circuit, but also it can affect the cell's overall cell performance via the concentration of the cations in the electrolyte.<sup>45,52-54</sup> The liquid electrolyte is one of the most classic electrolyte and the world record efficiency is always

achieved by liquid electrolyte for DSSCs. Generally, a liquid electrolyte includes four elements, containing electron mediators like  $I^-/I_3^-$ , additives like tert-butylpyridine (*t*-BP) and organic solvents used to dissolve everything. It is essential to specify that most of the efficient organic dyes are analysed with standard iodide/triiodide electrolyte in acetonitrile. On the other hand, it has been observed that the triiodide captured a non-negligible portion of the visible light and therefore is competitive with the dye. The make use of such high-performance cell using iodine-based electrolytes are thought to be result of superior dye regeneration by iodide. Besides the slow electron transfer from the  $TiO_2$  to triiodide making the dark current loss mechanism unfavourable. It contains few drawbacks, including high volatility, significant coloration and corrosive nature. Moreover, the redox potential of the iodine mediator is somewhat low (0.4 vs. NHE) and it would be desirable for a mediator which have a more positive redox potential, to show better match that of the sensitizer.<sup>55</sup> On the other hand, researchers are replaced  $I^-/I_3^-$  redox couples by cobalt bipyridine complexes which help enhancing the open circuit potentials. This is due to the low visible absorption of light, and the reduced corrosiveness with respect to metallic conductors existing by these redox couples.<sup>56,57</sup> One important significant feature of cobalt redox couple is the tuning of their redox potential are facile, which can be modulated to match the photo-sensitizer minimizing energy loss with respect to oxidation potential in the dye regeneration process. Furthermore, it has been promoted to slow mass transport.<sup>57</sup> The back reactions of injected electron are faster with respect to oxidized electrolyte<sup>58</sup> which connected with slow regeneration of cobalt redox species at the cathode electrode.<sup>59</sup> However, Power conversion efficiency with these cobalt redox couples were especially lower under full sunlight compared to the  $I^-/I_3^-$  redox electrolyte. Other alternative redox electrolyte systems that do not have these limitations towards the current research in the DSSC field. Therefore alternative redox mediators have been investigated.

Possible variations in DSSC redox mediators include:<sup>47</sup>

- Ionic dyes with liquid electrolytes
- Ionic liquids as electrolytes
- Solid electrolytes
- Gelification of the solvent

### 1.5.3 Counter Electrode

Counter electrode (CE) is the interface where the oxidized species are reduced in the electrolyte and those electrodes have been given equal important for DSSC performance. Generally, fluorine-doped tin oxide (FTO) glass is coated via pyrolysis, sputtering, and vapour deposition with platinum to afford more efficient reversible electron transfer with charge transfer resistance of less than  $1 \Omega \text{ cm}^2$ . However, Pt counter electrode is limited and more expensive. Hitherto, non-Pt materials, including graphite, <sup>60-62</sup> carbon black, <sup>63</sup> carbon nanotubes, <sup>63</sup> activated carbon, on FTO-glass and organic ion-doped conducting polymers of poly(3,4-ethylenedioxythiophene) (PEDOT) on both indium tin oxide (ITO) and FTO-glass, have been suggested as a counter electrode in DSSCs. Kay and Grätzel group developed a counter electrode with good electronic condition from a mixture of graphite and carbon black which has been used in DSSCs besides catalytic activity.<sup>64</sup> Deposited on a flexible substrate (ITO/PEN) it exceeds Pt on the same materials, with a charge transfer resistance down to  $1.8 \Omega \text{ cm}^2$ , at the same time thermal Pt on FTO provided  $1.3 \Omega \text{ cm}^2$  using the same ionic liquid electrolyte. The carbon catalyst-based DSSC were recently achieved rendering a new option with low cost and high corrosion resistance and gave over 9% efficiency under AM 1.5 simulated sunlight.<sup>63</sup>

### 1.6 Dye Design

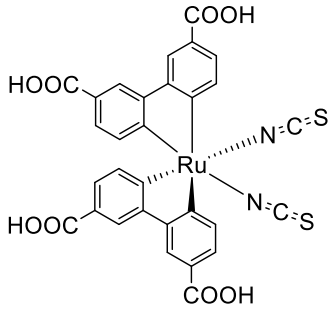
The sensitizer is one of the most important components to harvesting light in the DSSCs, converting the incident light into photocurrent. Its properties have a lot of effect on the overall power conversion efficiency and the light harvesting efficiency. The role of the sensitizer has more impact on the light harvesting as well as charge injection. The following properties are necessary for the dye to enable high power conversion efficiency (PCE) in the DSSC. First the sensitising dye should cover panchromatic absorption in visible as well as NIR region for high photocurrent, in particular high molar extinction coefficient in order to harvest as much photon as possible with thinner  $\text{TiO}_2$  film, respectively. Secondly, it must have anchoring groups and it persists several anchoring units which are commonly used such as carboxylic acid (-COOH), phosphonic acid ( $-\text{PO}_3\text{H}_2$ ) and sulfonic acid ( $-\text{SO}_3\text{H}$ ) to graft itself on the surface of  $\text{TiO}_2$  and to inject electrons from the excited dye to conduction band of the  $\text{TiO}_2$ . Thirdly, the ground state and excited state redox potentials must be positioned correctly for both electron injection and dye regeneration. Homo of sensitizers should be more positive potential than the electrochemical potential of redox couple that ensure the feasible regeneration of oxidised dye. The LUMO of the

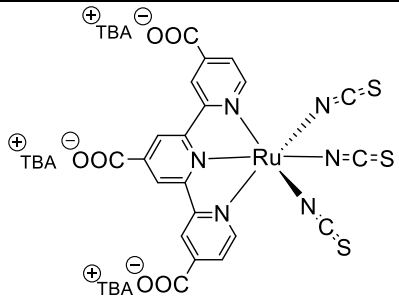
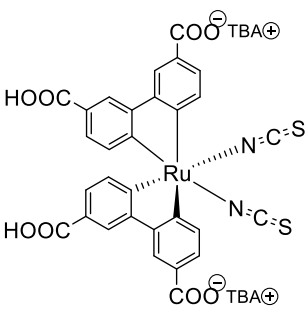
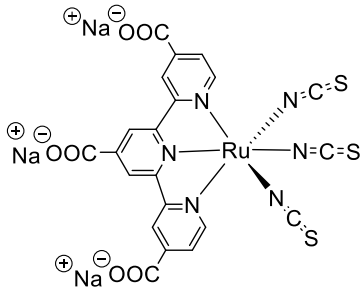
dyes should be more negative potential than conduction band edge of TiO<sub>2</sub> that ensure the electron injection process. In addition, the dyes should persist reasonably for both good thermal and chemical stabilities. Finally, it should persevere its photovoltaic activity a minimum of 20 years of throughout current generation cycle under illumination. Till now, there are two main class of sensitising dyes that metal complexes and metal-free organic dyes.

### 1.6.1 Ruthenium Complexes

In general, Ru(II)-bipyridine metal complexes were utilized for more than over decade and still it shows the higher end of power conversion efficiency nearly upto 11% compared to recent metal based complexes. The literature strategies showing the Ru based metal complexes have been studied for DSSC research purpose that listed in **Table 1.2. M**.

**Table 1.2** Initial literature reports and Ru-metal complexes reported for DSSC research

No	Metal Complexes	Remarks/Milestones
1.2.1	Grätzel first report on DSSCs <sup>42</sup>	Year of 1992
1.2.2	Grätzel review for Dye sensitised solar cell <sup>37</sup>	Year of 2003
1.2.3	N3 dye <sup>65</sup> 	PCE: 10% $J_{sc} = 17 \text{ mA/cm}^2$ $V_{oc} = 0.72 \text{ V}$ Electrolyte: I <sup>-</sup> /I <sub>3</sub> <sup>-</sup>
1.2.4	Black dye <sup>67</sup>	PCE: 10.4%, $J_{sc} = 20.5 \text{ mA/cm}^2$ $V_{oc} = 0.72 \text{ V}$ Electrolyte: I <sup>-</sup> /I <sub>3</sub> <sup>-</sup>

		
1.2.5	N719 dye <sup>66</sup> 	PCE: 11.18% $J_{sc} = 18.23 \text{ mA/cm}^2$ $V_{oc} = 0.86 \text{ V}$ Electrolyte: $\text{I}^-/\text{I}_3^-$
1.2.6	Highest certified efficiency for DSSC <sup>68</sup> 	PCE: 11.1% $J_{sc} = 20.9 \text{ mA/cm}^2$ $V_{oc} = 0.736 \text{ V}$ Electrolyte: $\text{I}^-/\text{I}_3^-$

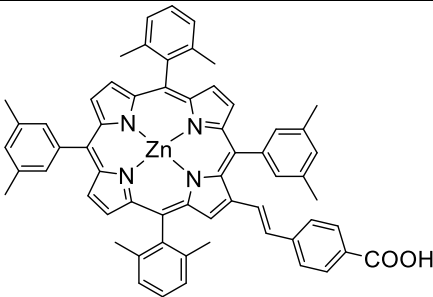
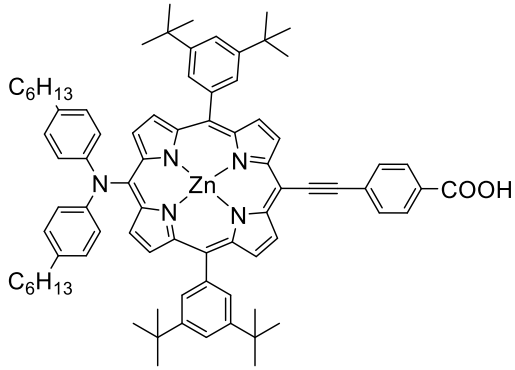
Grätzel was first reported N3 dye in 1993 and gave DSSC based solar cell that reached efficiency of 10%.<sup>65</sup> In addition, another type of N3 called black dye in which Ru-pyridyl complex consists of four carboxylic acid groups ( $-\text{COOH}$ ) that gave efficiency nearly 10.4%. The first N719 dye was studied and achieved at highest PCE of 11.18% and it was used as standard reference dye for DSSC device.<sup>66</sup> Until 2006, the Ru metal based complex, black dye was used and showed the best reported efficiency of 10.4%<sup>67</sup>. However, with optimised conditions and a certified efficiency of 11.1% was reported using high haze  $\text{TiO}_2$  electrode at 800 nm that was one of the best reported so far for any DSSC using a Ru metal based complex.<sup>68</sup> However, the use of

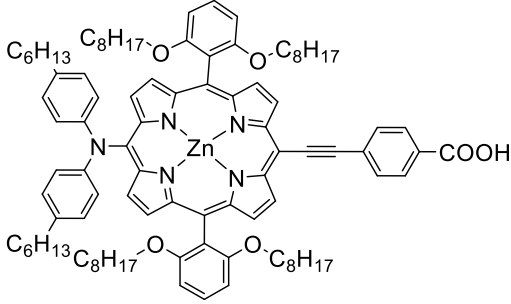
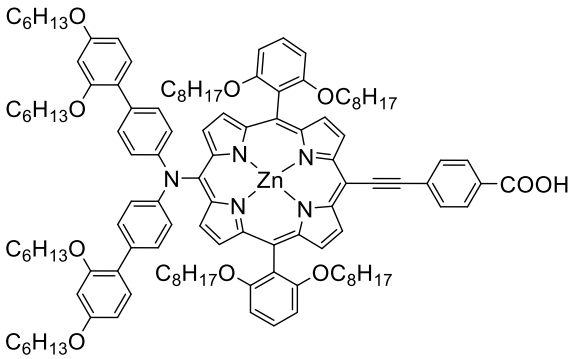
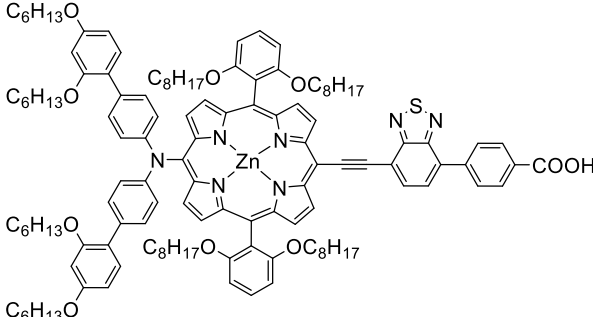
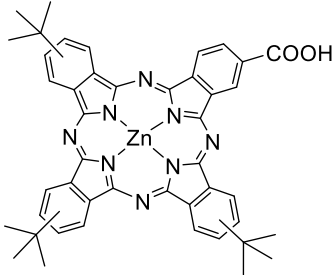
ruthenium metal based complex is undesirable owing to limited availability, cost of expensive, and environmental issues.<sup>69-73</sup>

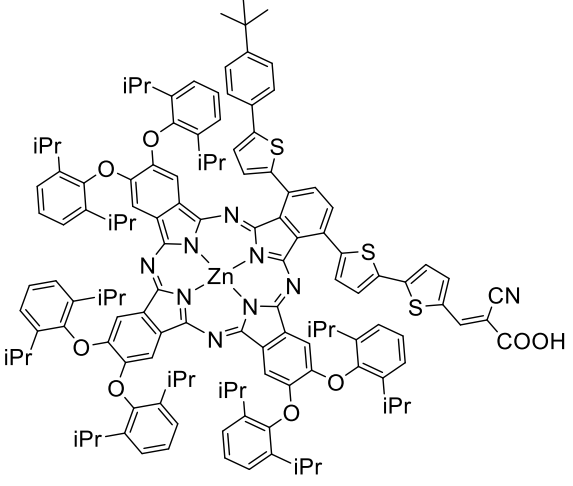
### 1.6.2 Porphyrin and Phthalocyanine Dyes

In general, porphyrin dyes are aromatic macrocyclic compound which existing intensely blue-green colour. In contrast to Ru complexes, porphyrin and phthalocyanine dyes showed an intense absorption in the 400-450 nm region as well as higher region in the 500-700 nm with good chemical, physical properties and thermal stability. The diamagnetic zinc based porphyrins dyes having carboxylic grafting groups is showed the best performance among the all the porphyrin and phthalocyanine<sup>34</sup> dyes in **Table 1.3**.

**Table 1.3** Initial literature reports and porphyrin and phthalocyanine based dyes for DSSC research.

Dye	Structure	PCE (%)
<b>D4</b> <sup>74</sup>		PCE: 4.8% $J_{sc} = 9.70 \text{ mA/cm}^2$ $V_{oc} = 0.66 \text{ V}$ Electrolyte: $\text{I}^-/\text{I}_3^-$
<b>YD-2</b> <sup>75</sup>		PCE: 5.6% $J_{sc} = 10.5 \text{ mA/cm}^2$ $V_{oc} = 0.75 \text{ V}$ Electrolyte: $\text{I}^-/\text{I}_3^-$

<b>YD-2-o- C8<sup>43</sup></b>		PCE: 11.9% $J_{sc} = 17.3 \text{ mA/cm}^2$ $V_{oc} = 0.96 \text{ V}$ Electrolyte: Co <sup>(II/III)</sup>
<b>SM371<sup>76</sup></b>		PCE: 12% $J_{sc} = 15.9 \text{ mA/cm}^2$ $V_{oc} = 0.96 \text{ V}$ Electrolyte: Co <sup>(II/III)</sup>
<b>SM315<sup>40</sup></b>		PCE: 13% $J_{sc} = 18.1 \text{ mA/cm}^2$ $V_{oc} = 0.91 \text{ V}$ Electrolyte: Co <sup>(II/III)</sup>
<b>TT1<sup>34</sup></b>		PCE: 3.2% $J_{sc} = 8.8 \text{ mA/cm}^2$ $V_{oc} = 0.55 \text{ V}$ Electrolyte: I <sup>-</sup> /I <sub>3</sub> <sup>-</sup>

$\alpha\text{PcS1}^{34}$		PCE: 5.5% $J_{sc} = 11.7 \text{ mA/cm}^2$ $V_{oc} = 0.61 \text{ V}$ Electrolyte: $\text{I}^-/\text{I}_3^-$
--------------------------	--	---

Nazeeruddin and co-workers used D- $\pi$ -A based D4 dye and gave overall efficiency of 4.8%.<sup>74</sup> But this class of dye having one problem that both the HOMO and LUMO are localised in the macrocycle, and it is not good for charge separation and it suppress the electron injection to the conduction band of semiconductor. To overcome this drawback along with aggregation of dyes, dye was designed and introduced the strong electron donors and acceptors with anchoring groups. Based on this idea **YD-2**,<sup>75</sup> its derivative YD-2-o-C8<sup>43</sup> as well as SM371<sup>76</sup> and its derivatives SM315 are one of the dyes used in the world record solar cell.

D-A- $\pi$ -A based SM315 dye showed an significant absorbance broadening features of Soret and Q-band compared to SM371, yielding improved light harvesting in both the green and red region of the spectrum. Recently, the panchromatic sensitizer SM315 achieved a record 13.0% PCE at full sun illumination without the requirement of a co-sensitizer.<sup>40</sup>

### 1.6.3 Metal-free organic Dyes

In general, metal-free organic dyes are alternatives option for the Ru based metal complexes. Because the structures of organic dyes are more diverse form that can be designed and synthesised without difficulty. In addition, without using any rare earth metal, research into this expanding field has mainly attracted on synthesising dyes, improving PCE ( $\eta$ ), cell lifetime, dye stability, concerning the cost and environment issues. The molar extinction coefficients of this class of dyes are normally higher than that of metal based Ru complexes, and made these dyes are very attractive for DSSC performance. In general, organic dyes are designed based on a donor-  $\pi$ - spacer-acceptor (D-  $\pi$  -A) and Donor-Acceptor- $\pi$ -Acceptor (D-A- $\pi$ -A) architecture. Upon photexcitation, the photoinduced excited electrons transfer from donor part to acceptor part

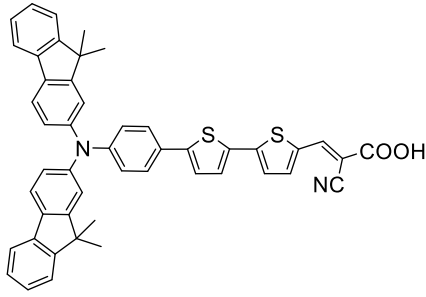
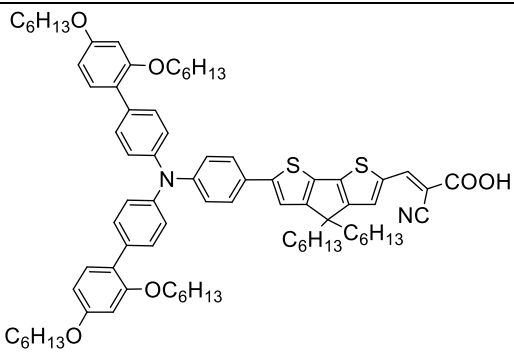
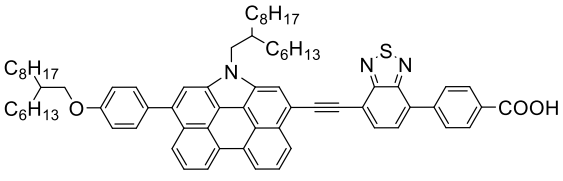


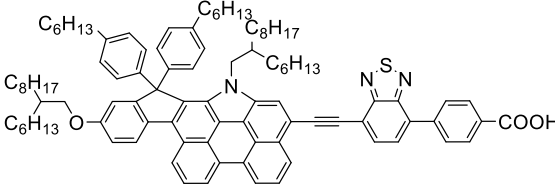
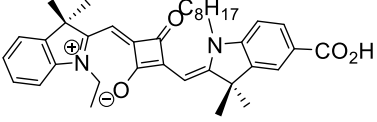
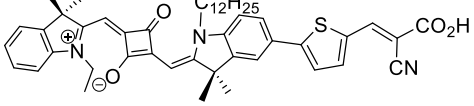
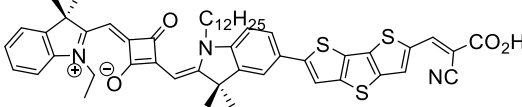
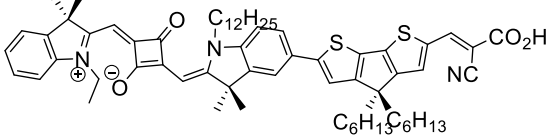
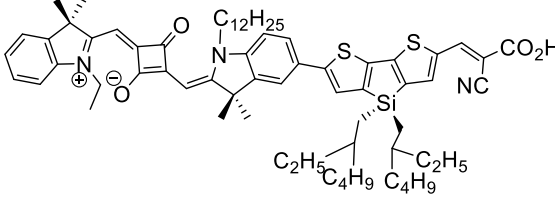
through the  $\pi$ -bridge towards conduction band of TiO<sub>2</sub> surface via electron accepting groups. Many essential efforts have been made to change the various parts of metal free organic dyes to optimize DSSC performance including coumarin dyes,<sup>77–81</sup> indoline dyes,<sup>82–86</sup> tetrahydroquinoline dyes,<sup>87–90</sup> triarylamine dyes,<sup>91–99</sup> heteroanthracene dyes,<sup>100–104</sup> carbazole dyes,<sup>73,105–108</sup> *N,N*-dialkylaniline dyes,<sup>93,109–111</sup> hemicyanine dyes,<sup>112–118</sup> merocyanine dyes,<sup>119–122</sup> squaraine dyes,<sup>123–130</sup> perylene dyes,<sup>131–134</sup> anthraquinone dyes,<sup>135</sup> oligothiophene dyes,<sup>136</sup> polymeric dyes,<sup>137–139</sup> and natural dyes<sup>140–142</sup> have been adopted to act as sensitizers for DSCs and have obtained impressive efficiencies.

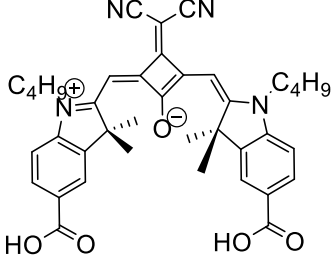
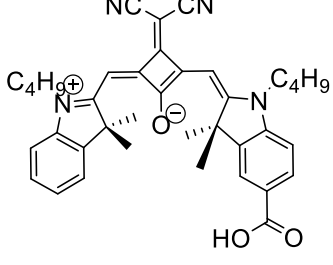
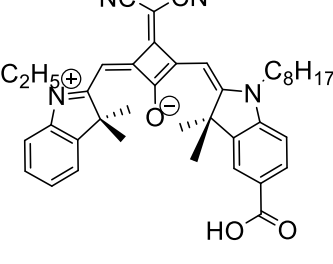
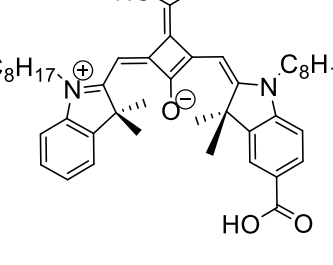
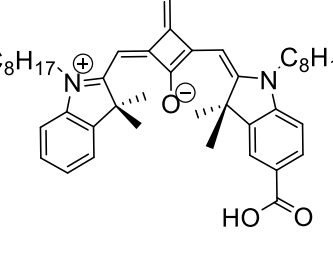
In general among the metal free organic dyes and squaraine chromophores that absorb in the red and NIR regions of the solar spectrum, besides squaraine dyes possess the transitions with high molar extinction coefficient in the far-red, and NIR regions ( $10^5 \text{ M}^{-1} \text{ cm}^{-1}$ ). These structures are very interesting for photovoltaic applications because they can harvest near-infrared (NIR) light and convert low-energy frequencies from solar irradiation. Further, squaraine dyes showing very intense and narrow absorption strongly in the NIR spectroscopic region.<sup>143</sup> Owing to their intense and narrow absorption in the NIR region, getting strong panchromatic incident-photon-to current conversion efficiencies (IPCEs) for such squaraine dyes are normally very difficult to achieve, thereby leading to PCEs of 3.9– 6.3%.<sup>144–147</sup> On the other hand, the efficient squaraine dye YR6 squaraine dye, which shows a PCE of 6.7%, and it exhibits a good IPCE response (>50%) in the range 450–700 nm,<sup>148</sup> and it is because of the presence of additional  $\pi$  bridge which gives extra higher-energy absorption features. Here, aggregation of dyes on the TiO<sub>2</sub> surface is one of the most important cause for suppressing the IPCE response of squaraine dyes.<sup>36,47</sup> But monomeric dye adsorption on the semiconductor metal oxide surface has efficient potential to improve the PCE of devices.<sup>36,120</sup> Further to improve IPCE response, di-*n*-hexyl- substituted cyclopentadithiophene (CPDT) bridge was introduced in place of thiophene bridge of YR6 dye to form JD10 which shows good  $J_{sc}$  and PCE of 7.3%.<sup>149</sup> In addition, the gem-dihexyl substituents suppressing the undesirable aggregation and disturb the any non-productive intermolecular charge transfer.<sup>150</sup> The use of a di-*n*-hexyl-substituted CPDT bridge in place of the thiophene bridge of YR6 is anticipated to significantly contribute to increasing the absorbance strength of high-energy bands, which may also provide a substantial increase in photocurrent.<sup>151</sup>

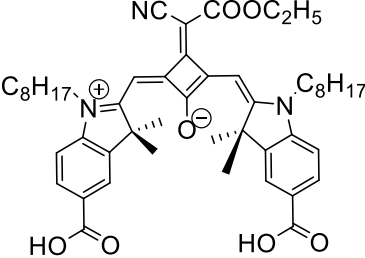
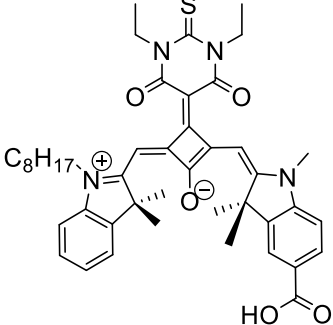
The effect of various  $\pi$ - bridges was studied which have high energy absorption bands corresponding to the NIR absorption of the squaraine to improve the panchromaticity and IPCE.<sup>149</sup> Ultimately to achieve those response, different  $\pi$  bridges were introduced covalently linked squaraine donor and acceptor such as, 4-hexyl-4H-dithieno[3,2-b:2',3'-d]pyrrole (DTP), dithieno[3,2-b:2',3'-d]thiophene (DTT), and 4,4-bis(2-ethylhexyl)-4Hsilolo[3,2-b:4,5-b']dithiophene (DTS). In addition DTS shows significantly contribute to increasing the absorbance strength of high-energy bands which provide significant photovoltaic performance and IPCE response and gives maximum efficiency of 8.9%.<sup>152</sup>

**Table 1.4** Initial literature reports and metal-free based organic dyes for DSSC research

Dye	Structure	PCE (%)
JK-2 <sup>154</sup>		PCE: 8.01% $J_{sc} = 14.2 \text{ mA/cm}^2$ $V_{oc} = 0.76 \text{ V}$ Electrolyte: $\text{I}^-/\text{I}_3^-$
YI23 <sup>155</sup>		PCE: 10% $J_{sc} = 13.06 \text{ mA/cm}^2$ $V_{oc} = 1.0 \text{ V}$ Electrolyte: $\text{Co}^{(II/III)}$
C272 <sup>156</sup>		PCE: 10% $J_{sc} = 15.92 \text{ mA/cm}^2$ $V_{oc} = 0.90 \text{ V}$ Electrolyte: $\text{Co}^{(II/III)}$

<b>C275</b> <sup>156</sup>		PCE: 12% $J_{sc} = 14.54 \text{ mA/cm}^2$ $V_{oc} = 0.92 \text{ V}$ Electrolyte: $\text{Co}^{(II/III)}$
<b>SQ01</b> <sup>129</sup>		PCE: 4.5% $J_{sc} = 10.5 \text{ mA/cm}^2$ $V_{oc} = 0.71 \text{ V}$ Electrolyte: $\text{I}^-/\text{I}_3^-$
<b>YR6</b> <sup>148</sup>		PCE: 6.7% $J_{sc} = 14.8 \text{ mA/cm}^2$ $V_{oc} = 0.71 \text{ V}$ Electrolyte: $\text{I}^-/\text{I}_3^-$
<b>DTT-CA</b> <sup>152</sup>		PCE: 5.8% $J_{sc} = 12.9 \text{ mA/cm}^2$ $V_{oc} = 0.64 \text{ V}$ Electrolyte: $\text{I}^-/\text{I}_3^-$
<b>JD10</b> <sup>149</sup>		PCE: 7.3% $J_{sc} = 16.4 \text{ mA/cm}^2$ $V_{oc} = 0.63 \text{ V}$ Electrolyte: $\text{I}^-/\text{I}_3^-$
<b>DTS-CA</b> <sup>152</sup>		PCE: 8.9% $J_{sc} = 19.1 \text{ mA/cm}^2$ $V_{oc} = 0.68 \text{ V}$ Electrolyte: $\text{I}^-/\text{I}_3^-$

<b>SQM1a</b> <sup>157</sup>		PCE: 3.6% $J_{sc} = 14.2 \text{ mA/cm}^2$ $V_{oc} = 0.50 \text{ V}$ Electrolyte: $\text{I}^-/\text{I}_3^-$
<b>SQM1b</b> <sup>157</sup>		PCE: 2.9% $J_{sc} = 10.3 \text{ mA/cm}^2$ $V_{oc} = 0.53 \text{ V}$ Electrolyte: $\text{I}^-/\text{I}_3^-$
<b>HSQ1</b> <sup>158</sup>		PCE: 4.1% $J_{sc} = 11.84 \text{ mA/cm}^2$ $V_{oc} = 0.55 \text{ V}$ Electrolyte: $\text{I}^-/\text{I}_3^-$
<b>HSQ2</b> <sup>159</sup>		PCE: 4.1% $J_{sc} = 11.55 \text{ mA/cm}^2$ $V_{oc} = 0.58 \text{ V}$ Electrolyte: $\text{I}^-/\text{I}_3^-$
<b>HSQ3</b> <sup>159</sup>		PCE: 4.6% $J_{sc} = 13.95 \text{ mA/cm}^2$ $V_{oc} = 0.58 \text{ V}$ Electrolyte: $\text{I}^-/\text{I}_3^-$

<b>HSQ4</b> <sup>159</sup>	 <p>The structure shows a central squaraine core with two N-phenyl rings. Each ring has an octyl chain (C<sub>8</sub>H<sub>17</sub>) and a carboxylic acid group (HO-C(=O)-). The central carbon of the squaraine is substituted with a cyano group (NC) and an ethyl ester group (COOC<sub>2</sub>H<sub>5</sub>).</p>	PCE:5.66% $J_{sc} = 15.61 \text{ mA/cm}^2$ $V_{oc} = 0.56 \text{ V}$ Electrolyte: I <sup>-</sup> /I <sub>3</sub> <sup>-</sup>
<b>HSQ5</b> <sup>147</sup>	 <p>The structure shows a central squaraine core with two N-phenyl rings. One ring has an octyl chain (C<sub>8</sub>H<sub>17</sub>) and a carboxylic acid group (HO-C(=O)-). The other ring has a methyl group. The central carbon of the squaraine is substituted with a thiobarbiturate group: -C(=O)-N(C<sub>2</sub>H<sub>5</sub>)<sub>2</sub>-C(=S)-N(C<sub>2</sub>H<sub>5</sub>)<sub>2</sub>-C(=O)-.</p>	PCE:4.7% $J_{sc} = 11.87 \text{ mA/cm}^2$ $V_{oc} = 0.57 \text{ V}$ Electrolyte: I <sup>-</sup> /I <sub>3</sub> <sup>-</sup>

Besides extending the conjugation by  $\pi$ -spacer, modification on the squaric unit has been also attempted to increase light harvesting efficiency of SQ dyes. Electron withdrawing barbiturate appended *cis*-configured squaraines dyes helped in extending the conjugation with better device efficiency than SQ1. Further design to improve the device performance with dicyano-, cyanoester derivatives and number of anchoring groups showed the cell efficiency up to 5.66% (**Table 1.4**).<sup>153</sup>

## 1.7 Challenges and Perspectives

### 1.7.1 Dye Aggregation on the Surface of Semiconductor Metal Oxide

Even though a lot of efforts have been made in the design strategies of organic dyes to enhance the efficiency, the overall DSSC performances are determined by some key factors such as the photo-excited state of the dyes, electronic overlapping between the LUMO and conduction band of the metal oxide semiconductor and more importantly the formation of dye aggregation. Most of the above concerns have been resolved by means of substitution of different donor/acceptor moieties. However controlling the aggregation of dyes on the TiO<sub>2</sub> surface is a challenging task.

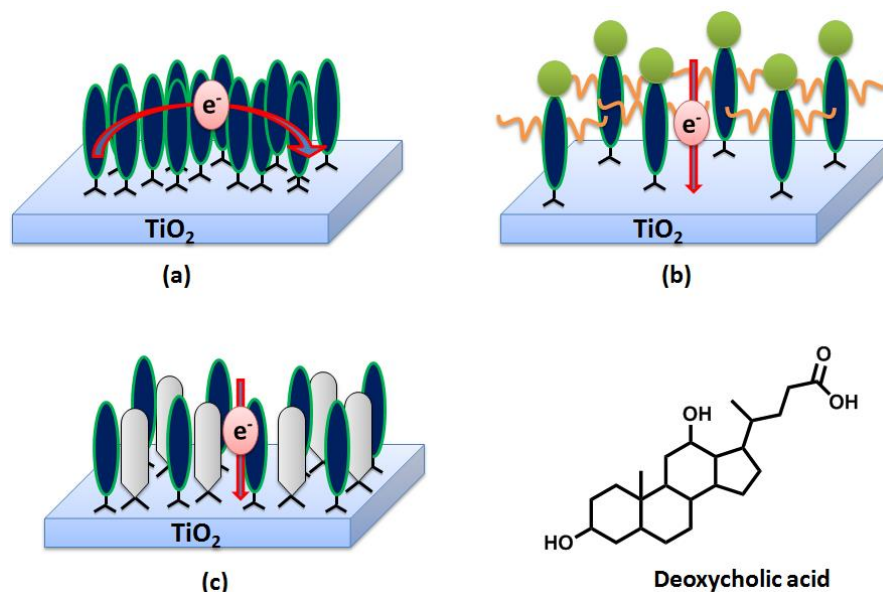


**Figure 1.4** Molecule arrangement of sensitizer on titanium dioxide film. (a)  $\pi$ -stacked dye molecules, (b) Alkyl chain for reducing the aggregation, (c) chenodeoxycholic acid to diminish the dye aggregation

In general metal free organic dyes have remarkable tendency towards the formation of aggregation when it adsorbs on the semiconductor surface due to the alignment of intrinsic molecular dipole. Such aggregated structure may have either blue shifted (H-aggregate) or red-shifted absorption (J-aggregate) with respect to that of the monomer. Intermolecular  $\pi$ - $\pi$  interaction of aggregated structures on  $\text{TiO}_2$  surface leads to varied DSSC device efficiency in **Figure 1.4**. Self-assembly of active layer components of this class of dyes on  $\text{TiO}_2$  surface hampers photovoltaic device performance due to the aggregation-induced self-quenching of photoexcited state has remained unexplored. There is one way to avoid aggregation using photoanode electrode has to adsorb in dye solutions containing coadsorbates such as chenodeoxycholic acid, which can help to control the self-assembly of dyes on the  $\text{TiO}_2$  surface or an efficient photovoltaic performance. In addition, the introduction of sterically hindered substituents (bulky groups), such as long alkyl chains and aromatic units, into dye structures should efficiently suppress dye aggregation owing to a disturbance in the intermolecular  $\pi$ - $\pi$  stacking.

### 1.7.2 Charge Recombination

The charge recombination is one of the significant factors involved at the TiO<sub>2</sub>-dye/electrolyte interface and it suppresses severely the photovoltaic device performance. In order to avoid this major drawback, a lot of effort has been dedicated to optimizing the molecular structure of these organic dyes, through controlling the self-assembling modes of the dyes and molecular dye orientation on the surface of TiO<sub>2</sub>. In addition, the introduction of bulky groups, long hydrophobic alkyl and alkoxy chains on the donor (D) moiety in **Figure 1.5**, which are effectively blocks the approach of hydrophilic I<sub>3</sub><sup>-</sup> ions to the TiO<sub>2</sub> surface. Further, it reduces the

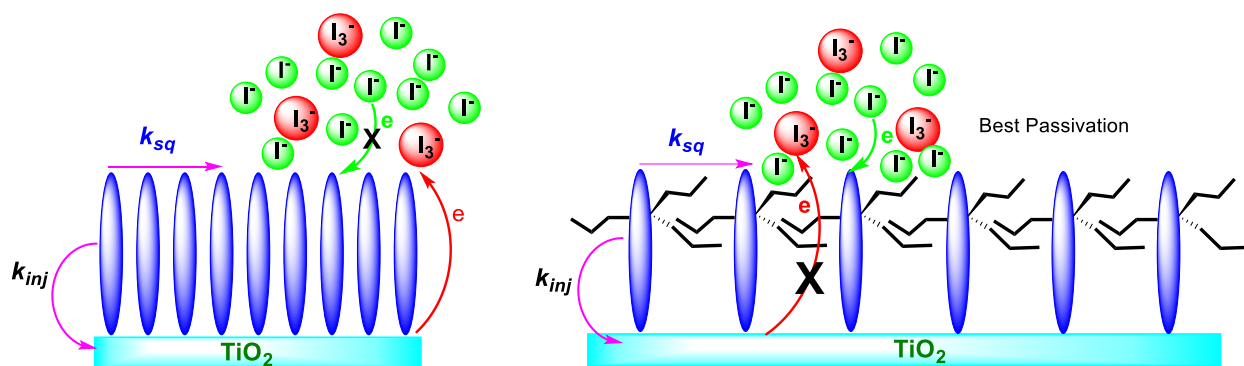


**Figure 1.5** Schematic diagrams for charge recombination process at TiO<sub>2</sub>-dye/electrolyte interface.

charge recombination, resulting an increase in the electron lifetime and  $V_{oc}$  value and also to decrease the self-assembly of dyes effectively for an efficient electron injection.

### 1.7.3 Position of Alky Groups and Importance on the Photovoltaic Cell

In general, alkyl groups have been introduced to control the packing of dyes on surface of semiconductor photoanode that can reduce the level of self-assembly of dyes besides increasing the photovoltaic parameter such as  $V_{oc}$  and  $J_{sc}$  to achieve high efficiency by avoiding the charge recombination. But there is a problem of facing that while introducing alkyl group in different position of organic dye systematically either near or far from the TiO<sub>2</sub> surface and it showed different kind of device performance. There were limited literature available related to the substitution of alkyl group in different position of organic dyes to get knowledge about the importance of position of alkyl group in the photovoltaic performance. It is essential to discuss the influence of alkyl groups in different position of organic dyes on arranging the conjugated backbone with respect to the surface of TiO<sub>2</sub>. Therefore, the strategies must be developed to deal with these factors and it is clear that many challenges still remain unanswered. In order to

understand the role alkyl group in different position of squaraine dyes in which the indoline unit is preferred to introduce in-plane and out-of plane alkyl groups through N- and  $sp^3$ -C atoms that are near or far away from the  $TiO_2$  surface which clearly explaining controlling the dye aggregation and the dye loading on the  $TiO_2$  surface, besides its photovoltaic performance.

#### 1.7.4 Optical Response towards Photovoltaic Cells

The spectrum is shown in **Figure 1.6** as the irradiance of the sun as a function of wavelength. Metal-free organic dyes were designed and synthesized to increase the intramolecular charge transfer and extend the absorption band from visible to NIR region, respectively. However, majority of these dyes were more efficiently involved in the visible region, but photocurrent response in the NIR region needed to be improved for better PCE due to the maximum short-circuit current ( $J_{sc}$ ) for a solar cell with an absorption onset of 800 nm is 26  $mA\ cm^{-2}$  in **Figure 1.6**. From the above information there are limited chromophores available that absorb in the NIR regions such as phthalocyanines, porphyrines, and polymethine dyes in which symmetric/unsymmetric squaraine dye structures with dicyano, cyanoester, and diethylthio barbiturate containing central squaraine units which help to extend the conjugation for panchromatic light absorption towards the NIR regions and then showing better photocurrent responses for better PCE.

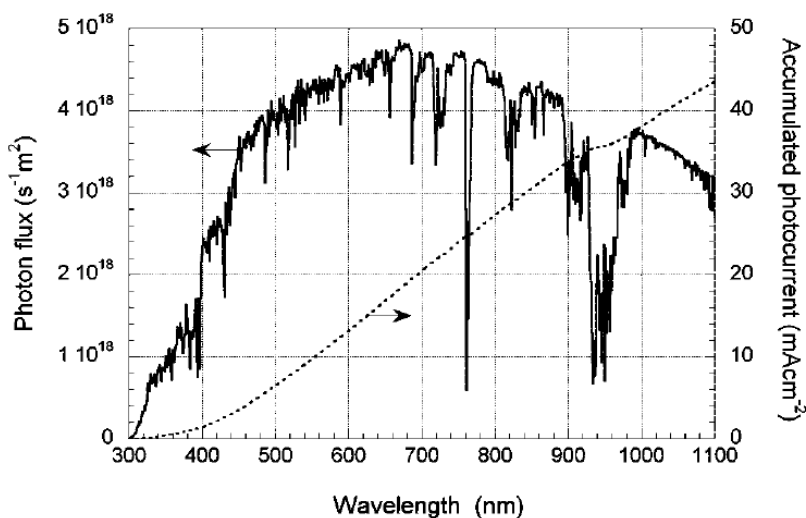


**Figure 1.6** Photon flux of the AM 1.5 G spectrum at  $1000\ W\ m^{-2}$  (ASTM G173-03), and calculated accumulated photocurrent.

#### 1.7.5 The Role of $\pi$ -bridges and Anchoring Groups on Solar Cell Performance



A series of unsymmetric squaraine-based dyes were prepared with various  $\pi$  spacer and anchoring group and studied in dye-sensitized solar cells in which the anchoring group was attached directly through  $\pi$  spacer with and without an ethynyl spacer. Most of the  $\pi$  spacer thiophene-based sensitizers YR6,<sup>148</sup> JD10<sup>149</sup> and DTS<sup>152</sup> provide photovoltaic performance from 6.74% to 8.9% than remaining ethynyl-spaced dyes in **Figure 1.7**.

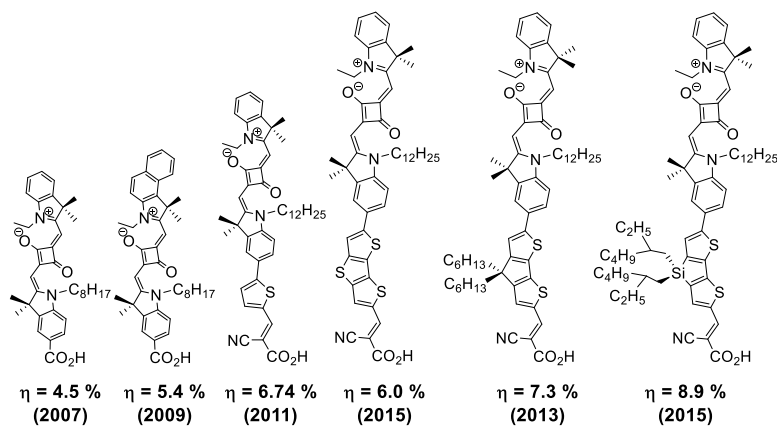


**Figure 1.7** Short summary of high-efficiency unsymmetric squaraine dyes for the DSSCs

Further, the thiophene-based dyes DTS dye are the most red shifted, with the onset of the IPCE curves extending 50 nm into the low energy region beyond the remaining dye. The role of  $\pi$ -spacer and anchoring group may tend to different molecular orientation on the TiO<sub>2</sub> surface. Due to the certain degree of curvature in the system, which may help in controlling the dye loading besides extending the conjugation in the NIR region and enhance visible absorption.

Finally this thesis work focused very important factors that has to be discussed and solved on squaraine based dye to enhance the better photovoltaic device performances such as,

- The importance of dye aggregation in charge injection at the aggregated dye-TiO<sub>2</sub> interface.
- Design and synthesis of more efficient panchromatic dyes by utilizing the benefit of steric, electronic and aggregation effects.
- By modulating the dye design and the orientation of dyes, the charge recombination can be controlled in dye sensitized solar cells (DSSC).

## 1.8 References

- (1) Lewis, N. S.; Nocera, D. G. Powering the Planet: Chemical Challenges in Solar Energy Utilization. *Proc. Natl. Acad. Sci.* **2006**, *103*, 15729–15735.
- (2) Metz, B.; Davidson, O. R.; Bosch, P. R.; Dave, R.; Meyer, L. A. Intergovernmental Panel on Climate Change. *Climate Change, 2007: Mitigation of Climate Change*; Cambridge University Press: Cambridge, United Kingdom and New York, NY, USA.
- (3) Eisenberg, R.; Nocera, D. G. Preface: Overview of the Forum on Solar and Renewable Energy. *Inorg. Chem.* **2005**, *44*, 6799–6801.
- (4) Yum, J.-H.; Baranoff, E.; Wenger, S.; Nazeeruddin, M. K.; Grätzel, M. Panchromatic Engineering for Dye-Sensitized Solar Cells. *Energy Environ. Sci.* **2011**, *4*, 842–857.
- (5) Schiermeier, Q.; Tollefson, J.; Scully, T.; Witze, A.; Morton, O. Energy Alternatives: Electricity without Carbon. *Nature* **2008**, *454*, 816–823.
- (6) Armaroli, N.; Balzani, V. The Future of Energy Supply: Challenges and Opportunities. *Angew. Chem. Int. Ed Engl.* **2007**, *46*, 52–66.
- (7) Barnham, K. W. J.; Mazzer, M.; Clive, B. Resolving the energy crisis: nuclear or photovoltaics? *Nature materials*, **2006**, *5*, 161–164.
- (8) Hoffmann, W.; Teske, S. Solar Generation - Solar Electricity for over One Billion People and Two Million Jobs by 2020, **2006**, Solar Generation Third Edition -2 ([www.greenpeace.org/sweden/Global/sweden/p2/klimat/report/2006/solar-generation-3rd-edition-2](http://www.greenpeace.org/sweden/Global/sweden/p2/klimat/report/2006/solar-generation-3rd-edition-2)).
- (9) Wolfgang P. Power for the World - The Emergence of Electricity from the Sun. World Council for Renewable Energy, Belgium (DOI: 10.4032/9789814303385).
- (10) Fritts, C. E. On a New Form of Selenium Cell, and Some Electrical Discoveries Made by Its Use. *Am. J. Sci.* **1883**, *26*, 465–472.
- (11) Chapin, D. M.; Fuller, C. S.; Pearson, G. L. A New Silicon P-n Junction Photocell for Converting Solar Radiation into Electrical Power. *J. Appl. Phys.* **1954**, *25*, 676–677.
- (12) Shockley, W.; Queisser, H. J. Detailed Balance Limit of Efficiency of P-n Junction Solar Cells. *J. Appl. Phys.* **1961**, *32*, 510–519.
- (13) Gratzel, M. Photovoltaic and Photoelectrochemical Conversion of Solar Energy. *Philos. Trans. R. Soc. Math. Phys. Eng. Sci.* **2007**, *365*, 993–1005.
- (14) Green, M. A. Consolidation of Thin-film Photovoltaic Technology: The Coming Decade of Opportunity. *Prog. Photovolt. Res. Appl.* **2006**, *14*, 383–392.

- 
- (15) Butler, D. Thin Films: Ready for Their Close-Up? *Nature* **2008**, *454*, 558–559.
- (16) Kim, M. R.; Ma, D. Quantum-Dot-Based Solar Cells: Recent Advances, Strategies, and Challenges. *J. Phys. Chem. Lett.* **2015**, *6*, 85–99.
- (17) Zhao, H.; Rosei, F. Colloidal Quantum Dots for Solar Technologies. *Chem* **2017**, *3*, 229–258.
- (18) Song, J. H.; Jeong, S. Colloidal Quantum Dot Based Solar Cells: From Materials to Devices. *Nano Converg.* **2017**, *4*, 21.
- (19) Jun, H. K.; Careem, M. A.; Arof, A. K. Quantum Dot-Sensitized Solar Cells—perspective and Recent Developments: A Review of Cd Chalcogenide Quantum Dots as Sensitizers. *Renew. Sustain. Energy Rev.* **2013**, *22*, 148–167.
- (20) Sogabe, T.; Shen, Q.; Yamaguchi, K. Recent Progress on Quantum Dot Solar Cells: A Review. *J. Photonics Energy* **2016**, *6*, 040901.
- (21) Mayer, A. C.; Scully, S. R.; Hardin, B. E.; Rowell, M. W.; McGehee, M. D. Polymer-Based Solar Cells. *Mater. Today* **2007**, *10*, 28–33.
- (22) Lu, L.; Zheng, T.; Wu, Q.; Schneider, A. M.; Zhao, D.; Yu, L. Recent Advances in Bulk Heterojunction Polymer Solar Cells. *Chem. Rev.* **2015**, *115*, 12666–12731.
- (23) Hau, S. K.; Yip, H. L.; Jen, A. K. Y. A Review on the Development of the Inverted Polymer Solar Cell Architecture. *Polym. Rev.* **2010**, *50*, 474–510.
- (24) Kang, H.; Lee, W.; Oh, J.; Kim, T.; Lee, C.; Kim, B. J. From Fullerene–Polymer to All-Polymer Solar Cells: The Importance of Molecular Packing, Orientation, and Morphology Control. *Acc. Chem. Res.* **2016**, *49*, 2424–2434.
- (25) Ahn, N.; Son, D. Y.; Jang, I.-H.; Kang, S. M.; Choi, M.; Park, N. G. Highly Reproducible Perovskite Solar Cells with Average Efficiency of 18.3% and Best Efficiency of 19.7% Fabricated via Lewis Base Adduct of Lead(II) Iodide. *J. Am. Chem. Soc.* **2015**, *137*, 8696–8699.
- (26) Yang, S.; Fu, W.; Zhang, Z.; Chen, H.; Li, C. Z. Recent Advances in Perovskite Solar Cells: Efficiency, Stability and Lead-Free Perovskite. *J. Mater. Chem. A* **2017**, *5*, 11462–11482.
- (27) Green, M. A.; Ho-Baillie, A. Perovskite Solar Cells: The Birth of a New Era in Photovoltaics. *ACS Energy Lett.* **2017**, *2*, 822–830.

- 
- (28) Asghar, M. I.; Zhang, J.; Wang, H.; Lund, P. D. Device Stability of Perovskite Solar Cells – A Review. *Renew. Sustain. Energy Rev.* **2017**, *77*, 131–146.
- (29) Ameri, T.; Dennler, G.; Lungenschmied, C.; Brabec, C. Organic Tandem Solar Cells: A Review. *Energy Environ. Sci.* **2009**, *2*, 347–363.
- (30) Huang, H.; Yang, L.; Sharma, B. Recent Advances in Organic Ternary Solar Cells. *J. Mater. Chem. A* **2017**, *5*, 11501–11517.
- (31) Gao, Y.; Jin, F.; Li, W.; Su, Z.; Chu, B.; Wang, J.; Zhao, H.; Wu, H.; Liu, C.; Hou, F.; et al. Highly Efficient Organic Tandem Solar Cell with a SubPc Interlayer Based on TAPC:C<sub>70</sub> Bulk Heterojunction. *Sci. Rep.* **2016**, *6*, 23916.
- (32) Petrozza, A.; Groves, C.; Snaith, H. J. Electron Transport and Recombination in Dye-Sensitized Mesoporous TiO<sub>2</sub> Probed by Photoinduced Charge-Conductivity Modulation Spectroscopy with Monte Carlo Modeling. *J. Am. Chem. Soc.* **2008**, *130*, 12912–12920.
- (33) Yeoh, M. -E.; Chan, K. -Y. Recent Advances in Photo-anode for Dye-sensitized Solar Cells: A Review. *Int. J. Energy Res.* **2017**, *41*, 2446–2467.
- (34) Brogdon, P.; Cheema, H.; Delcamp, J. H. Near-Infrared-Absorbing Metal-Free Organic, Porphyrin, and Phthalocyanine Sensitizers for Panchromatic Dye-Sensitized Solar Cells. *ChemSusChem* **2018**, *11*, 86–103.
- (35) Arjunan, T. V.; Senthil, T. S. Review: Dye Sensitised Solar Cells. *Mater. Technol.* **2013**, *28*, 9–14.
- (36) Hagfeldt, A.; Boschloo, G.; Sun, L.; Kloo, L.; Pettersson, H. Dye-Sensitized Solar Cells. *Chem. Rev.* **2010**, *110*, 6595–6663.
- (37) Grätzel, M. Dye-Sensitized Solar Cells. *J. Photochem. Photobiol. C Photochem. Rev.* **2003**, *4*, 145–153.
- (38) Gong, J.; Liang, J.; Sumathy, K. Review on Dye-Sensitized Solar Cells (DSSCs): Fundamental Concepts and Novel Materials. *Renew. Sustain. Energy Rev.* **2012**, *16*, 5848–5860.
- (39) Gong, J.; Sumathy, K.; Qiao, Q.; Zhou, Z. Review on Dye-Sensitized Solar Cells (DSSCs): Advanced Techniques and Research Trends. *Renew. Sustain. Energy Rev.* **2017**, *68*, 234–246.
- (40) Mathew, S.; Yella, A.; Gao, P.; Humphry-Baker, R.; Curchod, B. F. E.; Ashari-Astani, N.; Tavernelli, I.; Rothlisberger, U.; Nazeeruddin, M. K.; Grätzel, M. Dye-Sensitized Solar

- Cells with 13% Efficiency Achieved through the Molecular Engineering of Porphyrin Sensitizers. *Nat. Chem.* **2014**, *6*, 242–247.
- (41) Shen, S.; Jiang, P.; He, C.; Zhang, J.; Shen, P.; Zhang, Y.; Yi, Y.; Zhang, Z.; Li, Z.; Li, Y. Solution-Processable Organic Molecule Photovoltaic Materials with Bithienyl-Benzodithiophene Central Unit and Indenedione End Groups. *Chem. Mater.* **2013**, *25*, 2274–2281.
- (42) O'Regan, B.; Graetzel, M. A Low-Cost, High-Efficiency Solar Cell Based on Dye-Sensitized Colloidal TiO<sub>2</sub> Films. *Nature* **1991**, *353*, 737–740.
- (43) Yella, A.; Lee, H.-W.; Tsao, H. N.; Yi, C.; Chandiran, A. K.; Nazeeruddin, M. K.; Diau, E. W.-G.; Yeh, C.-Y.; Zakeeruddin, S. M.; Grätzel, M. Porphyrin-Sensitized Solar Cells with Cobalt (II/III)-Based Redox Electrolyte Exceed 12 Percent Efficiency. *Science* **2011**, *334*, 629–634.
- (44) Hardin, B. E.; Snaith, H. J.; McGehee, M. D. The Renaissance of Dye-Sensitized Solar Cells. *Nat. Photonics* **2012**, *6*, 162–169.
- (45) Ye, S.; Kathiravan, A.; Hayashi, H.; Tong, Y.; Infahsaeng, Y.; Chabera, P.; Pascher, T.; Yartsev, A. P.; Isoda, S.; Imahori, H.; et al. Role of Adsorption Structures of Zn-Porphyrin on TiO<sub>2</sub> in Dye-Sensitized Solar Cells Studied by Sum Frequency Generation Vibrational Spectroscopy and Ultrafast Spectroscopy. *J. Phys. Chem. C* **2013**, *117*, 6066–6080.
- (46) Snaith H. J.; Grätzel M. The Role of a “Schottky Barrier” at an Electron-Collection Electrode in Solid-State Dye-Sensitized Solar Cells. *Adv. Mater.* **2006**, *18* (14), 1910–1914.
- (47) Mishra, A.; Fischer, M. K. R.; Bäuerle, P. Metal-Free Organic Dyes for Dye-Sensitized Solar Cells: From Structure: Property Relationships to Design Rules. *Angew. Chem. Int. Ed.* **2009**, *48*, 2474–2499.
- (48) Matsumura, M.; Nomura, Y.; Tsubomura, H. Dye-Sensitization on the Photocurrent at Zinc Oxide Electrode in Aqueous Electrolyte Solution. *Bull. Chem. Soc. Jpn. - BULL CHEM SOC JPN* **1977**, *50*, 2533–2537.
- (49) V, N. A.; Beley, M.; Chartier, P.; Ern, V. Dye Sensitization of Ceramic Semiconducting Electrodes for Photoelectrochemical Conversion. *Rev. Phys. Appliquée* **1981**, *16* (1), 5–10.
- (50) Liu, D.; Fessenden, R. W.; Hug, G. L.; Kamat, P. V. Dye Capped Semiconductor Nanoclusters. Role of Back Electron Transfer in the Photosensitization of SnO<sub>2</sub> Nanocrystallites with Cresyl Violet Aggregates. *J. Phys. Chem. B* **1997**, *101*, 2583–2590.

- 
- (51) Peng, B.; Jungmann, G.; Jäger, C.; Haarer, D.; Schmidt, H.-W.; Thelakkat, M. Systematic Investigation of the Role of Compact TiO<sub>2</sub> Layer in Solid State Dye-Sensitized TiO<sub>2</sub> Solar Cells. *Coord. Chem. Rev.* **2004**, *248*, 1479–1489.
- (52) Fredin, K.; Nissfolk, J.; Boschloo, G.; Hagfeldt, A. The Influence of Cations on Charge Accumulation in Dye-Sensitized Solar Cells. *J. Electroanal. Chem.* **2007**, *609*, 55–60.
- (53) Pelet, S.; Moser, J.-E.; Grätzel, M. Cooperative Effect of Adsorbed Cations and Iodide on the Interception of Back Electron Transfer in the Dye Sensitization of Nanocrystalline TiO<sub>2</sub>. *J. Phys. Chem. B* **2000**, *104*, 1791–1795.
- (54) Wang, H.; Bell, J.; Desilvestro, J.; Bertoz, M.; Evans, G. Effect of Inorganic Iodides on Performance of Dye-Sensitized Solar Cells. *J. Phys. Chem. C* **2007**, *111*, 15125–15131.
- (55) Zhang Z.; Chen P.; Murakami T.N.; Zakeeruddin S.M.; Grätzel M. The 2,2,6,6-Tetramethyl-1-piperidinyloxy Radical: An Efficient, Iodine- Free Redox Mediator for Dye-Sensitized Solar Cells. *Adv. Funct. Mater.* **2008**, *18*, 341–346.
- (56) Sapp, S. A.; Elliott, C. M.; Contado, C.; Caramori, S.; Bignozzi, C. A. Substituted Polypyridine Complexes of Cobalt(II/III) as Efficient Electron-Transfer Mediators in Dye-Sensitized Solar Cells. *J. Am. Chem. Soc.* **2002**, *124*, 11215–11222.
- (57) Nusbaumer, H. N.; Zakeeruddin, S. M.; Moser, J. E.; Grätzel, M. An Alternative Efficient Redox Couple for the Dye-Sensitized Solar Cell System. *Chem. Eur. J.* **2003**, *9*, 3756–3763.
- (58) Wang, H.; Nicholson, P. G.; Peter, L.; Zakeeruddin, S. M.; Grätzel, M. Transport and Interfacial Transfer of Electrons in Dye-Sensitized Solar Cells Utilizing a Co(Dbbip)<sub>2</sub> Redox Shuttle. *J. Phys. Chem. C* **2010**, *114*, 14300–14306.
- (59) Cameron, P. J.; Peter, L. M.; Zakeeruddin, S. M.; Grätzel, M. Electrochemical Studies of the Co(III)/Co(II)(Dbbip)<sub>2</sub> Redox Couple as a Mediator for Dye-Sensitized Nanocrystalline Solar Cells. *Coord. Chem. Rev.* **2004**, *248*, 1447–1453.
- (60) Kay, A.; Grätzel, M. Low Cost Photovoltaic Modules Based on Dye Sensitized Nanocrystalline Titanium Dioxide and Carbon Powder. *Sol. Energy Mater. Sol. Cells* **1996**, *44*, 99–117.
- (61) Lindström, H.; Holmberg, A.; Magnusson, E.; Lindquist, S.-E.; Malmqvist, L.; Hagfeldt, A. A New Method for Manufacturing Nanostructured Electrodes on Plastic Substrates. *Nano Lett.* **2001**, *1*, 97–100.
-

- 
- (62) Imoto, K.; Takahashi, K.; Yamaguchi, T.; Komura, T.; Nakamura, J.; Murata, K. High-Performance Carbon Counter Electrode for Dye-Sensitized Solar Cells. *Sol. Energy Mater. Sol. Cells* **2003**, *79*, 459–469.
- (63) Murakami, T. N.; Ito, S.; Wang, Q.; Nazeeruddin, M. K.; Bessho, T.; Cesar, I.; Liska, P.; Humphry-Baker, R.; Comte, P.; Péchy, P.; et al. Highly Efficient Dye-Sensitized Solar Cells Based on Carbon Black Counter Electrodes. *J. Electrochem. Soc.* **2006**, *153*, A2255–A2261.
- (64) Pettersson, H.; Gruszecki, T.; Bernhard, R.; Häggman, L.; Gorlov, M.; Boschloo, G.; Edvinsson, T.; Kloo, L.; Hagfeldt, A. The Monolithic Multicell: A Tool for Testing Material Components in Dye-sensitized Solar Cells. *Prog. Photovolt. Res. Appl.* **2006**, *15*, 113–121.
- (65) Nazeeruddin, M. K.; Kay, A.; Rodicio, I.; Humphry-Baker, R.; Mueller, E.; Liska, P.; Vlachopoulos, N.; Graetzel, M. Conversion of Light to Electricity by *Cis*-X<sub>2</sub>bis(2,2'-Bipyridyl-4,4'-Dicarboxylate)Ruthenium(II) Charge-Transfer Sensitizers (X = Cl-, Br-, I-, CN-, and SCN-) on Nanocrystalline Titanium Dioxide Electrodes. *J. Am. Chem. Soc.* **1993**, *115*, 6382–6390.
- (66) Nazeeruddin, M. K.; De Angelis, F.; Fantacci, S.; Selloni, A.; Viscardi, G.; Liska, P.; Ito, S.; Takeru, B.; Grätzel, M. Combined Experimental and DFT-TDDFT Computational Study of Photoelectrochemical Cell Ruthenium Sensitizers. *J. Am. Chem. Soc.* **2005**, *127*, 16835–16847.
- (67) Nazeeruddin, M. K.; Péchy, P.; Renouard, T.; Zakeeruddin, S. M.; Humphry-Baker, R.; Comte, P.; Liska, P.; Cevey, L.; Costa, E.; Shklover, V.; et al. Engineering of Efficient Panchromatic Sensitizers for Nanocrystalline TiO<sub>2</sub>-Based Solar Cells. *J. Am. Chem. Soc.* **2001**, *123*, 1613–1624.
- (68) Chiba, Y.; Islam, A.; Watanabe, Y.; Komiya, R.; Koide, N.; Han, L. Dye-Sensitized Solar Cells with Conversion Efficiency of 11.1%. *Jpn. J. Appl. Phys.* **2006**, *45*, L638–L640.
- (69) Campbell, W. M.; Burrell, A. K.; Officer, D. L.; Jolley, K. W. Porphyrins as Light Harvesters in the Dye-Sensitised TiO<sub>2</sub> Solar Cell. *Coord. Chem. Rev.* **2004**, *248*, 1363–1379.
- (70) Campbell, W. M.; Jolley, K. W.; Wagner, P.; Wagner, K.; Walsh, P. J.; Gordon, K. C.; Schmidt-Mende, L.; Nazeeruddin, M. K.; Wang, Q.; Grätzel, M.; et al. Highly Efficient
-

- Porphyrin Sensitizers for Dye-Sensitized Solar Cells. *J. Phys. Chem. C* **2007**, *111*, 11760–11762.
- (71) Hara, K.; Kurashige, M.; Dan-oh, Y.; Kasada, C.; Shinpo, A.; Suga, S.; Sayama, K.; Arakawa, H. Design of New Coumarin Dyes Having Thiophene Moieties for Highly Efficient Organic-Dye-Sensitized Solar Cells. *New J. Chem.* **2003**, *27*, 783–785.
- (72) Ito S.; Zakeeruddin S. M.; Humphry-Baker R.; Liska P.; Charvet R.; Comte P.; Nazeeruddin M. K.; Péchy P.; Takata M.; Miura H.; et al. High-Efficiency Organic-Dye-Sensitized Solar Cells Controlled by Nanocrystalline-TiO<sub>2</sub> Electrode Thickness. *Adv. Mater.* **2006**, *18*, 1202–1205.
- (73) Koumura, N.; Wang, Z.-S.; Mori, S.; Miyashita, M.; Suzuki, E.; Hara, K. Alkyl-Functionalized Organic Dyes for Efficient Molecular Photovoltaics. *J. Am. Chem. Soc.* **2006**, *128*, 14256–14257.
- (74) Nazeeruddin, M. K.; Humphry-Baker, R.; Officer, D. L.; Campbell, W. M.; Burrell, A. K.; Grätzel, M. Application of Metalloporphyrins in Nanocrystalline Dye-Sensitized Solar Cells for Conversion of Sunlight into Electricity. *Langmuir* **2004**, *20*, 6514–6517.
- (75) Bessho, T.; Zakeeruddin, S. M.; Yeh, C.-Y.; Diau, E. W.-G.; Grätzel, M. Highly Efficient Mesoscopic Dye-Sensitized Solar Cells Based on Donor–Acceptor-Substituted Porphyrins. *Angew. Chem. Int. Ed.* **2010**, *49*, 6646–6649.
- (76) Gao, P.; Kim, Y. J.; Yum, J.-H.; Holcombe, T. W.; Nazeeruddin, M. K.; Grätzel, M. Facile Synthesis of a Bulky BPTPA Donor Group Suitable for Cobalt Electrolyte Based Dye Sensitized Solar Cells. *J. Mater. Chem. A* **2013**, *1*, 5535–5544.
- (77) Hara, K.; Wang, Z.-S.; Sato, T.; Furube, A.; Katoh, R.; Sugihara, H.; Dan-oh, Y.; Kasada, C.; Shinpo, A.; Suga, S. Oligothiophene-Containing Coumarin Dyes for Efficient Dye-Sensitized Solar Cells. *J. Phys. Chem. B* **2005**, *109*, 15476–15482.
- (78) Hara, K.; Sato, T.; Katoh, R.; Furube, A.; Ohga, Y.; Shinpo, A.; Suga, S.; Sayama, K.; Sugihara, H.; Arakawa, H. Molecular Design of Coumarin Dyes for Efficient Dye-Sensitized Solar Cells. *J. Phys. Chem. B* **2003**, *107*, 597–606.
- (79) Hara, K.; Sayama, K.; Ohga, Y.; Shinpo, A.; Suga, S.; Arakawa, H. A Coumarin-Derivative Dye Sensitized Nanocrystalline TiO<sub>2</sub> Solar Cell Having a High Solar-Energy Conversion Efficiency up to 5.6%. *Chem. Commun.* **2001**, *0*, 569–570.



- 
- (80) Wang Z. S.; Cui Y.; Hara K.; Dan-oh Y.; Kasada C.; Shinpo A. A High-Light-Harvesting-Efficiency Coumarin Dye for Stable Dye-Sensitized Solar Cells. *Adv. Mater.* **2007**, *19*, 1138–1141.
- (81) Wang, Z.-S.; Cui, Y.; Dan-oh, Y.; Kasada, C.; Shinpo, A.; Hara, K. Molecular Design of Coumarin Dyes for Stable and Efficient Organic Dye-Sensitized Solar Cells. *J. Phys. Chem. C* **2008**, *112*, 17011–17017.
- (82) Ito, S.; Miura, H.; Uchida, S.; Takata, M.; Sumioka, K.; Liska, P.; Comte, P.; Péchy, P.; Grätzel, M. High-Conversion-Efficiency Organic Dye-Sensitized Solar Cells with a Novel Indoline Dye. *Chem. Commun.* **2008**, *0*, 5194–5196.
- (83) Schmidt-Mende L.; Bach U.; Humphry-Baker R.; Horiuchi T.; Miura H.; Ito S.; Uchida S.; Grätzel M. Organic Dye for Highly Efficient Solid-State Dye-Sensitized Solar Cells. *Adv. Mater.* **2005**, *17*, 813–815.
- (84) Kuang, D.; Uchida, S.; Humphry-Baker, R.; Zakeeruddin, S. M.; Grätzel, M. Organic Dye-Sensitized Ionic Liquid Based Solar Cells: Remarkable Enhancement in Performance through Molecular Design of Indoline Sensitizers. *Angew. Chem. Int. Ed Engl.* **2008**, *47*, 1923–1927.
- (85) Dentani, T.; Kubota, Y.; Funabiki, K.; Jin, J.; Yoshida, T.; Minoura, H.; Miura, H.; Matsui, M. Novel Thiophene-Conjugated Indoline Dyes for Zinc Oxide Solar Cells. *New J. Chem.* **2009**, *33*, 93–101.
- (86) Liu, B.; Zhu, W.; Zhang, Q.; Wu, W.; Xu, M.; Ning, Z.; Xie, Y.; Tian, H. Conveniently Synthesized Isophoronedyes for High Efficiency Dye-Sensitized Solar Cells: Tuning Photovoltaic Performance by Structural Modification of Donor Group in Donor- $\pi$ -acceptor System. *Chem. Commun.* **2009**, *0*, 1766–1768.
- (87) Chen, R.; Yang, X.; Tian, H.; Sun, L. Tetrahydroquinoline Dyes with Different Spacers for Organic Dye-Sensitized Solar Cells. *J. Photochem. Photobiol. Chem.* **2007**, *189*, 295–300.
- (88) Chen, R.; Yang, X.; Tian, H.; Wang, X.; Hagfeldt, A.; Sun, L. Effect of Tetrahydroquinoline Dyes Structure on the Performance of Organic Dye-Sensitized Solar Cells. *Chem. Mater.* **2007**, *19*, 4007–4015.
- (89) Chen, R.; Zhao, G.; Yang, X.; Jiang, X.; Liu, J.; Tian, H.; Gao, Y.; Liu, X.; Han, K.; Sun, M.; et al. Photoinduced Intramolecular Charge-Transfer State in Thiophene- $\pi$ -Conjugated Donor-acceptor Molecules. *J. Mol. Struct.* **2008**, *876*, 102–109.
-

- 
- (90) Hao, Y.; Yang, X.; Cong, J.; Tian, H.; Hagfeldt, A.; Sun, L. Efficient near Infrared D- $\pi$ -A Sensitizers with Lateral Anchoring Group for Dye-Sensitized Solar Cells. *Chem. Commun.* **2009**, *0*, 4031–4033.
- (91) Zhang, G.; Bala, H.; Cheng, Y.; Shi, D.; Lv, X.; Yu, Q.; Wang, P. High Efficiency and Stable Dye-Sensitized Solar Cells with an Organic Chromophore Featuring a Binary  $\pi$ -Conjugated Spacer. *Chem. Commun.* **2009**, *0*, 2198–2200.
- (92) Marinado, T.; Hagberg, D. P.; Hedlund, M.; Edvinsson, T.; Johansson, E. M. J.; Boschloo, G.; Rensmo, H.; Brinck, T.; Sun, L.; Hagfeldt, A. Rhodanine Dyes for Dye-Sensitized Solar Cells: Spectroscopy, Energy Levels and Photovoltaic Performance. *Phys. Chem. Chem. Phys.* **2008**, *11*, 133–141.
- (93) Kitamura, T.; Ikeda, M.; Shigaki, K.; Inoue, T.; Anderson, N. A.; Ai, X.; Lian, T.; Yanagida, S. Phenyl-Conjugated Oligoene Sensitizers for TiO<sub>2</sub> Solar Cells. *Chem. Mater.* **2004**, *16*, 1806–1812.
- (94) Justin, T. K. R.; Hsu, Y. C.; Lin, J. T.; Lee, K. M.; Ho, K. C.; Lai, C. H.; Cheng, Y. M.; Chou, P.T. 2,3-Disubstituted Thiophene-Based Organic Dyes for Solar Cells. *Chem. Mater.* **2008**, *20*, 1830–1840.
- (95) Hagberg, D. P.; Edvinsson, T.; Marinado, T.; Boschloo, G.; Hagfeldt, A.; Sun, L. A Novel Organic Chromophore for Dye-Sensitized Nanostructured Solar Cells. *Chem. Commun.* **2006**, *0*, 2245–2247.
- (96) Tian Haining; Yang Xichuan; Pan Jingxi; Chen Ruikui; Liu Ming; Zhang Qingyu; Hagfeldt Anders; Sun Licheng. A Triphenylamine Dye Model for the Study of Intramolecular Energy Transfer and Charge Transfer in Dye-Sensitized Solar Cells. *Adv. Funct. Mater.* **2008**, *18*, 3461–3468.
- (97) Yum, J. H.; Hagberg, D. P.; Moon, S. J.; Karlsson, K. M.; Marinado, T.; Sun, L.; Hagfeldt, A.; Nazeeruddin, M. K.; Grätzel, M. A Light-Resistant Organic Sensitizer for Solar-Cell Applications. *Angew. Chem. Int. Ed Engl.* **2009**, *48*, 1576–1580.
- (98) Wang, M.; Xu, M.; Shi, D.; Li, R.; Gao, F.; Zhang, G.; Yi, Z.; Humphry, B. R.; Wang, P.; Zakeeruddin, S. M. High-Performance Liquid and Solid Dye-Sensitized Solar Cells Based on a Novel Metal-Free Organic Sensitizer. *Adv. Mater.* **2008**, *20*, 4460–4463.

- 
- (99) Nakazono, S.; Easwaramoorthi, S.; Kim, D.; Shinokubo, H.; Osuka, A. Synthesis of Arylated Perylene Bisimides through C–H Bond Cleavage under Ruthenium Catalysis. *Org. Lett.* **2009**, *11*, 5426–5429.
- (100) Mann, J. R.; Gannon, M. K.; Fitzgibbons, T. C.; Detty, M. R.; Watson, D. F. Optimizing the Photocurrent Efficiency of Dye-Sensitized Solar Cells through the Controlled Aggregation of Chalcogenoxanthylum Dyes on Nanocrystalline Titania Films. *J. Phys. Chem. C* **2008**, *112*, 13057–13061.
- (101) Zhou, G.; Pschirer, N.; Schöneboom, J. C.; Eickemeyer, F.; Baumgarten, M.; Müllen, K. Ladder-Type Pentaphenylene Dyes for Dye-Sensitized Solar Cells. *Chem. Mater.* **2008**, *20*, 1808–1815.
- (102) Hattori, S.; Ohkubo, K.; Urano, Y.; Sunahara, H.; Nagano, T.; Wada, Y.; Tkachenko, N. V.; Lemmetyinen, H.; Fukuzumi, S. Charge Separation in a Nonfluorescent Donor-Acceptor Dyad Derived from Boron Dipyrromethene Dye, Leading to Photocurrent Generation. *J. Phys. Chem. B* **2005**, *109*, 15368–15375.
- (103) Tian, H.; Yang, X.; Chen, R.; Pan, Y.; Li, L.; Hagfeldt, A.; Sun, L. Phenothiazine Derivatives for Efficient Organic Dye-Sensitized Solar Cells. *Chem. Commun.* **2007**, *0*, 3741–3743.
- (104) Tian, H.; Yang, X.; Chen, R.; Hagfeldt, A.; Sun, L. A Metal-Free “Black Dye” for Panchromatic Dye-Sensitized Solar Cells. *Energy Environ. Sci.* **2009**, *2*, 674–677.
- (105) Wang, Z. S.; Koumura, N.; Cui, Y.; Takahashi, M.; Sekiguchi, H.; Mori, A.; Kubo, T.; Furube, A.; Hara, K. Hexylthiophene-Functionalized Carbazole Dyes for Efficient Molecular Photovoltaics: Tuning of Solar-Cell Performance by Structural Modification. *Chem. Mater.* **2008**, *20*, 3993–4003.
- (106) Kim, D.; Lee, J. K.; Kang, S. O.; Ko, J. Molecular Engineering of Organic Dyes Containing N-Aryl Carbazole Moiety for Solar Cell. *Tetrahedron* **2007**, *63*, 1913–1922.
- (107) Ooyama, Y.; Shimada, Y.; Kagawa, Y.; Imae, I.; Harima, Y. Photovoltaic Performance of Dye-Sensitized Solar Cells Based on Donor–acceptor  $\pi$ -Conjugated Benzofuro[2,3-c]Oxazolo[4,5-a]Carbazole-Type Fluorescent Dyes with a Carboxyl Group at Different Positions of the Chromophore Skeleton. *Org. Biomol. Chem.* **2007**, *5*, 2046–2054.
- (108) Ooyama, Y.; Shimada, Y.; Ishii, A.; Ito, G.; Kagawa, Y.; Imae, I.; Komaguchi, K.; Harima, Y. Photovoltaic Performance of Dye-Sensitized Solar Cells Based on a Series of New-Type
-

- Donor–acceptor  $\pi$ -Conjugated Sensitizer, Benzofuro[2,3-c]Oxazolo[4,5-a]Carbazole Fluorescent Dyes. *J. Photochem. Photobiol. Chem.* **2009**, *203*, 177–185.
- (109) Hara, K.; Kurashige, M.; Ito, S.; Shinpo, A.; Suga, S.; Sayama, K.; Arakawa, H. Novel Polyene Dyes for Highly Efficient Dye-Sensitized Solar Cells. *Chem. Commun.* **2003**, *0*, 252–253.
- (110) Hara K.; Sato T.; Katoh R.; Furube A.; Yoshihara T.; Murai M.; Kurashige M.; Ito S.; Shinpo A.; Suga S.; et al. Novel Conjugated Organic Dyes for Efficient Dye-Sensitized Solar Cells. *Adv. Funct. Mater.* **2005**, *15*, 246–252.
- (111) Li, S. L.; Jiang, K. J.; Shao, K. F.; Yang, L. M. Novel Organic Dyes for Efficient Dye-Sensitized Solar Cells. *Chem. Commun. Camb. Engl.* **2006**, *26*, 2792–2794.
- (112) Wang, Z.; Huang, Y.; Huang, C.; Zheng, J.; Cheng, H.; Tian, S. Photosensitization of ITO and Nanocrystalline TiO<sub>2</sub> Electrode with a Hemicyanine Derivative. *Synth. Met.* **2000**, *114*, 201–207.
- (113) Wang, Z. S.; Li, F.Y.; Huang, C. H. Highly Efficient Sensitization of Nanocrystalline TiO<sub>2</sub> Films with Styryl Benzothiazolium Propylsulfonate. *Chem. Commun.* **2000**, *0*, 2063–2064.
- (114) Wang, Z. S.; Li, F.Y.; Huang, C. H.; Wang, L.; Wei, M.; Jin, L.-P.; Li, N.-Q. Photoelectric Conversion Properties of Nanocrystalline TiO<sub>2</sub> Electrodes Sensitized with Hemicyanine Derivatives. *J. Phys. Chem. B* **2000**, *104*, 9676–9682.
- (115) Wang, Z.-S.; Li, F.-Y.; Huang, C.-H. Photocurrent Enhancement of Hemicyanine Dyes Containing RSO<sub>3</sub>- Group through Treating TiO<sub>2</sub> Films with Hydrochloric Acid. *J. Phys. Chem. B* **2001**, *105*, 9210–9217.
- (116) Yao, Q.-H.; Meng, F.-S.; Li, F.-Y.; Tian, H.; Huang, C.-H. Photoelectric Conversion Properties of Four Novel Carboxylated Hemicyanine Dyes on TiO<sub>2</sub> Electrode. *J. Mater. Chem.* **2003**, *13*, 1048–1053.
- (117) Chen, Y.-S.; Li, C.; Zeng, Z.-H.; Wang, W.-B.; Wang, X.-S.; Zhang, B.-W. Efficient Electron Injection Due to a Special Adsorbing Group's Combination of Carboxyl and Hydroxyl: Dye-Sensitized Solar Cells Based on New Hemicyanine Dyes. *J. Mater. Chem.* **2005**, *15*, 1654–1661.
- (118) Stathatos, E.; Lianos, P.; Laschewsky, A.; Ouari, O.; Van, C. P. Synthesis of a Hemicyanine Dye Bearing Two Carboxylic Groups and Its Use as a Photosensitizer in Dye-Sensitized Photoelectrochemical Cells. *Chem. Mater.* **2001**, *13*, 3888–3892.

- (119) Khazraji, A. C.; Hotchandani, S.; Das, S.; Kamat, P. V. Controlling Dye (Merocyanine-540) Aggregation on Nanostructured TiO<sub>2</sub> Films. An Organized Assembly Approach for Enhancing the Efficiency of Photosensitization. *J. Phys. Chem. B* **1999**, *103*, 4693–4700.
- (120) Sayama, K.; Hara, K.; Mori, N.; Satsuki, M.; Suga, S.; Tsukagoshi, S.; Abe, Y.; Sugihara, H.; Arakawa, H. Photosensitization of a Porous TiO<sub>2</sub> Electrode with Merocyanine Dyes Containing a Carboxyl Group and a Long Alkyl Chain. *Chem. Commun.* **2000**, *0*, 1173–1174.
- (121) Sayama, K.; Tsukagoshi, S.; Hara, K.; Ohga, Y.; Shinpou, A.; Abe, Y.; Suga, S.; Arakawa, H. Photoelectrochemical Properties of J Aggregates of Benzothiazole Merocyanine Dyes on a Nanostructured TiO<sub>2</sub> Film. *J. Phys. Chem. B* **2002**, *106*, 1363–1371.
- (122) Sayama, K.; Tsukagoshi, S.; Mori, T.; Hara, K.; Ohga, Y.; Shinpou, A.; Abe, Y.; Suga, S.; Arakawa, H. Efficient Sensitization of Nanocrystalline TiO<sub>2</sub> Films with Cyanine and Merocyanine Organic Dyes. *Sol. Energy Mater. Sol. Cells* **2003**, *80*, 47–71.
- (123) Zhao, W.; Jun Hou, Y.; Song Wang, X.; Wen Zhang, B.; Cao, Y.; Yang, R.; Bo Wang, W.; Rui Xiao, X. Study on Squarylium Cyanine Dyes for Photoelectric Conversion. *Sol. Energy Mater. Sol. Cells* **1999**, *58*, 173–183.
- (124) Alex, S.; Santhosh, U.; Das, S. Dye Sensitization of Nanocrystalline TiO<sub>2</sub>: Enhanced Efficiency of Unsymmetrical versus Symmetrical Squaraine Dyes. *J. Photochem. Photobiol. Chem.* **2005**, *172*, 63–71.
- (125) Chen, Y.; Zeng, Z.; Li, C.; Wang, W.; Wang, X.; Zhang, B. Highly Efficient Co-Sensitization of Nanocrystalline TiO<sub>2</sub> Electrodes with Plural Organic Dyes. *New J. Chem.* **2005**, *29*, 773–776.
- (126) Li, C.; Wang, W.; Wang, X.; Zhang, B.; Cao, Y. Molecular Design of Squaraine Dyes for Efficient Far-Red and Near-IR Sensitization of Solar Cells. *Chem. Lett.* **2005**, *34*, 554–555.
- (127) Burke, A.; Schmidt, M. L.; Ito, S.; Grätzel, M. A Novel Blue Dye for Near-IR ‘Dye-Sensitised’ Solar Cell Applications. *Chem. Commun.* **2007**, *0*, 234–236.
- (128) Tatay, S.; Haque, S. A.; O’Regan, B.; Durrant, J. R.; Verhees, W. J. H.; Kroon, J. M.; Vidal-Ferran, A.; Gaviña, P.; Palomares, E. Kinetic Competition in Liquid Electrolyte and Solid-State Cyanine Dye Sensitized Solar Cells. *J. Mater. Chem.* **2007**, *17*, 3037–3044.

- (129) Yum, J. H.; Walter, P.; Huber, S.; Rentsch, D.; Geiger, T.; Nüesch, F.; De Angelis, F.; Grätzel, M.; Nazeeruddin, M. K. Efficient Far Red Sensitization of Nanocrystalline TiO<sub>2</sub> Films by an Unsymmetrical Squaraine Dye. *J. Am. Chem. Soc.* **2007**, *129*, 10320–10321.
- (130) Burke, A.; Ito, S.; Snaith, H.; Bach, U.; Kwiatkowski, J.; Grätzel, M. The Function of a TiO<sub>2</sub> Compact Layer in Dye-Sensitized Solar Cells Incorporating “Planar” Organic Dyes. *Nano Lett.* **2008**, *8*, 977–981.
- (131) Edvinsson, T.; Li, C.; Pschirer, N.; Schöneboom, J.; Eickemeyer, F.; Sens, R.; Boschloo, G.; Herrmann, A.; Müllen, K.; Hagfeldt, A. Intramolecular Charge-Transfer Tuning of Perylenes: Spectroscopic Features and Performance in Dye-Sensitized Solar Cells. *J. Phys. Chem. C* **2007**, *111*, 15137–15140.
- (132) Zafer, C.; Kus, M.; Turkmen, G.; Dincalp, H.; Demic, S.; Kuban, B.; Teoman, Y.; Icli, S. New Perylene Derivative Dyes for Dye-Sensitized Solar Cells. *Sol. Energy Mater. Sol. Cells* **2007**, *91*, 427–431.
- (133) Jin, Y.; Hua, J.; Wu, W.; Ma, X.; Meng, F. Synthesis, Characterization and Photovoltaic Properties of Two Novel near-Infrared Absorbing Perylene Dyes Containing Benzo[e]Indole for Dye-Sensitized Solar Cells. *Synth. Met.* **2008**, *158*, 64–71.
- (134) Li, C.; Yum, J. -H.; Moon, S. -J.; Herrmann, A.; Eickemeyer, F.; Pschirer, N. G.; Erk, P.; Schöneboom, J.; Müllen, K.; Grätzel, M. An Improved Perylene Sensitizer for Solar Cell Applications. *ChemSusChem* **2008**, *1*, 615–618.
- (135) Li, C.; Yang, X.; Chen, R.; Pan, J.; Tian, H.; Zhu, H.; Wang, X.; Hagfeldt, A.; Sun, L. Anthraquinone Dyes as Photosensitizers for Dye-Sensitized Solar Cells. *Sol. Energy Mater. Sol. Cells* **2007**, *91*, 1863–1871.
- (136) Tanaka, K.; Takimiya, K.; Otsubo, T.; Kawabuchi, K.; Kajihara, S.; Harima, Y. Development and Photovoltaic Performance of Oligothiophene-Sensitized TiO<sub>2</sub> Solar Cells. *Chem. Lett.* **2006**, *35*, 592–593.
- (137) Hao, Y.; Yang, M.; Yu, C.; Cai, S.; Liu, M.; Fan, L.; Li, Y. Photoelectrochemical Studies on Acid-Doped Polyaniline as Sensitizer for TiO<sub>2</sub> Nanoporous Film. *Sol. Energy Mater. Sol. Cells* **1998**, *56*, 75–84.
- (138) Mwaura, J. K.; Zhao, X.; Jiang, H.; Schanze, K. S.; Reynolds, J. R. Spectral Broadening in Nanocrystalline TiO<sub>2</sub> Solar Cells Based on Poly(p-Phenylene Ethynylene) and Polythiophene Sensitizers. *Chem. Mater.* **2006**, *18*, 6109–6111.

- (139) Liu, X.; Zhu, R.; Zhang, Y.; Liu, B.; Ramakrishna, S. Anionic Benzothiadiazole Containing Polyfluorene and Oligofluorene as Organic Sensitizers for Dye-Sensitized Solar Cells. *Chem. Commun.* **2008**, *0*, 3789–3791.
- (140) Garcia, C. G.; Polo, A. S.; Murakami Iha, N. Y. Fruit Extracts and Ruthenium Polypyridinic Dyes for Sensitization of TiO<sub>2</sub> in Photoelectrochemical Solar Cells. *J. Photochem. Photobiol. Chem.* **2003**, *160*, 87–91.
- (141) Yamazaki, E.; Murayama, M.; Nishikawa, N.; Hashimoto, N.; Shoyama, M.; Kurita, O. Utilization of Natural Carotenoids as Photosensitizers for Dye-Sensitized Solar Cells. *Sol. Energy* **2007**, *81*, 512–516.
- (142) Meng, S.; Ren, J.; Kaxiras, E. Natural Dyes Adsorbed on TiO<sub>2</sub> Nanowire for Photovoltaic Applications: Enhanced Light Absorption and Ultrafast Electron Injection. *Nano Lett.* **2008**, *8*, 3266–3272.
- (143) Beverina Luca; Salice Patrizio. Squaraine Compounds: Tailored Design and Synthesis towards a Variety of Material Science Applications. *Eur. J. Org. Chem.* **2010**, *2010*, 1207–1225.
- (144) Warnan, J.; Buchet, F.; Pellegrin, Y.; Blart, E.; Odobel, F. Panchromatic Trichromophoric Sensitizer for Dye-Sensitized Solar Cells Using Antenna Effect. *Org. Lett.* **2011**, *13*, 3944–3947.
- (145) Paek, S.; Choi, H.; Kim, C.; Cho, N.; So, S.; Song, K.; K. Nazeeruddin, M.; Ko, J. Efficient and Stable Panchromatic Squaraine Dyes for Dye -Sensitized Solar Cells. *Chem. Commun.* **2011**, *47*, 2874–2876.
- (146) Geiger, T.; Kuster, S.; Yum, J. H.; Moon, S. J.; Nazeeruddin, M. K.; Grätzel, M.; Nüesch, F. Molecular Design of Unsymmetrical Squaraine Dyes for High Efficiency Conversion of Low Energy Photons into Electrons Using TiO<sub>2</sub> Nanocrystalline Films. *Adv. Funct. Mater.* **2009**, *19*, 2720–2727.
- (147) Beverina, L.; Ruffo, R.; Mari, C. M.; Pagani, G. A.; Sassi, M.; De, A. F.; Fantacci, S.; Yum, J. H.; Grätzel, M.; Nazeeruddin, M. K. Panchromatic Cross-Substituted Squaraines for Dye-Sensitized Solar Cell Applications. *ChemSusChem* **2009**, *2*, 621–624.
- (148) Shi, Y.; Hill, R. B. M.; Yum, J. H.; Dualeh, A.; Barlow, S.; Grätzel, M.; Marder, S. R.; Nazeeruddin, M. K. A High-Efficiency Panchromatic Squaraine Sensitizer for Dye-Sensitized Solar Cells. *Angew. Chem.* **2011**, *123*, 6749–6751.

- (149) Delcamp, J. H.; Shi, Y.; Yum, J. H.; Sajoto, T.; Dell, O. E.; Barlow, S.; Nazeeruddin, M. K.; Marder Seth R.; Grätzel, M. The Role of  $\pi$  Bridges in High-Efficiency DSCs Based on Unsymmetrical Squaraines. *Chem. Eur. J.* **2012**, *19*, 1819–1827.
- (150) Pastore, M.; De Angelis, F. Aggregation of Organic Dyes on TiO<sub>2</sub> in Dye-Sensitized Solar Cells Models: An Ab Initio Investigation. *ACS Nano* **2010**, *4*, 556–562.
- (151) Li, J. Y.; Chen, C. Y.; Lee, C. P.; Chen, S. C.; Lin, T. H.; Tsai, H. H.; Ho, K. C.; Wu, C. G. Unsymmetrical Squaraines Incorporating the Thiophene Unit for Panchromatic Dye-Sensitized Solar Cells. *Org. Lett.* **2010**, *12*, 5454–5457.
- (152) Jradi, F. M.; Kang, X.; O’Neil, D.; Pajares, G.; Getmanenko, Y. A.; Szymanski, P.; Parker, T. C.; El-Sayed, M. A.; Marder, S. R. Near-Infrared Asymmetrical Squaraine Sensitizers for Highly Efficient Dye Sensitized Solar Cells: The Effect of  $\pi$ -Bridges and Anchoring Groups on Solar Cell Performance. *Chem. Mater.* **2015**, *27*, 2480–2487.
- (153) Saccone, D.; Galliano, S.; Barbero, N.; Quagliotto, P.; Viscardi, G.; Barolo, C. Polymethine Dyes in Hybrid Photovoltaics: Structure–Properties Relationships. *Eur. J. Org. Chem.* **2016**, *2016*, 2244–2259.
- (154) Kim, S.; Lee, J. K.; Kang, S. O.; Ko, J.; Yum, J.-H.; Fantacci, S.; De Angelis, F.; Di Censo, D.; Nazeeruddin, M. K.; Grätzel, M. Molecular Engineering of Organic Sensitizers for Solar Cell Applications. *J. Am. Chem. Soc.* **2006**, *128*, 16701–16707.
- (155) Yum, J. H.; Baranoff, E.; Kessler, F.; Moehl, T.; Ahmad, S.; Bessho, T.; Marchioro, A.; Ghadiri, E.; Moser, J.-E.; Yi, C.; et al. A Cobalt Complex Redox Shuttle for Dye-Sensitized Solar Cells with High Open-Circuit Potentials. *Nat. Commun.* **2012**, *3*, 631.
- (156) Yao, Z.; Zhang, M.; Wu, H.; Yang, L.; Li, R.; Wang, P. Donor/Acceptor Indenoperylene Dye for Highly Efficient Organic Dye-Sensitized Solar Cells. *J. Am. Chem. Soc.* **2015**, *137*, 3799–3802.
- (157) Maeda, T.; Mineta, S.; Fujiwara, H.; Nakao, H.; Yagi, S.; Nakazumi, H. Conformational Effect of Symmetrical Squaraine Dyes on the Performance of Dye-Sensitized Solar Cells. *J. Mater. Chem. A* **2012**, *1*, 1303–1309.
- (158) Qin, C.; Numata, Y.; Zhang, S.; Islam, A.; Yang, X.; Sodeyama, K.; Tateyama, Y.; Han, L. A Near-Infrared *Cis*-configured Squaraine Co-Sensitizer for High-Efficiency Dye-Sensitized Solar Cells. *Adv. Funct. Mater.* **2013**, *23*, 3782–3789.



- (159) Qin, C.; Numata, Y.; Zhang, S.; Yang, X.; Islam, A.; Zhang, K.; Chen, H.; Han, L. Novel Near-Infrared Squaraine Sensitizers for Stable and Efficient Dye-Sensitized Solar Cells. *Adv. Funct. Mater.* **2014**, *24*, 3059–3066.

## Chapter 2

**Interplay Between  $\pi$ -Bridge and Position of Branched-Alkyl Groups of Unsymmetrical D-A-D- $\pi$ -A Squaraine in Dye-Sensitized Solar Cells: Mode of Dye Anchoring and Charge Transfer Process at TiO<sub>2</sub>-dye/Electrolyte Interface**

Punitharasu, V.; Kavungathodi, M. F. M.; Nithyanandhan, J. *ACS Appl. Mater. Interfaces* **2017**, *9*, 32698–32712.

## 2.1 Introduction

Photovoltaics (PV) are emerging as a viable renewable energy technology, as an alternative to conventional fuel. Dye sensitized solar cell is one of the most important photovoltaic technology that has been attracted much attention and extended into the possibility of inexpensive and efficient solar energy conversion. In 1991 O'Regan and Grätzel published the first remarkable report which led more efficient mesoscopic DSSCs towards consistent and potential photovoltaic technology with PCE more than 10%.<sup>1-3</sup> There are few important key components pushed in-depth research like molecular sensitizers, n-type semiconductors, redox couples and cathode materials which showed the importance in chemistry and suitable interfaces of these functional materials.<sup>4-10</sup> On the other hand, sensitizers are significant part of DSSC due to the photoinduced charge separation takes place at the TiO<sub>2</sub>-dye/electrolyte interface.<sup>11-12</sup> The structure-property relationships of sensitizing chromophore were studied and employed its relevance in further improvement of dye cell's PCE.<sup>13</sup> The panchromatic structures of ruthenium based complex were demonstrated a significant improvement in efficiency from 7.12% for homoleptic dye to 11.8% for heteroleptic dye.<sup>14-16</sup> Molecularly engineered zinc based porphyrin dye, SM315, which replaced structure of YD2-*o*-C8 donor- $\pi$ -acceptor (D- $\pi$ -A) dye with PCE of 11.9%, showed a record of PCE of 13% under 1 sun illumination using cobalt redox couple.<sup>17-18</sup> However, difficulty in synthesis, expensive transition metal precursors, and moderate molar extinction coefficient of metallated dyes which found a more consistent way of tuning the spectral properties of sensitizers using metal-free organic systems.<sup>19-21</sup>

Recently, the literature survey of metal-free organic dyes, were reported and showed significant PCE more than 10% using either single dye or co-sensitization of multiple dyes.<sup>5</sup> Triarylamine based D- $\pi$ -A and D-A- $\pi$ -A dyes exhibited new insight into the effect of electronic and steric factors on light harvesting and interfacial process.<sup>13</sup> Recently, indenepeylene based D-A- $\pi$ -A dyes (C257) showed PCE of 11.5% using cobalt redox electrolyte under 1 sun irradiation.<sup>22</sup> When comparing the optical and photovoltaic properties of NIR active squaraines, their high molar extinction coefficient of NIR region and good performance of PCE using I<sup>-</sup>/I<sub>3</sub><sup>-</sup> redox electrolyte of the later which attracts them like an significant molecular structure in dye cell.<sup>23-24</sup> NIR light-harvesting polymethine dyes such as squaraines, and cyanines have been recently studied without compromising device cell performances.<sup>25-26</sup> In general squaraine dyes showed high photovoltaic performance compared to other polymethine dyes and their

unsymmetrical  $\pi$ -framework favors unidirectional charge injection which is due to the strong coupling between lowest unoccupied molecular orbitals (LUMO) of dye with TiO<sub>2</sub> conduction band edge ( $E_{CB}$ ) through carboxylic acid anchoring group.<sup>27</sup> After chemisorption of squaraine dyes on the TiO<sub>2</sub> surface which exhibited strong intramolecular charge transfer (ICT) towards NIR region besides broadening of absorption spectrum renders them as important class of sensitizers.<sup>28</sup> The solar cell efficiency of polymethine dyes govern many parameters apart from photophysical and electrochemical properties. Self-assembly and orientation of dyes on TiO<sub>2</sub> surface plays very important role in achieving the high efficiency device cells.<sup>29-30</sup> The orientation of dyes on TiO<sub>2</sub> surface were controlled by changing length, position of in-plane and out-of-plane hydrophobic functionalities; type, number and position of anchoring groups; dipping solvent, co-adsorbents and co-sensitizer were studied in the literature.<sup>31-42</sup> Unsymmetrical squaraine structure of silalodithiophene  $\pi$ -spacer having out-of-plane branched alkyl groups showed a PCE of 8.9% implying both electronic and steric effects.<sup>43</sup> In-plane and out-of-plane branched alkyl group on sp<sup>3</sup>-C and N-alkyl position in D-A-D dyes were showed a PCE of 9.1% for top-alkylated SQ5 is also recently reported.<sup>44</sup> Extending the length of branched alkyl groups away from anchoring group which helps the orientation of dyes with controlled aggregate formation upon chemisorption that can passivate TiO<sub>2</sub> surface besides broadening the absorption spectrum to enhance  $J_{sc}$  and  $V_{oc}$ .<sup>42,45</sup> When comparing the relative orientation of para, meta, and *ortho* carboxyphenyl functionalized porphyrin dyes adsorbed on TiO<sub>2</sub> surface, the more parallel orientation of *meta*- and *para*- showed more than *ortho*- dyes to the surface are attained better PCE.<sup>46,47</sup>

Dipole-dipole interaction of self-assembly of dyes on TiO<sub>2</sub> surface, which leads to H (hypochromic shift) and J (bathochromic shift)-type aggregation on the surface and their contribution revealed a significant broad spectral coverage in spectrum for PCE. However, aggregation induces excited state quenching and results in inefficient electron injection.<sup>28,48-51</sup> There are a selective ways used which helps to control the dye aggregation and enhance the device cell performance such as (i) addition of optically transparent co-adsorbent (CDCA), (ii) co-sensitization using a sterically dominated dye, (iii) supramolecular host-guest complex, and (iv) by attaching branched alkyl groups.<sup>44, 52-54</sup> The role of  $\pi$ -bridges were introduced in squaraine DSSC and studied the unsymmetrical D- $\pi$ -A based dyes, JD10 gave 7.3% efficiency in

liquid electrolyte.<sup>55</sup> Sensitizers have persists different orientation depending upon the  $\pi$ -spacers and D-A-D unit dihedral angle in squaraine dyes.<sup>56</sup> D-A-D based far red active unsymmetrical squaraines dyes can be functionalized with in-plane and out-of-plane alkyl groups and observed the formation stable aggregate that can also efficiently participate in the charge injection process<sup>44, 57</sup>

In this chapter, effects of (i) position of in-plane and out-of-plane alkyl groups and (ii)  $\pi$ -spacer have been examined on a D-A-D- $\pi$ -Anchoring group based unsymmetrical squaraine dyes. The design and molecular structures of five dyes **PSQ1-5** were showed in **Figure 2.1**.

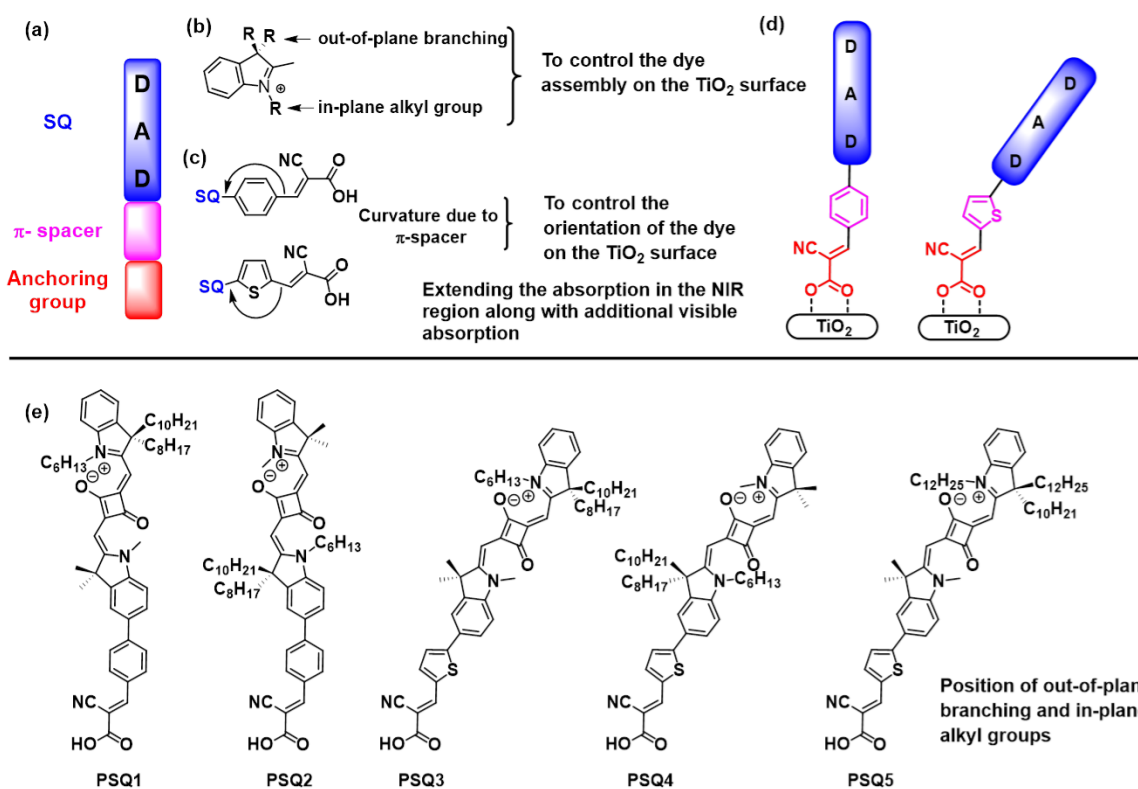
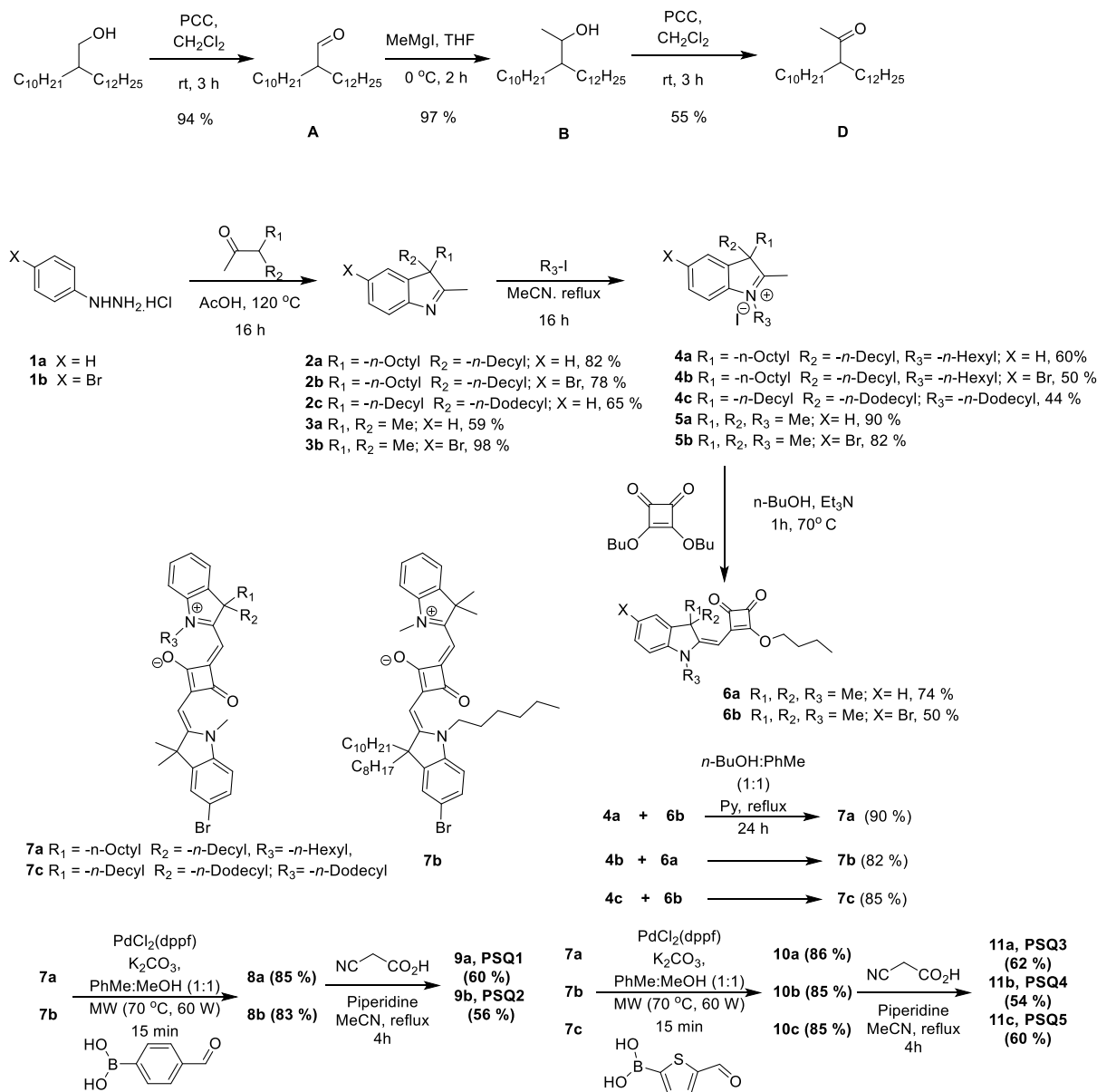


**Figure 2.1** (a) D-A-D- $\pi$ -A dye based on unsymmetrical squaraine dyes, (b) in-plane and out-of-plane branching on indoline, (c) curvature due to  $\pi$ -spacer, (d) schematic representation of mode of anchoring on  $\text{TiO}_2$  surface, and (e) the  $\pi$ -extended structure of alkyl functionalized unsymmetrical D-A-D- $\pi$ -A squaraine dyes, **PSQ1-5**.

## 2.2 Results and Discussions

### 2.2.1 Synthesis of PSQ Sensitizers

**Figure 2.1** shows the structures of D-A-D- $\pi$ -A unsymmetrical squaraine sensitizers (**PSQ1-5**) and its multi-step synthesis is carried out according to **Scheme 2.1**. The starting material, a branched ketone, 3-octyl-2-tridecanone<sup>44</sup> and 3-decyl-2-pentadecanone was synthesized from corresponding branched alcohols 2-octyldodecanol and 2-decyltetradecanol.



**Scheme 2.1** Synthesis of branched alkyl group containing  $\pi$ -extended D-A-D- $\pi$ -A squaraine dyes, **PSQ1-5**.

Unsymmetrical squaraine dyes (**D-A-D- $\pi$ -A**) with  $\pi$ -spacer and cyanoacetic acid requires three segment of synthesis, where bromo group functionalized unsymmetrical squaraine (**D-A-D**) needs to be synthesized first and further Suzuki coupling with  $\pi$ -spacer provides the aldehyde terminated precursor and further Knoevenagel condensation with cyanoacetic acid provides the required products. Microwave mediated Pd catalyzed Suzuki coupling provided the aldehyde precursor in good yield in short reaction time. The branched alcohol was oxidized in the presence of PCC to give the branched aldehyde, **A** and it was reacted with MeMgI to afford the branched secondary alcohol, **B**. Oxidation of **B** in the presence of PCC afforded the required branched methyl ketone in moderate yield, which was then reacted with phenyl hydrazine to give the indoline derivative (**2a-3b**), followed by N-alkylation with methyl/hexyl/dodecyl iodide afforded the required indolium salt (**4a-5b**). The indolium salts were condensed with the bromo functionalized semi squaraine to afford the unsymmetrical squaraines (**7a-7c**). After microwave-assisted Suzuki coupling with 4-formylphenylboronic acid and 5-formylthiophen-2-ylboronic acid, the aldehyde precursors (**8a-b**, and **10a-c**) were isolated in high yield; this precursor was further condensed with cyanoacetic acid to afford **PSQ 1-5** dyes.

**2.2.2 Photophysical Properties** The optical properties of **PSQ1-5** in solution ( $\text{CHCl}_3$ ) and on transparent thin film of  $\text{TiO}_2$  (6  $\mu\text{m}$ ) are shown in **Figure 2.2**, and summarized in **Table 2.2**. Squaraine dyes show strong and intense absorption/emission properties at far-red region with an extinction coefficient of  $\geq 10^5 \text{ M}^{-1} \text{ cm}^{-1}$ . UV-vis absorption spectra of dyes, **Figure 3a**, exhibit a strong  $S_0$ - $S_1$  intramolecular charge transfer (ICT) transition at far-red region with a vibronic shoulder at higher energy, and also a weak absorption band between 400-500 nm ( $\epsilon \sim 10^5 \text{ M}^{-1} \text{ cm}^{-1}$ ). Such high energy transitions were observed for SQ dyes upon increasing the conjugation with  $\pi$ -spacer or the dicyano derivatives of SQ dyes.<sup>57</sup> PSQ dyes were having wavelength at absorption maxima ( $\lambda_{\text{max}}$ ) around 654 to 667 nm and for **PSQ1** and **PSQ3** substituting phenyl group with thiophene causes red shifted absorption band (11 nm), and for positional isomers  $\lambda_{\text{max}}$  were almost same. For **PSQ1** and **PSQ2**, the position of  $\text{sp}^3$ -alkyl group produce small changes in molar absorptivity ( $\sim 2 \times 10^5 \text{ M}^{-1} \text{ cm}^{-1}$ ) and  $\lambda_{\text{max}}$  of 654 nm in solution. For **PSQ1** and **PSQ3**, absorption onset was increased in later and found a slight decrease in molar absorptivity. In case of **PSQ3** and **PSQ4**, both shows close similarity in their  $\lambda_{\text{max}}$  and  $\epsilon$  values, even after extending the length of top indoline  $\text{sp}^3$ -alkyl chain, **PSQ5**. Emission  $\lambda_{\text{max}}$  of **PSQ1-5** shows intense peak

between 664-676 nm, optical band gap of thiophene  $\pi$ -spacer based dyes were decreased and shifted towards long wavelength.

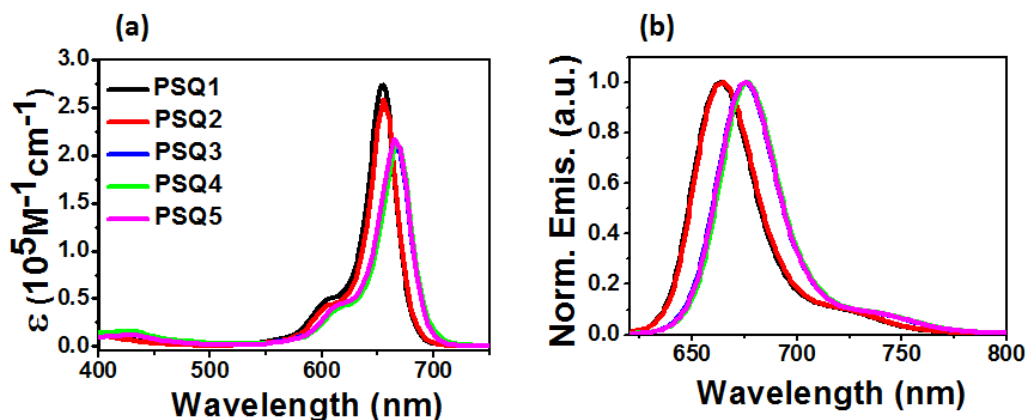


**Figure 2.2** Optical properties of **PSQ1-5** dyes. (a) UV-vis absorption spectra in  $\text{CHCl}_3$  (blue, magenta and green colored curves are overlapping), (b) Normalized emission spectra in  $\text{CHCl}_3$  (excitation wavelength: 610 nm) (blue, magenta and green colored curves are overlapping).

Absorption and emission studies were carried out in solvents with different polarity (**Figure 2.3-2.6**) and found that gradual increase in polarity increases the excitation energy, this solvatochromism shift attributed to the more polar nature of ground state than excited state, and the results are listed in **Table 2.1**. The Stokes shift of  $\sim 10$  nm for PSQ series shows the change in dipole moment in the excited state is small. Fluorescence quantum yield ( $\phi$ ) in different solvents was measured via relative method<sup>44</sup> and in chloroform  $\phi$  shows an increasing order of  $[\text{PSQ1} \approx \text{PSQ2}] > [\text{PSQ3} = \text{PSQ4} = \text{PSQ5}]$ . The excitation transition energy ( $E_{0-0}$ ) was calculated from the intersection of absorption and emission spectra and **PSQ1-5** exhibited optical band gap between 1.85-1.88 eV (**Table 2.2**).

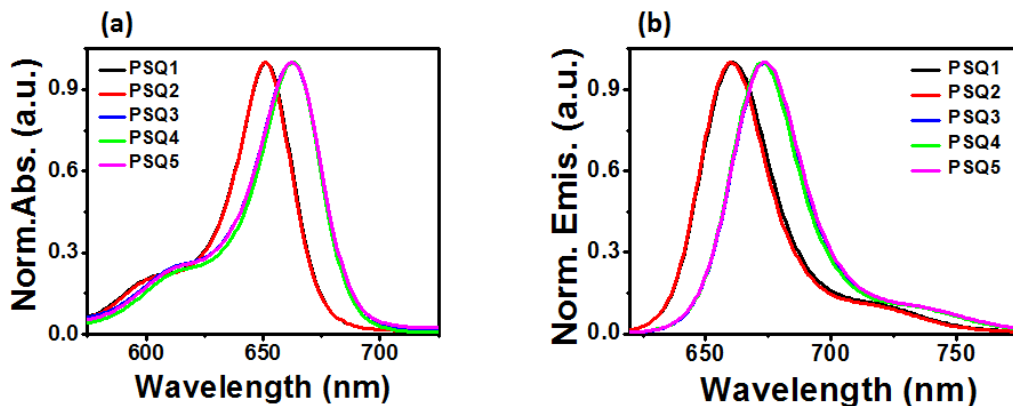


**Figure 2.3** Normalized UV-vis absorption (a) and fluorescence spectra (b) of **PSQ1-5** in EtOH.



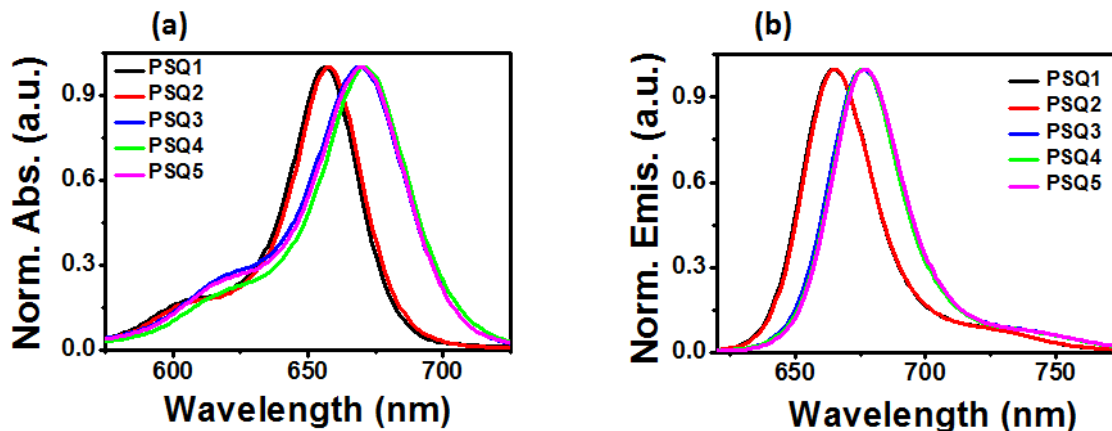


**Figure 2.4** Normalized UV-vis absorption (a) and fluorescence spectra (b) of PSQ1-5 in  $\text{CH}_2\text{Cl}_2$ .

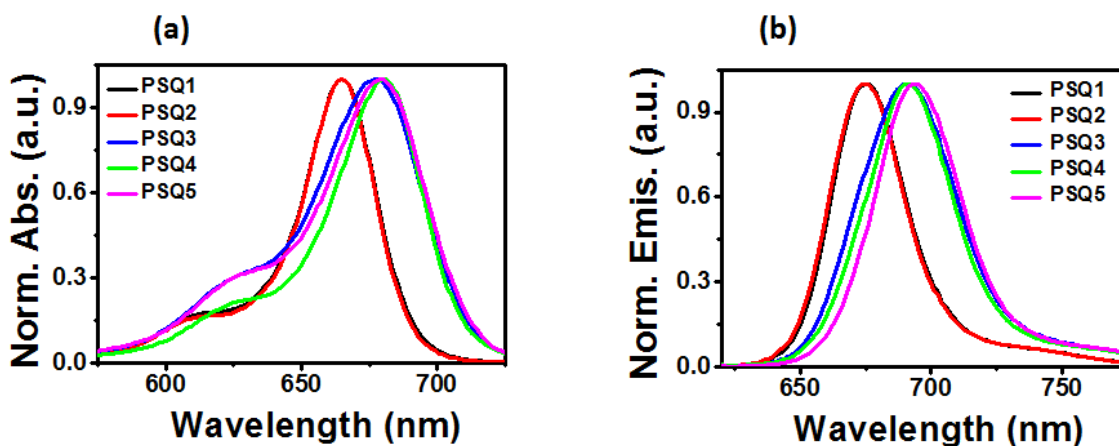


**Figure 2.5** Normalized UV-vis absorption (a) and fluorescence spectra (b) of PSQ1-5 in PhMe.

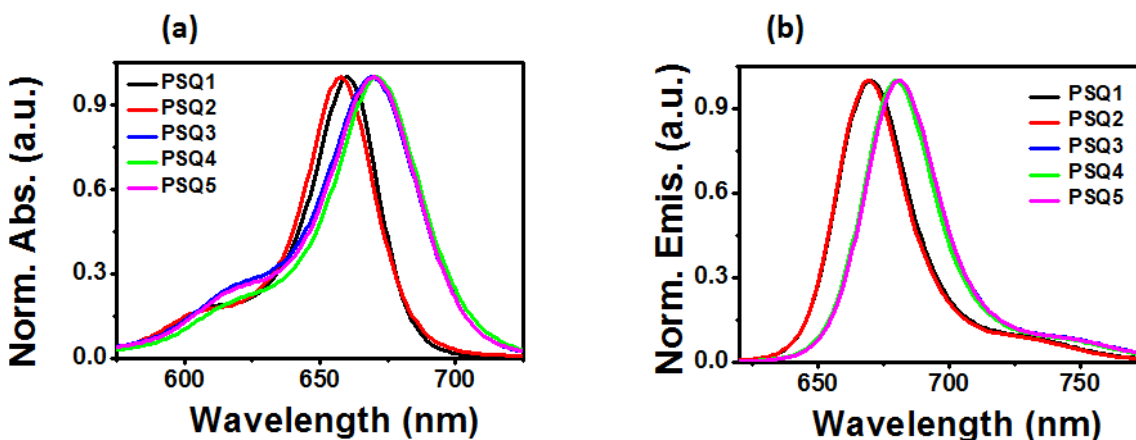


**Figure 2.6** Normalized UV-vis absorption (a) and fluorescence spectra (b) of PSQ1-5 in DMF.

**Table 2.1** UV-vis absorption and fluorescence properties of **PSQ1-5** in different solvents and at excitation wavelength ( $\lambda_{ex}$ ) was 610 nm

Dye	$\lambda_{max}^{abs}/\lambda_{max}^{emis}$ (n m), $\phi$ , in PhMe	$\lambda_{max}^{abs}/\lambda_{max}^{emis}$ (n m), $\phi$ , in CH <sub>2</sub> Cl <sub>2</sub>	$\lambda_{max}^{abs}/\lambda_{max}^{emis}$ (n m), $\phi$ , in CHCl <sub>3</sub>	$\lambda_{max}^{abs}/\lambda_{max}^{emis}$ (n m), $\phi$ , in EtOH	$\lambda_{max}^{abs}/\lambda_{max}^{emis}$ (n m), $\phi$ , in DMF
<b>PSQ1</b>	665/675, 0.42	657/665, 0.31	654/664, 0.47	651/660, 0.41	658/669, 0.33
<b>PSQ2</b>	665/675, 0.47	658/676, 0.27	654/664, 0.48	651/660, 0.34	660/670, 0.28
<b>PSQ3</b>	671/691, 0.23	669/676, 0.14	665/675, 0.39	662/673, 0.34	669/680, 0.29
<b>PSQ4</b>	680/691, 0.30	671/676, 0.35	667/676, 0.39	662/673, 0.32	671/680, 0.25
<b>PSQ5</b>	679/694, 0.25	669/677, 0.14	665/675, 0.39	662/673, 0.36	670/681, 0.29

Effect of chemisorption on TiO<sub>2</sub> surface in dye absorption features showed in **Figure 2.7a**. A transparent, 6  $\mu$ m thick, TiO<sub>2</sub> film dipped in 0.1 mM dye solution for a short time (30 min); dyes **PSQ1-5** showed a broadened absorption spectrum due to aggregation on the surface. Ratio of optical density of monomer with dimer given in **Table 2.2**, which helps to conclude extend of aggregation for each dyes on surface and found that top alkylated PSQ dyes are more aggregated than the down branched dyes (**PSQ2** and **PSQ4**). Effects of position of out-of-plane alkyl group in **PSQ1** and **PSQ2** exhibited 21% decrease in the ratio of  $A_{dimer}/A_{monomer}$ . But **PSQ1** and **PSQ3**

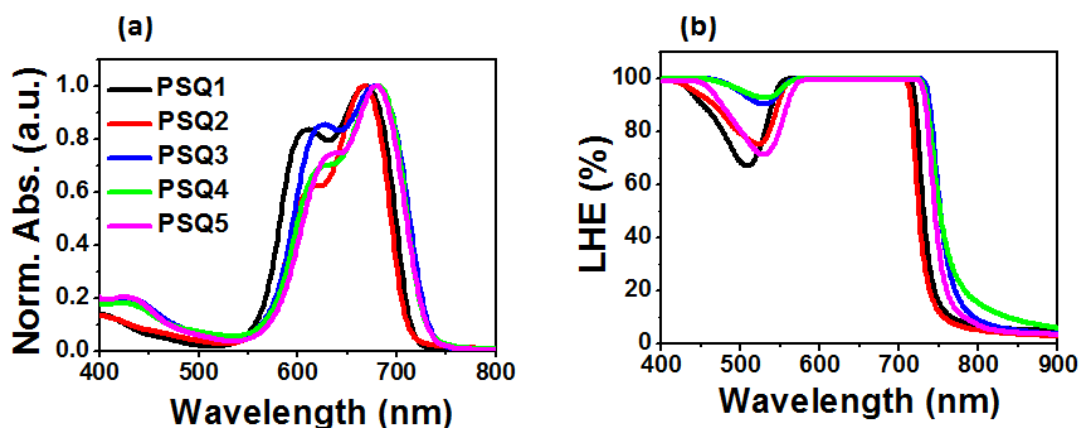


**Figure 2.7** Optical properties of **PSQ1-5** dyes. (a) Normalized absorption spectra on thin film of TiO<sub>2</sub>, thickness = 6  $\mu$ m, dipping time = 30 min, and [PSQ] = 0.1 mM in chloroform, (b) Absorbance in % on thin film recorded after 12 h dipping in 0.1 mM solution of PSQs in CHCl<sub>3</sub>.

showed similar ratio after exchanging  $\pi$ -spacer. Controlling the aggregation ratio was realized by

increasing the alkyl chains at both  $sp^3$ -C and N-centers as in the case of **PSQ5**. Prolonged dipping of thin film in 0.1 mM dye solution revealed the both H and J-type pattern in absorbance, and in addition to better spectral coverage in visible and far-red, these dyes LHE (LHE =  $1-10^{-A}$ ) extends to near-infrared region. **PSQ1-5** have shown broad LHE (from 400 to 800 nm) profile in the visible and far-red region of spectrum, which would contribute significantly for their PCE.

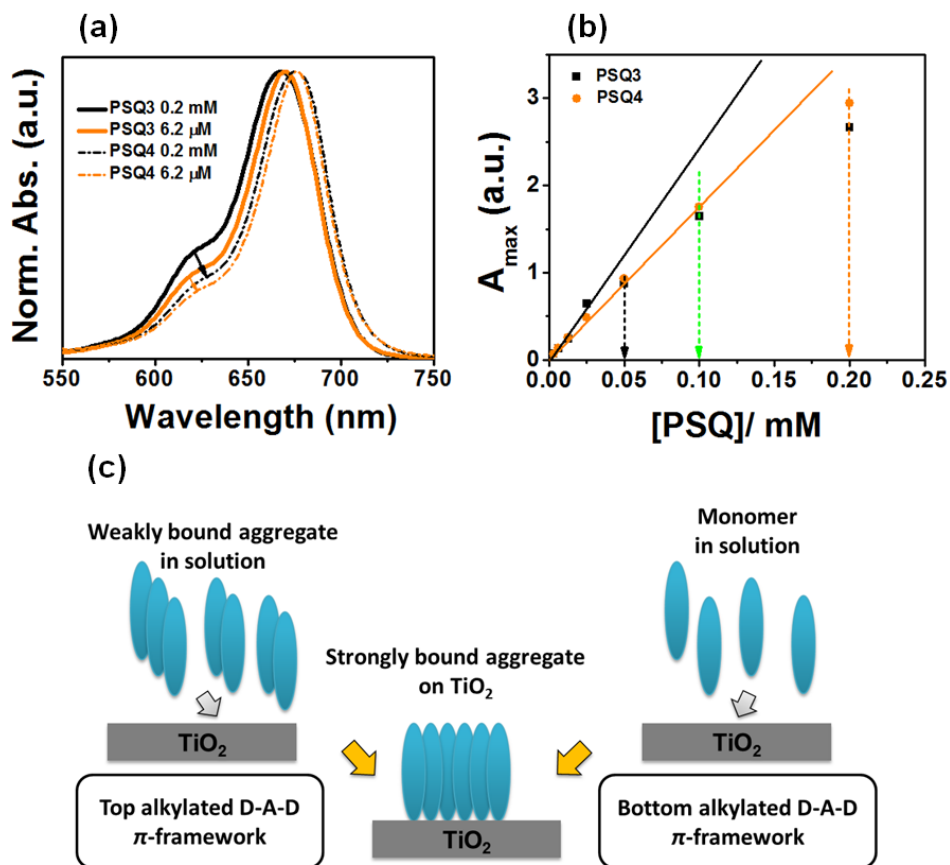
**Table 2.2** Photophysical and electrochemical properties of **PSQ1-5** at rt

Dye	$\lambda_{\max}/\text{abs}$ (nm) <sup>a</sup>	$\epsilon_a, \epsilon_b$ $10^5(\text{M}^{-1}\text{cm}^{-1})^b$	$\lambda_{\max}/e$ mis (nm) <sup>c</sup>	$\phi_{\text{emis}}$ (%) <sup>d</sup>	$\lambda_{\max}/\text{abs}/$ <b>TiO<sub>2</sub></b> (nm) <sup>e</sup>	$A_{\text{dimer}}/$ $A_{\text{monomer}}$ (%)	$E_{\text{HOMO}}^f$ (eV)	$\Delta E_{0-0}^g$ (eV)	$E_{\text{LUMO}}$ (eV) <sup>h</sup>
<b>PSQ1</b>	400,654	0.11,2.7	664	0.47	610,669	84	0.77	1.88	-1.12
<b>PSQ2</b>	399,654	0.12,2.5	664	0.48	618,667	63	0.82	1.88	-1.07
<b>PSQ3</b>	426,665	0.14,2.1	675	0.39	626,678	85	0.77	1.85	-1.08
<b>PSQ4</b>	427,667	0.16,2.1	676	0.39	629,682	70	0.81	1.85	-1.04
<b>PSQ15</b>	429,665	0.12,2.2	675	0.39	637/680	75	0.73	1.85	-1.12

<sup>a</sup>UV-vis absorption in  $\text{CHCl}_3$ . <sup>b</sup>Molar extinction coefficient in visible region peak  $\epsilon_a$ , and charge transfer peak  $\epsilon_b$ . <sup>c</sup>Emission studies. <sup>d</sup>Quantum yield by relative method in  $\text{CHCl}_3$ . <sup>e</sup>On thin film of  $\text{TiO}_2$ , thickness = 6  $\mu\text{m}$ , dipping time = 30 min, and  $[\text{PSQ}] = 0.1 \text{ mM}$  in  $\text{CHCl}_3$ . <sup>f</sup> $E_{\text{HOMO}}$  of **PSQ1-5** in  $\text{CH}_2\text{Cl}_2$ ,  $\text{Fc}^+/\text{Fc}$  was used as external standard and potential measured vs  $\text{Fc}/\text{Fc}^+$  (eV) were converted to NHE (V) by addition of 0.7 V<sup>64</sup>. <sup>g</sup> $E_{0-0}$  deduced at the intersection of absorption and emission spectra using the eq  $E_{0-0} \text{ (eV)} = 1240/\lambda_{\max}$ . <sup>h</sup> $E_{\text{LUMO}}$  levels were measured by subtracting  $E_{\text{HOMO}}$  from  $E_{0-0}$ .

To study the aggregation characteristics of these dyes in solution, we have recorded the absorption spectrum of **PSQ3** and **PSQ4** in various concentrations in dipping solvent ( $\text{CHCl}_3$ ), and observed that **PSQ3** exist as loosely bound aggregate (called as dynamic aggregate) in solution and deviated the Beer-Lambert law when the concentration reached around 0.025 mM. Whereas for **PSQ4**, non-linearity starts when the concentration of dye dipping solution goes beyond 0.1 mM (**Figure 2.8b**). This observation is important in the sense that the out-of-plane

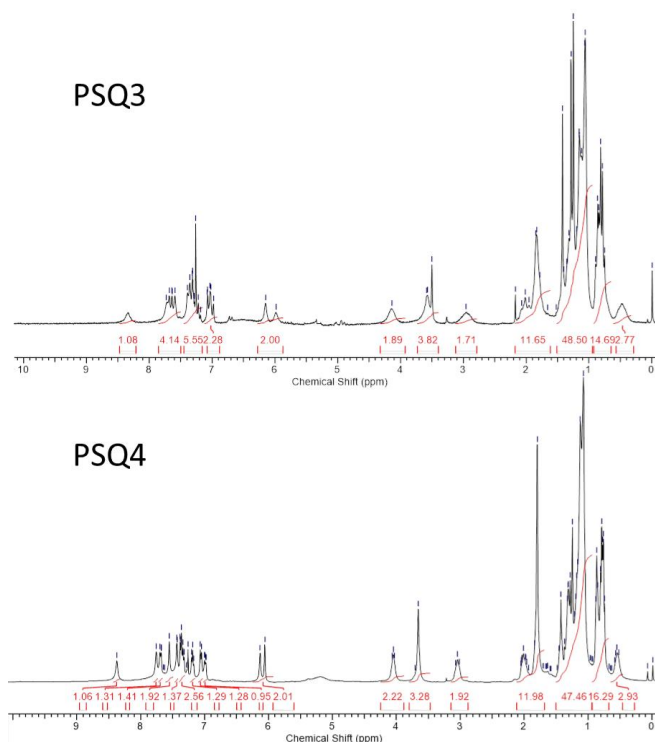
group that was far away from the anchoring groups allows the strong intermolecular interaction even in solution, and in the case of **PSQ4**, the dye exist as monomer at 100  $\mu\text{M}$  which was the concentration of dye that was used for dipping the electrode for device fabrication. The mechanism of transferring the dynamic aggregate in solution to static aggregate on  $\text{TiO}_2$  surface for dye cell application have given in **Figure 2.8c**.



**Figure 2.8** Aggregation of dyes in solution. (a) UV-vis absorption spectrum in  $\text{CHCl}_3$  in different concentration (path length of the cuvette 0.1 cm), (b) Deviation from Beer-Lambert law (**PSQ3** and **PSQ4**) and (c) Schematic representation of adsorption of top and bottom alkylated PSQ dyes on  $\text{TiO}_2$  surface.

**2.2.3 Mode of adsorption on  $\text{TiO}_2$  and Structure of PSQ dyes** Absorbance study showed that the aggregation of PSQ dyes having fingerprints of monomer, dimer and larger aggregated structures on mesoporous  $\text{TiO}_2$  in **Figure 2.7**. It is essential to discuss the influence of  $\pi$ -spacers or position of out-of-plane and in-plane alkyl groups on arranging the conjugated backbone with respect to surface. The association of  $\pi$ -functional molecules in solution can be studied using  $^1\text{H}$ -

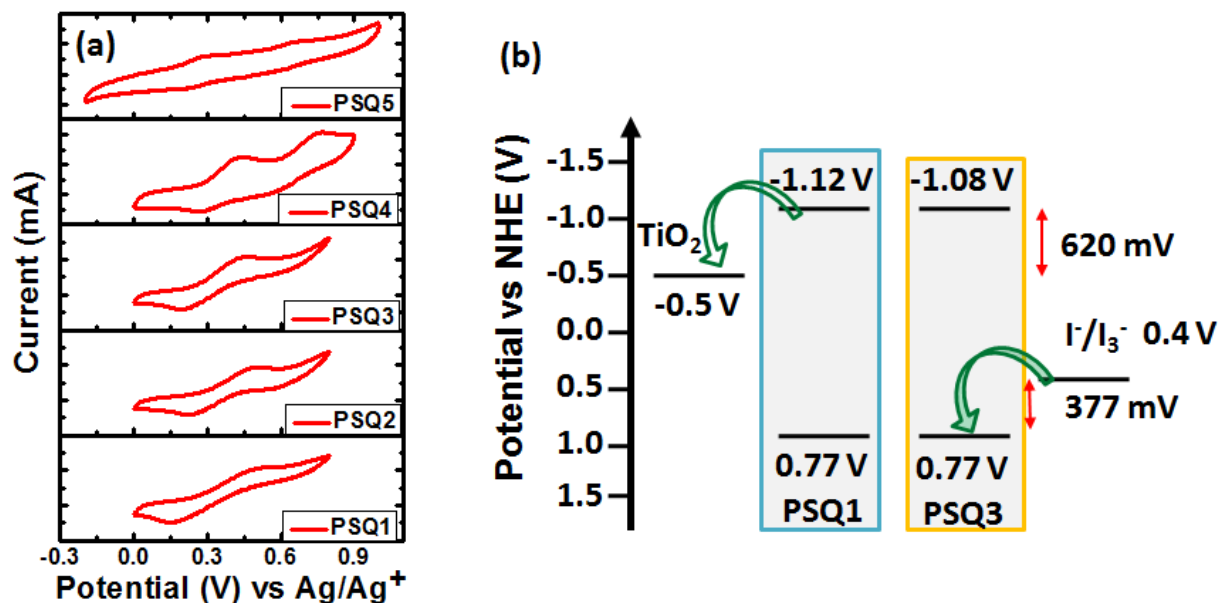
NMR spectroscopy (**Figure 2.9**) and UV-vis absorption studies (**Figure 2.8**). NMR studies are widely used but at higher concentration signals are broadened owing to aggregated structure.<sup>65</sup> Absorption studies of different dye concentration (6.2  $\mu\text{M}$  to 0.2 mM), cuvette path length was 1 mm, exhibited distinct absorption behavior for upper-indoline-alkylated and bottom-indoline-alkylated dyes. **Figure 2.8** shows Beer-Lambert plot for **PSQ3** and **PSQ4**. The optical density of vibronic peak of later set of dyes in chloroform and on thin film (dipping time of 30 min) was less compared to their isomers. Line broadening effects in the  $^1\text{H}$ -NMR spectra of **PSQ3** and **PSQ4** were compared to ascertain the presence of aggregates in the solution that can be transferred to form a static aggregate on  $\text{TiO}_2$  surface. In case of **PSQ4** even at higher concentration NMR peaks were more resolved than **PSQ3** owing to formation of strong intermolecular attraction in the later class of dyes. Utilizing the van der Waals interaction for assembling molecules is well known in literature but more proximity of dyes through  $\pi$ - $\pi$  interactions leads to least efficiency, and hence this study proves the control over dye-dye distance in solution is important in DSSC.



**Figure 2.9**  $^1\text{H}$ -NMR spectra of **PSQ3** (top) and **PSQ4** (bottom) in  $\text{CDCl}_3$  at rt.

### 2.2.4 Electrochemical Characterization

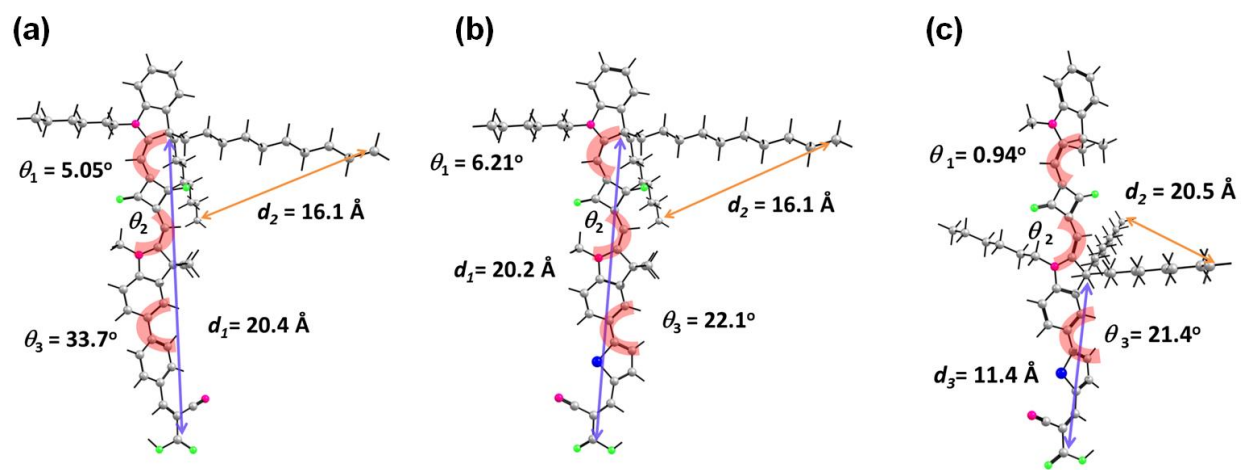
The electrochemical properties of **PSQ1-5** dyes in solution were investigated by recording cyclic voltammograms to understand the feasibility of electron injection and dye regeneration (**Figure 2.10 and Table 2.2**). All the dyes showed quasi-reversible first oxidation peak. First-ground-state oxidation potentials ( $E_{S/S^+}$ ) of **PSQ1-5** were calculated from the oxidation onset of cyclic voltammograms with potential window of 0-0.8 V and which can be attributed to the oxidation of indoline part of D-A-D unit. **Figure 2.10** shows cyclic voltammograms of upper branched **PSQ1**, **PSQ3** and **PSQ5** and the remaining plots (**PSQ2**, **PSQ4**). The more positive potential of **PSQ1** and **PSQ3** (770 mV) than the electrochemical potential of iodide/triiodide redox couple (400 mV vs NHE) ensure the feasible regeneration of oxidized dye. The large dye regeneration driving force ( $\Delta G_{\text{reg}}$ ) of PSQ dyes was higher than the required minimum offset of ca. 200 mV (**Figure 2.10b**) and showed a loss-in-potential of 377 mV.<sup>25, 66-67</sup> For **PSQ1-5** dyes the  $E_{\text{ox}}$  was around 0.73-0.82 V vs NHE, suggests that the changes in  $\pi$ -spacers do not make large difference, in contrast the position of out-of-plane alkyl groups showed a notable difference. **Table 2.2** shows the electrochemical properties of **PSQ1-5** dyes. The more negative shift in the HOMO levels of **PSQ1**, **PSQ3** and **PSQ5** compared to bottom alkylated **PSQ2** and **PSQ4** can be because of the difference in the interaction between top and bottom alkylated PSQ dyes with the electrode. The LUMO energy levels of PSQ dyes (-1.04 to -1.12 V vs NHE) were more negative than the conduction band edge of  $\text{TiO}_2$  ( $E_{\text{CB/TiO}_2}$ ) ca. -0.5 V vs NHE and which is sufficiently higher than the required over-potential ca. 100 to 150 mV.<sup>25</sup> The higher lying LUMO brings large injection driving force ( $\Delta G_{\text{inj}}$ ) of ca. 620 mV for PSQ dyes helps in efficient electron injection ( $\eta_{\text{inj}}$ ). But the loss-in-potential was almost similar for the series. Structural changes in isomers **PSQ1** and **PSQ2** or **PSQ3** and **PSQ4**, kept the optical band gap same. Shift in the conduction band-edge of  $\text{TiO}_2$  in presence of charged species would be attenuated using hydrophobic functionalities of PSQ dyes. For **PSQ5**, the HOMO and LUMO is at 0.73 V and -1.12 V vs NHE, respectively and there was no significant difference after extending the out-of-plane alkyl length. Comparison of **PSQ1** and **PSQ3** showed the addition of more electron withdrawing thiophene in the later dye has a greater influence in LUMO than their HOMO. Close similarity in the energy levels of PSQ dyes directs the question of significant difference in PCE towards nanoscopic structure of dye/ $\text{TiO}_2$  heterogeneous interface.



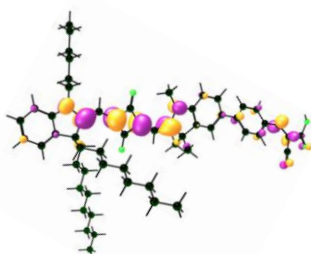
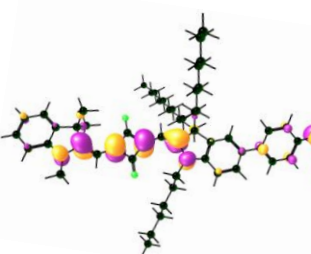
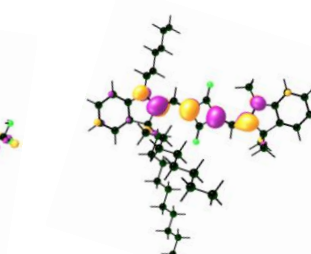
**Figure 2.10** Electrochemical properties of **PSQ** dyes. (a) Cyclic voltammograms for **PSQ1-5** and (b) Energy level diagram of **PSQ** dyes (V vs NHE) with TiO<sub>2</sub>, and electrolyte (iodide/triiodide).

**2.2.5 Density Functional Theory (DFT) Calculations and Energy Levels** To understand the electronic structure of the **PSQ1-5** dyes, their ground-state geometries and energies were fully optimized by B3LYP/6-31G\*\* level with the Gaussian 09 program<sup>59-63</sup>. **Figure 2.11** shows energy minimized structures of **PSQ1**, **PSQ3** and **PSQ4**, and the detailed parameters are listed in **Table 2.3**. The isosurface plots of four selected frontier molecular orbitals HOMO+1, HOMO, LUMO and LUMO-1 were depicted in **Figure 2.12-2.13**. Theoretical result elucidates there is no such a significant difference in the distribution of electronic density of MOs after changing the  $\pi$ -framework at gaseous state of these dyes. Distinct partition of HOMO towards D-A-D unit and LUMO close to cyanoacetic acid group helps in strong intramolecular charge transfer (ICT) and which favors strong coupling of LUMO with TiO<sub>2</sub> conduction band edge. The electrons in the HOMO-1 are completely delocalized on squaric acid unit, and for LUMO+1 the major part on D- $\pi$ -D and found remaining at cyanoacetic unit. The peculiar behavior of electronic distribution in HOMO and LUMO of **PSQ** dyes would be owing to fast dye regeneration and charge injection. Self-assembly of **PSQ1-5** dyes plays crucial role in PCE. Distance between terminal carbon atoms of top and bottom-indoline out-of-plane alkyl chains were calculated and enlisted in **Table**

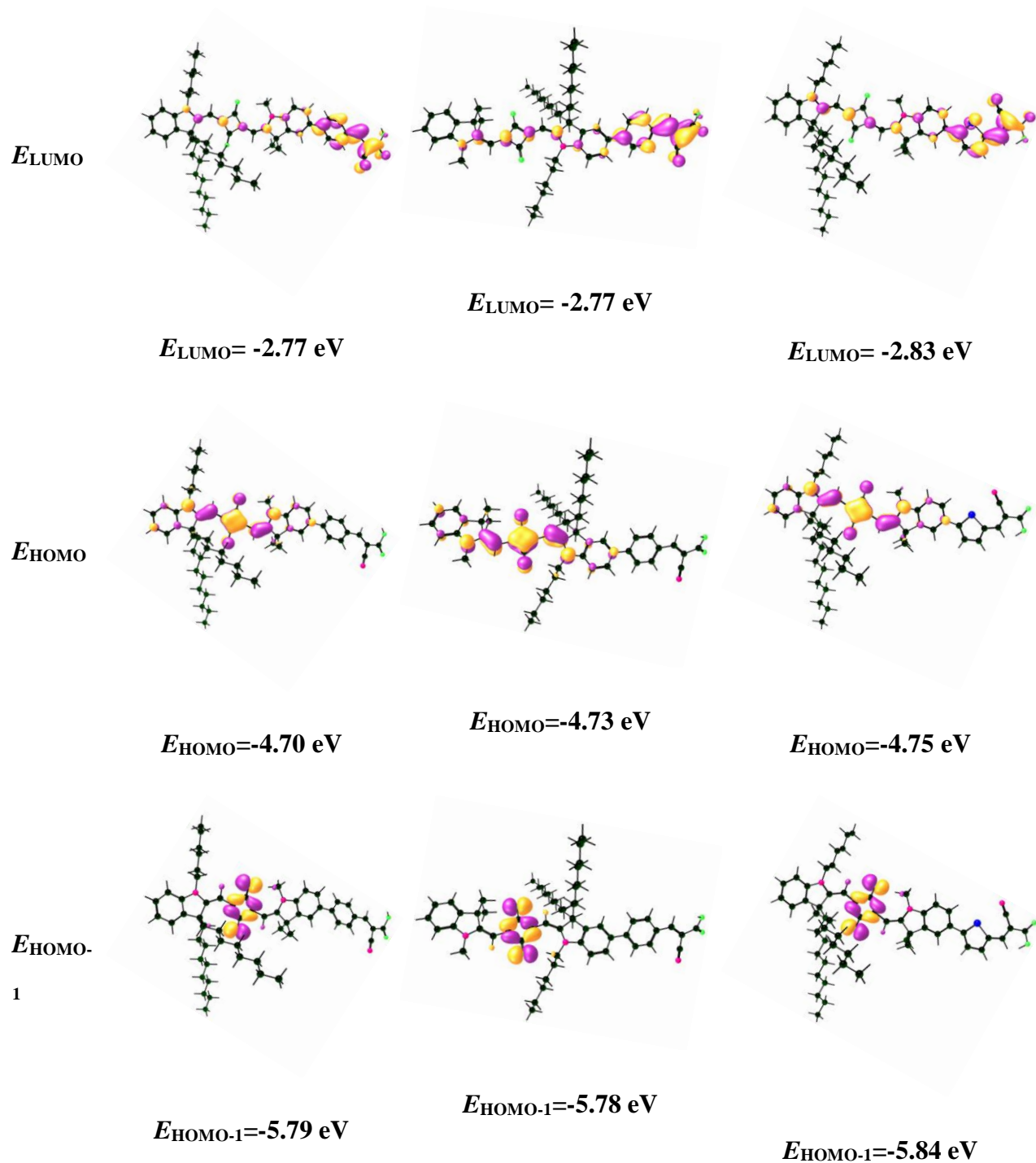
**2.3.** For **PSQ1**, **PSQ2** and **PSQ5** the distance ( $d_1$ ) was 16.1 Å and in case of bottom branched **PSQ2** and **PSQ4**,  $d_2$  showed 4.4 Å increase in length. Dihedral angle of phenyl shares with D-A-D unit of **PSQ1** and **PSQ2** was larger (33.7°) than thiophene derivatives **PSQ3-5** (22.1°), which in turn decreases extend of conjugation and reflected in the absorption spectrum. All three important dihedral angles,  $\theta_1$ ,  $\theta_2$ , and  $\theta_3$  are listed in **Table 2.3**. Position of out-of-plane alkyl groups at top indoline unit which is away from the anchoring group showed the distance  $d_1$  of 20.4 Å and 20.2 Å for **PSQ1** and **PSQ3**, respectively.



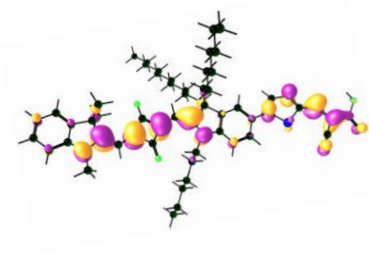
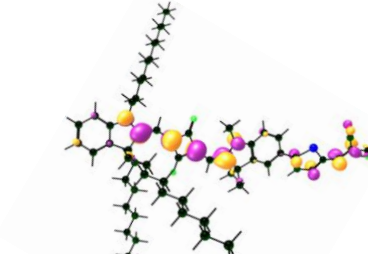
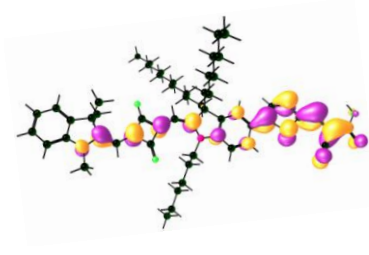
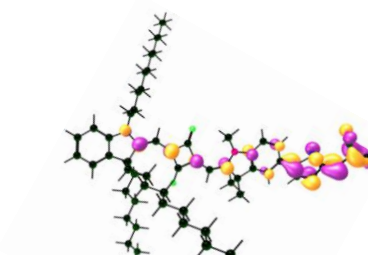
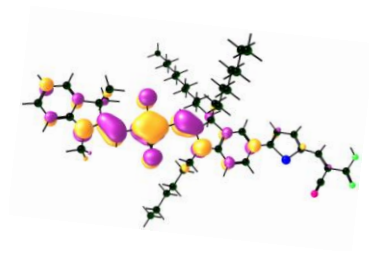
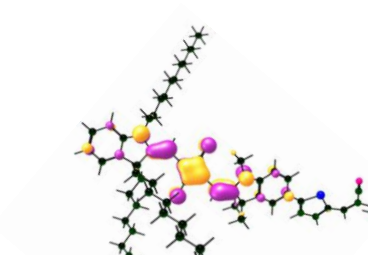
**Figure 2.11** Energy minimized structures of (a) **PSQ1**, (b) **PSQ3** and (c) **PSQ4**.

State	PSQ1	PSQ2	PSQ3
$E_{\text{LUMO}+1}$ +1			
	$E_{\text{LUMO}+1} = -2.45 \text{ eV}$	$E_{\text{LUMO}+1} = -2.45 \text{ eV}$	$E_{\text{LUMO}+1} = -2.47 \text{ eV}$





**Figure 2.12.** Isosurface plots of selected frontier orbitals (HOMO, HOMO-1, LUMO, LUMO+1) of **PSQ1**, **PSQ3** and **PSQ3**. Fully optimised at DFT B3LYP/6-31G\*\* level. (Isovalue set to 0.036 a.u.)

Energy State	PSQ4	PSQ5
$E_{LUMO+1}$	 $E_{LUMO+1} = -2.46 \text{ eV}$	 $E_{LUMO+1} = -2.44 \text{ eV}$
$E_{LUMO}$	 $E_{LUMO} = -2.83 \text{ eV}$	 $E_{LUMO} = -2.83 \text{ eV}$
$E_{HOMO}$	 $E_{HOMO} = -4.77 \text{ eV}$	 $E_{HOMO} = -4.74 \text{ eV}$

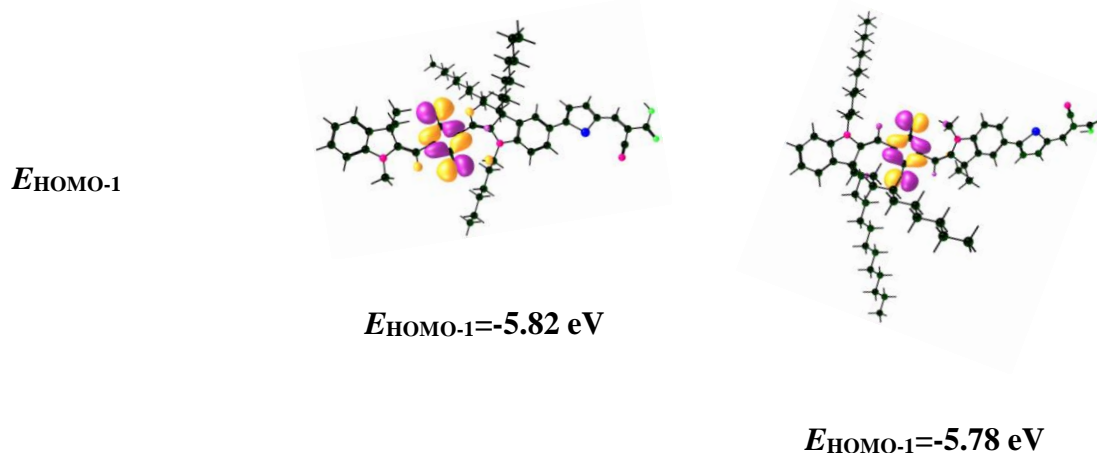


**Figure 2.13** Isosurface plots of selected frontier orbitals (HOMO, HOMO-1, LUMO, LUMO+1) of **PSQ4** and **PSQ5**. Fully optimised at DFT B3LYP/6-31G\*\* level. (Isovalue set to 0.036 a.u.)

**Table 2.3** Theoretical values of dihedral angles, distances and energy levels of selected MOs<sup>a</sup>

Dye	Distance between alkyl groups			Dihedral Angle (degree)			$E_{HOMO}^T$	$E_{HOMO-1}^T$	$E_{LUMO}^T$	$E_{LUMO+1}^T$	$E_g^T$
	$d_1$	$d_2$	$d_3$	$\theta_1$	$\theta_2$	$\theta_3$	(eV)	(eV)	(eV)	(eV)	(eV)
<b>PSQ1</b>	20.4	16.1		5.05	0.29	33.7	-4.70	-5.79	-2.77	-2.45	1.93
<b>PSQ2</b>		20.4	11.6	0.02	0.05	33.7	-4.73	-5.78	-2.77	-2.45	1.96
<b>PSQ3</b>	20.2	16.1		6.21	0.79	22.1	-4.75	-5.84	-2.83	-2.47	1.92
<b>PSQ4</b>		20.5	11.4	0.94	1.31	21.4	-4.77	-5.82	-2.83	-2.46	1.94
<b>PSQ5</b>	20.1	20		5.23	12.2	21.4	-4.74	-5.78	-2.83	-2.44	1.91

<sup>a</sup> for the description of  $d$  and  $\theta$ , refer the **figure 2.11**.

**2.2.6 Photovoltaic Studies of PSQ1-5** Current-voltage ( $I$ - $V$ ) characterization of **PSQ1-5** were measured using iodide/triiodide ( $I^-/I_3^-$ ) liquid electrolyte under standard conditions (AM 1.5G, 100 mW cm<sup>-2</sup>), and the cells average device parameters with and without co-adsorbent 3 $\alpha$ ,7 $\alpha$ -dihydroxy-5 $\beta$ -cholic acid are summarized in **Table 2.4** and **Table 2.5**. In the previous report from our group, whenever the in-plane and out-of-plane branched alkyl groups on D-A-D part of squaraine dye situate away from the anchoring group gave better PCE.<sup>44</sup> Upper branched **PSQ1** having phenyl  $\pi$ -spacer showed 4.28% PCE with a  $J_{sc}$  of 11.05 mA cm<sup>-2</sup> and  $V_{oc}$  of 0.589 V.

Addition of minimum amount of coadsorbent increased both the  $J_{sc}$  and  $V_{oc}$  and further increase in the concentration of CDCA reduced the number of dyes on  $TiO_2$  (**Figure 2.14 and Table 2.4**). For the isomer, **PSQ2**, in absence of CDCA  $J_{sc}$  was comparatively similar and showed 11.7% reduction in PCE because of low  $V_{oc}$  (0.557 V). Efficiency of these cells was increasing till the addition of 4 equiv of CDCA by the concomitant improvement in  $J_{sc}$  and  $V_{oc}$  values but further addition of CDCA reduced the cell performance. The  $J$ - $V$  characteristics of **PSQ1** and **PSQ3** infer the effect of phenyl and thiophene  $\pi$ -spacers in D-A-D- $\pi$ -A unsymmetrical squaraine dyes. The small dihedral angle of thiophene unit shared with D-A-D part could accelerate the charge injection than **PSQ1** (**Table 2.3**). Though the PCE of **PSQ3** was moderate in absence of CDCA, addition of 0.1 mM (1:1 equiv of Dye vs CDCA) into the dye solution enhanced the efficiency (**Figure 2.15**). A PCE of 7.21% was achieved for 1:3 equiv of dye: co-adsorbent ratio and the corresponding  $J_{sc}$  and  $V_{oc}$  were 17.11 mA cm<sup>-2</sup> and 600 mV, respectively. Photovoltaic parameters with different concentrations of CDCA were summarized in **Table 2.5** for **PSQ3-5**. As observed in the case of **PSQ2**, the bottom out-of-plane branching of **PSQ4** displayed a 6.7% decrease in efficiency, but reached the overall PCE of 6.36%, and which was higher than **PSQ2** (5.55%). Hence the typical characteristics of bottom alkylated dyes, reduction in amount of dyes on  $TiO_2$  compared to their isomers as reported in the earlier study was changed after increasing distance between anchoring group and alkyl functionalities, and the desorption studies are showed in **Table 2.4**. Extending the length of out-of-plane and in-plane alkyl groups of **PSQ3** shows significant improvement in current and voltage and which in turn brings high efficiency for **PSQ5** sensitized solar cells. For a dye cell measured without co-adsorbent for **PSQ5** showed 14.28 mA cm<sup>-2</sup> of  $J_{sc}$  and 590 mV of  $V_{oc}$ , its PCE was 33.4% higher than **PSQ3**, which is attributed to the controlled organization surface using extended alkyl functionalities. The best efficiency of PSQ series was achieved at one equiv of CDCA in 0.1 mM **PSQ5** with a PCE of 8.15% ascribed to the  $J_{sc}$  of 19.73 mA cm<sup>-2</sup> and  $V_{oc}$  of 0.630 V. After increasing the out-of-plane chain length increase in both  $J_{sc}$  and  $V_{oc}$  was observed.

The distinct profile of photon-to-current conversion of upper branched PSQ dyes indicates the extended aggregation behavior of them in compared to isomers which showed narrowed profile. The loosely bound aggregates in the solution where electrodes are dipped for chemisorption of PSQ dyes help to control the assembly on surface and which is emphasized via studying the absorptance of **PSQ1-5** in presence of CDCA. Self-assembled monolayers of upper-

branched dyes were exhibited comparatively small difference up on increasing the concentration of co-adsorbent in solution than weakly bound **PSQ2** and **PSQ4**. IPCE response of **PSQ1**, **PSQ3**, and **PSQ5** showed better conversion in dimer, trimer and larger aggregated region. In the absence of co-adsorbent **PSQ1** showed a broad profile than **PSQ2**, which is attributed to the long range H-type aggregation as shown in the **Figure 2.8a**.

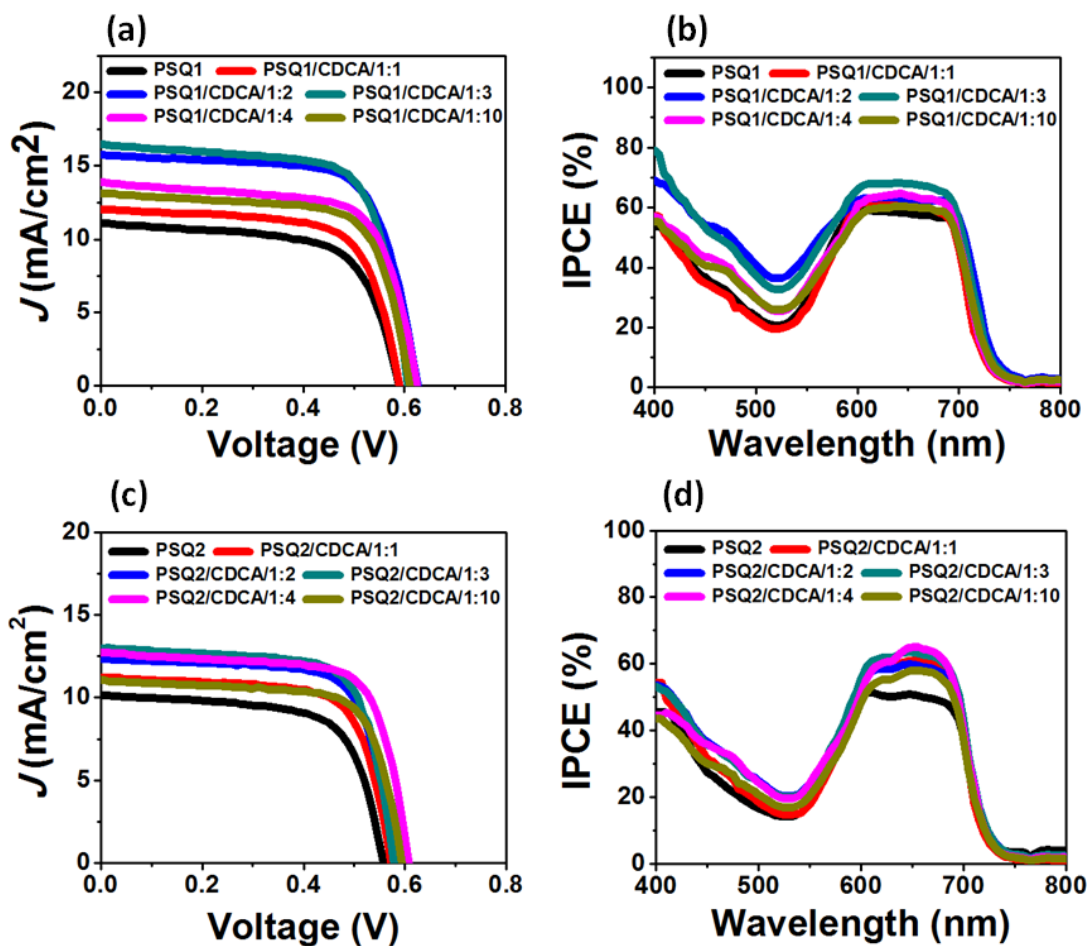


**Figure 2.14**  $I$ - $V$  curve and IPCE profile of **PSQ1-2**, a-d, in  $\text{CHCl}_3$ . (a) and (b)  $I$ - $V$  and IPCE curves for **PSQ1-5** in absence of CDCA. (c) and (d)  $I$ - $V$  and IPCE curves of best device for **PSQ1-5** in presence of CDCA (TiO<sub>2</sub> electrode thickness = 8 + 4  $\mu\text{m}$  (transparent+scattering layer), area = 0.22 cm<sup>2</sup>, [Dye] = 0.1 mM in  $\text{CHCl}_3$ , dipping time 12 h at rt, electrolyte: iodolyte Z-50 from Solaronix).

Whenever the branching was close to anchoring group sensitizers showed a narrow profile and which in turn decreased the  $J_{sc}$ . The assumption of strong secondary interactions for **PSQ1**,

**PSQ3** and **PSQ5** were clearly observed in the IPCE profile that after CDCA addition molecules moves away and possessing more dimeric and monomeric nature. After all, the synergic effect of controlled organization and effective conjugation of **PSQ5** have high photon-to-current profile with and without CDCA.

**Table 2.4** *I-V* characteristics of **PSQ1** and **PSQ2** dyes with and without CDCA

[Dye]/ mM	[CDCA]/mM	$J_{sc}$ (mA/cm <sup>2</sup> )	$V_{oc}$ (V)	$ff$ (%)	$\eta$ (%)	Dye loading mol/cm <sup>2</sup>
<b>PSQ1/0.1</b>	0	11.05	0.589	65.8	4.28	$1.58 \times 10^{-7}$
<b>PSQ1/0.1</b>	0.1	12.06	0.591	68.7	4.89	$1.15 \times 10^{-7}$
<b>PSQ1/0.1</b>	0.2	15.79	0.626	70.1	6.92	$1.25 \times 10^{-7}$
<b>PSQ1/0.1</b>	0.3	16.47	0.607	70.2	7.01	$1.20 \times 10^{-7}$
<b>PSQ1/0.1</b>	0.4	13.90	0.625	68.8	5.98	$0.96 \times 10^{-7}$
<b>PSQ1/0.1</b>	1	13.12	0.611	70.2	5.62	$0.66 \times 10^{-7}$
<b>PSQ2/0.1</b>	0	10.12	0.557	67.4	3.78	$1.34 \times 10^{-7}$
<b>PSQ2/0.1</b>	0.1	11.22	0.572	70.6	4.53	$0.99 \times 10^{-7}$
<b>PSQ2/0.1</b>	0.2	12.35	0.582	71.5	5.14	$0.98 \times 10^{-7}$
<b>PSQ2/0.1</b>	0.3	12.94	0.579	71.2	5.37	$0.94 \times 10^{-7}$
<b>PSQ2/0.1</b>	0.4	12.74	0.608	71.7	5.55	$0.95 \times 10^{-7}$
<b>PSQ2/0.1</b>	1	11.05	0.594	71.6	4.70	$0.54 \times 10^{-7}$

<sup>a</sup>TiO<sub>2</sub> electrode thickness = 8 + 4  $\mu$ m (transparent+scattering layer), area = 0.22 cm<sup>2</sup>, [Dye] = 0.1 mM in CHCl<sub>3</sub>, dipping time was 12 h at rt, electrolyte was iodolyte Z-50 (Solaronix) and summarize the result of best six devices with deviation.

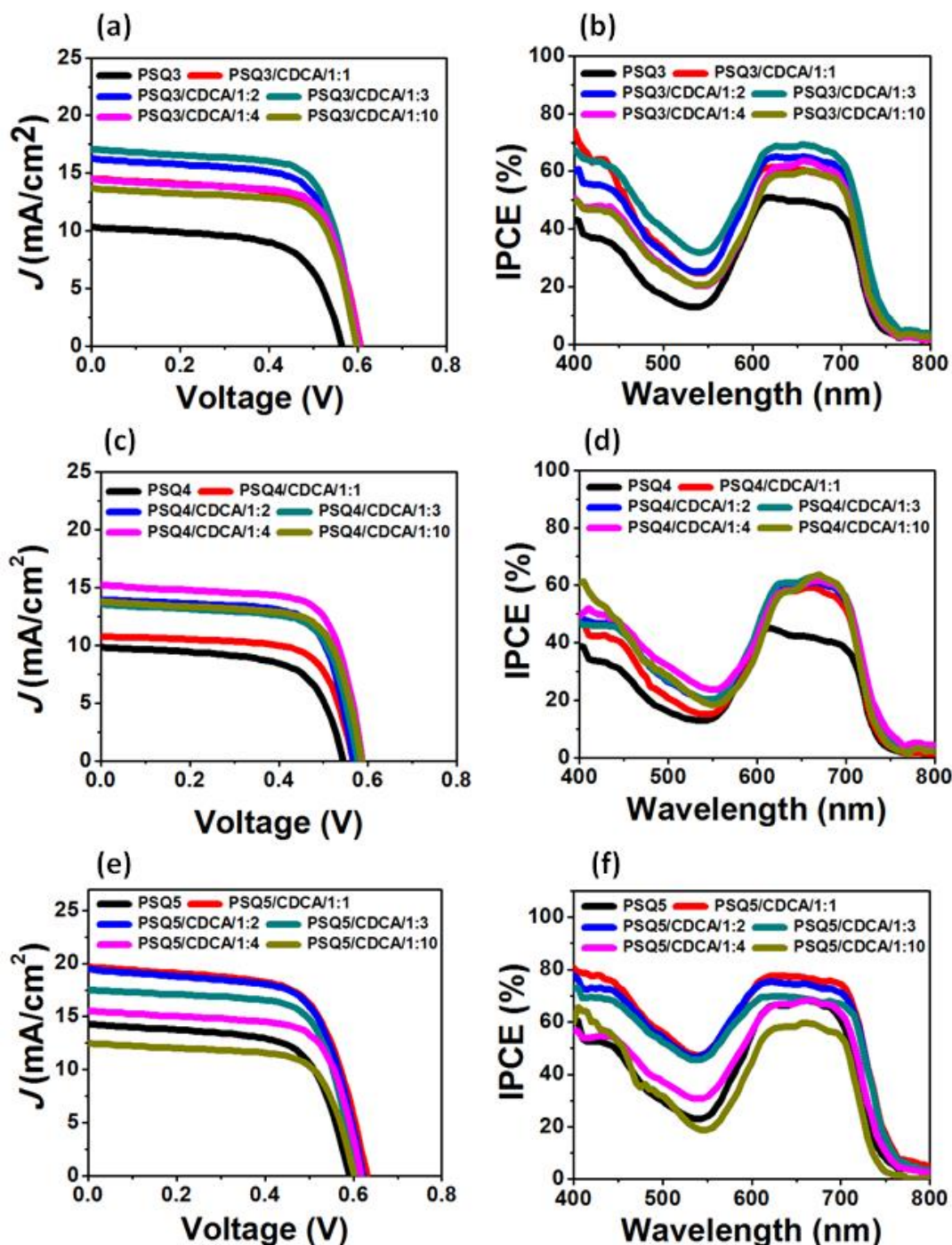


**Figure 2.15** I-V curve and IPCE profile of PSQ3-5, a-f, in  $\text{CHCl}_3$ . (a) and (b) I-V and IPCE curves for PSQ1-5 in absence of CDCA. (c) and (d) I-V and IPCE curves of best device for PSQ1-5 in presence of CDCA (TiO<sub>2</sub> electrode thickness = 8 + 4  $\mu\text{m}$  (transparent+scattering layer), area = 0.22 cm<sup>2</sup>, [Dye] = 0.1 mM in  $\text{CHCl}_3$ , dipping time 12 h at rt, electrolyte: iodolyte Z-50 from Solaronix).

**Table 2.5** *I-V* characteristics of **PSQ3**, **PSQ4** and **PSQ5** dyes with and without CDCA

[Dye]/ mM	[CDCA]/mM	$J_{sc}$ (mA/cm <sup>2</sup> )	$V_{oc}$ (V)	$ff$ (%)	$\eta$ (%)	Dye loading mol/cm <sup>2</sup>
<b>PSQ3/0.1</b>	0	10.30	0.565	63.8	3.71	$2.09 \times 10^{-7}$
<b>PSQ3/0.1</b>	0.1	14.55	0.607	68.1	6.01	$1.29 \times 10^{-7}$
<b>PSQ3/0.1</b>	0.2	16.25	0.598	69.2	6.72	$1.39 \times 10^{-7}$
<b>PSQ3/0.1</b>	0.3	17.11	0.600	70.2	7.21	$1.26 \times 10^{-7}$
<b>PSQ3/0.1</b>	0.4	14.47	0.604	71.1	6.21	$1.21 \times 10^{-7}$
<b>PSQ3/0.1</b>	1	13.68	0.597	71.5	5.84	$0.77 \times 10^{-7}$
<b>PSQ4/0.1</b>	0	9.83	0.545	64.6	3.46	$1.6 \times 10^{-7}$
<b>PSQ4/0.1</b>	0.1	10.82	0.567	69.9	4.29	$0.86 \times 10^{-7}$
<b>PSQ4/0.1</b>	0.2	13.94	0.567	71.1	5.62	$0.89 \times 10^{-7}$
<b>PSQ4/0.1</b>	0.3	14.28	0.577	70.4	5.80	$0.91 \times 10^{-7}$
<b>PSQ4/0.1</b>	0.4	15.21	0.587	71.3	6.36	$0.72 \times 10^{-7}$
<b>PSQ4/0.1</b>	1	13.84	0.586	70.7	5.73	$0.56 \times 10^{-7}$
<b>PSQ5/0.1</b>	0	14.28	0.590	66.1	5.57	$1.45 \times 10^{-7}$
<b>PSQ5/0.1</b>	0.1	19.73	0.630	65.6	8.15	$1.17 \times 10^{-7}$
<b>PSQ5/0.1</b>	0.2	19.47	0.621	66.7	8.06	$1.22 \times 10^{-7}$
<b>PSQ5/0.1</b>	0.3	17.45	0.606	70.1	7.41	$1.13 \times 10^{-7}$
<b>PSQ5/0.1</b>	0.4	15.57	0.617	69.5	6.68	$1.09 \times 10^{-7}$
<b>PSQ5/0.1</b>	1	12.51	0.602	69.5	5.23	$0.82 \times 10^{-7}$

### 2.2.7 Electrochemical Impedance Analysis

The dye cell performance can be correlated with electron injection and collection efficiency, electron transport resistance and interfacial charge transfer processes. In this report, the influence of dye structure on PCE was explained using interfacial charge transfer process.<sup>68-70</sup> Difference



in the  $J_{sc}$  and  $V_{oc}$  of top indoline in-plane and out-of-plane alkylated **PSQ1** and **PSQ3** versus bottom indoline alkylated **PSQ2** and **PSQ4** showed a unique effect of position of alkyl groups on D-A-D- $\pi$ -A  $\pi$ -framework. Apart from that, the smaller dihedral angle ( $\theta$ ) of thiophene  $\pi$ -spacers sharing with D-A-D unit can increase the injection efficiency ( $\eta_{inj}$ ) of **PSQ3-5** and these dyes may possess different way of orientation on  $TiO_2$ . To get insight into the contribution of  $\pi$ -spacers and position of in-plane/out-of-plane alkyl groups to PCE, the electron transfer reactions at the interfaces were examined. Particularly, the recombination reaction between  $TiO_2$  electrons and electrolyte at dye cell's heterogeneous interfaces has been studied using impedance analysis to clarify the  $I$ - $V$  characteristics of PSQ series. The Nyquist plot of best PSQ devices, **Figure 2.16a** shows the current response to the application of an ac voltage as a function of the frequency, all measurements carried out in the dark. The radius of intermediate frequency region reveals  $TiO_2$ -Dye/Electrolyte interface charge recombination resistance ( $R_{ct}$ ). Generally the uncertainty of dye cell's  $V_{oc}$  originates from a shift of the  $TiO_2$  electron quasi-Fermi-level ( $E_{F,n}$ ) and the position of Fermi level of electrolyte ( $E_{F,redox}$ ), Eq 2.1.<sup>71-72</sup> For this study electrolytes used in **PSQ1-5** were same, so the contribution from the movement of  $E_{F,redox}$  is negligible. The Eq 2.2 shows the parameters effecting  $E_{F,n}$ , where  $k_B$  is the Boltzmann constant,  $T$  is the absolute temperature (293 K),  $n_c$  is the free electron density, and  $N_c$  represents the density of accessible states in the conduction band.<sup>4</sup> Thus either conduction band edge shift or change in chemical capacitance of  $TiO_2$  infers the cell potential. (**Table 2.6**)

$$V_{oc} = E_{(F,redox)} - E_{(F,n)} \quad (2.1)$$

$$E_{(F,n)} = E_{CB} + k_B T \ln(n_c/N_c) \quad (2.2)$$

Among the five PSQ dyes, **PSQ5** showed large radius for mid frequency region at -0.5V applied bias in **Figure 2.16** and showed the high  $R_{ct}$  of **PSQ5** vs applied potentials. The high impedance at the  $TiO_2$ -dye/Electrolyte interface indicates the minimum recombination reactions and which is mainly due to the passivation of  $TiO_2$  by closely packed dye monolayer. Recombination resistance for upper-branched PSQ dyes was higher than their isomers, and after increasing the chain length of out-of-plane branching from  $C_8C_{10}$  (**PSQ3**) to  $C_{10}C_{12}$  (**PSQ5**) the  $R_{ct}$  value also increased. For applied bias of -0.5 V,  $R_{ct}$  of PSQs were in the order of **PSQ5** (32.86  $\Omega$ )>**PSQ3** (25.67  $\Omega$ )> **PSQ1** (20.24  $\Omega$ )>**PSQ4** (16.75  $\Omega$ )>**PSQ2** (15.66  $\Omega$ ). For **PSQ5**, this result was ascribed to the high impedance of injected electrons present in the conduction

band of TiO<sub>2</sub> against oxidizing agents in the electrolyte under dark condition. The similar trend of  $R_{ct}$  was observed in  $V_{oc}$  of PSQs as **PSQ5**>(630 mV), **PSQ3** (600 mV), >**PSQ4** (587 mV).

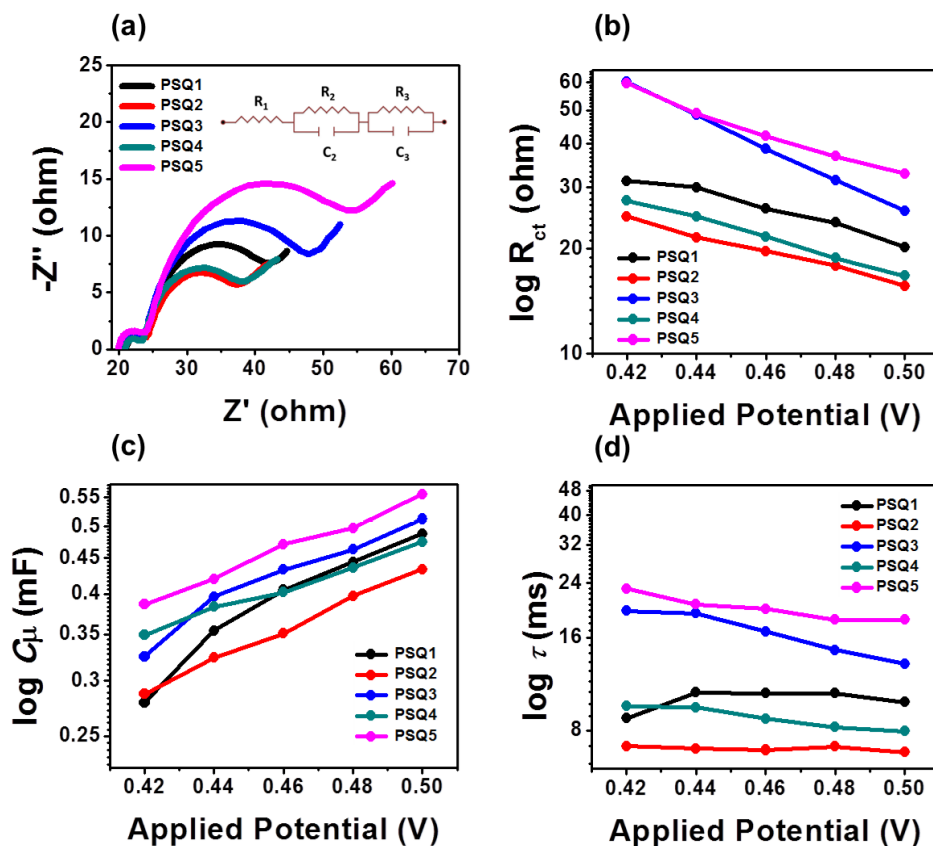


**Figure 2.16** Impedance analysis of PSQ dyes: (a) Nyquist plot (inset shows the equivalent circuit), (b)  $\log R_{ct}$  vs applied potential, (c)  $\log C_{\mu}$  vs applied potential and (d)  $\log \tau$  vs applied potential for best efficiency devices (**PSQ1**: CDCA 1:3, **PSQ2**: CDCA 1:4, **PSQ3**: CDCA 1:3, **PSQ4**: CDCA 1:4, **PSQ5**: CDCA 1:1).

Therefore the observed high  $R_{ct}$  of **PSQ5** indicates the better passivation of surface from redox couple than other PSQs, which reduces the recombination reactions and increases the PCE. Capacitance ( $C_{\mu}$ ) of the sensitized TiO<sub>2</sub> film closely related to the  $V_{oc}$  of the DSSC as shown in eq 2.2, shift in the conduction-band-edge or the number free electrons in the density states governs the potential of PSQ dye cell. **Figure 2.16c** explains the observed increase in the  $V_{oc}$  of **PSQ5** and the difference in PSQ isomers as the capacitance of **PSQ1** and **PSQ3** were higher than the **PSQ2** and **PSQ4**. Long electron lifetime ( $\tau = R_{ct} \times C_{\mu}$ ) of **PSQ1** and **PSQ3** than their isomers, as shown in **Figure 2.16d**, elucidated the improvement in their  $J_{sc}$  and  $V_{oc}$  values. Better

orientation of top-alkylated PSQ dyes, via transferring a dynamic aggregation to more organized static aggregation on surface, passivated the charge in conduction band from triiodide present at the interface of thiophene substituted **PSQ3** and **PSQ5** exhibited improved the current and voltage.

**Table 2.63** EIS parameters of PSQ dye cells at -0.5 V applied potential in dark

DSSC	$R_s$ (ohm)	$R_{ct}$ (ohm)	$C_{\mu}$ (mF)	$\tau$ (ms)
<b>PSQ1/CDCA</b> (1:3)	21.01	20.24	0.49	9.92
<b>PSQ2/CDCA</b> (1:4)	20.78	15.66	0.43	6.73
<b>PSQ3/CDCA</b> (1:3)	19.89	25.67	0.51	13.09
<b>PSQ4/CDCA</b> (1:4)	20.90	16.75	0.47	7.87
<b>PSQ5/CDCA</b> (1:1)	20.05	32.86	0.56	18.41

### 2.3 Summary

In summary, a systematic study was carried out to understand the role of  $\pi$ -spacers and position of alkyl functionalities in D-A-D- $\pi$ -A unsymmetrical squaraine dye for device cell. Furthermore, squaraines possess well known aggregated induced spectral features and their controlled aggregated nature on TiO<sub>2</sub> surface was not well explored by utilizing the formation of dynamic aggregation in solution for DSSC. Selective alkyl functionalisation of indoline units in D-A-D part of the sensitizer becomes one of the crucial part in the nature of self-assembled monolayers on TiO<sub>2</sub> surface. These transient aggregates in solution would be controlled the mode of dye anchoring and showed more impact on PCE. The contribution of four positional isomers were examined to elucidate the significance in position of in-plane out-of-plane branching, in which their photovoltaic properties enhanced in case these positional units are far away from the dye anchoring TiO<sub>2</sub> surface. Thiophene-based **PSQ3** showed PCE of 7.21% which was comparatively high  $J_{sc}$  than phenyl counterpart. Even though the amount of each dyes (**PSQ1** to

**PSQ4**) adsorbed on TiO<sub>2</sub> surface were almost same, the difference in  $J_{sc}$  and  $V_{oc}$  further highlight our hypothesis. **PSQ5** showed a significant improvement in  $J_{sc}$  and  $V_{oc}$  after extending the length of out-of-plane of PSQ3 in absence of optically transparent co-adsorbent. Furthermore, a DSSC sensitized with **PSQ5** showed PCE of 8.15% with a corresponding  $J_{sc}$  and  $V_{oc}$  of 19.73 mA cm<sup>-2</sup> and 630 mV, respectively. Orientation and dye loading on TiO<sub>2</sub> surface is effectively depending on the sensitizer's structure as well as extend of aggregation in solution. This is the first report whereas mimicking the molecular structure of loosely bound aggregates in solution on nanoscopic surface of a dye cell.

## 2.4 Experimental Section

**2.4.1 Materials and Characterization** For dye synthesis and DSSC fabrication, all reagents and solvents purchased from commercial sources were used without further purification unless otherwise noted. Tetrahydrofuran and toluene were dried by standard procedure prior to use. Required precursors **2a**, **3a**, **3b**, **4a**, **5a**, **5b** and **6a** were synthesized according to the reported literature procedure.<sup>44, 58</sup> All oxygen- and moisture-sensitive reactions were performed under nitrogen atmosphere. <sup>1</sup>H NMR spectra were recorded on a 200 MHz or 400 MHz or 500 MHz spectrometers, using CDCl<sub>3</sub>. All chemical shifts were reported in parts per million (ppm). <sup>1</sup>H NMR chemical shifts were referenced to TMS (0 ppm). <sup>13</sup>C NMR chemical shifts were referenced to CDCl<sub>3</sub> (77.23 ppm, and recorded on either 100 MHz or 125 MHz NMR spectrometer). HRMS and MALDI-TOF-MS were recorded on SYNAPT G2 HDM spectrometer and ABSciex 5800 MALDI TOF mass spectrometer, respectively. UV-vis absorption spectra were recorded on Analytikjena (SPECORD 210 PLUS) spectrophotometer. A three electrode cell was used for cyclic voltammetric (CV) analysis was performed on BioLogic SP300 potentiostat. Platinum wire used as a working electrode, a thin platinum foil was used as a counter electrode, and dyes were dissolved in dry dichloromethane. Measurements were carried out at the scan rate of 50 mV s<sup>-1</sup> after addition of 0.1 M of tetra butyl ammonium perchlorate (TBAP) as the supporting electrolyte and non-aqueous Ag/Ag<sup>+</sup> (0.01M in CH<sub>3</sub>CN) used as reference electrode. The reference electrode was calibrated by recording the cyclic voltammograms of ferrocene in the same electrolyte as external standard; the potential values are on the basis of the estimated value of the ferrocene redox potential in dichloromethane 0.7 V versus NHE.<sup>64</sup> EIS analysis was performed under dark condition by applying external bias to dye cells using a BioLogic SP300

potentiostat equipped with frequency response analyzer. Frequency range was fixed from 1 MHz to 10 mHz with AC amplitude of 10 mV. *I-V* characteristics of the dye cells were measured under a solar simulator (PET, CT200AAA) in clean room conditions, which is controlled by a source measurement unit (Keithley 2420). A certified 4 cm<sup>2</sup> silicon solar cell (NREL) was calibrated to an intensity of 1000 W m<sup>-2</sup> (xenon lamp, 450 W, USHIO INC) of a solar simulator (AM1.5 G light). IPCE spectra measurements were conducted by Newport QE measurement kit including a xenon light source, a monochromator, and a power meter. The set-up was calibrated using a reference silicon solar cell before the device measurement.

**2.4.2 Device Fabrication Procedure** For fabricating photoanode of DSSC, FTO (F-doped SnO<sub>2</sub> glass; 6-8 Ω/sq) was cleaned sequentially by mucasol (2% in water), deionized water, and isopropanol using an ultra-sonication for 15 min. A blocking layer of TiO<sub>2</sub> was prepared by dipping cleaned FTO substrate in freshly prepared aqueous 0.05 M TiCl<sub>4</sub> solution at 70 °C for 30 min, and washed immediately with deionized water, and followed by annealing in air at 125 °C for 10 min. And the mesoscopic transparent thin layer (6-8 μm thickness) of TiO<sub>2</sub> onto buffer layer modified FTO was coated using TiO<sub>2</sub> paste (< 20 nm, Ti-Nanoxide T/SP) by the doctor-blade technique. Then kept in air for 5 min and annealed at 125 °C in air for 15 min before coating scattering layer on it. Dyesol, WER2-O paste was used to coat a 4-6 μm thick TiO<sub>2</sub> layer, kept in air for 5 min and annealed at 125 °C in air for 15 min. Resulting 0.22 cm<sup>2</sup> active area films were sintered at 325 °C for 5 min, 375 °C for 5 min, 450 °C for 15 min and 500 °C for 15 min with heating rate of 5 °C per min in air. After reaching the furnace temperature at 50 °C, sintered films were treated in TiCl<sub>4</sub> solution as described before. After sintering the layer-by-layer deposited film again at 500 °C for 30 min, allowed to reach 50 °C and were immediately immersed in 0.1 mM **PSQ1-5** dye solution in chloroform at room temperature for 12 h. The dye loaded electrodes are washed thoroughly with chloroform, to remove physisorbed molecules. Successive addition of co-adsorbent 3α,7α-dihydroxy-5β-cholanic acid (CDCA) was varied the concentration of de-aggregating agent in the dye solution and studied the device performance at 1, 2, 3, 4 and 10 equiv of CDCA. Finally the dye cell was assembled by joining the electrolyte (Iodolyte Z50) filled photoanode and platinum cathode using a 25 μm thick spacer. Photovoltaic parameters have been evaluated without masking the device.

**2.4.3 Relative method Procedure** Fluorescence quantum yields were measured by the relative method<sup>44</sup> using optically matched dilute solutions. 4, 4'-[Bis-(N, N-dimethylamino) phenyl]-squaraine dye (DM-SQ) was used as the standard. The quantum yields of fluorescence were calculated using the eq 2.3,

$$\Phi_u = (A_s F_u n_u^2 / A_u F_s n_s^2) \times \Phi_s \dots \dots \dots (2.3)$$

where  $A_s$  and  $A_u$  are the absorbance of the standard (DM-SQ) and unknown (SQ) dye, respectively;  $F_s$  and  $F_u$  are the integrated areas of fluorescence peaks of the DM-SQ and SQ dye, respectively; and  $n_s$  and  $n_u$  are the refractive indices of the solvents in which standard and unknown compounds were dissolved, respectively.  $\Phi_s$  and  $\Phi_u$  are the fluorescence quantum yields of the standard (DM-SQ) and unknown (SQ) dye, respectively.

To synthesise of 4,4'-[Bis-(N,N-dimethylamino) phenyl]-squaraine (DM-SQ), 3,4-dihydroxycyclobut-3-ene-1,2-dione (250 mg, 2.2 mmol) and N,N-dimethylaniline (532 mg, 4.4 mmol) were dissolved in a mixture of n-Butanol: benzene (7.5: 3 mL) and refluxed in Dean-Stark apparatus for 12 h in presence of  $N_2$  gas. After cooling at room temperature the blue coloured compound was precipitated and the solvent was decanted. The precipitate was washed four times with a mixture of dichloromethane (4 mL) and hexane (1 mL).

#### 2.4.4 Synthetic Procedures and Characterization Data

**2-Decyltetradecanal (A):** 2-Decyl-1-tetradecanol (4.4 g, 12.5 mmol) was taken in a 100 mL round bottomed flask, pyridiniumchlorochromate (8.1 g, 37.6 mmol) was added to it and the mixture was dissolved in anhydrous  $CH_2Cl_2$  (120 mL). The reaction mixture was stirred at room temperature for 3 h and filtered through a short pad of silica gel to provide the required aldehyde as a colourless liquid. Yield: 4.1 g, 94%.  $^1H$  NMR (500 MHz,  $CDCl_3$ )  $\delta$ : 9.55 (d,  $J = 3.2$  Hz, 1H), 2.40–2.29 (m, 1H), 1.62–1.56 (m, 2H), 1.47–1.43 (m, 2H), 1.25 (br. s, 36 H), 0.89–0.87 (m, 6H);

**3-Decylpentadecan-2-ol (B):** 2-Decyltetradecanal (4.4 g, 12.5 mmol) was dissolved in dry THF (20 mL) at 0 °C, and then MeMgI (3.3 mL, 25.1 mmol) was slowly added. The mixture was stirred at 0 °C for half h, and then it was allowed to stir for 2 h at room temperature, then quenched by adding saturated aqueous solution of ammonium chloride, extracted with ethyl acetate and dried over  $Na_2SO_4$ . The organic layer was concentrated under reduced pressure to

afford as a colourless liquid. Yield: 4.5 g, 97%. This product was used further reaction without purification.

**3-Decylpentadecan-2-one (C):** 3-Decylpentadecan-2-ol (4.3 g, 11.8 mmol) was taken in a 100 mL round bottomed flask, pyridiniumchlorochromate (5.1 g, 23.6 mmol) was added to it and the mixture was dissolved in anhydrous  $\text{CH}_2\text{Cl}_2$  (120 mL). The reaction mixture was stirred at room temperature for 3 h and filtered through a short pad of silica gel to provide the required ketone as a colourless liquid. 2.4 g, Yield: 55%.  $^1\text{H}$  NMR (500 MHz,  $\text{CDCl}_3$ )  $\delta$ : 2.48 - 2.28 (m, 1 H), 2.10 (s, 3 H), 1.65 - 1.48 (m, 2 H), 1.44 - 1.34 (m, 2 H), 1.33 - 1.11 (m, 36 H), 0.87 (t,  $J = 7.1$  Hz, 6 H);  $^{13}\text{C}$  NMR (126 MHz,  $\text{CDCl}_3$ )  $\delta$ : 213.2, 53.4, 31.9, 31.7, 29.7, 29.6, 29.6, 29.5, 29.3, 28.6, 27.4, 22.7, 14.1; MALDI-TOF ( $m/z$ ):  $[\text{M}+\text{Na}]^+$  calcd for  $\text{C}_{25}\text{H}_{50}\text{O}$ : 389.3762; found: 389.3605.

**General procedure for the synthesis of 5-bromo-2-methyl-3,3-dialkyl-3H-indole (2b) and 2-methyl-3,3-dialkyl-3H-indole (2c):**

4-Bromo Phenyl hydrazine hydrochloride or phenyl hydrazine hydrochloride (1 equiv.), corresponding 3-alkyl-2-alkanone (2 equiv.) were dissolved in acetic acid (50mL) in a 100 mL round bottom flask. The reaction mixture was heated to reflux for 16 h under nitrogen atmosphere. The reaction mixture was cooled and then solvent was removed under reduced pressure and purified by column chromatography (100-200 mesh  $\text{SiO}_2$ , EtOAc: Pet.ether, 2:98) to provide the required compound as a viscous liquid.

**5-Bromo-3-decyl-2-methyl-3-octyl-3H-indole (2b):** Started with 0.4 g (1.8 mmol) of (4-bromophenyl)hydrazine hydrochloride, product obtained: 0.64 g, Yield: 78%;  $^1\text{H}$  NMR (400MHz,  $\text{CDCl}_3$ )  $\delta$ : 7.42 (dd,  $J = 8.2$  Hz,  $J = 2.0$  Hz, 1 H), 7.37 (d,  $J = 8.2$  Hz, 1 H), 7.2 (d,  $J = 2.0$  Hz, 1 H), 2.18 (s, 3 H), 1.91 - 1.61 (m, 4 H), 1.33 - 1.03 (m, 24 H), 0.85 (q,  $J = 7.2$  Hz, 6 H), 0.75 - 0.62 (m, 2 H), 0.62 - 0.47 (m, 2 H);  $^{13}\text{C}$  NMR (100 MHz,  $\text{CDCl}_3$ )  $\delta$ : 187.2, 154.1, 144.7, 130.6, 124.9, 120.9, 118.9, 63.3, 36.9, 31.9, 31.8, 31.7, 30.3, 30.2, 29.7, 29.6, 29.5, 29.3, 29.2, 29.2, 29.1, 23.7, 23.5, 22.6, 22.6, 16.1, 14.1, 14.1; MALDI-TOF ( $m/z$ ):  $[\text{M}]^+$  calcd for  $\text{C}_{27}\text{H}_{44}\text{BrN}$ : 462.2736; found: 462.1292.

**3-Decyl-3-dodecyl-2-methyl-3H-indole (2c):** Started with 0.65 g (4.5 mmol) of phenylhydrazine hydrochloride, product obtained: 1.2 g, Yield: 65%;  $^1\text{H}$  NMR (500 MHz,

CDCl<sub>3</sub>) δ: 7.50 (d, *J* = 7.6 Hz, 1 H), 7.29 (td, *J* = 4.1, 8.1 Hz, 1 H), 7.18 (d, *J* = 4.2 Hz, 2 H), 2.20 (s, 3 H), 1.92 - 1.78 (m, 2 H), 1.78 - 1.64 (m, 2 H), 1.30 - 1.06 (m, 32 H), 0.97 - 0.81 (m, 6 H), 0.78 - 0.64 (m, 2 H), 0.62 - 0.43 (m, 2 H); <sup>13</sup>C NMR (126 MHz, CDCl<sub>3</sub>) δ: 186.5, 155.3, 142.3, 127.4, 124.8, 121.6, 119.6, 62.6, 37.0, 31.9, 31.8, 29.8, 29.6, 29.5, 29.5, 29.3, 29.2, 29.2, 23.5, 22.7, 22.6, 16.1, 14.1; MALDI-TOF (*m/z*): [M]<sup>+</sup>calcd for C<sub>31</sub>H<sub>53</sub>N: 439.4178; found: 439.4259.

**General procedure for Synthesis of 5-bromo-1,2,3,3-tetraalkyl-3H-indol-1-ium iodide (4b) and 1-alkyl-2-methyl-3,3-dialkyl-3H-indol-1-ium iodide (4c):**

Alkyl iodide (2 equiv.) and indole derivative (1 equiv.) were dissolved in MeCN (30 mL) in a 100 mL round bottom flask and refluxed for 16 h under inert atmosphere for 24 h. The reaction mixture was cooled to room temperature; the solvent was removed under reduced pressure. The precipitate was washed with diethyl ether (4× 5 mL) to afford the required compound and 90% petroleum ether to afford the required compound.

**5-Bromo-3-decyl-1-hexyl-2-methyl-3-octyl-3H-indol-1-ium iodide (4b):** Started with 0.4 g (0.86 mmol) of 5-bromo-3-decyl-2-methyl-3-octyl-3H-indole, product obtained: 0.26 g, Yield: 50%; <sup>1</sup>H NMR (500 MHz, CDCl<sub>3</sub>) δ: 7.84 (d, *J* = 8.8 Hz, 1 H), 7.76 (dd, *J* = 8.0 Hz, *J* = 2.0 Hz, 1 H), 7.64 (d, *J* = 2.0 Hz, 1 H), 4.83 (t, *J* = 7.5 Hz, 2 H), 3.08 (s, 3 H), 2.19 - 1.99 (m, 4 H), 1.94 - 1.84 (m, 2 H), 1.84 - 1.67 (m, 1 H), 1.54 - 1.39 (m, 2 H), 1.31 - 1.07 (m, 30H), 0.90 - 0.70 (m, 11 H), 0.69 - 0.53 (m, 2 H); <sup>13</sup>C NMR (100 MHz, CDCl<sub>3</sub>) δ: 195.7, 141.1, 140.7, 133.0, 126.7, 124.6, 117.4, 63.8, 50.7, 37.1, 33.4, 31.7, 31.5, 31.2, 30.6, 30.0, 29.3, 29.1, 28.9, 28.9, 28.8, 28.5, 26.4, 24.0, 22.5, 22.4, 22.3, 22.2, 17.4, 13.9, 13.9, 13.8; MALDI-TOF (*m/z*): [M]<sup>+</sup>calcd for C<sub>33</sub>H<sub>57</sub>BrN<sup>+</sup>: 546.3669; found: 546.2598.

**3-Decyl-1,3-didodecyl-2-methyl-3H-indol-1-ium iodide (4c):** Started with 0.73 g (1.6 mmol) of 3-decyl-3-dodecyl-2-methyl-3H-indole, product obtained: 0.54 g, Yield: 44%; <sup>1</sup>H NMR (500 MHz, CDCl<sub>3</sub>) δ: 7.76 (d, *J* = 6.5 Hz, 1 H), 7.67 - 7.56 (m, 2 H), 7.51 (d, *J* = 6.5 Hz, 1 H), 4.80 (t, 2 H), 3.08 (s, 3 H), 2.22 - 2.02 (m, 4 H), 1.97 - 1.78 (m, 4 H), 1.52 - 1.40 (m, 3 H), 1.40 - 1.10 (m, 45 H), 0.90 - 0.70 (m, 11 H), 0.65 - 0.50 (m, 2 H); <sup>13</sup>C NMR (126 MHz, CDCl<sub>3</sub>) δ: 195.5, 142.1, 138.7, 130.1, 129.7, 123.6, 115.4, 77.3, 76.7, 63.7, 50.3, 37.3, 33.4, 31.7, 31.7, 30.3, 29.8, 29.4, 29.4, 29.3, 29.3, 29.2, 29.1, 29.0, 28.9, 28.5, 28.4, 26.8, 23.9, 22.5, 17.1, 13.9; MALDI-TOF (*m/z*): [M]<sup>+</sup>calcd for C<sub>43</sub>H<sub>78</sub>N<sup>+</sup>: 608.6129; found: 608.5602.



---

**General procedure for Synthesis of 3-Butoxy-4-[(1-methyl-1,3-dihydro-3,3-dimethyl-2H-indol-2-ylidene)methyl]-3-cyclobutene-1,2-dione (6a) and 3-Butoxy-4-[5-bromo-((1-methyl-1,3-dihydro-3,3-dimethyl-2H-indol-2-ylidene)methyl)]-3-cyclobutene-1,2-dione (6b):**

5-bromo-1,2,3,3-tetraalkyl-3H-indol-1-ium iodide (1 equiv.) and 3, 4-dibutoxycyclobut-3-ene-1,2-dione (1 equiv) were dissolved in 1-butanol in a 50 mL two necked round bottom flask and triethylamine (1.2 equiv) was added into the reaction mixture. The reaction mixture was heated at 70°C for 1 h under nitrogen atmosphere. The reaction mixture cooled to room temperature, and the solvents were removed under reduced pressure. The reaction mixture was purified by column chromatography (SiO<sub>2</sub>, 100-200 mesh, 10% ethyl acetate and 90% petroleum ether) to afford the required compound as a yellow solid.

**3-Butoxy-4-[5-bromo-((1-methyl-1,3-dihydro-3,3-dimethyl-2H-indol-2-ylidene)methyl)]-3-cyclobutene-1,2-dione (6b):** Started with 0.5 g (1.3 mmol) of 5-Bromo-3-decyl-1-hexyl-2-methyl-3-octyl-3H-indol-1-ium iodide, product obtained: 0.26 g, Yield: 50%. <sup>1</sup>H NMR (400 MHz, CDCl<sub>3</sub>) δ: 7.41 - 7.33 (m, 2 H), 6.74 (d, *J* = 8.5 Hz, 1 H), 4.84 (t, *J* = 6.7 Hz, 2 H), 3.33 (s, 3 H), 1.90 - 1.78 (m, 2 H), 1.60 (s, 6 H), 1.54 - 1.44 (m, 2 H), 0.99 (t, *J* = 7.3 Hz, 3 H); <sup>13</sup>C NMR (100 MHz, CDCl<sub>3</sub>) δ: 192.3, 188.3, 188.1, 173.3, 167.9, 142.7, 142.2, 130.6, 125.3, 115.4, 115.0, 109.3, 82.0, , 73.9, 47.7, 32.1, 30.0, 29.6, 26.9, 18.6, 13.6 ; MALDI-TOF (*m/z*): [M]<sup>+</sup>calcd for C<sub>20</sub>H<sub>22</sub>BrNO<sub>3</sub>: 403.0783; found: 403.9487.

**General procedure for Synthesis of Unsymmetrical Bromo Squaraine Precursor (7 a, 7 b and 7c):**

1,2,3,3-Tetraalkyl-3H-indol-1-ium iodide (1 equiv.) **4a-c** and semisquaraine derivatives, **6a-b** (1 equiv.) were dissolved in 1-butanol and dry toluene (1:1, 3 mL each) in a 50 mL two necked round bottom flask, dry pyridine (1.5 equiv.) was added to it and charged with Dean-Stark apparatus. The reaction mixture was refluxed for 24 h under inert atmosphere. The reaction mixture was cooled to room temperature and the solvents were removed under reduced pressure. The reaction mixture was subjected to column chromatography (SiO<sub>2</sub>, 100-200 mesh, 5% MeOH and 95% CH<sub>2</sub>Cl<sub>2</sub>) to afford the required dye as blue colored compound.

**5-Bromo-2-[[3-[(1,3-dihydro-3-decyl-1-hexyl-3-octyl-2H-indol-2-ylidene)methyl]-4-oxo-2-cyclobuten-2-olate-1-ylidene]methyl]-1,3,3-trimethyl-3H-indolium (7a):**

Started with 1.1 g (2.7 mmol) of **6b**, product obtained: 1.9 g, Yield: 90%. <sup>1</sup>H NMR (400 MHz, CDCl<sub>3</sub>) δ: 7.43 - 7.36 (m, 2 H), 7.34 - 7.30 (m, 2 H), 7.28 (m, 1 H), 7.02 (d, *J* = 8.0 Hz, 1 H), 6.82 (d, *J* = 8.4 Hz, 1 H), 6.10 (br s, 1 H), 5.89 (s, 1 H), 4.03 (br s, 2 H), 3.47 (s, 3 H), 3.03 (br s, 2 H), 1.93 (m, 2 H), 1.8 (s., 6 H), 1.6 - 1 (m, 32 H), 1 - 0.6 (m, 11 H), 0.47 (m, 2 H); <sup>13</sup>C NMR (100 MHz, CDCl<sub>3</sub>) δ: 181.6, 177.6, 169.8, 168.2, 144.0, 143.9, 142.2, 139.2, 130.5, 127.7, 127.1, 125.5, 124.1, 122.3, 122.0, 117.8, 115.7, 109.8, 109.3, 104.4, 87.8, 86.9, 59.0, 48.7, 43.9, 39.9, 31.8, 31.7, 31.6, 31.5, 30.3, 29.9, 29.6, 29.5, 29.5, 29.4, 29.3, 29.2, 29.1, 29.0, 27.3, 27.2, 26.9, 26.8, 26.0, 24.0, 24.0, 23.9, 22.5, 22.5, 14.0, 13.9; MALDI-TOF (*m/z*): [M]<sup>+</sup> cald for C<sub>49</sub>H<sub>69</sub>BrN<sub>2</sub>O<sub>2</sub>: 796.4542; found: 796.3585.

**5-Bromo-2-[[3-[(1,3-dihydro-1,3,3-trimethyl-2H-indol-2-ylidene)methyl]-4-oxo-2-cyclobuten-2-olate-1-ylidene]methyl]-3-decyl-1-hexyl-3-octyl-3H-indolium (7b):**

Started with 0.16 g (0.59 mmol) of **6a**, product obtained: 0.39 g, Yield: 82 %; <sup>1</sup>H NMR (500 MHz, CDCl<sub>3</sub>) δ: 7.42 (dd, *J* = 8.2, 1.7 Hz, 1 H), 7.39 - 7.29 (m, 3 H), 7.16 (t, *J* = 7.4 Hz, 1 H), 7.02 (d, *J* = 8.0 Hz, 1 H), 6.82 (d, *J* = 8.4 Hz, 1 H), 6.04 (s, 1 H), 5.96 (br. s., 1 H), 3.94 (t, *J* = 7.6 Hz, 2 H), 3.56 (br s, 3 H), 3.17 - 2.93 (m, 2 H), 2.02 - 1.87 (m, 2 H), 1.87 - 1.63 (m, 6 H), 1.49 - 1.37 (m, 2 H), 1.37 - 1.28 (m, 4 H), 1.27 - 1.03 (m, 26 H), 0.94 - 0.71 (m, 11 H), 0.60 - 0.40 (m, 2 H); <sup>13</sup>C NMR (126 MHz, CDCl<sub>3</sub>) δ: 182.3, 180.1, 179.5, 170.8, 167.0, 143.4, 141.1, 130.5, 127.7, 125.4, 123.8, 122.1, 116.3, 110.0, 109.1, 87.6, 86.9, 58.5, 49.2, 43.7, 40.0, 40.0, 40.0, 31.7, 31.7, 31.4, 29.5, 29.4, 29.3, 29.1, 29.1, 29.0, 27.1, 27.0, 26.9, 26.8, 24.0, 23.9, 22.5, 22.5, 22.4, 14.0, 13.9, 13.8; MALDI-TOF (*m/z*): [M]<sup>+</sup> cald for C<sub>49</sub>H<sub>69</sub>BrN<sub>2</sub>O<sub>2</sub>: 796.4542; found: 796.3453.

**5-Bromo-2-[[3-[(1,3-dihydro-1,3-didodecyl-3-decyl-2H-indol-2-ylidene)methyl]-4-oxo-2-cyclobuten-2-olate-1-ylidene]methyl]-1,3,3-trimethyl-3H-indolium (7c):**

Started with 0.3 g (0.74 mmol) of **6b**, product obtained: 0.59 g, Yield: 85 %. <sup>1</sup>H NMR (400 MHz, CDCl<sub>3</sub>) δ: 7.42 - 7.38 (m, 2 H), 7.36 - 7.3 (m, 2 H), 7.24 - 7.15 (m, 1 H), 7.02 (d, *J*=8 Hz, 1 H), 6.81 (d, *J*=8.4 Hz, 1 H), 6.11 (br s, 1 H), 5.90 (s, 1 H), 4.03 (br s, 2 H), 3.46 (br s, 3 H), 3.03 (br s, 2 H), 2.09 - 1.9 (m, 2 H), 1.81 (br s, 8 H), 1.50 - 1.04 (m, 52 H), 0.93 - 0.68 (m, 11 H), 0.56 - 0.44 (m, 2 H); <sup>13</sup>C NMR (100 MHz, CDCl<sub>3</sub>) δ: 181.5, 177.5, 169.7, 168.1, 144.0, 143.9, 143.8, 142.1, 139.1, 130.4, 127.6, , 125.4, 124.1, 122.2, 115.7, 109.8, 109.3, 87.8, 86.9, 58.9, 48.6, 43.8, 39.9,

32.0, 31.8, 30.2, 29.9, 29.5, 29.4, 29.2, 29.18, 29.12, 27.3, 27.1, 23.9, 22.6, 22.4, 14.0; MALDI-TOF ( $m/z$ ):  $[M]^+$  calcd for  $C_{49}H_{69}BrN_2O_2$ : 936.6107; found: 936.313.

**General procedure for synthesis of aldehyde derivative of unsymmetrical SQ compounds**

**(8a, 8b, 10a, 10b and 10c):** Bromofunctionalized unsymmetrical squaraine precursors, **7a-c** (1 equiv.) was dissolved in 1:1 ratio of toluene and methanol (total volume 5 mL) in 50 mL microwave reactor vessel and 4-formylphenylboronic acid or 5-formylthiopheneboronic acid (2 equiv.) and  $K_2CO_3$  (5 equiv.) were added to it under  $N_2$  atmosphere. The solution was purged with nitrogen for 20 min and then  $PdCl_2(dppf)$  (0.1 equiv.) was added and the reaction was carried out under microwave condition at 60 W, 70 °C for 15 min. The reaction mixture cooled to room temperature, and the solvents were removed under reduced pressure. The reaction mixture was purified by column chromatography ( $SiO_2$ , 100-200 mesh 5% methanol and 95% dichloromethane to afford the required compound.

**5-(4-Formyl-phen-1-yl)-2-[[3-[(1,3-dihydro-3-decyl-1-hexyl-3-octyl-2H-indol-2-**

**ylidene)methyl]-4-oxo-2-cyclobuten-2-olate-1-ylidene]methyl]-1,3,3-trimethyl-3H-indolium**

**(8a):** Started with 0.1 g (0.12 mmol) of **7a**, product obtained: 87 mg, Yield: 85 %.  $^1H$  NMR (400 MHz,  $CDCl_3$ )  $\delta$ : 10.06 (s, 1 H), 7.96 (d,  $J = 8$  Hz, 2 H), 7.77 (m, 2 H), 7.60 (m, 2 H), 7.32 (m, 2 H), 7.20 (d,  $J = 7.2$  Hz, 1 H), 7.05 (m, 2 H), 6.12 (br. s., 1 H), 5.96 (s, 1 H), 4.04 (br. s, 2 H), 3.54 (s, 3 H), 3.04 (br. s., 2 H), 1.88 (s, 6 H), 1.80 (m, 2 H), 1.5-1.0 (m, 30 H), 1.0-0.8 (m, 11 H), 0.48 (m, 2 H);  $^{13}C$  NMR (100 MHz,  $CDCl_3$ )  $\delta$ : 191.7, 181.3, 177.4, 169.8, 168.7, 146.7, 144.0, 143.6, 142.8, 134.8, 134.6, 130.3, 127.7, 127.2, 127.1, 124.1, 122.3, 121.0, 109.4, 109.0, 87.8, 87.2, 58.9, 48.7, 43.9, 40.0, 39.9, 31.8, 31.7, 31.6, 31.4, 30.3, 30.2, 29.6, 29.5, 29.5, 29.4, 29.3, 29.3, 29.2, 29.1, 29.0, 27.3, 26.8, 24.0, 23.9, 22.5, 22.5, 14.0, 13.9; MALDI-TOF ( $m/z$ ):  $[M]^+$  calcd for  $C_{56}H_{74}N_2O_3$ : 822.5699; found: 822.4362.

**5-(4-Formyl-phen-1-yl)-2-[[3-[(1,3-dihydro-1,3,3-trimethyl-2H-indol-2-ylidene)methyl]-4-**

**oxo-2-cyclobuten-2-olate-1-ylidene]methyl]-3-decyl-1-hexyl-3-octyl-3H-indolium** **(8b):**

Started with 0.1 g (0.12 mmol) of **7b**, product obtained: 83 mg, Yield: 83%.  $^1H$  NMR (500 MHz,  $CDCl_3$ )  $\delta$ : 10.06 (s, 1 H), 7.97 (d,  $J = 8.5$  Hz, 2 H), 7.82 (d,  $J = 8.0$  Hz, 2 H), 7.63 (d,  $J = 10$  Hz, 1 H), 7.55 (s, 1 H), 7.37 (d,  $J = 7$  Hz, 1 H), 7.33 (m, 1 H), 7.28 (m, 1 H), 7.17 (d,  $J = 7.5$  Hz, 1 H), 7.02 (d,  $J = 7.5$  Hz, 1 H), 6.11 (s, 1 H), 5.97 (br. s., 1 H), 4.01 (t,  $J = 7.5$  Hz, 2 H), 3.57

br, s, 3 H), 3.07 ( dt,  $J = 8$  Hz,  $J = 2.5$  Hz, 2 H ), 2.03 (m, 2 H), 1.80 (br, s, 8 H) , 1.5 - 1.06 (m, 30 H), 0.89 - 0.80 (m, 11 H), 0.75 (m, 2 H);  $^{13}\text{C}$  NMR (100 MHz,  $\text{CDCl}_3$ )  $\delta$ : 191.7, 182.4, 179.6, 179.0, 170.9, 167.7, 146.6, 144.8, 139.9, 134.9, 132.2, 130.3, 128.6, 127.3, 127.1, 123.8, 122.2, 120.9, 116.3, 109.2, 88.0, 86.9, 58.5, 49.2, 43.8, 40.1, 31.8, 31.7, 31.5, 29.6, 29.5, 29.5, 29.4, 29.3, 29.2, 29.1, 29.0, 28.8, 27.2, 27.0, 26.8, 24.0, 24.0, 22.6, 22.5, 22.5, 14.0, 13.9; MALDI-TOF ( $m/z$ ):  $[\text{M}]^+$  cald for  $\text{C}_{56}\text{H}_{74}\text{N}_2\text{O}_3$ :822.5699; found: 822.4290.

**5-(5-Formyl-thiophen-2-yl)-2-[[3-[(1,3-dihydro-3-decyl-1-hexyl-3-octyl-2H-indol-2-ylidene)methyl]-4-oxo-2-cyclobuten-2-olate-1-ylidene]methyl]-1,3,3-trimethyl-3H-indolium (10a):** Started with 0.1 g (0.12 mmol) of **7a**, product obtained: 89 mg, Yield: 86%.  $^1\text{H}$  NMR (500 MHz,  $\text{CDCl}_3$ )  $\delta$ : 9.87 (s, 1 H), 7.73 (d,  $J = 4$  Hz, 1 H), 7.62 - 7.60 (dd,  $J = 8$  Hz, 2.5 Hz 1 H ), 7.34-7.28 (m, 2 H), 7.2 (m, 1 H), 7.02 (d,  $J = 8$  Hz, 1 H), 6.96 (d,  $J = 8.5$  Hz, 1 H), 6.11 (br.,s, 1 H), 5.93 (br.,s, 1 H), 4.03 (br.,s, 2 H), 3.49 (br.,s, 3 H), 3.49 (s, 3 H), 3.01 (br.,s, 2 H), 2.0 (m, 2 H), 1.84 (m, 8 H), 1.4 - 1.03 (m, 30 H), 0.82 - 0.72 (m, 11 H), 0.45 - 0.43 (m, 2 H);  $^{13}\text{C}$  NMR (100 MHz,  $\text{CDCl}_3$ )  $\delta$ : 182.5, 181.9, 176.9, 170.4, 168.1, 154.3, 144.3, 144.0, 142.9, 141.7, 137.6, 128.0, 127.8, 126.5, 124.8, 124.4, 123.3, 122.4, 120.1, 109.6, 109.0, 88.1, 87.6, 59.1, 48.5, 44.1, 39.9, 31.9, 31.8, 31.7, 31.6, 31.5, 30.4, 30.3, 29.6, 29.5, 29.52, 29.47, 29.38, 29.3, 29.2, 29.1, 29.0, 27.34, 27.3, 26.8, 24.0, 23.9, 22.6, 22.5, 22.5, 14.0, 13.9; MALDI-TOF ( $m/z$ ):  $[\text{M}+1]^+$  cald for  $\text{C}_{54}\text{H}_{72}\text{N}_2\text{O}_3\text{S}$ :829.5343; found: 829.4586.

**5-(5-Formyl-thiophen-2-yl)-2-[[3-[(1,3-dihydro-1,3,3-trimethyl-2H-indol-2-ylidene)methyl]-4-oxo-2-cyclobuten-2-olate-1-ylidene]methyl]-3-decyl-1-hexyl-3-octyl-3H-indolium (10b):** Started with 0.1 g (0.12 mmol) of **7b**, product obtained: 88 mg, Yield: 85 %.  $^1\text{H}$  NMR (400 MHz,  $\text{CDCl}_3$ )  $\delta$ : 9.87 (s, 1 H), 7.74 (d,  $J = 4.4$  Hz, 1 H), 7.63 (d,  $J = 8.4$  Hz, 1 H), 7.53 (s, 1 H), 7.41 (d,  $J = 4.4$  Hz, 1 H), 7.34 (q, 2 H), 7.164 (t, 1 H), 7.02 (d,  $J = 8$  Hz, 1 H), 6.96 (d,  $J = 8.8$  Hz, 1 H), 6.07 (br.s, 1 H), 5.97 (br. s., 1 H), 3.97 (t, 2 H), 3.58 (br. s., 3 H), 3.03 (t, 2 H), 1.96 (m, 2 H), 1.79 (br. s., 8 H), 1.43 - 1.04 (m, 30 H), 0.895 - 0.73 (m, 11H), 0.5 - 0.49 (m, 2 H);  $^{13}\text{C}$  NMR (100 MHz,  $\text{CDCl}_3$ )  $\delta$ : 182.5, 182.3, 180.8, 179.0, 171.4, 166.8, 154.3, 145.6, 142.8, 141.7, 140.1, 137.5, 128.2, 127.8, 126.5, 124.1, 123.4, 122.3, 119.9, 109.4, 109.2, 88.2, 87.1, 58.3, 49.4, 43.8, 40.1, 31.8, 31.7, 31.5, 30.2, 29.6, 29.5, 29.4, 29.3, 29.2, 29.1, , 29.0, 27.1, 26.9, 26.8, 24.1, 24.0, 22.6, 22.5, 14.0, 13.9; MALDI-TOF ( $m/z$ ):  $[\text{M}+1]^+$  cald for  $\text{C}_{54}\text{H}_{72}\text{N}_2\text{O}_3\text{S}$ :829.5343; found: 829.4407.

**5-(5-Formyl-thiophen-2-yl)-2-[[3-[(1,3-dihydro-1,3-didodecyl-3-decyl-2H-indol-2-ylidene)methyl]-4-oxo-2-cyclobuten-2-olate-1-ylidene]methyl]-1,3,3-trimethyl-3H-indolium (10c):** Started with 0.1 g (0.11 mmol) of **7c**, product obtained: 87 mg, Yield: 85 %. <sup>1</sup>H NMR (500 MHz, CDCl<sub>3</sub>) δ: 9.87 (s, 1 H), 7.7 (d, *J* = 4.2 Hz, 1 H), 7.59 (d, *J* = 8.5 Hz, 1 H), 7.56 (s, 1 H), 7.36 (d, *J* = 4 Hz, 1 H), 7.3 (q, 2 H), 7.18 (t, 1 H), 7.0 (d, *J* = 8 Hz, 1 H), 6.95 (d, *J* = 8.5 Hz, 1 H), 6.09 (br. s., 1 H), 5.91 (s, 1 H), 4.01 (br. s., 2 H), 3.47 (s, 3 H), 3 (br. s., 2 H), 2.0-1.948 (m, 2 H), 1.85 (m, 8 H), 1.43-1.01 (m, 52 H), 0.85 - 0.70 (m, 11 H), 0.47- 0.40 (m, 2 H); <sup>13</sup>C NMR (126 MHz, CDCl<sub>3</sub>) δ: 182.4, 177.1, 170.2, 167.9, 154.2, 144.2, 143.9, 142.8, 141.6, 139.2, 137.5, 131.9, 131.4, 131.3, 131.19, 128.2, 128.1, 128.0, 127.9, 127.7, 126.4, 124.3, 123.3, 122.3, 120.0, 109.5, 108.9, 88.0, 87.5, 69.6, 59.1, 48.4, 44.0, 43.0, 39.9, 31.8, 31.7, 30.3, 29.5, 29.4, 29.3, 29.2, 29.1, 27.3, 27.2, 27.1, 23.9, 22.6, 22.5, 22.5, 14.0, 13.9; MALDI-TOF (*m/z*): [M+Na]<sup>+</sup> calcd for C<sub>64</sub>H<sub>92</sub>N<sub>2</sub>O<sub>3</sub>S:991.6729; found: 991.8636.

**General procedure for synthesis of unsymmetrical SQ final compounds (PSQ1-PSQ5):**

The aldehyde precursor (1 equiv.) was dissolved in dry CH<sub>3</sub>CN (5 mL) in a 50 mL single necked round bottomed flask, cyano acetic acid (3 equiv.) was added and then finally piperidine (2 equiv.) was added into it. The reaction mixture was allowed to reflux for 6 h. After the reaction completion, the solvent was removed and work up with dil. acetic acid and then it was purified by column chromatography.

**5-[4-(2-carboxy-2-cyanovinyl)phen-1-yl]-2-[[3-[(1,3-dihydro-3-decyl-1-hexyl -3-octyl-2H-indol-2-ylidene)methyl]-4-oxo-2-cyclobuten-2-olate-1-ylidene]methyl]-1,3,3-trimethyl-3H-indolium (PSQ 1):** Started with 0.1 g (0.12 mmol) of **8a**, product obtained: 64 mg, Yield: 60%. <sup>1</sup>H NMR (400 MHz, CDCl<sub>3</sub>) δ: 8.34 (br. s., 1 H), 8.07 (br. s., 2 H), 7.7 (br. s., 2 H), 7.57 (br. s., 2 H), 7.31 (m, 2 H), 7.20 (t, *J*=7.6 Hz 1 H), 7.03 (m, 2 H), 6.13 (br. s., 1 H), 5.98 (br. s., 1 H), 4.09 (br. s., 2 H), 3.57 (br. s., 3 H), 2.98 (br. s., 2 H), 2.01 (m, 2 H), 1.83 (m, 8 H), 1.43 (m, 2 H), 1.31 - 1.04 (m, 28 H), 0.86 - 0.76 (m, 11 H), 0.48 (m, 2 H); <sup>13</sup>C NMR (101 MHz, CDCl<sub>3</sub>) δ: 182.8, 177.0, 169.6, 169.1, 167.26, 152.6, 144.1, 143.2, 142.7, 139.2, 134.8, 131.2, 130.8, 129.5, 127.7, 127.3, 126.8, 124.0, 123.7, 123.3, 122.3, 120.6, 109.4, 87.8, 87.3, 77.3, 58.9, 48.7, 44, 41.2, 39.9, 34.8, 31.9, 31.8, 31.7, 31.6, 31.5, 30.4, 30.2, 29.6, 29.5, 29.5, 29.5, 29.4, 29.3, 29.2, 29.1, 29.0,

27.3, 27.2, 27.2, 26.8, 24.0, 22.6, 22.5, 22.5, 14.0, 13.9; MALDI-TOF ( $m/z$ ):  $[M]^+$  calcd for  $C_{59}H_{75}N_3O_4$ : 889.5758; found: 889.4904.

**5-[4-(2-carboxy-2-cyanovinyl)phen-1-yl]-2-[[3-[(1,3-dihydro-1,3,3-trimethyl-2H-indol-2-ylidene)methyl]-4-oxo-2-cyclobuten-2-olate-1-ylidene]methyl]-3-decyl-1-hexyl-3-octyl-3H-indolium (PSQ2):** Started with 0.1 g (0.12 mmol) of **8b**, product obtained: 60 mg, Yield: 56%.  $^1H$  NMR (400 MHz,  $CDCl_3$ )  $\delta$ : 8.36 (br. s., 1 H), 8.12 (d,  $J = 8.4$  Hz, 2 H), 7.77 (d,  $J = 7.6$  Hz, 2 H), 7.66-7.56 (m, 2 H), 7.50-6.90 (m, 5 H), 6.13 (br. s., 1 H), 6.03 (br. s., 1 H), 4.05 (br. s., 2 H), 3.63 (br. s., 3 H), 3.05 (br. s., 2 H), 2.25 - 1.6 (m, 10 H), 1.50-0.87 (m, 30 H), 0.79 - 0.72 (m, 11 H), 0.55 (m, 2 H);  $^{13}C$  NMR (100 MHz,  $CDCl_3$ )  $\delta$ : 183.0, 176.1, 175.4, 171.7, 168.4, 164.3, 154.0, 145.0, 144.8, 142.8, 142.0, 140.1, 135.0, 131.7, 130.4, 129.7, 128.0, 127.9, 127.8, 127.6, 127.5, 127.3, 127.1, 124.2, 122.2, 120.8, 116.4, 109.5, 103.3, 88.1, 87.1, 58.6, 49.3, 44.0, 44.0, 40.0, 34.7, 31.8, 31.7, 31.5, 31.4, 31.1, 29.6, 29.5, 29.5, 29.4, 29.2, 29.2, 29.1, 29.0, 27.3, 26.8, 26.6, 24.2, 24.0, 24.0, 24.0, 22.5, 22.5, 22.5, 14.0, 13.9; MALDI-TOF ( $m/z$ ):  $[M]^+$  calcd for  $C_{59}H_{75}N_3O_4$ : 889.5758; found: 889.4180.

**5-[5-(2-carboxy-2-cyanovinyl)thiophen-2-yl]-2-[[3-[(1,3-dihydro-3-decyl-1-hexyl -3-octyl-2H-indol-2-ylidene)methyl]-4-oxo-2-cyclobuten-2-olate-1-ylidene]methyl]-1,3,3-trimethyl-3H-indolium (PSQ 3):** Started with 0.1 g (0.12 mmol) of **10a**, product obtained: 67 mg, Yield: 62%.  $^1H$  NMR (200 MHz,  $CDCl_3$ )  $\delta$ : 8.34 (br. s., 1 H), 7.7 - 7.59 (m, 4 H), 7.4 - 7.18 (m, 4 H), 7.1 - 6.92 (m, 2 H), 6.15 (br. s., 1 H), 5.98 (br. s., 1 H), 4.14 (br. s., 2 H), 3.58 (br. s., 3 H), 2.95 (br. s., 2 H), 2.17 - 1.95 (m, 2 H), 1.83 (m, 8 H), 1.42-1.06 (m, 30H), 0.89 - 0.75 (m, 11 H), 0.92 - 0.65 (m, 2 H);  $^{13}C$  NMR (100 MHz,  $CDCl_3$ )  $\delta$ : 181.9, 181.1, , 175.9, 169.9, 168.6, 153.8, 152.9, 144.1, 143.7, 142.7, 141.8, , 135.2, 135.01, 128.4, 127.7, 126.4, 124.1, 123.7, 123.3, 119.8, 116.0, 109.4, 88.0, 87.5, 59.0, 48.6, 44.0, 39.9, 36.6, 34.8, 34.1, 31.8, 31.7, 31.6, 31.5, 30.4, 30.3, 29.6, 29.5, 29.5, 29.5, 29.4, 29.2, 29.1, 29.0, 28.4, 27.3, 27.3, 27.2, 26.8, 24.7, 24.0, 23.9, 23.4, 22.6, 22.5, 14.0, 13.9; MALDI-TOF ( $m/z$ ):  $[M]^+$  calcd for  $C_{57}H_{73}N_3O_4S$ : 895.5322; found: 895.3006.

**5-[5-(2-carboxy-2-cyanovinyl)thiophen-2-yl]-2-[[3-[(1,3-dihydro-1,3,3-trimethyl-2H-indol-2-ylidene)methyl]-4-oxo-2-cyclobuten-2-olate-1-ylidene]methyl]-3-decyl-1-hexyl-3-octyl-3H-indolium (PSQ 4):** Started with 0.1 g (0.12 mmol) of **10b**, product obtained: 58 mg, Yield: 54%.  $^1H$  NMR (400 MHz,  $CDCl_3$ )  $\delta$ : 8.37 (br. s., 1 H), 7.76 (br. s., 1 H), 7.69 (d,  $J=8$ Hz, 1 H), 7.55

(br. s., 2 H), 7.43 (br. s., 1 H), 7.38 - 7.32 (m, 2 H), 7.19 (t, 1 H), 7.06 (d, J=8Hz, 1 H), 6.99 (d, J=8.8Hz, 1 H), 6.13 (br. s., 1 H), 6.06 (br. s., 1 H), 4.05 (br. s., 1 H), 3.66 (br. s., 1 H), 3.04 (br. s., 2 H), 2.05-1.93 (m, 2 H), 1.75 (m, 11 H), 1.4-1.072 (m, 30 H), 0.87-0.74 (m, 11 H), 0.583-0.52 (m, 2 H);  $^{13}\text{C}$  NMR (100 MHz,  $\text{CDCl}_3$ )  $\delta$ : 182.6, 177.7, 175.7, 175.6, 172.1, 167.4, 164.9, 154.1, 146.4, 145.6, 142.8, 142.0, 140.2, 139.0, 134.6, 128.2, 127.9, 126.7, 124.3, 123.8, 122.2, 119.8, 116.7, 109.7, 109.5, 98.5, 88.4, 87.4, 58.4, 49.5, 43.9, 40.0, 31.8, 31.7, 31.6, 31.5, 31.4, 31.2, 30.2, 29.6, 29.5, 29.4, 29.3, 29.2, 29.1, 29.0, 27.3, 26.8, 26.8, 26.6, 24.3, 24.1, 24.1, 24.0, 22.6, 22.6, 22.5, 22.5, 14.1, 14.0, 13.9; MALDI-TOF ( $m/z$ ):  $[\text{M}+\text{K}]^+$  calcd for  $\text{C}_{57}\text{H}_{73}\text{N}_3\text{O}_4\text{S}$ : 934.6302; found: 834.2532.

**5-[5-(2-carboxy-2-cyanovinyl)thiophen-2-yl]-2-[[3-[(1,3-dihydro-1,3-didodecyl-3-decyl-2H-indol-2-ylidene)methyl]-4-oxo-2-cyclobuten-2-olate-1-ylidene]methyl]-1,3,3-trimethyl-3H-indolium (PSQ 5):** Started with 0.1 g (0.10 mmol) of **10c**, product obtained: 64 mg, Yield: 60%.  $^1\text{H}$  NMR (500 MHz,  $\text{CDCl}_3$ )  $\delta$ : 8.39 (br. s, 1H), 7.62 - 7.47 (m, 2 H), 7.36-7.28 (m, 3 H), 7.19 (br. s., 2 H), 7.05-6.9 (m, 2 H), 6.85 (br. s., 1 H), 6.12 (br. s., 1 H), 5.93 (br. s., 1 H), 4.03 (br. s., 2 H), 3.46 (br. s., 1 H), 3.02 (br. s., 3 H), 2.06-1.97 (m, 2 H), 1.82-1.80 (m, 8H), 1.44-1.03 (m, 50H), 0.88-0.79 (m, 11H), 0.4-0.45 (m, 2 H);  $^{13}\text{C}$  NMR (126 MHz,  $\text{CDCl}_3$ )  $\delta$ : 183.1, 182.14, 177.2, 176.9, 169.6, 168.3, 152.9, 152.1, 144.1, 142.6, 141.8, 139.3, 139.2, 135.0, 127.7, 123.9, 123.7, 123.3, 122.4, 121.9, 119.8, 119.07, 116.0, 109.49, 108.8, 88.0, 87.5, 59.0, 48.6, 43.9, 40.0, 34.8, 34.2, 31.8, 31.8, 31.6, 31.4, 30.3, 30.3, 30.1, 29.6, 29.6, 29.5, 29.4, 29.3, 29.2, 29.2, 28.9, 27.4, 27.2, 24.0, 22.6, 22.6, 22.6, 14.1; MALDI-TOF ( $m/z$ ):  $[\text{M}+1]^+$  calcd for  $\text{C}_{67}\text{H}_{93}\text{N}_3\text{O}_4\text{S}$ : 1036.6966; found: 1036.9155.

## 2.5 References

- (1) O'Regan, B.; Grätzel, M. A Low-Cost, High-Efficiency Solar Cell Based on Dye-Sensitized Colloidal  $\text{TiO}_2$  films. *Nature* **1991**, *353*, 737-740.
- (2) Grätzel, M. Recent Advances in Sensitized Mesoscopic Solar Cells. *Acc. Chem. Res.* **2009**, *42*, 1788-1798.
- (3) Hagfeldt, A.; Boschloo, G.; Sun, L.; Kloo, L.; Pettersson, H. Dye Sensitized Solar Cells. *Chem. Rev.* **2010**, *110*, 6595-6663.

- (4) Mishra, A.; Fischer, M. K. R.; Bäuerle, P. Metal-Free Organic Dyes for Dye-Sensitized Solar Cells: From Structure: Property Relationships to Design Rules. *Angew. Chem. Int. Ed.* **2009**, *48*, 2474-2499.
- (5) Liang, M.; Chen, J. Arylamine Organic Dyes for Dye-Sensitized Solar Cells. *Chem. Soc. Rev.* **2013**, *42*, 3453-3488.
- (6) Ye, M.; Wen, X.; Wang, M.; Iocozzia, J.; Zhang, N.; Lin, C.; Lin, Z. Recent Advances in Dye-Sensitized Solar Cells: from Photoanodes, Sensitizers and Electrolytes to Counter Electrodes. *Mater. Today* **2015**, *18*, 155-162.
- (7) Li, W.; Wu, Z.; Wang, J.; Elzatahry, A. A.; Zhao, D. A Perspective on Mesoporous TiO<sub>2</sub> Materials. *Chem. Mater.* **2014**, *26*, 287-298.
- (8) Anta, J. A.; Guillén, E.; Tena-Zaera, R. ZnO-Based Dye-Sensitized Solar Cells. *J. Phys. Chem. C* **2012**, *116*, 11413-11425.
- (9) Wu, J.; Lan, Z.; Lin, J.; Huang, M.; Huang, Y.; Fan, L.; Luo, G. Electrolytes in Dye-Sensitized Solar Cells. *Chem. Rev.* **2015**, *115*, 2136-2173.
- (10) Thomas, S.; Deepak, T. G.; Anjusree, G. S.; Arun, T. A.; Nair, S. V.; Nair, A. S. A Review on Counter Electrode Materials in Dye-Sensitized Solar Cells. *J. Mater. Chem. A* **2014**, *2*, 4474-4490.
- (11) Cahen, D.; Hodes, G.; Grätzel, M.; Guillemoles, J. F.; Riess, I. Nature of Photovoltaic Action in Dye-Sensitized Solar Cells. *J. Phys. Chem. B* **2000**, *104*, 2053-2059.
- (12) Listorti, A.; O'Regan, B.; Durrant, J. R. Electron Transfer Dynamics in Dye-Sensitized Solar Cells. *Chem. Mater.* **2011**, *23*, 3381-3399.
- (13) Clifford, J. N.; Martínez-Ferrero, E.; Viterisi, A.; Palomares, E. Sensitizer Molecular Structure-Device Efficiency Relationship in Dye-Sensitized Solar Cells. *Chem. Soc. Rev.* **2011**, *40*, 1635-1646.
- (14) Nazeeruddin, M. K.; Péchy, P.; Renouard, T.; Zakeeruddin, S. M.; Humphry-Baker, R.; Comte, P.; Liska, P.; Cevey, L.; Costa, E.; Shklover, V.; Spiccia, L.; Deacon, G. B.; Bignozzi, C.



---

A.; Grätzel, M. Engineering of Efficient Panchromatic Sensitizers for Nanocrystalline TiO<sub>2</sub>-Based Solar Cells. *J. Am. Chem. Soc.* **2001**, *123*, 1613-1624.

(15) Nazeeruddin, M. K.; De Angelis, F.; Fantacci, S.; Selloni, A.; Viscardi, G.; Liska, P.; Ito, S.; Takeru, B.; Grätzel, M. Combined Experimental and DFT-TDDFT Computational Study of Photoelectrochemical Cell Ruthenium Sensitizers. *J. Am. Chem. Soc.* **2005**, *127*, 16835-16847.

(16) Chen, C.-Y.; Wang, M.; Li, J.-Y.; Pootrakulchote, N.; Alibabaei, L.; Ngoc-le, C.; Decoppet, J.-D.; Tsai, J.-H.; Grätzel, C.; Wu, C.-G.; Zakeeruddin, S. M.; Grätzel, M. Highly Efficient Light-Harvesting Ruthenium Sensitizer for Thin-Film Dye-Sensitized Solar Cells. *ACS Nano* **2009**, *3*, 3103-3109.

(17) Mathew, S.; Yella, A.; Gao, P.; Humphry-Baker, R.; Curchod, B. F. E.; Ashari-Astani, N.; Tavernelli, I.; Rothlisberger, U.; Nazeeruddin, M. K.; Grätzel, M. Dye-Sensitized Solar Cells with 13% Efficiency Achieved through the Molecular Engineering of Porphyrin Sensitizers. *Nat. Chem.* **2014**, *6*, 242-247.

(18) Yella, A.; Lee, H.-W.; Tsao, H. N.; Yi, C.; Chandiran, A. K.; Nazeeruddin, M. K.; Diao, E. W.-G.; Yeh, C.-Y.; Zakeeruddin, S. M.; Grätzel, M. Porphyrin-Sensitized Solar Cells with Cobalt (II/III)-Based Redox Electrolyte Exceed 12 Percent Efficiency. *Science*. **2011**, *334*, 629–634.

(19) Gong, J.; Liang, J.; Sumathy, K. Review on Dye-Sensitized Solar Cells (DSSCs): Fundamental Concepts and Novel Materials. *Renewable Sustainable Energy Rev.* **2012**, *16*, 5848–5860.

(20) Ahmad, S.; Guillén, E.; Kavan, L.; Grätzel, M.; Nazeeruddin, M. K.; Hauge, R. H.; Li, J.; Lou, J.; Lin, H.; Han, H.; Grätzel, M.; Cao, A.; Ruoff, R. S.; Bello, I.; Lee, S. T. Metal Free Sensitizer and Catalyst for Dye Sensitized Solar Cells. *Energy Environ. Sci.* **2013**, *6*, 3439-3466.

(21) Schmidt-Mende, L.; Bach, U.; Humphry-Baker, R.; Horiuchi, T.; Miura, H.; Ito, S.; Uchida, S.; Grätzel, M. Organic Dye for Highly Efficient Solid-State Dye-Sensitized Solar Cells. *Adv. Mater.* **2005**, *17*, 813–815.

(22) Zhang, M.; Wang, Y.; Xu, M.; Ma, W.; Li, R.; Wang, P.; Wang, P. Design of High-

---

Efficiency Organic Dyes for Titania Solar Cells Based on the Chromophoric Core of Cyclopentadithiophene-Benzothiadiazole. *Energy Environ. Sci.* **2013**, 6 (10), 2944-2949.

(23) Bricks, J. L.; Kachkovskii, A. D.; Slominskii, Y. L.; Gerasov, A. O.; Popov, S. V. Molecular Design of Near Infrared Polymethine Dyes: A Review. *Dyes Pigm.* **2015**, 121, 238 - 255.

(24) Saccone, D.; Galliano, S.; Barbero, N.; Quagliotto, P.; Viscardi, G.; Barolo, C. Polymethine Dyes in Hybrid Photovoltaics: Structure-Properties Relationships. *Eur. J. Org. Chem.* **2016**, 2016, 2244-2259.

(25) Hardin, B. E.; Snaith, H. J.; McGehee, M. D. The Renaissance of Dye-Sensitized Solar Cells. *Nat. Photonics* **2012**, 6, 162–169.

(26) Qin, C.; Wong, W.-Y.; Han, L. Squaraine Dyes for Dye-Sensitized Solar Cells: Recent Advances and Future Challenges. *Chem. Asian J.* **2013**, 8, 1706–1719.

(27) Yum, J.-H.; Walter, P.; Huber, S.; Rentsch, D.; Geiger, T.; Nüesch, F.; De Angelis, F.; Grätzel, M.; Nazeeruddin, M. K. Efficient Far Red Sensitization of Nanocrystalline TiO<sub>2</sub> Films by an Unsymmetrical Squaraine Dye. *J. Am. Chem. Soc.* **2007**, 129, 10320–10321.

(28) Sreejith, S.; Carol, P.; Chithra, P.; Ajayaghosh, A. Squaraine Dyes: A Mine of Molecular Materials. *J. Mater. Chem.* **2008**, 18, 264–274.

(29) Anselmi, C.; Mosconi, E.; Pastore, M.; Ronca, E.; De Angelis, F. Adsorption of Organic Dyes on TiO<sub>2</sub> Surfaces in Dye-Sensitized Solar Cells: Interplay of Theory and Experiment. *Phys. Chem. Chem. Phys.* **2012**, 14, 15963–15974.

(30) Monti, S.; Pastore, M.; Li, C.; De Angelis, F.; Carravetta, V. Theoretical Investigation of Adsorption, Dynamics, Self-Aggregation, and Spectroscopic Properties of the D102 Indoline Dye on an Anatase (101) Substrate. *J. Phys. Chem. C* **2016**, 120, 2787–2796.

(31) Chai, Q.; Li, W.; Wu, Y.; Pei, K.; Liu, J.; Geng, Z.; Tian, H.; Zhu, W. Effect of a Long Alkyl Group on Cyclopentadithiophene as a Conjugated Bridge for D–A– $\pi$ –A Organic Sensitizers: IPCE, Electron Diffusion Length, and Charge Recombination. *ACS Appl. Mater. Interfaces* **2014**, 6, 14621–14630.

- (32) Cao, Y.; Cai, N.; Wang, Y.; Li, R.; Yuan, Y.; Wang, P. Modulating the Assembly of Organic Dye Molecules on Titania Nanocrystals via Alkyl Chain Elongation for Efficient Mesoscopic Cobalt Solar Cells. *Phys. Chem. Chem. Phys.* **2012**, *14*, 8282–8286.
- (33) Koumura, N.; Wang, Z. S.; Mori, S.; Miyashita, M.; Suzuki, E.; Hara, K. Alkyl-Functionalized Organic Dyes for Efficient Molecular Photovoltaics. *J. Am. Chem. Soc.* **2006**, *128*, 14256–14257.
- (34) Ning, Z.; Zhang, Q.; Pei, H.; Luan, J.; Lu, C.; Cui, Y.; Tian, H. Photovoltage Improvement for Dye-Sensitized Solar Cells via Cone Shaped Structural Design. *J. Phys. Chem. C* **2009**, *113*, 10307–10313.
- (35) Zhang, X.; Xu, Y.; Giordano, F.; Schreier, M.; Pellet, N.; Hu, Y.; Yi, C.; Robertson, N.; Hua, J.; Zakeeruddin, S. M. Molecular Engineering of Potent Sensitizers for Very Efficient Light Harvesting in Thin-Film Solid-State Dye-Sensitized Solar Cells. *J. Am. Chem. Soc.* **2016**, *138*, 10742–10745.
- (36) Yella, A.; Humphry-Baker, R.; Curchod, B. F. E.; Ashari Astani, N.; Teuscher, J.; Polander, L. E.; Mathew, S.; Moser, J.-E.; Tavernelli, I.; Rothlisberger, U. Molecular Engineering of a Fluorene Donor for Dye-Sensitized Solar Cells. *Chem. Mater.* **2013**, *25*, 2733–2739.
- (37) Pastore, M.; De Angelis, F. Computational Modelling of TiO<sub>2</sub> Surfaces Sensitized by Organic Dyes With Different Anchoring Groups: Adsorption Modes, Electronic Structure and Implication for Electron Injection/Recombination. *Phys. Chem. Chem. Phys.* **2012**, *14*, 920–928.
- (38) Zhang, L.; Cole, J. M. Anchoring Groups for Dye-Sensitized Solar Cells. *ACS Appl. Mater. Interfaces* **2015**, *7*, 3427–3455.
- (39) Marquet, P.; Andersson, G.; Snedden, A.; Kloo, L.; Atkin, R. Molecular Scale Characterization of the Titania-Dye-Solvent Interface in Dye-Sensitized Solar Cells. *Langmuir* **2010**, *26*, 9612–9616.
- (40) Hayashi, H.; Higashino, T.; Kinjo, Y.; Fujimori, Y.; Kurotobi, K.; Chabera, P.; Sundström, V.; Isoda, S.; Imahori, H. Effects of Immersion Solvent on Photovoltaic and Photophysical

---

Properties of Porphyrin-Sensitized Solar Cells. *ACS Appl. Mater. Interfaces* **2015**, *7*, 18689–18696

(41) Li, G.; Liang, M.; Wang, H.; Sun, Z.; Wang, L.; Wang, Z.; Xue, S. Significant Enhancement of Open-Circuit Voltage in Indoline-Based Dye-Sensitized Solar Cells via Retarding Charge Recombination. *Chem. Mater.* **2013**, *25*, 1713–1722.

(42) Ooyama, Y.; Ohshita, J.; Harima, Y. Control of Molecular Arrangement and/or Orientation of D- $\pi$ -A Fluorescent Dyes for Dye-Sensitized Solar Cells. *Chem. Lett.* **2012**, *41*, 1384–1396.

(43) Jradi, F. M.; Kang, X. W.; O’Neil, D.; Pajares, G.; Getmanenko, Y. A.; Szymanski, P.; Parker, T. C.; El-Sayed, M. A.; Marder, S. R. Near-Infrared Asymmetrical Squaraine Sensitizers for Highly Efficient Dye Sensitized Solar Cells: The Effect of  $\pi$ -Bridges and Anchoring Groups on Solar Cell Performance. *Chem. Mater.* **2015**, *27*, 2480–2487.

(44) Alagumalai, A.; Kavungathodi, M. F. M.; Vellimalai, P.; Sil, M. C.; Nithyanandhan, J. Effect of Out-of-Plane Alkyl Group’s Position in Dye-Sensitized Solar Cell Efficiency: A Structure-Property Relationship Utilizing Indoline Based Unsymmetrical Squaraine Dyes, *ACS Appl. Mater. Interfaces* **2016**, *8*, 35353–35367.

(45) Barea, E. M.; Bisquert, J. Properties of Chromophores Determining Recombination at the TiO<sub>2</sub>-Dye-Electrolyte Interface. *Langmuir* **2013**, *29*, 8773–8781.

(46) Hart, A. S.; KC, C. B.; Gobeze, H. B.; Sequeira, L. R.; D ’Souza, F. Porphyrin-Sensitized Solar Cells: Effect of Carboxyl Anchor Group Orientation on the Cell Performance. *ACS Appl. Mater. Interfaces* **2013**, *5*, 5314–5323.

(47) Rochford, J.; Chu, D.; Hagfeldt, A.; Galoppini, E. Tetrachelate Porphyrin Chromophores for Metal Oxide Semiconductor Sensitization: Effect of the Spacer Length and Anchoring Group Position. *J. Am. Chem. Soc.* **2007**, *129*, 4655–4665.

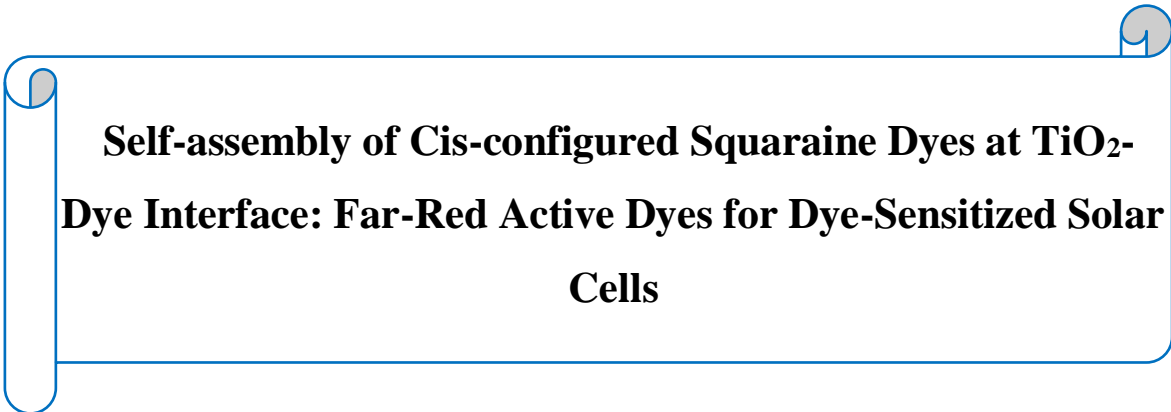
(48) Mulhern, K. R.; Detty, M. R.; Watson, D. F. Aggregation Induced Increase of the Quantum Yield of Electron Injection from Chalcogenorhodamine Dyes to TiO<sub>2</sub>. *J. Phys. Chem. C* **2011**, *115*, 6010–6018.

- (49) Kryman, M. W.; Nasca, J. N.; Watson, D. F.; Detty, M. R. Selenorhodamine Dye-Sensitized Solar Cells: Influence of Structure and Surface-Anchoring Mode on Aggregation, Persistence, and Photoelectrochemical Performance. *Langmuir* **2016**, *32*, 1521–1532
- (50) Pastore, M.; De Angelis, F. Intermolecular Interactions in Dye-Sensitized Solar Cells: A Computational Modeling Perspective. *J. Phys. Chem. Lett.* **2013**, *4*, 956–974.
- (51) de Miguel, G.; Ziółek, M.; Zitnan, M.; Organero, J. A.; Pandey, S. S.; Hayase, S.; Douhal, A. Photophysics of H- and J-Aggregates of Indole-Based Squaraines in Solid State. *J. Phys. Chem. C* **2012**, *116*, 9379–9389.
- (52) Lu, H.-P.; Tsai, C.-Y.; Yen, W.-N.; Hsieh, C.-P.; Lee, C.-W.; Yeh, C.-Y.; Diao, E. W.-G. Control of Dye Aggregation and Electron Injection for Highly Efficient Porphyrin Sensitizers Adsorbed on Semiconductor Films with Varying Ratios of Coadsorbate. *J. Phys. Chem. C* **2009**, *113*, 20990–20997.
- (53) Kimura, M.; Nomoto, H.; Masaki, N.; Mori, S. Dye Molecules for Simple Co-Sensitization Process: Fabrication of Mixed-Dye-Sensitized Solar Cells. *Angew. Chem., Int. Ed.* **2012**, *51*, 4371–4374.
- (54) Choi, H.; Kang, S.; Ko, J.; Gao, G.; Kang, H.; Kang, M.-S.; Nazeeruddin, M.; Grätzel, M. An Efficient Dye-Sensitized Solar Cell with an Organic Sensitizer Encapsulated in a Cyclodextrin Cavity. *Angew. Chem., Int. Ed.* **2009**, *48*, 5938–5941.
- (55) Delcamp, J. H.; Shi, Y.; Yum, J.-H.; Sajoto, T.; Dell’Orto, E.; Barlow, S.; Nazeeruddin, M. K.; Marder, S. R.; Grätzel, M. The Role of  $\pi$  Bridges in High-Efficiency DSCs Based on Unsymmetrical Squaraines. *Chem. Eur. J.* **2013**, *19*, 1819–1827.
- (56) Tsai, H.-H. G.; Tan, C.-J.; Tseng, W.-H. Electron Transfer of Squaraine-Derived Dyes Adsorbed on TiO<sub>2</sub> Clusters in Dye-Sensitized Solar Cells: A Density Functional Theory Investigation. *J. Phys. Chem. C* **2015**, *119*, 4431–4443.
- (57) Shi, Y.; Hill, R. B.; Yum, J. H.; Dualeh, A.; Barlow, S.; Grätzel, M.; Marder, S. R.; Nazeeruddin, M. K. A High-Efficiency Panchromatic Squaraine Sensitizer for Dye-Sensitized Solar Cells. *Angew. Chem., Int. Ed.* **2011**, *50*, 6619–6621.

- (58) M. Schulz Senft, M.; Gates, P. J.; Soennichsen, F. D.; Staubitz, A.; Diversely halogenated spiropyrans - Useful synthetic building blocks for a versatile class of molecular switches . *Dyes Pigm.* **2017**, *136*, 292–301.
- (59) Becke, A. D. Density-Functional Thermochemistry. III. The Role of Exact Exchange. *J. Chem. Phys.* **1993**, *98*, 5648–5652.
- (60) Lee, C.; Yang, W.; Parr, R. G.; Development of the Colle-Salvetti Correlation-Energy Formula into a Functional of the Electron Density. *Phys. Rev. B: Condens. Matter Mater. Phys.* **1988**, *37*, 785–789.
- (61) Becke, A. D.; A New Mixing of Hartree-Fock and Local DensityFunctional Theories. *J. Chem. Phys.* **1993**, *98*, 1372–1377.
- (62) Frisch, M. J.; Pople, J. A.; Binkley, J. S.; Self-Consistent Molecular Orbital Methods. 25. Supplementary Functions for Gaussian Basis Sets. *J. Chem. Phys.* **1984**, *80*, 3265–3269.
- (63) Frisch, M. J.; Trucks, G. W.; Schlegel, H. B.; Scuseria, G. E.; Robb, M. A.; Cheeseman, J. R.; Scalmani, G.; Barone, V.; Mennucci, B.; Petersson, G. A.; Nakatsuji, H.; Caricato, M.; Li, X.; Hratchian, H. P.; Izmaylov, A. F.; Bloino, J.; Zheng, G.; Sonnenberg, J. L.; Hada, M.; Ehara, M.; Toyota, K.; Fukuda, R.; Hasegawa, J.; Ishida, M.; Nakajima, T.; Honda, Y.; Kitao, O.; Nakai, H.; Vreven, T.; Montgomery, J. A., Jr.; Peralta, J. E.; Ogliaro, F.; Bearpark, M.; Heyd, J. J.; Brothers, E.; Kudin, K. N.; Staroverov, V. N.; Kobayashi, R.; Normand, J.; Raghavachari, K.; Rendell, A.; Burant, J. C.; Iyengar, S. S.; Tomasi, J.; Cossi, M.; Rega, N.; Millam, J. M.; Klene, M.; Knox, J. E.; Cross, J. B.; Bakken, V.; Adamo, C.; Jaramillo, J.; Gomperts, R.; Stratmann, R. E.; Yazyev, O.; Austin, A. J.; Cammi, R.; Pomelli, C.; Ochterski, J. W.; Martin, R. L.; Morokuma, K.; Zakrzewski, V. G.; Voth, G. A.; Salvador, P.; Dannenberg, J. J.; Dapprich, S.; Daniels, A. D.; Farkas, Ö.; Foresman, J. B.; Ortiz, J. V.; Cioslowski, J.; Fox, D. J. Gaussian, Inc., Wallingford CT, 2009.
- (64) Aghazada, S.; Gao, P.; Yella, A.; Marotta, G.; Moehl, T.; Teuscher, J.; Moser, J.-E.; De Angelis, F.; Grätzel, M.; Nazeeruddin, M. K. Ligand Engineering for the Efficient Dye-Sensitized Solar Cells with Ruthenium Sensitizers and Cobalt Electrolytes. *Inorg. Chem.* **2016**, *55*, 6653–6659.

- (65) Chen, Z.; Lohr, A.; Saha-Möller, C. R.; Würthner, F. Self-Assembled  $\pi$ -Stacks of Functional Dyes in Solution: Structural and Thermodynamic Features. *Chem. Soc. Rev.* **2009**, *38*, 564–584.
- (66) Snaith, H. J. Estimating the Maximum Attainable Efficiency in Dye-Sensitized Solar Cells. *Adv. Funct. Mater.* **2010**, *20*, 13–19
- (67) Daeneke, T.; Mozer, A. J.; Uemura, Y.; Makuta, S.; Fekete, M.; Tachibana, Y.; Koushida, N.; Bach, U.; Spiccia, L., Dye Regeneration Kinetics in Dye-Sensitized Solar Cells. *J. Am. Chem. Soc.* **2012**, *134*, 16925-16928.
- (68) Eom, Y. K.; Kang, S. H.; Choi, I. T.; Yoo, Y.; Kim, J.; Kim, H. K. Significant Light Absorption Enhancement by a Single Heterocyclic Unit Change in the P-Bridge Moiety from thieno[3,2-B]benzothiophene to thieno[3,2-B]indole for High Performance Dye- Sensitized and Tandem Solar Cells. *J. Mater. Chem. A* **2017**, *5*, 2297–2308.
- (69) Kang, S. H.; Jeong, M. J.; Eom, Y. K.; Choi, I. T.; Kwon, S. M.; Yoo, Y.; Kim, J.; Kwon, J.; Park, J. H.; Kim, H. K. Porphyrin Sensitizers with Donor Structural Engineering for Superior Performance Dye-Sensitized Solar Cells and Tandem Solar Cells for Water Splitting Applications. *Adv. Energy Mater.* **2017**, *7*, 1602117.
- (70) Fabregat-Santiago, F.; Bisquert, J.; Garcia-Belmonte, G.; Boschloo, G.; Hagfeldt, A. Influence of Electrolyte in Transport and Recombination in Dye-Sensitized Solar Cells Studied by Impedance Spectroscopy. *Sol. Energy Mater. Sol. Cells* **2005**, *87*, 117–131.
- (71) Wang, Q.; Moser, J.-E.; Grätzel, M. Electrochemical Impedance Spectroscopic Analysis of Dye-Sensitized Solar Cells. *J. Phys. Chem. B* **2005**, *109*, 14945–14953.
- (72) Raga, S. R.; Barea, E. M.; Fabregat-Santiago, F. Analysis of the Origin of Open Circuit Voltage in Dye Solar Cells. *J. Phys. Chem. Lett.* **2012**, *3*, 1629–1634.

## Chapter 3



### **Self-assembly of Cis-configured Squaraine Dyes at TiO<sub>2</sub>- Dye Interface: Far-Red Active Dyes for Dye-Sensitized Solar Cells**

Punitharasu, V.; Kavungathodi, M. F. M.; Nithyanandhan, J. *ACS Appl. Mater. Interfaces* **2018**, *10*, Article ASAP, DOI: 10.1021/acsami.8b03106.



### 3.1 Introduction

Design and syntheses of both metal containing and organic sensitizers have been evolved as an important research for highly potential photovoltaic DSSC device since 1991 by Grätzel.<sup>1-2</sup> TiO<sub>2</sub>-dye/electrolyte interface showed very important role for enhancing photon to current conversion process and recombination processes in dye-sensitized solar cells (DSSC).<sup>3</sup> To enhance the efficient charge injection process, the electronic coupling should be modulated between the dye and TiO<sub>2</sub> by having an suitable anchoring group on the dye and TiO<sub>2</sub> surface.<sup>4-6</sup> Here there are very important critical factors observed from the orientation of dyes on the TiO<sub>2</sub> surface, and the distance between the oxidized donor unit of the dye from the surface to govern the charge recombination process besides passivating the surface.<sup>7-8</sup> D- $\pi$ -A<sup>9</sup>, D-A- $\pi$ -A<sup>10</sup> dyes have been systematically designed showed the device efficiency of 13% and 12.5%, respectively.

Dipole-dipole interaction of dye aggregated monolayers formation plays very important role in spectroscopy as well as various applications. Furthermore, self-assembly active layers of aggregated structures having good responses in the sense that it broadens the absorption spectrum like H-aggregation and J-aggregation showed blue and red shifted absorption peaks compared to monomer, respectively. On the other hand, these aggregation properties have been observed thoroughly in solution<sup>11-12</sup> and solid surfaces<sup>13-20</sup> that has been widely used in photoconductive material,<sup>21</sup> chemsensor,<sup>22</sup> photovoltaics,<sup>23-26</sup> optoelectronics,<sup>27</sup> and xerography.<sup>21</sup> But comparing to dye-sensitized solar cell (DSSCs), the self-assembly of periodically arranged aggregated structure on the TiO<sub>2</sub> surface plays a negative role owing to the self quenching of photoexcited dyes to the surface besides the inefficient charge injection process which leads to decrease the DSSC device efficiency. However, few reports showed the advantage of those aggregation which helps to enhance the light harvesting efficiency and device performance<sup>15</sup> where better charge transport properties have been observed for well-defined dye aggregated structures besides broadening the light absorbing properties. Therefore controlling the aggregation and orientation of the dyes on the TiO<sub>2</sub> surface to attain both efficient charge injections as well as light harvesting efficiency at the dye-TiO<sub>2</sub> interface is very important challenging task.

Among the porphyrin,<sup>28-29</sup> phthalocyanine,<sup>30-32</sup> and squaraine dyes that constitute with donor-acceptor-donor (D-A-D)  $\pi$ -conjugated framework which absorbs in the red and NIR regions of the solar spectrum, and possess high molar extinction coefficient in the far-red, and

NIR regions ( $10^5 \text{ M}^{-1} \text{ cm}^{-1}$ ). The systematic extended  $\pi$ -conjugation was introduced in squaraine based dyes SQ1<sup>32</sup>, YR6<sup>33</sup>, JD10<sup>34</sup>, DTS-CA<sup>35</sup>, and Psil-SC12-DTS35 which helps to enhancing the device efficiency ranging from 4.5% to 8.9%. Herein, we have recently reported on the structures of squaraine that D-A-D based far red active unsymmetrical squaraines dyes in which indoline moiety as donor units and carboxylic acid as an anchoring group. In addition, donor moiety can be functionalized with in-plane and out-of-plane alkyl groups and observed the controlled aggregate formation that can be efficiently contributed in the charge injection process.<sup>36</sup> As investigated in the previous sections that extending the conjugation of  $\pi$ -spacer in D-A-D based far red active unsymmetrical squaraines dyes which played very important role to enhance the light harvesting efficiency of SQ dyes.<sup>37</sup> On the other hand, modulated *cis*-

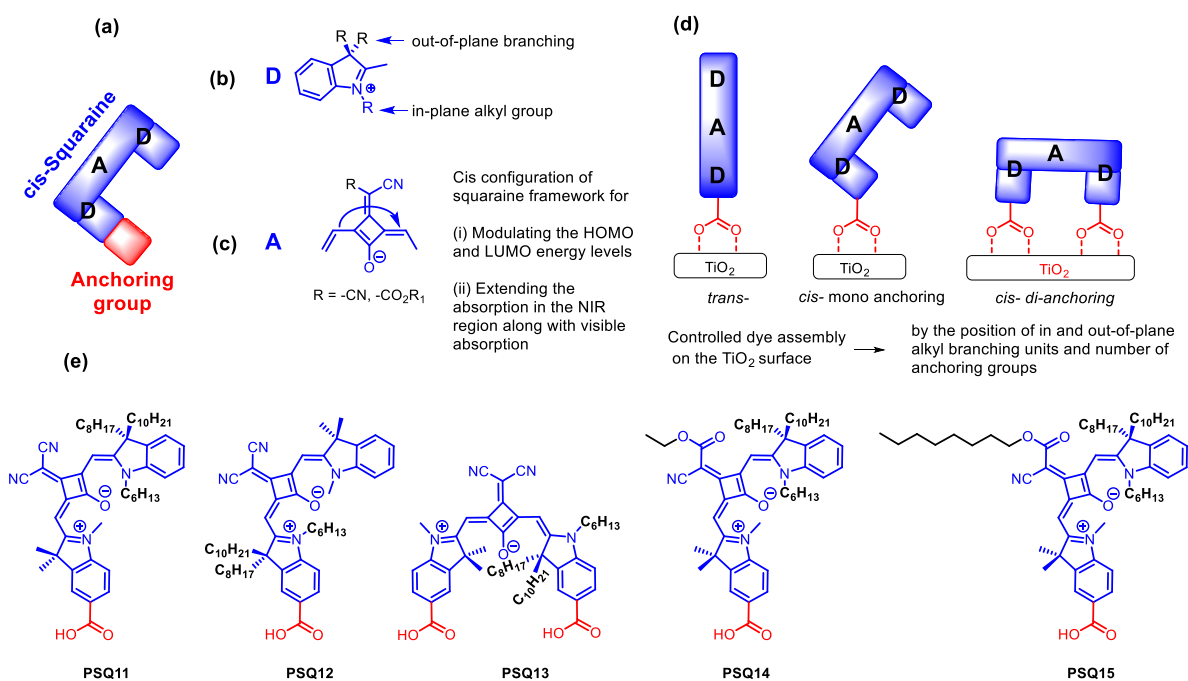


**Figure 3.1** (a) D-A-D framework based on *cis*-configured unsymmetrical squaraine dyes, (b) in-plane and out-of-plane branching alkyl groups on indoline unit, (c) *cis*-configured squaranyl unit, (d) schematic representation of mode of *trans*- and *cis*-SQ dyes anchored on TiO<sub>2</sub> surface, and (e) structures of alkyl groups functionalized *cis*-configured unsymmetrical squaraine dyes, PSQ11-15.

configured squaric unit consists of electron withdrawing barbiturate<sup>38</sup> unit which helped further extending the conjugation with efficient device efficiency than SQ1. Besides designing central

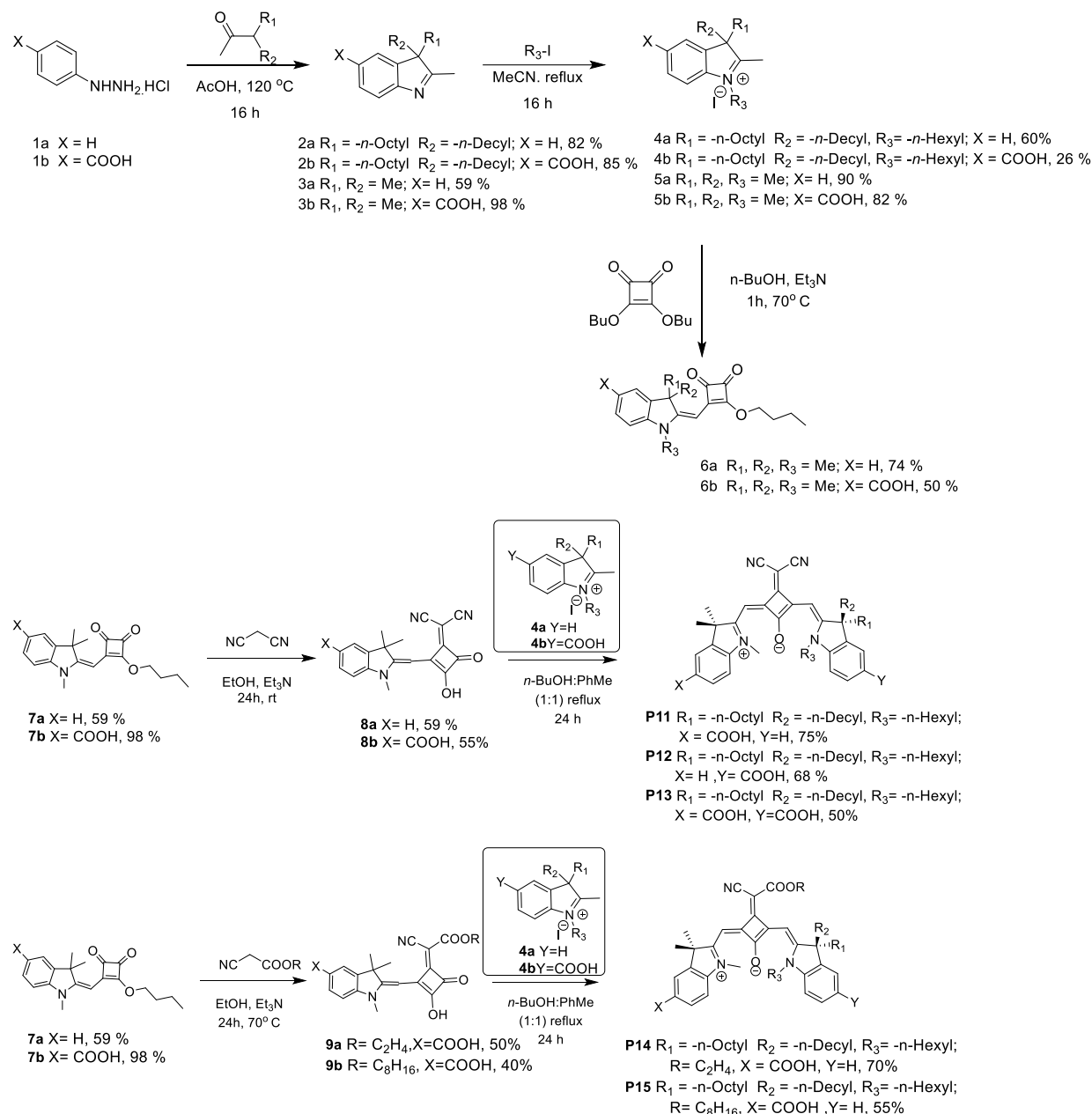
squaraine units with dicyano-,<sup>39-40</sup> cyanoester derivatives<sup>41</sup> and number of anchoring groups to enhance the device cell efficiency up to 5.66%. Similarly, such designed NIR active dyes has been achieved the better device performance to 7.77% by co-sensitization with visible active dyes.<sup>42</sup>

In this chapters, design and synthesis of a series of *cis*-configured squaraine dyes and self-assembly on TiO<sub>2</sub> surface is studied further DSSC device fabrication has been carried out. A series of *cis*-configured unsymmetrical PSQ dyes (**PSQ11-15**) (**Figure 3.1**) has been designed and synthesized with following features (i) in-plane and out-of-plane alkyl groups, which modulated to control the self-assembly of dye and orientation of dyes on the TiO<sub>2</sub> surface (ii) appending electron withdrawing groups such as dicyano and cyanoester to the squaric unit to maintain the *cis*-configuration besides extend the light harvesting in NIR region as well as visible region and (iii) number of anchoring group which helps strengthening the interaction between dye and TiO<sub>2</sub> surface.

## 3.2 Results and Discussions

### 3.2.1 Syntheses of *Cis*-configured Squaraine Sensitizers

**Figure 3.1** showed the structures of D-A-D- $\pi$ -A unsymmetrical *cis*-squaraine sensitizers (**PSQ11-15**) and its synthetic route (**Scheme 3.1**). Syntheses of unsymmetrical *cis*-squaraine dyes require a suitably substituted semi-squaric acid (**6a-6b**), and branched indolium salts (**4a-4b**), dicyanovinylene, cyanoester vinylene appended semi-squaric acid derivatives of **8a-9b**. The starting material, a branched ketone, 3-octyl-2-tridecanone was synthesized from corresponding branched alcohols 2-octyldodecanol and procedure followed from the previous work. The semisquaric acid derivatives (**7a-7b**) were condensed with malononitrile afforded the dicyanovinylene or cyanoester vinylene substituted squaric acid derivative (**8a-9b**). The final condensation reaction was carried out with the corresponding indolium salts **4a** and **4b** by refluxing in presence of pyridine base in a 1:1 mixture of benzene and n-butanol under azeotropic reaction condition to afford the *cis*-configured unsymmetrical squaraine dyes **PSQ11-PSQ15** in moderate yield (**Scheme 3.1**).

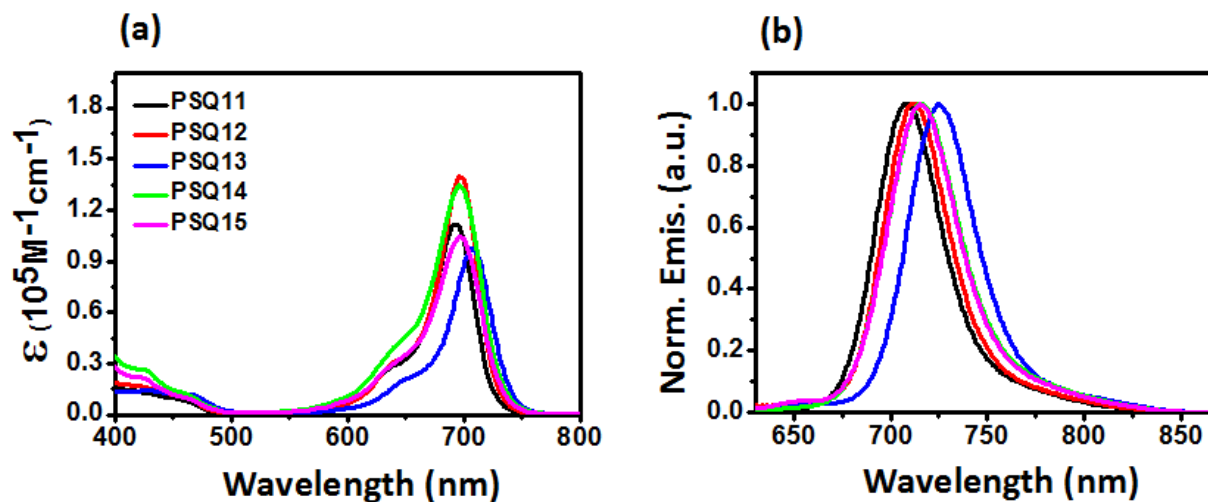


**Scheme 3.1** Syntheses of *cis*-configured unsymmetrical squaraine dyes, **PSQ11-15**

### 3.2.2 Photophysical Properties

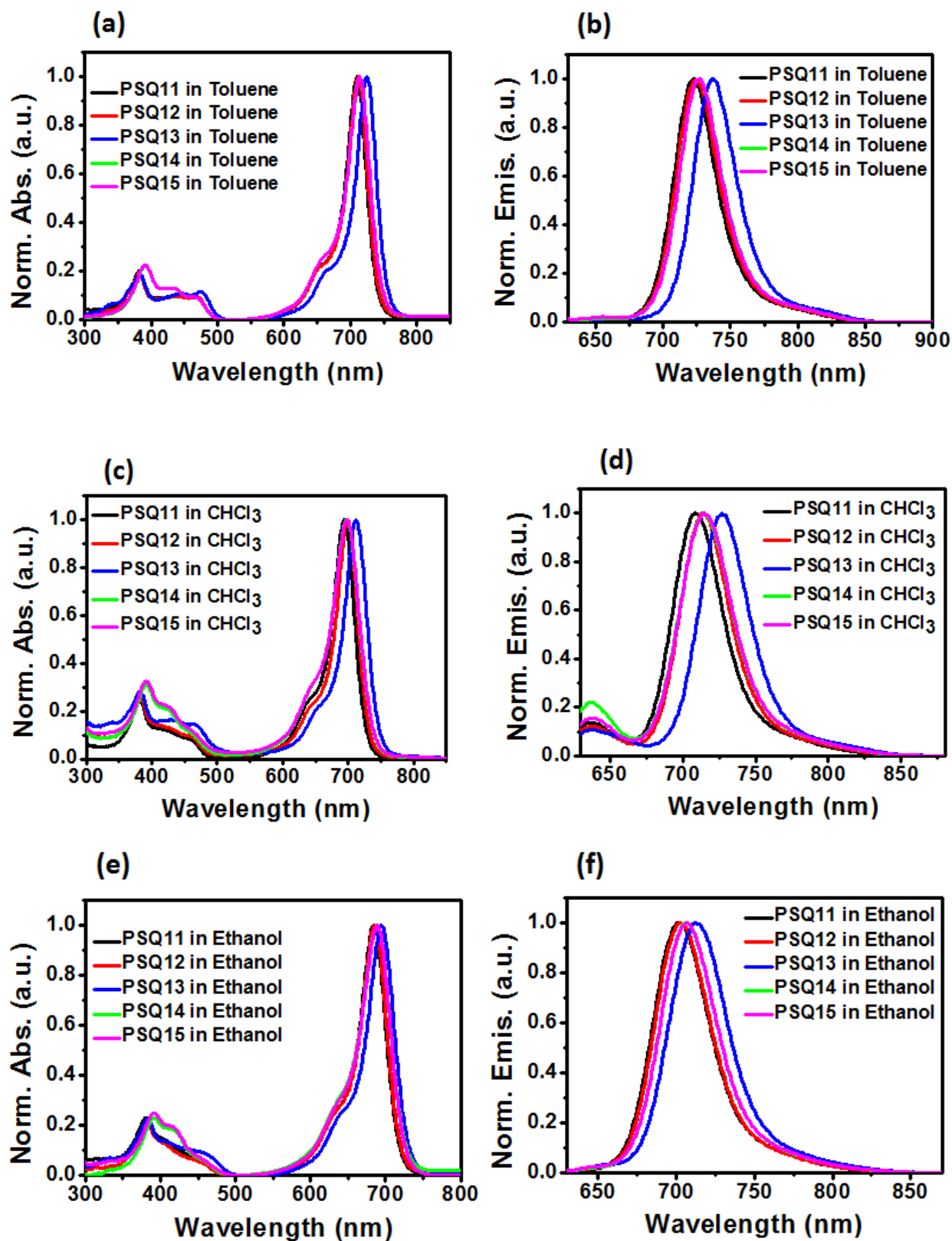
The UV-Vis absorption spectra of dyes **PSQ11-15** in CH<sub>2</sub>Cl<sub>2</sub> and on transparent TiO<sub>2</sub> film (particle size: <20 nm, film thickness: 6 μm) were shown in **Figure 3.2** and summarized in **Table 3.3**. **PSQ11-15** dyes exhibited two absorption bands, a sharp intense intramolecular charge-transfer (ICT) band between 600-750 nm with an extinction coefficient of  $\geq 10^5 \text{ M}^{-1} \text{ cm}^{-1}$  and a visible absorption peak between 400-500 nm ( $\epsilon \sim 10^4 \text{ M}^{-1} \text{ cm}^{-1}$ ), respectively. Such high

energy transition was observed by substituting with a dicyanovinyl or cyano ester group in squaraine dyes. Within the isomeric dyes of **PSQ11-PSQ13**, introducing a second carboxylic acid group as in **PSQ13** caused 10 nm bathochromic shift compared to **PSQ11** and **PSQ12** due to the electron withdrawing nature of carboxylic acid group. Dyes **PSQ14** and **PSQ15** showed 5 nm red shifted absorption compared to **PSQ11**.



**Figure 3.2** Optical properties of **PSQ11-15** dyes. (a) UV-vis absorption spectra in  $\text{CH}_2\text{Cl}_2$ , (b) Normalized emission spectra in  $\text{CH}_2\text{Cl}_2$  (excitation wavelength: 610 nm), (c) Normalized absorption spectra on thin film of  $\text{TiO}_2$ , thickness = 6  $\mu\text{m}$ , dipping time = 10 min, and  $[\text{PSQ}] = 0.1 \text{ mM}$  in  $\text{CH}_2\text{Cl}_2$ , (d) LHE (%) on  $\text{TiO}_2$  thin film recorded after 12 h dipping in 0.1 mM solution in  $\text{CH}_2\text{Cl}_2$ .

Optical properties of **PSQ11-PSQ15** were carried out in different solvents (PhMe,  $\text{CHCl}_3$ ,  $\text{CH}_2\text{Cl}_2$ , EtOH and DMF) and these dyes exhibited a red shifted absorption in  $\lambda_{\text{max}}$  from least polar PhMe to DMF (**Table 3.1**). Emission spectra of **PSQ11-15** in  $\text{CH}_2\text{Cl}_2$  showed intense peak between 707-725 nm. The Stokes shift of ~15-19 nm for **PSQ11-15** indicated that the dipole moments of the photo-excited states have been changed significantly. By relative method the fluorescence quantum yield ( $\phi$ ) in different solvents were measured and in dichloromethane  $\phi$  shows an increasing order of  $[\text{PSQ13}=\text{PSQ15}] < [\text{PSQ14}\approx\text{PSQ11}\approx\text{PSQ12}]$ . The optical band gap ( $E_{0.0}$ ) was calculated from the intersection point of the respective absorption and emission spectra and it varied between 1.73-1.76 eV for **PSQ11-PSQ15** dyes (**Figure 3.3 and Table 3.1**).



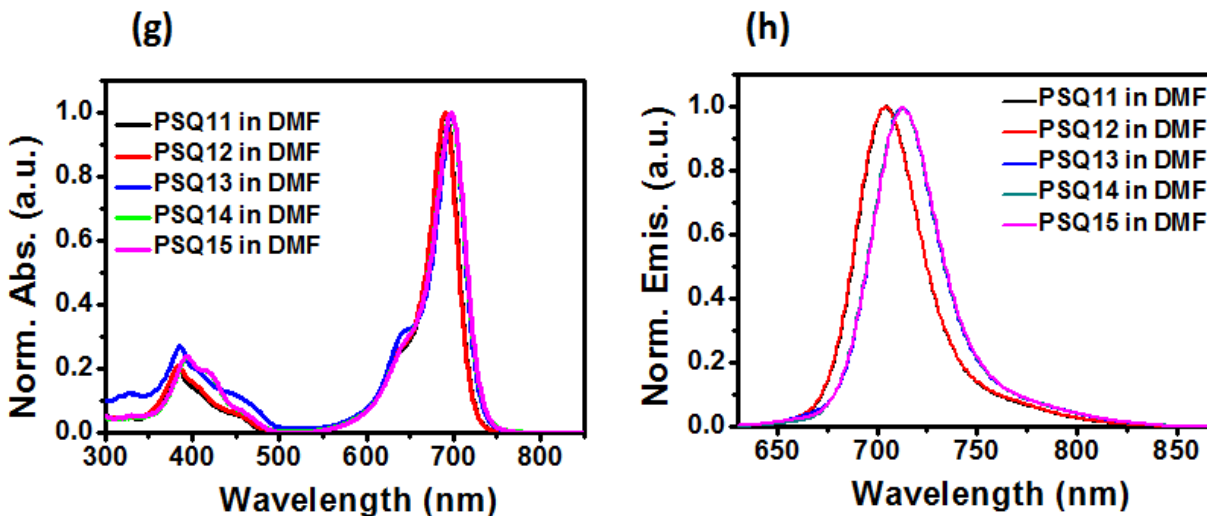


**Figure 3.3** Normalized UV-vis absorption and fluorescence spectra of **PSQ11-15** dye of (a-h) in different solvents.

**Table 3.1** Absorption and emission properties of **PSQ11-15** dyes in different solvents. Excitation wavelength ( $\lambda_{\text{ex}}$ ) was 610 nm

Dye	$\lambda_{\text{abs}}/\lambda_{\text{emis}}$	$\lambda_{\text{abs}}/\lambda_{\text{emis}}$	$\lambda_{\text{abs}}/\lambda_{\text{emis}}$	$\lambda_{\text{abs}}/\lambda_{\text{emis}}$	$\lambda_{\text{abs}}/\lambda_{\text{emis}}$
	(nm), $\phi$ in PhMe	(nm), $\phi$ in $\text{CH}_2\text{Cl}_2$	(nm), $\phi$ in $\text{CHCl}_3$	(nm), $\phi$ in EtOH	(nm), $\phi$ in DMF
<b>PSQ11</b>	710/723, 0.12	657/665, 0.31	694/709, 0.16	684/702, 0.17	691/704, 0.09
<b>PSQ12</b>	712/724, 0.11	658/676, 0.27	699/714, 0.11	686/703, 0.13	690/704, 0.08
<b>PSQ13</b>	724/737, 0.06	669/676, 0.14	712/727, 0.07	695/713, 0.13	698/712, 0.07
<b>PSQ14</b>	714/727, 0.07	671/676, 0.35	699/715, 0.08	689/707, 0.08	697/712, 0.05
<b>PSQ15</b>	714/727, 0.07	669/677, 0.14	699/715, 0.08	689/707, 0.09	697/712, 0.05

To understand the self-assembling nature of **PSQ11-PSQ15** dyes in solution, the UV-vis absorption studies were carried out in different concentrations of **PSQ11-PSQ13** dyes in  $\text{CH}_2\text{Cl}_2$  and a non-linear Beer-Lambert plot indicated that **PSQ11**, **PSQ13** and **PSQ14** exist as aggregate in solution with the threshold concentration of dyes were about 0.05 mM. Whereas for **PSQ12** and **PSQ15**, non-linear behavior observed beyond the dye concentration of 0.1 mM (**Figure 3.4**). This observation indicated that keeping the branched alkyl groups away from the anchoring groups allows the strong intermolecular interaction even in solution, and in the case of **PSQ12** and **PSQ15**, the dye exist as monomer even at 100  $\mu\text{M}$  that was the dye bath concentration used for dipping the electrode for device fabrication.

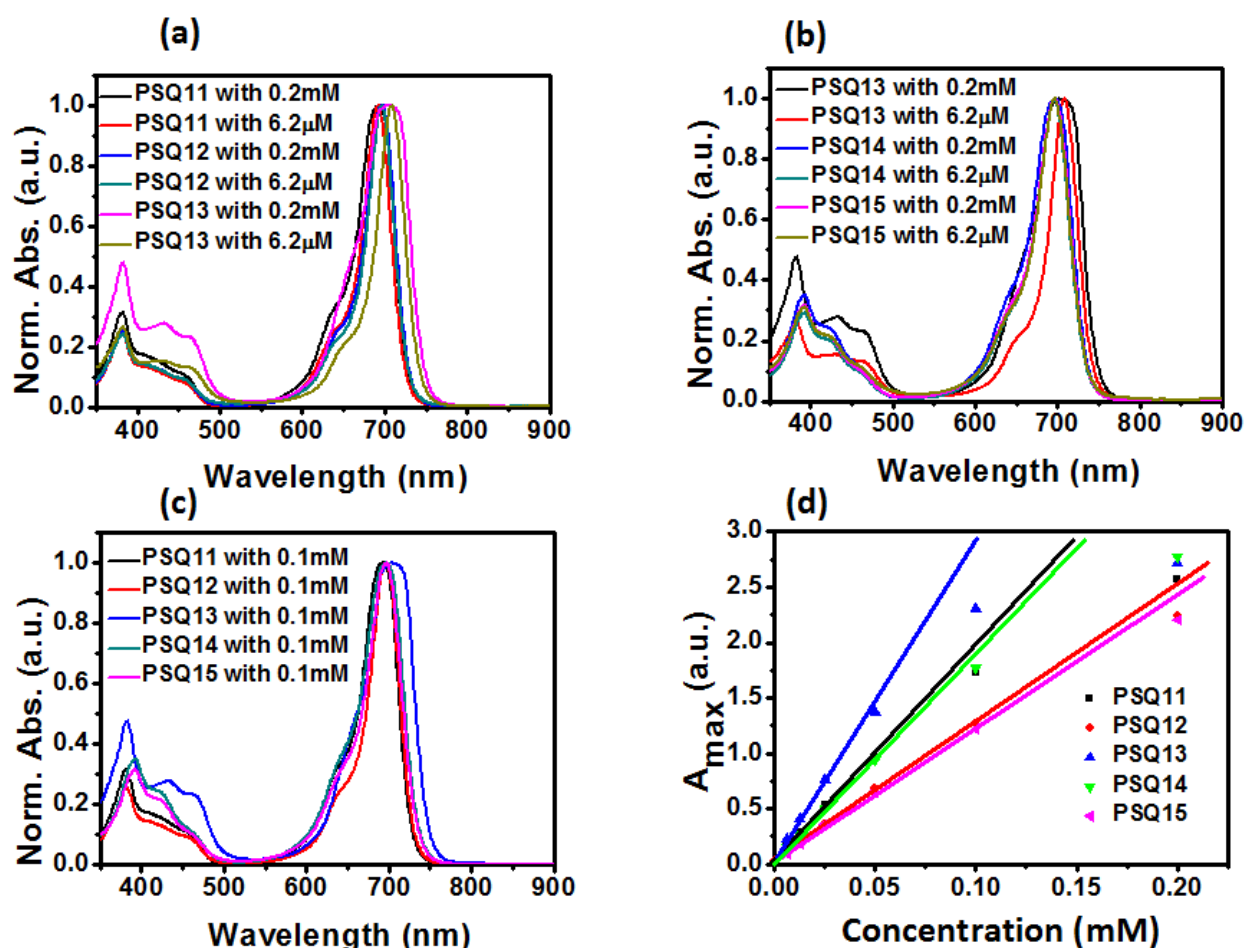


**Figure 3.4** Aggregation of dyes in solution. (a-b) UV-vis absorption spectra of **PSQ11** in  $\text{CH}_2\text{Cl}_2$  in different concentration (path length of the cuvette 0.1 cm), (c) Normalized UV-vis absorption spectrum of 0.1 mM **PSQ11-15** in  $\text{CH}_2\text{Cl}_2$  (d) Deviation from Beer-Lambert law (**PSQ11-PSQ15**).



### 3.2.3 Photophysical Characterization on the Surface

Controlling the self assembly of dyes on TiO<sub>2</sub> surface and in solution are often dictated by the molecular structure. In terms of structure, **PSQ11-15** dyes possess bulkiness offered by sp<sup>3</sup>-C and N-alkyl groups either near or far away from the anchoring group on a *cis*-configured squaraine framework. Further the orientation of dye at the TiO<sub>2</sub> surface has been controlled by number of anchoring groups and hydrophobic alkyl chains present in the dye molecules.

To understand the dye-dye interaction on the surface, the UV-vis studies on dye coated TiO<sub>2</sub> electrode has been carried out. TiO<sub>2</sub> electrode (6 μm) dipped in the **PSQ11-PSQ15** solutions 0.1 mM for 30 min. For the dye **PSQ11**, the ICT band at 692 nm was broadened along with the appearance of a broad peak at 638 nm. Broadening of the absorption spectrum on TiO<sub>2</sub> surface can be explained by the polar interaction of dye and deprotonation of carboxylic acid on the surface.<sup>45-47</sup> Hence the broad peaks at 692 nm and 638 nm were corresponds to the monomer and H-aggregates, respectively. However the isomeric **PSQ12** dye showed reduced H-aggregate at 644 nm along with the monomer. Having an additional –COOH group appended with **PSQ11** or **PSQ12** as in **PSQ13** provides completely different dye organization on the surface. Besides the monomer (727 nm), H-aggregate (658 nm) predominant formation of J-aggregate with red shifted absorption at 750 nm has been observed. Though, formation of H-type aggregation (Head-to-Head) of dyes on the TiO<sub>2</sub> surface can be very facile, formation of J-aggregate on TiO<sub>2</sub> surface by suitably functionalizing the squaraine dyes with in- and out-of plane alkyl groups can be envisaged by (i) parallel alignment of molecular dipoles with respect to the TiO<sub>2</sub> surface and (ii) slipped arrangement of dyes on the surface.<sup>48-49</sup> The above design can be realized by integrating *cis*-squaraine units with two anchoring groups and further one of the two indoline units were functionalized with steric demanding alkyl groups as in the case of **PSQ13** compared to **PSQ11** or **PSQ12**. The formation aggregated structure further controlled by appending on alkyl group through ester bond as in **PSQ14** and **PSQ15**, though it possess both N- and sp<sup>3</sup>-alkyl groups on the indoline unit which was far away from the anchoring group. Ratio of optical density of monomer with aggregate is listed in **Table 3.3** which helps to evaluate to extent of aggregation of dyes on the TiO<sub>2</sub> surface. These features have also been depicted in LHE profile, where **PSQ11**, **PSQ12** and **PSQ13** dyes have shown different profiles. The LHE profile is narrowed down with **PSQ13** where the chromophore was isolated to some extent with the

presence of alkyl groups at  $sp^3$ -C and N-atoms and the alkyl groups present at the cyanoester moiety.

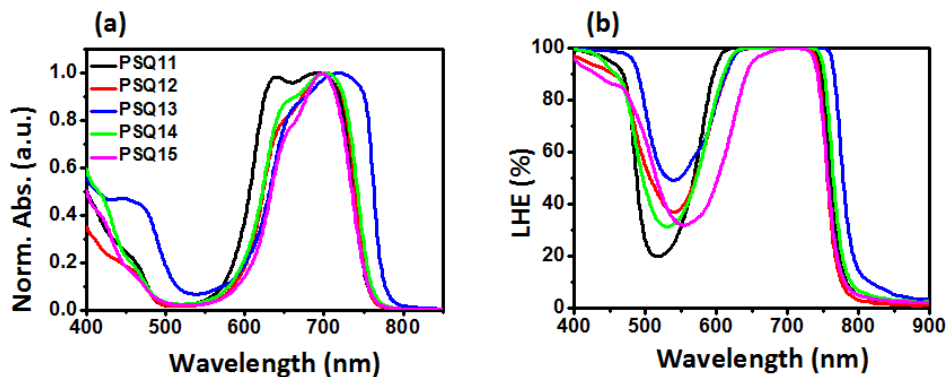


**Figure 3.5** Optical properties of PSQ11-15 dyes. (a) Normalized absorption spectra on thin film of  $TiO_2$ , thickness = 6  $\mu m$ , dipping time = 10 min, and  $[PSQ] = 0.1$  mM in  $CH_2Cl_2$ , (b) LHE (%) on  $TiO_2$  thin film recorded after 12 h dipping in 0.1 mM solution in  $CH_2Cl_2$ .

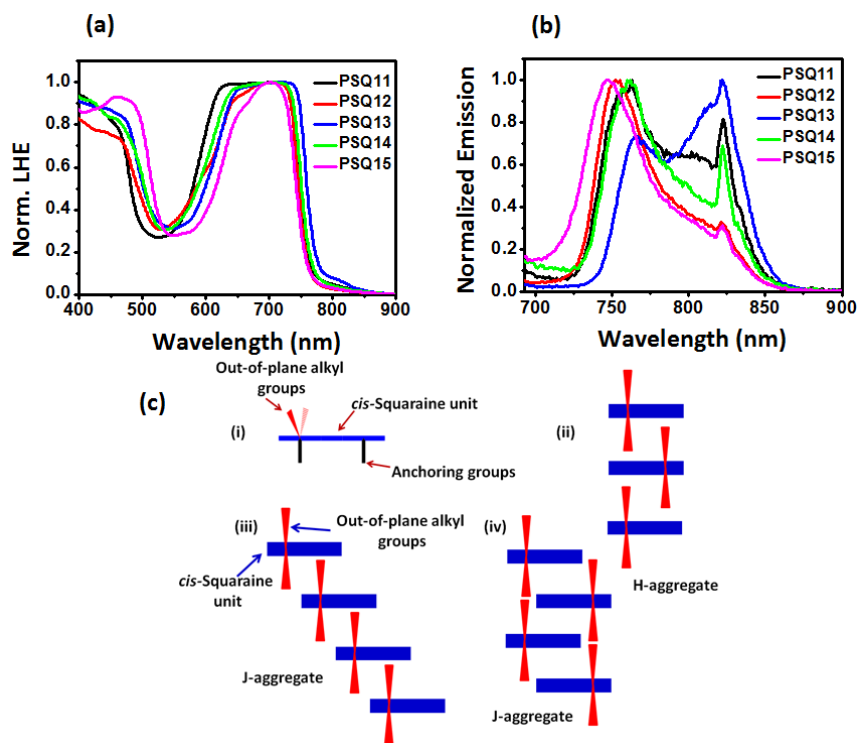


**Figure 3.6** Optical properties of PSQ11-15 dyes on  $Al_2O_3$  surface. (a) Normalized LHE on  $Al_2O_3$  thin film recorded after 12 h dipping in 0.1 mM solution in  $CH_2Cl_2$ . (b) Normalized emission spectra on thin film of  $Al_2O_3$ , excitation wavelength: 683 nm, thickness = 6  $\mu m$ , dipping time = 12 h and  $[PSQ] = 0.1$  mM in  $CH_2Cl_2$ . (c) possible arrangements of dyes on the surface for the observed H and J- type aggregations.

Emission studies on  $\text{Al}_2\text{O}_3$  surface has been carried out to understand the nature of aggregate formation with the **PSQ11-PSQ13** dyes. The  $\text{Al}_2\text{O}_3$  film was dipped in dye solution (0.1 mM of **PSQ11-PSQ13** in  $\text{CH}_2\text{Cl}_2$ ) for 12 h. The LHE profiles of **PSQ11-PSQ13** on both  $\text{TiO}_2$  and  $\text{Al}_2\text{O}_3$  surfaces have similar features (**Figures 3.5b** and **3.6a**). Emission spectra of **PSQ11-PSQ13** on  $\text{Al}_2\text{O}_3$  were consists of two peaks corresponding to monomer and J-aggregate (822 nm) emissions (**Figure 3.6b**). Possibility of such J-type aggregates emanate from the structures of the **PSQ11-PSQ13** dyes, for example, dye **PSQ13** possess inbuilt steric factor in one side of the molecule, which helps organizing the dyes on the  $\text{TiO}_2$  surface as described in **Figure 3.6c** that helps to the formation of prominent J-type aggregate.

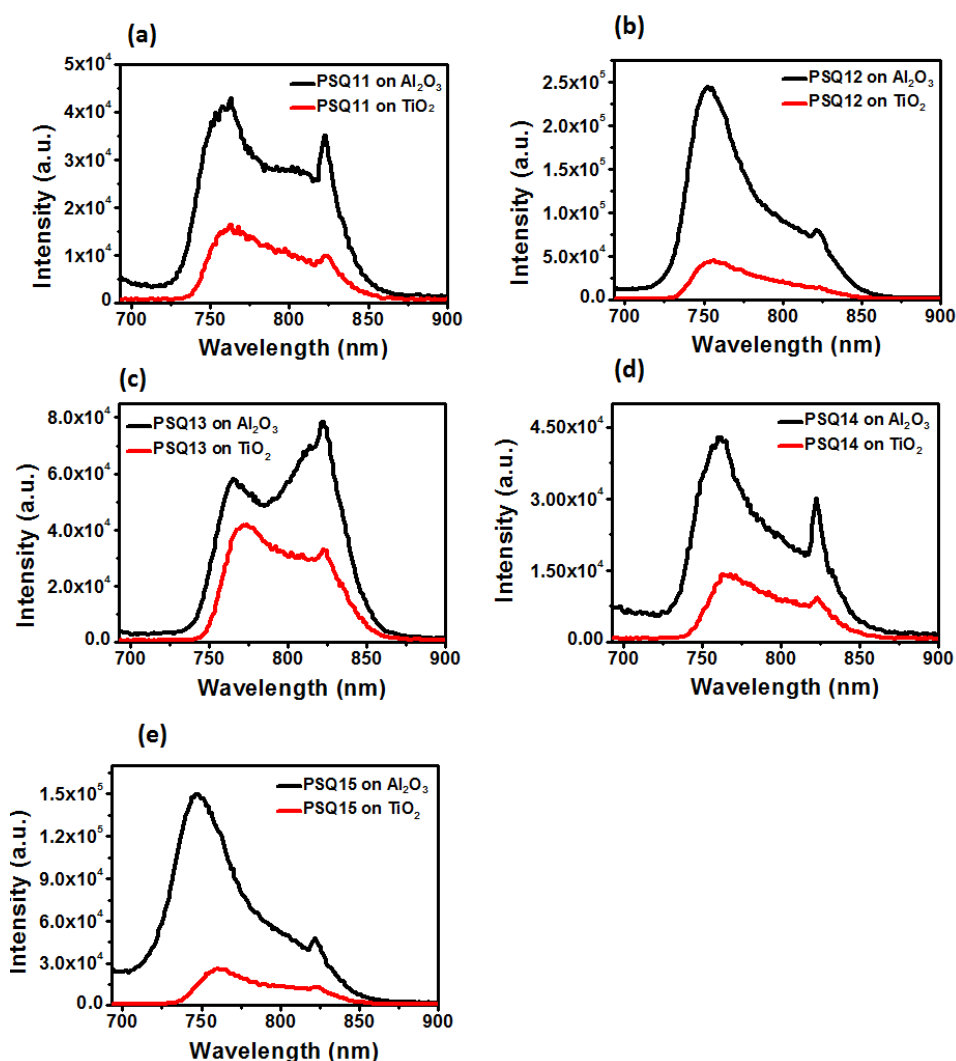


**Figure 3.7** Emission spectra of **PSQ11-PSQ15** dye of (a-e) on  $\text{Al}_2\text{O}_3$  (black line) and  $\text{TiO}_2$  (redline), excitation wavelength: 683 nm.

However the ratio of  $I_{\text{monomer}}/I_{\text{J-aggregate}}$  was different for all the dyes that indicate different arrangement of the dye on the surface. For example emission spectrum of **PSQ11** on  $\text{Al}_2\text{O}_3$  showed the monomer emission at 763 nm and the sharp J-aggregate emission at 822 nm. The isomeric **PSQ12** dye, showed the  $I_{\text{monomer}}/I_{\text{J-aggregate}}$  ratio of 3.03 which indicates more monomer formation compared to **PSQ11** that possess the  $I_{\text{monomer}}/I_{\text{J-aggregate}}$  ratio of 1.23. It is interesting to note that the emission from J-aggregate is predominant compared to monomer in case of **PSQ13**. The  $I_{\text{monomer}}/I_{\text{J-aggregate}}$  ratio for **PSQ11** and **PSQ13** were comparable as both the dyes are functionalized with N- and  $\text{sp}^3\text{-C}$  out-of-plane alkyl groups on the indoline unit that was far away from the anchoring groups. In case of **PSQ13**, due to the additional long alkyl group the formation of aggregate has been avoided which resembles the dye that possess in-plane, out-of-plane alkyl groups which were placed near to the anchoring group as in case of **PSQ12** (Table 3.2). In addition to emission study on  $\text{Al}_2\text{O}_3$ , emission from dye adsorbed  $\text{TiO}_2$  also monitored and the changes in radiative emission of dyes were compiled in Figure 3.7.

**Table 3.2** Emission properties of **PSQ11-15** on  $\text{Al}_2\text{O}_3$  at excitation wavelength of 683 nm.

Dye	Maximum $\lambda_{\text{max}}$ of monomer on $\text{Al}_2\text{O}_3(\text{nm})$	Maximum $\lambda_{\text{max}}$ of J-aggregate on $\text{Al}_2\text{O}_3(\text{nm})$	Fluorescence Intensity of monomer on $\text{Al}_2\text{O}_3$	Fluorescence Intensity of J-aggregate on $\text{Al}_2\text{O}_3$	$I_{\text{monomer}}/I_{\text{J-aggregate}}$
<b>PSQ11</b>	763	822	1	0.81	1.23
<b>PSQ12</b>	753	822	1	0.33	3.03
<b>PSQ13</b>	766	822	0.74	1	0.74
<b>PSQ14</b>	761	822	1	0.691	1.44
<b>PSQ15</b>	747	822	1	0.311	3.21

### 3.2.4 Electrochemical Characterization.

**PSQ11-15** chromophores were characterized by voltammetric analysis (DPV and CV) to understand the feasibility of electron injection from the LUMO of dye into conduction band of the  $\text{TiO}_2$  and the dye regeneration by the redox couple (Figure 3.8 and Table 3.3). The HOMO

energy level of **PSQ11**, **PSQ12** and **PSQ13** were 0.85 V and 0.93 V vs NHE, respectively. For **PSQ13** and **PSQ13** it was 0.70 V vs NHE, respectively. The more positive potential of **PSQ11-PSQ13** than the electrochemical potential of  $I^-/I_3^-$  redox couple (0.4 V vs NHE) warrants the regeneration of oxidized dye. The oxidation potential of **PSQ11-PSQ13** dyes were around 0.70-0.93 V vs NHE, suggests that the changes in position of out-of-plane alkyl groups do not make large difference, in contrast the insertion of COOH group, as in the case of **PSQ13** and different acceptor groups showed a notable difference. As described above,  $-CN$  group is more electron withdrawing than  $-COOEt$ , which is consistent with the observed change in the oxidation potential. The optical energy gaps ( $E_{0-0}$ ) was calculated from the intersection of absorption and emission spectra and **PSQ11-PSQ13** dyes exhibited optical band gap between 1.73-1.76 eV. The LUMO energy level of **PSQ11**, **PSQ12** and **PSQ13** was found at  $-0.92$  V,  $-0.91$  V and  $-0.80$  V vs NHE, respectively as well as for **PSQ13** and **PSQ13** it was  $-1.06$  V vs NHE, respectively. The LUMO energy level of **PSQ11-PSQ13** series was calculated by subtracting  $E_{0-0}$  from  $E_{HOMO}$  and tabulated results are more negative than  $E_{CB}$  of  $TiO_2$  ( $-0.5$  V vs NHE), which may result in a larger driving force for electron injection from the excited state of the sensitizer to the  $TiO_2$  conduction band. For **PSQ13**, the HOMO and LUMO is at 0.70 V and  $-1.06$  V vs NHE, respectively and there was no significant difference after extending the length of alkyl chain in acceptor groups.

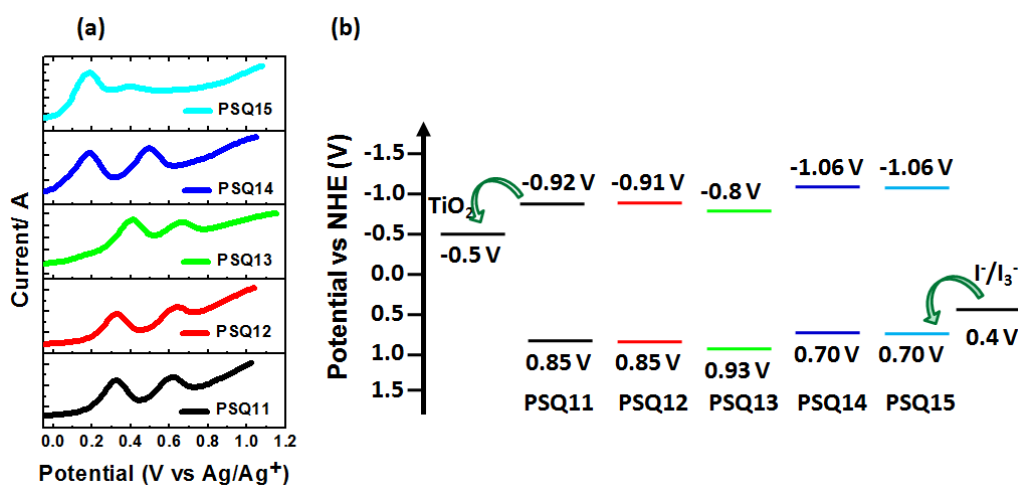


**Figure 3.8** Electrochemical properties of **PSQ11-15** dyes. (a) Differential pulse voltammetry for **PSQ11-PSQ15** dyes and (b) Energy level diagram of PSQ dyes (V vs NHE) with  $TiO_2$ , and electrolyte ( $I^-/I_3^-$ ).

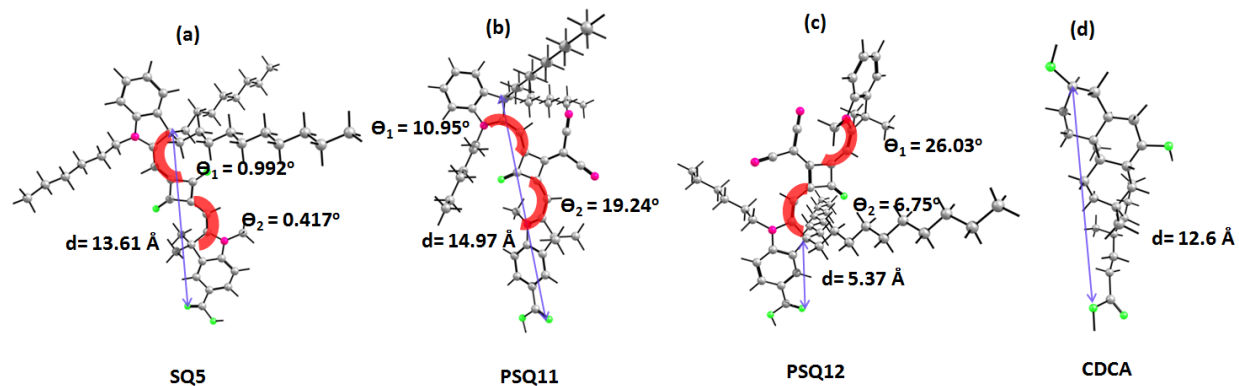
**Table 3.3** Photophysical and electrochemical properties of **PSQ11-15** at room temperature

Dye	$\lambda_{\max}/\text{abs}$ (nm) <sup>a</sup>	$\epsilon_a, \epsilon_b$ $10^5(\text{M}^{-1}\text{cm}^{-1})^b$	$\lambda_{\max}/\text{e}$ mis (nm) <sup>c</sup>	$\phi_{\text{emis}}$ (%) <sup>d</sup>	$\lambda_{\max, \text{abs}}/\text{TiO}_2$ (nm) <sup>e</sup>	$A_{\text{dimer}}/A_{\text{monomer}}$ (%)	$E_{\text{HOMO}}^f$ (eV)	$\Delta E_{0-0}^g$ (eV)	$E_{\text{LUMO}}$ (eV) <sup>h</sup>
<b>PSQ11</b>	381,692	0.27,1.1	707	0.23	638,692	98	0.85	1.77	-0.92
<b>PSQ12</b>	381,697	0.33,1.4	712	0.17	644,705	77	0.85	1.76	-0.91
<b>PSQ13</b>	381,707	0.26,1.0	725	0.14	658,727	84	0.93	1.73	-0.80
<b>PSQ14</b>	391,697	0.41,1.4	716	0.11	647,703	87	0.70	1.76	-1.06
<b>PSQ15</b>	391,697	0.35,1.1	715	0.13	651/699	73	0.70	1.76	-1.06

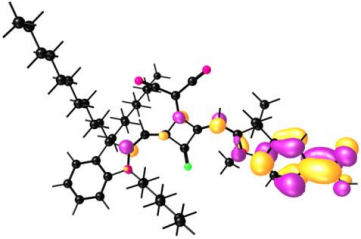
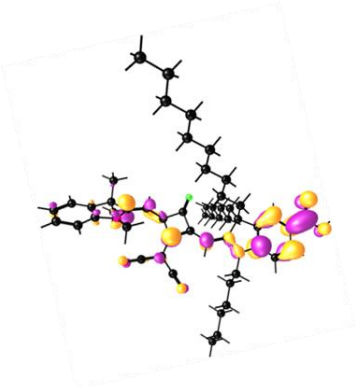
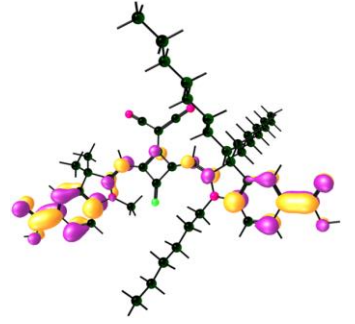
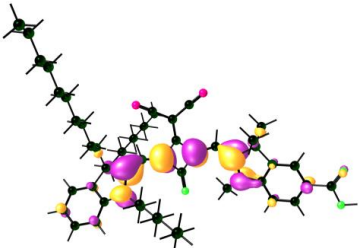
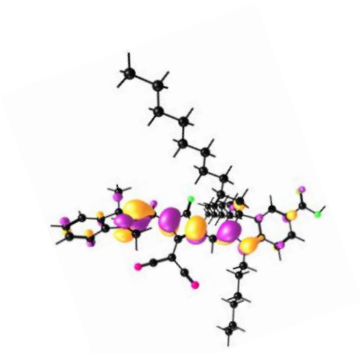
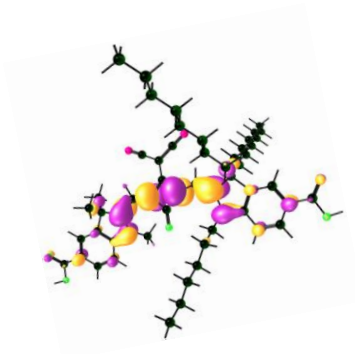
<sup>a</sup>UV-vis absorption in CH<sub>2</sub>Cl<sub>2</sub>. <sup>b</sup> $\epsilon_a$  and  $\epsilon_b$  are molar extinction coefficients for the peaks in visible and charge transfer peaks, respectively. <sup>c</sup>Emission studies (excitation wavelength 610 nm). <sup>d</sup>by relative method in CH<sub>2</sub>Cl<sub>2</sub>. <sup>e</sup>TiO<sub>2</sub> electrode (6  $\mu\text{m}$ , dipped for 30 min in 0.1 mM of **PSQ11-PSQ13** dyes in CHCl<sub>3</sub>. <sup>f</sup> $E_{\text{HOMO}}$  of **PSQ11-15** in CH<sub>2</sub>Cl<sub>2</sub> vs, Fc<sup>+</sup>/Fc (eV), further the potentials were converted with respect to NHE (V) by addition of 0.7 V. <sup>g</sup> $E_{0-0}$  (eV) =  $1240/\lambda$  ( $\lambda$  = intersection wavelength between absorption and emission spectra). <sup>h</sup> $E_{\text{LUMO}} = E_{\text{HOMO}} - E_{0-0}$ .

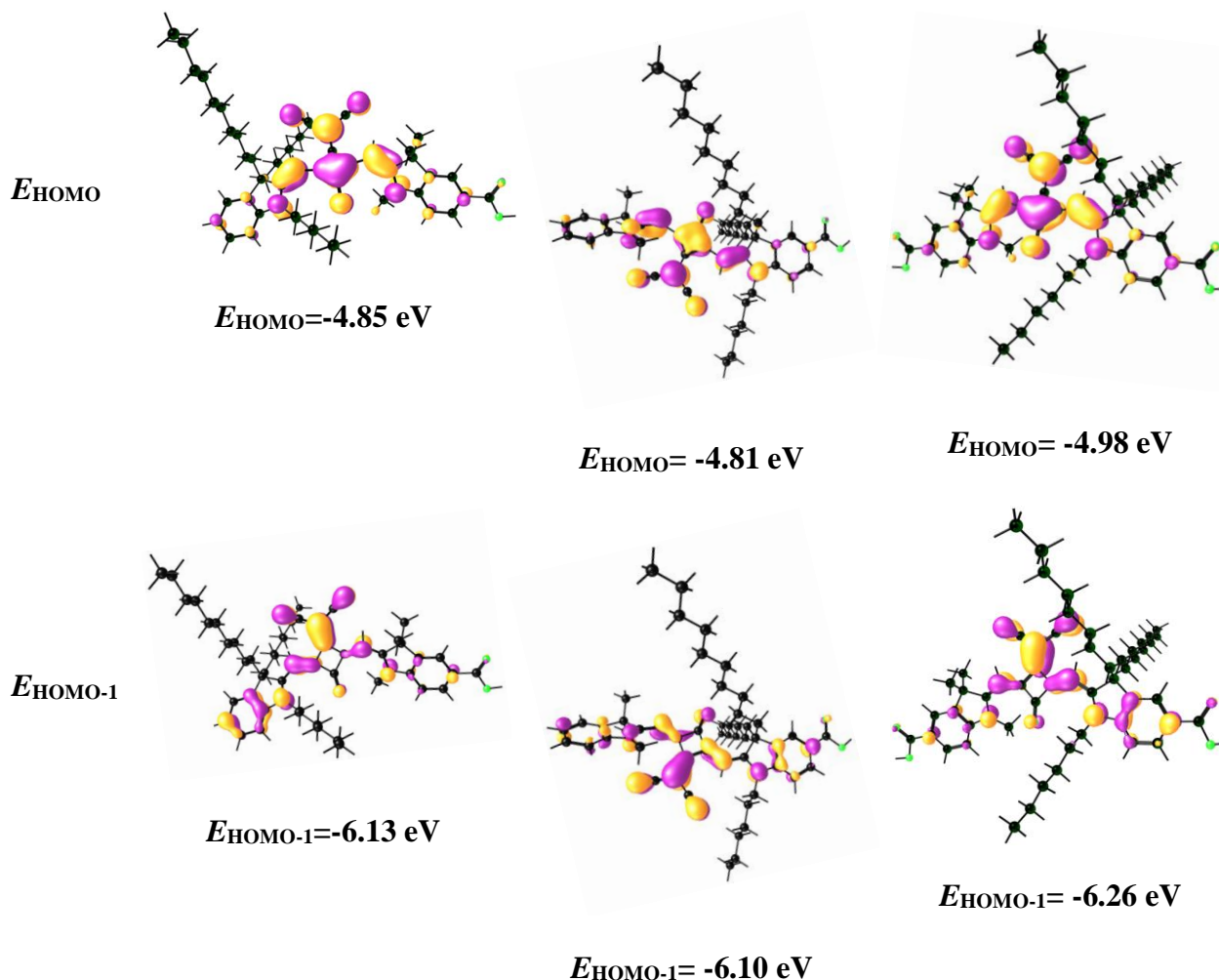
### 3.2.5 Density Functional Theory (DFT) Calculations

To gain insight into the electronic structures of **PSQ11-PSQ13** dyes, their ground state geometries and energies were fully optimized using density functional theory (DFT) by B3LYP/6-31G\*\* level with the Gaussian 09 program. Energy minimized structures of **PSQ11**, **PSQ12**, **PSQ13**, and CDCA were presented in **Figure 3.9** and the detailed parameters are summarized in **Table 3.4**. The iso-surface plots of four selected frontier molecular orbitals HOMO+1, HOMO, LUMO and LUMO-1 were depicted in **Figure 3.10-3.11**. In **PSQ11-PSQ13** dyes, the electron density of HOMO was localized over the dicyanovinyl or cyanoestervinyl groups in addition to the squaraine unit, while the electron distribution of HOMO-1 was



**Figure 3.9** Energy minimized structures of (a) SQ5, (b) PSQ11, (c) PSQ12 and (d) CDCA.

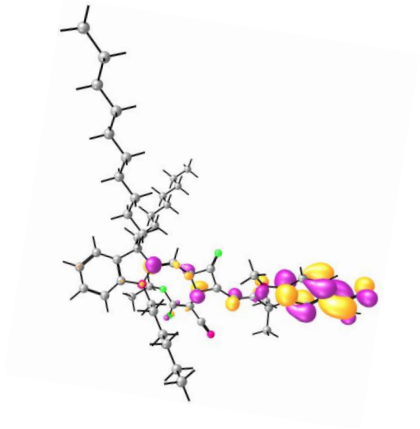
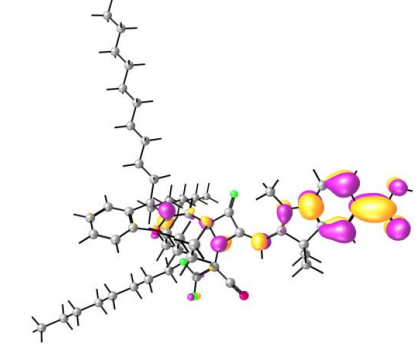
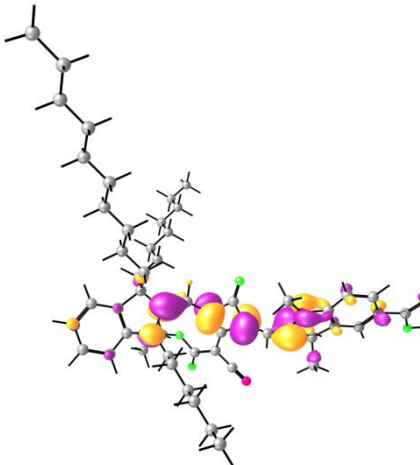
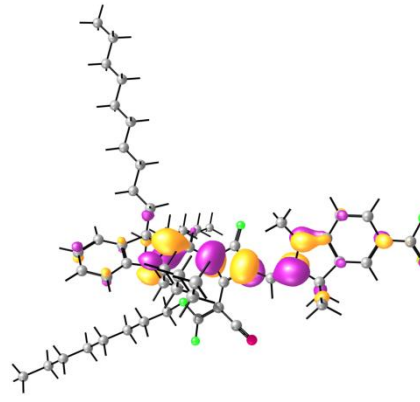
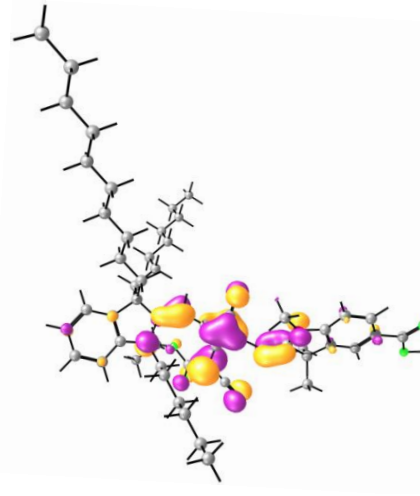
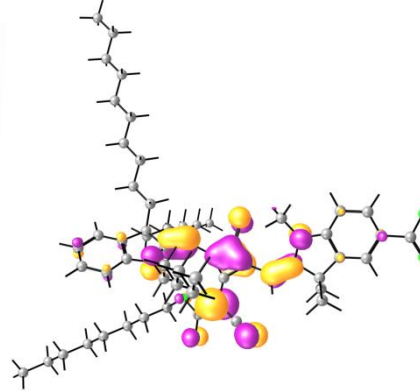
Energy State	PSQ11	PSQ12	PSQ13
$E_{LUMO+1}$	 $E_{LUMO+1} = -1.37$ eV	 $E_{LUMO+1} = -1.27$ eV	 $E_{LUMO+1} = -1.55$ eV
$E_{LUMO}$	 $E_{LUMO} = -2.85$ eV	 $E_{LUMO} = -2.79$ eV	 $E_{LUMO} = -3.01$ eV



**Figure 3.10.** Isosurface plots of selected frontier orbitals (HOMO, HOMO-1, LUMO, LUMO+1) of **PSQ11**, **PSQ12** and **PSQ13**. Fully optimised at DFT B3LYP/6-31G\*\* level. (Isovalue set to 0.036 a.u.)

delocalized over squarate derivatives which contain electron withdrawing group. The LUMOs are delocalized along the backbone of the molecules, and the LUMO+1 is located on the central core and the carboxylate-substituted indolinium moieties. In particular, the LUMO+1 of **PSQ13** showed electron densities at both sides of the two anchoring units, which favour highly efficient electron injection to conduction band of  $\text{TiO}_2$  surface. Such electron distribution in HOMO and LUMO or LUMO+1 suggests the effective electron transfer from dyes to  $\text{TiO}_2$  through anchoring unit. Though there was no significant change in electronic structures, functionalization with alkyl groups helps avoiding the dye-dye interaction.



Energy State	PSQ14	PSQ15
$E_{LUMO+1}$	 $E_{LUMO+1} = -1.55 \text{ eV}$	 $E_{LUMO+1} = -1.54 \text{ eV}$
$E_{LUMO}$	 $E_{LUMO} = -2.61 \text{ eV}$	 $E_{LUMO} = -2.60 \text{ eV}$
$E_{HOMO}$	 $E_{HOMO} = -4.60 \text{ eV}$	 $E_{HOMO} = -4.59 \text{ eV}$

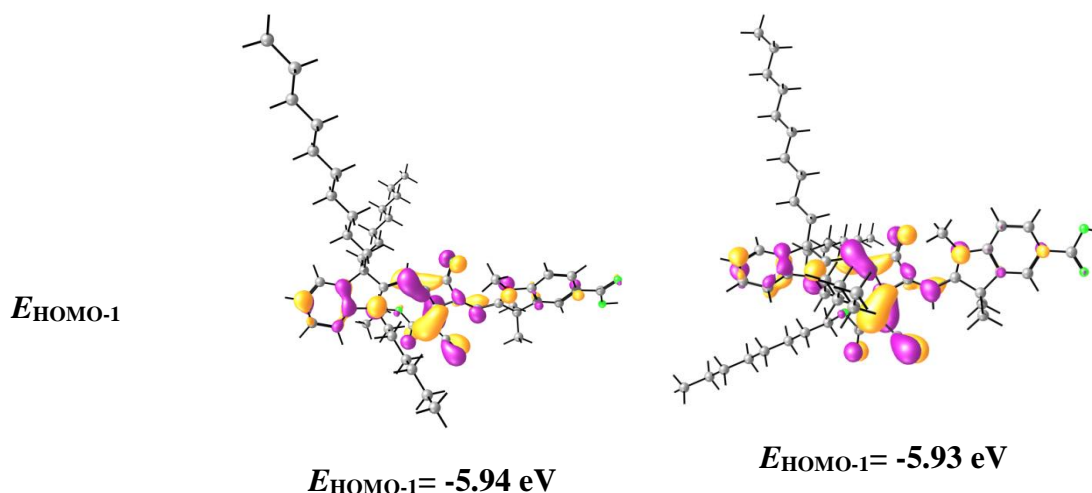


**Figure 3.11.** Isosurface plots of selected frontier orbitals (HOMO, HOMO-1, LUMO, LUMO+1) of **PSQ14** and **PSQ15**. Fully optimised at DFT B3LYP/6-31G\*\* level. (Isovalue set to 0.036 a.u.)

These structural features of top and down alkyl groups enhance the charge injection by reducing the dye aggregation and diminish the charge recombination by surface passivation due to hydrophobic moiety. The distance between the oxygen atom of carboxylic acid and the out-of-plane alkyl groups at top and down indoline units were found to be 14.97 Å and 5.36 Å for **PSQ11** and **PSQ12**, respectively (**Figure 3.9**).

**Table 3.4** Theoretical energy levels of selected MOs

Dye	$E_{\text{HOMO}}$ (eV)	$E_{\text{HOMO-1}}$ (eV)	$E_{\text{LUMO}}$ (eV)	$E_{\text{LUMO+1}}$ (eV)	$\Delta E_{0-0}$ (eV)
<b>PSQ11</b>	-4.85	-6.13	-2.85	-1.37	1.93
<b>PSQ12</b>	-4.81	-6.10	-2.79	-1.27	1.96
<b>PSQ13</b>	-4.98	-6.26	-3.01	-1.55	1.92
<b>PSQ14</b>	-4.60	-5.94	-2.61	-1.55	1.94
<b>PSQ15</b>	-4.59	-5.93	-2.60	-1.54	1.91

### 3.2.6 Photovoltaic Studies of PSQ11-15

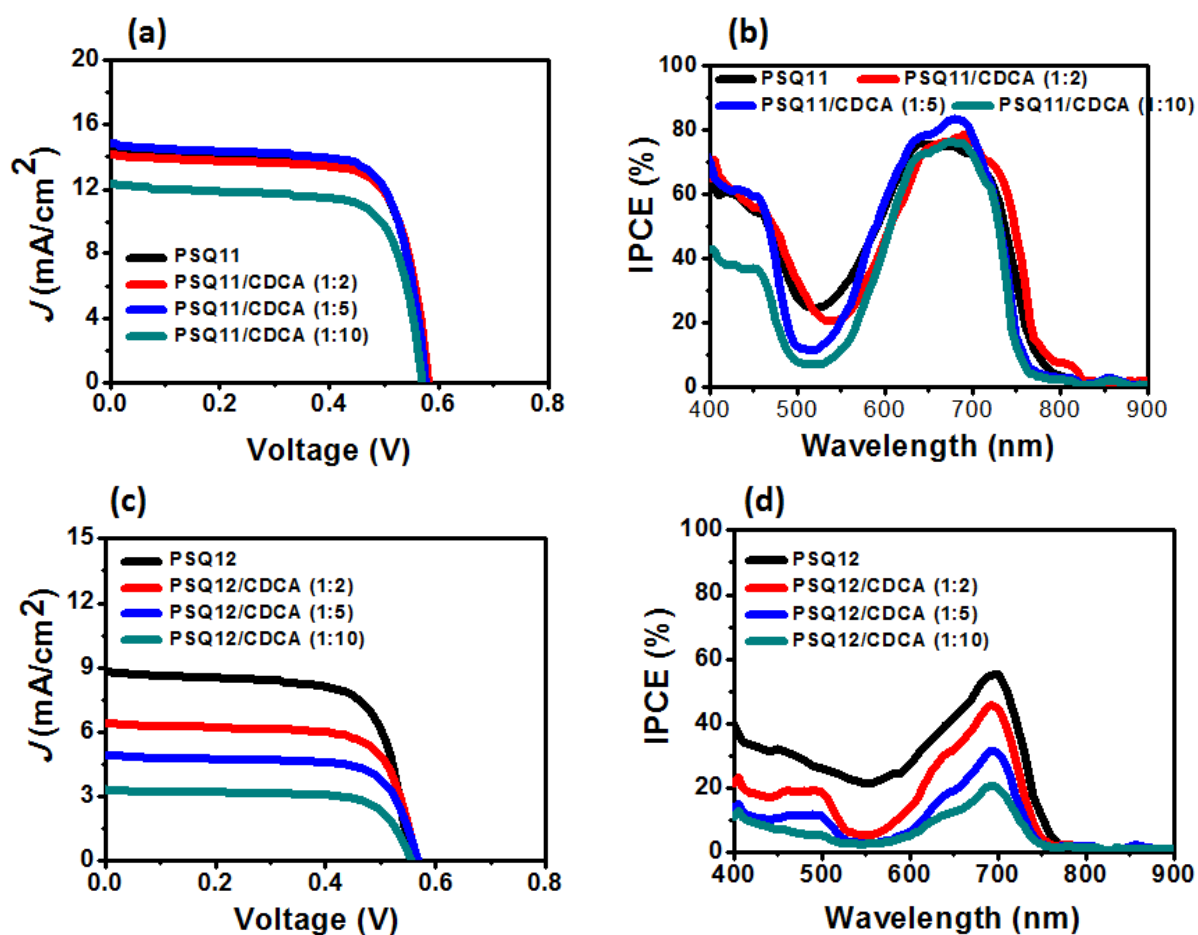
The photovoltaic device performances of DSSC devices based on **PSQ11–PSQ13** dyes under standard conditions (AM 1.5 G, 100 mW/cm<sup>2</sup>) were evaluated using I<sup>-</sup>/I<sub>3</sub><sup>-</sup> electrolyte. The current-voltage (*I-V*) characterization and IPCE profiles of **PSQ11-PSQ13** dyes were shown in **Figure 3.12** and the best cells device performance data with and without co-adsorbent 3 $\alpha$ ,7 $\alpha$ -dihydroxy-5 $\beta$ -cholanic acid (CDCA) were listed in **Table 3.5**. The DSSC devices based on **PSQ11** dye having dicyanovinylene group with in-plane and out-of-plane of branched alkyl chain on sp<sup>3</sup> carbon of indoline units which is away from the TiO<sub>2</sub> surface showed 5.98% PCE with a  $J_{sc}$  of 14.46 mA cm<sup>-2</sup>,  $V_{oc}$  of 0.576V and *ff* of 71.8%. Addition of upto 5 equiv of CDCA increased the device performance to 6.03%. Further addition of CDCA caused significant decreased in photocurrent due to the decreased dye amount on TiO<sub>2</sub> (**Figure 3.12**). When the insertion of in-plane and out-of-plane branched alkyl chain in indoline units which is placed near to TiO<sub>2</sub> anchoring carboxylic acid group as in **PSQ12**, a significant reduction in  $J_{sc}$ ,  $V_{oc}$  and the PCE of 3.45% was achieved in the absence of CDCA and showed 73.33% reduction in PCE compared to isomer of **PSQ11** because of low  $J_{sc}$  of 8.78 mA cm<sup>-2</sup> and  $V_{oc}$  of 0.554V. The reduction of photocurrent was due to significant drop in dye loading, as the branched alkyl group near to the TiO<sub>2</sub> surface facilitates in blocking the dye anchoring 5-coordinated Ti site. Further, the addition of CDCA reduced the cell performance and difference in the PCE appeared because of the less stable monolayer of **PSQ12** on TiO<sub>2</sub> compared to **PSQ11**. **PSQ13** dyes possess additional COOH group compared to **PSQ11** and **PSQ12** dye and exhibited the device performance of 6.07% with  $J_{sc}$  of 14.46 mA cm<sup>-2</sup>,  $V_{oc}$  of 605 mV and *ff* of 0.72. The  $\eta$  and  $V_{oc}$  values were significantly increased in the presence of coadsorbent CDCA. Addition of 2 eq. of CDCA showed improved device efficiency of 7.58%. Photovoltaic parameters with different concentrations of CDCA were showed in **Figure 3.12** for **PSQ11-15**. The reduction photocurrent in isomeric **PSQ11** and **PSQ12** dyes can be explained by the amount of dyes adsorbed on the TiO<sub>2</sub> surface. Dye desorption study in 2NHCl in EtOH was carried out to calculate the dye loading on TiO<sub>2</sub> films. The amount of dye loaded on TiO<sub>2</sub> for **PSQ11-PSQ13** sensitized DSSC was found to be 1.71 $\times 10^{-7}$  mol/cm<sup>2</sup>, 0.88 $\times 10^{-7}$  mol/cm<sup>2</sup> and 1.86 $\times 10^{-7}$  mol/cm<sup>2</sup> respectively. As observed in the case of **PSQ11**, adjusting electron withdrawing group by choosing ethyl cyano acetate of **PSQ13** displayed a 29.5% decrease in efficiency; the overall PCE was 4.26% in absence of CDCA. Extending the length of alkyl chain in electron acceptor unit from ethyl to

octyl as in **PSQ13** dye shows significant improvement in current and voltage and which in turn brings high efficiency of 5.29% with the  $J_{sc}$  and  $V_{oc}$  of 12.47 mA cm<sup>-2</sup> and 592 mV, respectively.

Incident photon-to-current conversion efficiency (IPCE) of **PSQ11-PSQ13** DSSCs is shown in **Figure 3.12**. **PSQ11** based DSSC showed greater IPCE response in the region of 525–800 nm, which corresponds to the absorption by monomers and aggregates. Further **PSQ11** showed high IPCE response between 400 and 510 nm, which corresponds to the absorption from the result of the substitution with dicyanovinylene groups. In absence of CDCA **PSQ11** showed IPCE with maximum of 60% and 76% at 426 and 638 nm, respectively. In contrast **PSQ12** dye showed narrow IPCE response with maximum of 54% at 692 nm because of branched long alkyl group was closer to the TiO<sub>2</sub> surface which suppressed the dye aggregation as well as more dye anchoring. After the addition of CDCA, **PSQ11** and **PSQ12** showed a further increase in IPCE in the far red region, and at 690 nm of **PSQ11** and **PSQ12** exhibit an IPCE response of 79%, and 45%, respectively. Compared to **PSQ11**, **PSQ13** exhibited a broad IPCE profile towards NIR region as it showed the photo-response on set from 800 nm. Similar to **PSQ11**, **PSQ13** also formed a stable monolayer of dyes, as the response from aggregated structure is pronounced in the presence of CDCA (~650 nm). These results suggest that the electron injection efficiency in the NIR region could be improved by introduction of in-plane and out-of-plane alkyl chains due to the modulated self assemblies of **PSQ11-PSQ13**. In case of **PSQ12**, **PSQ13** and **PSQ13**, showed narrow IPCE profile with maximum of 56% at 700 nm under same condition and its extended aggregation was reduced towards monomer which is ascribed to its adsorption status on the surface.

It is interesting to note that position of alkyl group and the number of anchoring groups determined the stability of dye monolayer in the TiO<sub>2</sub> surface. Through the IPCE profile, (i) **PSQ11** and **PSQ12**, among top and down functionalized *cis*-configured squaraine dyes, **PSQ11** showed stable monolayer formation compared to **PSQ12** as the IPCE profile did not change appreciably in the presence of CDCA, on the other hand the CDCA sensitive current response for **PSQ12** indicates the dye-dye interaction is reduced in the case of **PSQ12** on TiO<sub>2</sub>. And for (ii) **PSQ11** and **PSQ13**, besides top alkylated derivatives of the dyes, choice of substituent on the squaryl moiety also makes the self-assembly sensitive to the co-adsorbent. In order to increase the efficiency of formation of self-assembly, a further long alkyl chain is introduced as in **PSQ13**, exhibit the reduced dye-dye interaction which indicates the importance of position of

alkyl groups and the substituent effect on the squaryl moiety to control the aggregation of dyes on the TiO<sub>2</sub> surface to modulate the photocurrent. Further, dyes **PSQ11** and **PSQ13** have the IPCE response with the onset from 800 nm, with a distinctive peak at ~725 nm in the presence of CDCA, which indicates that the J-type aggregate may also effectively participate in the power conversion process. As mentioned before, combining the effect of (i) aligning the molecular dipole parallel to the TiO<sub>2</sub> surface by two anchoring groups and (ii) slipped arrangement of molecular dipoles by sterically demanding structural features offered by in-plane and out-of-plane alkyl groups on one of the indoline units as in **PSQ13** promotes the formation of J-aggregates.



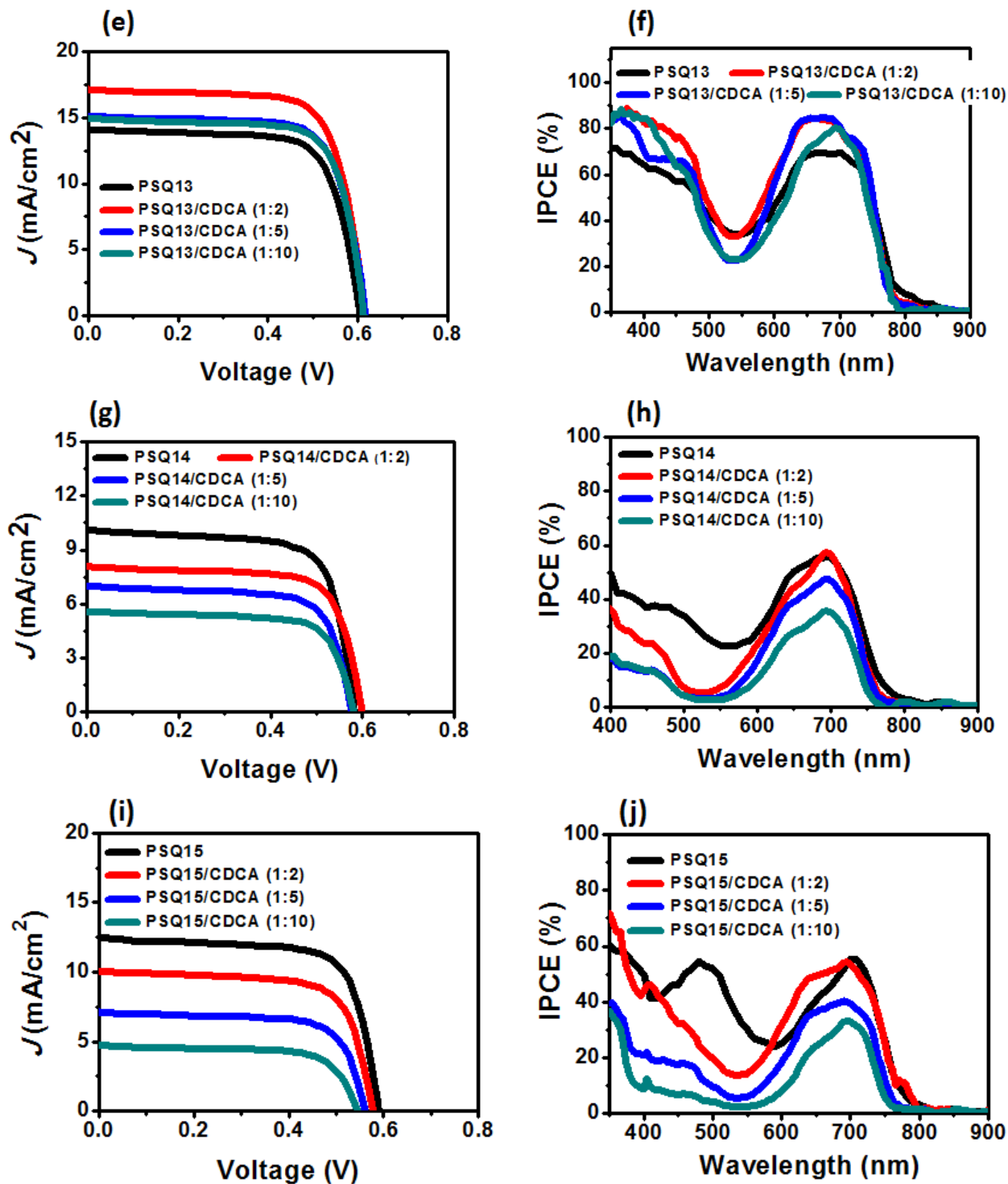


**Figure 3.12** *I-V* and IPCE characterization of **PSQ11-15** dyes. (a, c, e, g and i) and (b, d, f and j) *I-V* and IPCE curves for **PSQ11-15** in presence and absence of CDCA ( $\text{TiO}_2$  electrode thickness =  $8 + 4 \mu\text{m}$  (transparent+scattering layer), area =  $0.22 \text{ cm}^2$ , [Dye] =  $0.1 \text{ mM}$  in  $\text{CHCl}_3$ , dipping time 12 h at rt, electrolyte: iodolyte Z-50 from Solaronix).

**Table 3.5** *I-V* characteristics of **PSQ11-15** dyes best devices with and without CDCA<sup>a</sup>

<b>Dyes</b>	<b><math>J_{sc}</math> mA/cm<sup>2</sup></b>	<b><math>V_{oc}</math> (V)</b>	<b><math>ff</math> (%)</b>	<b>PCE (%)</b>
<b>PSQ11</b>	14.29±0.17	0.577±0.001	71.6±0.20	5.90±0.08
<b>PSQ11/CDCA (1:2)</b>	14.19±0.04	0.579±0.002	70.20±1.2	5.77±0.09
<b>PSQ12</b>	8.69±0.09	0.553±0.001	70.6±0.30	3.39±0.06
<b>PSQ12/CDCA (1:2)</b>	6.26±0.08	0.562±0.001	70.75±0.55	2.49±0.05
<b>PSQ13</b>	13.97±0.07	0.603±0.002	70.85±0.65	5.96±0.11
<b>PSQ13/CDCA (1:2)</b>	17.16±0.04	0.616±0.002	71.5±0.20	7.55±0.02
<b>PSQ14</b>	10.17±0.05	0.581±0.002	71.7±0.70	4.21±0.05
<b>PSQ14/CDCA (1:2)</b>	7.96±0.08	0.594±0.004	72.2±0.70	3.41±0.09
<b>PSQ15</b>	12.29±0.17	0.593±0.002	70.95±0.75	5.17±0.12
<b>PSQ15/CDCA (1:2)</b>	9.91±0.11	0.581±0.001	69.05±0.15	3.98±0.03

<sup>a</sup>TiO<sub>2</sub> electrode thickness = 8 + 4 μm (transparent + scattering layer), area = 0.22 cm<sup>2</sup>, [Dye] = 0.1 mM in CHCl<sub>3</sub>, dipping time was 12 h at rt, electrolyte was iodolyte Z-50 (Solaronix) and summarize the result of best six devices with deviation.

### 3.2.7 Electrochemical Impedance Analysis

To gain insights into the significant variations in  $J_{sc}$  and  $V_{oc}$  arising in DSSC devices and to study the interfacial charge recombination dynamics between the injected electrons in TiO<sub>2</sub> conduction band (CB<sub>TiO2</sub>) and I<sub>3</sub><sup>-</sup> in electrolyte at interfaces of TiO<sub>2</sub>-dye/electrolyte, electrochemical impedance spectroscopy (EIS) measurement was performed under dark experimental conditions. For DSSC,  $V_{oc}$  is the potential difference between quasi- Fermi level of electron in the TiO<sub>2</sub> ( $E_{Fn}$ ) and the fermi level of redox potential of electrolyte ( $E_{F, redox}$ ) (Eq 3.1). For this study, the chemical potential of redox electrolyte used in **PSQ11-PSQ13** were kept constant, so the contribution from the movement of  $E_{F, redox}$  is negligible. Further, changes in  $J_{sc}$

and  $V_{oc}$  parameters affecting  $E_{F,n}$  (Eq 3.2), ( $E_{CB}$  is the position of  $TiO_2$  conduction band,  $k_B$  is the Boltzmann constant,  $T$  is the absolute temperature (293 K),  $n_c$  is free electron density in the semiconductor, and  $N_c$  represents the density of accessible states in the conduction band). Thus, either the conduction band edge shift or the change in the chemical capacitance of  $TiO_2$  infers the cell potential (**Table 3.6**).

$$V_{oc} = E_{(F,redox)} - E_{(F,n)} \quad (3.1)$$

$$E_{(F,n)} = E_{CB} + k_B T \ln(n_c/N_c) \quad (3.2)$$

The Nyquist plots of the DSSC devices based **PSQ11-PSQ13** dye cells were acquired in the dark with applied bias of -0.47 V in **Figure 3.13a**. The impedance of electron transfer at the Pt/electrolyte interface was represented as a smaller semicircle at high frequency region, whereas the larger semicircle at mid frequency range represents the charge recombination resistance at the  $TiO_2$ -dye/electrolyte interface. Among the five PSQ dyes, **PSQ13** showed large radius for mid frequency region at applied bias -0.47 V and **Figure 3.13b** showed the high charge transfer resistance ( $R_{ct}$ ). The high impedance at the  $TiO_2$ -dye/electrolyte interface represents the minimum recombination reactions due to the effective passivation of  $TiO_2$  surface by closely packed dye monolayer. Further, top-branched unsymmetrical *cis*-squaraine dyes **PSQ11**, **PSQ13** and **PSQ13** dyes were exhibited higher charge recombination resistances compared to **PSQ12** dye due to the good passivation of top alkylated dyes on the  $TiO_2$  surface. In this study, both  $sp^3$ -C alkylated and di anchoring groups containing **PSQ13** dye exhibited high  $R_{ct}$  compared to other unsymmetrical *cis*-SQ dyes with branching units at the  $sp^3$ -C atom and mono anchoring group. For the applied bias of -0.47 V,  $R_{ct}$  of *cis*-SQ dyes were in the order of **PSQ13** (17.23  $\Omega$ )>**PSQ11** (14.92  $\Omega$ )> **PSQ14** (13.03  $\Omega$ )>**PSQ13** (12.88  $\Omega$ )>**PSQ12** (10.14  $\Omega$ ). The similar trend of  $R_{ct}$  was observed in  $V_{oc}$  of unsymmetrical *cis*-squaraine dyes which were in the order of **PSQ13**>(618 mV)>**PSQ11** (581 mV)>**PSQ12** (562 mV). Therefore, the observed high  $R_{ct}$  of **PSQ13** indicates the better passivation of surface from redox couple than other dyes. Capacitance ( $C_{\mu}$ ) of the *cis*-SQ dyes on the  $TiO_2$  surface which is closely related to the  $V_{oc}$  of the DSSC as shown in eq 3.2. **Figure 3.13c** explains the observed increase in the  $V_{oc}$  as the capacitance and  $R_{ct}$  of **PSQ11** and **PSQ13** were higher than the **PSQ12**, **PSQ13** and **PSQ13** dyes. This result indicates the importance of two carboxylic acid anchoring groups in dye **PSQ13** for the significant variation in  $C_{\mu}$  in **Figure 3.13c**. Electron lifetime ( $\tau = R_{ct} \times C_{\mu}$ ) for **PSQ11** and



PSQ13 than other PSQ dyes was showed in **Figure 3.13d**, which explains the significant improvement in both  $J_{sc}$  and  $V_{oc}$ . Introduction of ethyl and octyl group on the squaryl unit, further enhances the charge recombination pathways, hence the lower  $R_{ct}$  values were observed for PSQ13 and PSQ13, though it possess top  $sp^3$ -C and N-alkyl groups. It may be due to the formation of unstable monolayer formation for PSQ13 and PSQ13 compared to PSQ11 which is summarized in **Table 3.6**.

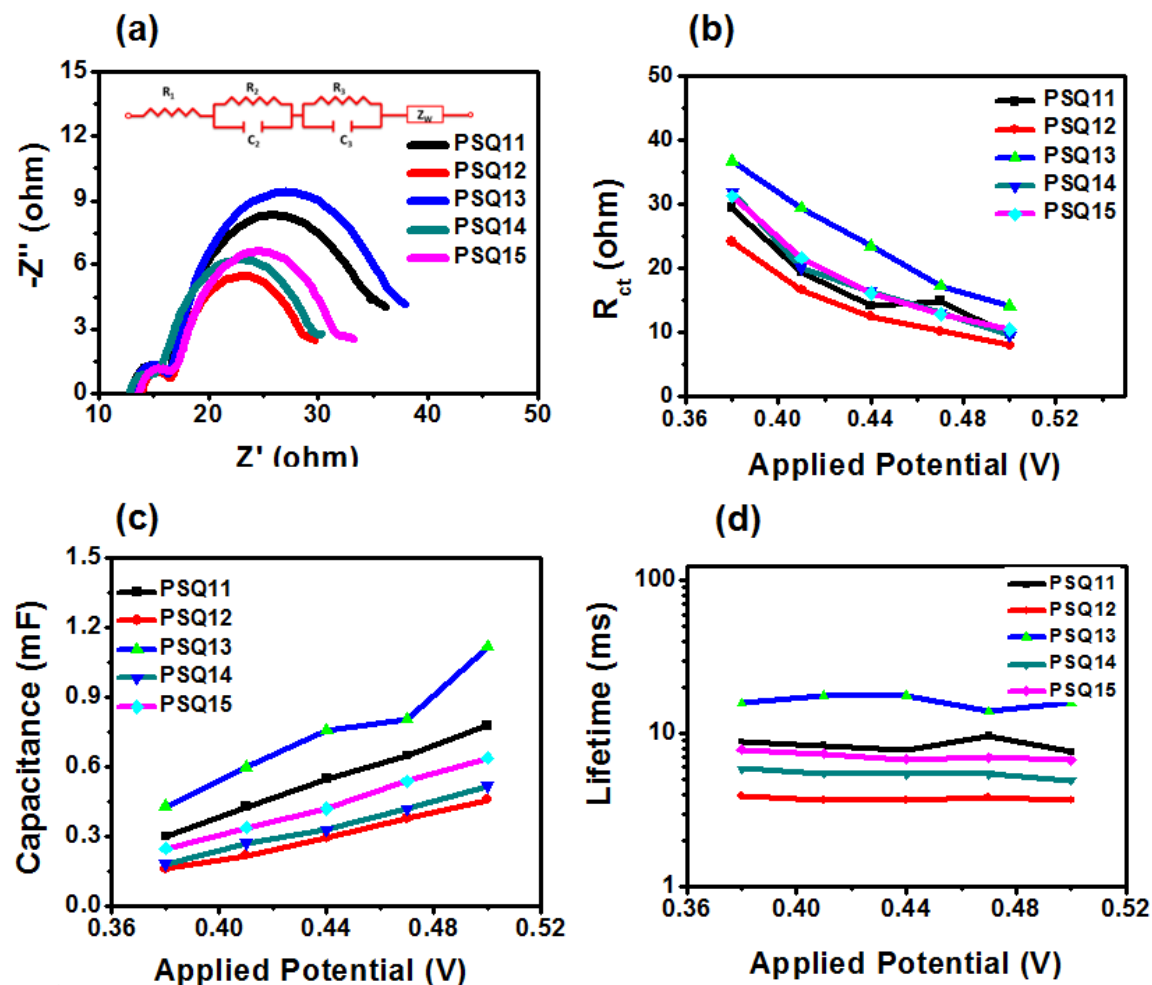


**Figure 3.13** Impedance analysis of PSQ11-15 dyes: (a) Nyquist plot, (b)  $R_{ct}$  vs applied potential, (c)  $C_{\mu}$  vs applied potential and (d)  $\tau$  vs applied potential

**Table 3.6** EIS Parameters of **PSQ11-15** dye cells at an applied potential of  $-0.47$  V in the dark

Dyes	$R_s(\text{ohm})$	$R_{ct}$ (ohm)	$C\mu$ (mF)	$\tau$ (ms)
<b>PSQ11</b>	12.90	14.92	0.65	9.7
<b>PSQ12</b>	13.86	10.14	0.38	3.85
<b>PSQ13</b>	12.93	17.23	0.806	13.89
<b>PSQ14</b>	12.89	13.03	0.42	5.47
<b>PSQ15</b>	13.62	12.88	0.54	6.95

### 3.3 Summary

In summary, a series of *cis*-configured unsymmetrical squaraine dyes **PSQ11-15** were designed with suitably functionalized out-of-plane branched alkyl groups on the  $sp^3$ -C atoms of indoline units of squaraine dyes for dye sensitized solar cells (DSSCs). Factors containing the position of in-plane and out-of-plane alkyl groups, number of anchoring groups that enhanced the self-assembly of dyes and their interaction between  $TiO_2$  and dyes were systematically studied.

However with respect to mono- and di-anchoring groups exhibited different photophysical properties and those studies were carried out on  $Al_2O_3$  surface and then showed different dye orientation on the  $TiO_2$  surface. Sensitivity of dye aggregation was studied by carrying out dye-dipping process in the presence of optically transparent CDCA coadsorbent and monitored that **PSQ11** and **PSQ13** dyes exhibited a stable self-assembly of dyes whereas the photocurrent properties did not show any drastic change upon increasing the CDCA concentration. On the other hand, **PSQ13** dye showed superior performance of 7.58% ( $J_{sc}$  of  $17.12 \text{ mA cm}^{-2}$ ,  $V_{oc}$  of  $0.618 \text{ V}$  and ff of 71.7%) than that of the **PSQ11** and **PSQ12**.

### 3.4 Experimental Section

**3.4.1 Materials and Characterization** Required precursors **1a**<sup>43</sup>, **1b**<sup>36</sup>, **2a**<sup>44</sup>, **3a**<sup>36</sup> and **3b**<sup>36</sup> were synthesized according to the reported literature procedure. All oxygen- and moisture-sensitive reactions were carried out under inert atmosphere. <sup>1</sup>H NMR spectra were recorded on a 200 MHz or 400 MHz or 500 MHz spectrometers, using CDCl<sub>3</sub>. All chemical shifts were reported in parts per million (ppm). <sup>1</sup>H NMR chemical shifts were referenced to TMS (0 ppm). <sup>13</sup>C NMR chemical shifts were referenced to CDCl<sub>3</sub> (77.23 ppm, and recorded on either 100 MHz or 126 MHz NMR spectrometer). HRMS and MALDI-TOF-MS were recorded on SYNAPT G2 HDM spectrometer and ABSciex 5800 MALDI TOF mass spectrometer, respectively. UV-vis absorption spectra were recorded on Analytikjena (SPECORD 210 PLUS) spectrophotometer. For cyclic and differential pulse voltammetric analysis (CV and DPV), a three electrode cell was used for and which was performed on BioLogic SP300 potentiostat. Platinum wire used as a working electrode, a thin platinum foil was used as a counter electrode, and dyes were dissolved in dry dichloromethane. Measurements were carried out at the scan rate of 50 mVs<sup>-1</sup> after addition of 0.1 M of tetra butyl ammonium perchlorate (TBAP) as the supporting electrolyte and non-aqueous Ag/Ag<sup>+</sup> (0.01 M in CH<sub>3</sub>CN) used as reference electrode. The reference electrode was calibrated by recording the cyclic voltammograms of ferrocene in the same electrolyte as external standard; the potential values are on the basis of the estimated value of the ferrocene redox potential in dichloromethane 0.7V versus NHE. The EIS analysis was performed under dark condition by applying external bias to dye cells using a BioLogic SP300 potentiostat equipped with frequency response analyzer. Frequency range was fixed from 1 MHz to 10 mHz with AC amplitude of 10 mV. *I-V* characteristics of the dye cells were measured under a solar simulator (PET, CT200AAA) in clean room conditions, which is controlled by a source measurement unit (Keithley 2420). A certified 4 cm<sup>2</sup> silicon solar cell (NREL) was calibrated to an intensity of 1000 W m<sup>-2</sup> (xenon lamp, 450 W, USHIO INC) of a solar simulator (AM1.5 G light). IPCE spectra measurements were conducted by Newport QE measurement kit including a xenon light source, a monochromator, and a power meter. The set-up was calibrated using a reference silicon solar cell before the device measurement.

**3.4.2 Device Fabrication Procedure** For fabricating photoanode of DSSC, FTO (F-doped SnO<sub>2</sub> glass; 6-8 Ω/sq) was cleaned sequentially by mucasol (2% in water), deionized water, and isopropanol using an ultra-sonication for 15 min. A blocking layer of TiO<sub>2</sub> was prepared by dipping cleaned FTO substrate in freshly prepared aqueous 0.05 M TiCl<sub>4</sub> solution at 70 °C for 30

min, and washed immediately with deionized water, and followed by annealing in air at 125 °C for 10 min. And the mesoscopic transparent thin layer (6-8 μm thickness) of TiO<sub>2</sub> onto buffer layer modified FTO was coated using TiO<sub>2</sub> paste (< 20 nm, Ti-Nanoxide T/SP) by the doctor-blade technique. Then kept in air for 5 min and annealed at 125 °C in air for 15 min before coating scattering layer on it. Dyesol, WER2-O paste was used to coat a 4-6 μm thick TiO<sub>2</sub> layer, kept in air for 5 min and annealed at 125 °C in air for 15 min. Resulting 0.22 cm<sup>2</sup> active area films were sintered at 325 °C for 5 min, 375 °C for 5 min, 450 °C for 15 min and 500 °C for 15 min with heating rate of 5 °C per min in air. After reaching the furnace temperature at 50 °C, sintered films were treated in TiCl<sub>4</sub> solution as described before. After sintering the layer-by-layer deposited film again at 500 °C for 30 min, allowed to reach 50 °C and were immediately immersed in 0.1 mM **PSQ11-15** dye solution in chloroform at room temperature for 12 h. The dye loaded electrodes are washed thoroughly with chloroform, to remove physisorbed molecules. Successive addition of co-adsorbent 3α,7α-dihydroxy-5β-cholanic acid (CDCA) was varied the concentration of de-aggregating agent in the dye solution and studied the device performance at 1, 2, 3, 4 and 10 equiv of CDCA. Finally the dye cell was assembled by joining the electrolyte (Iodolyte Z50) filled photoanode and platinum cathode using a 25 μm thick spacer. Photovoltaic parameters have been evaluated without masking the device.

### 3.4.3 Synthetic Procedures and Characterization Data

#### 2-[(1-Methyl-5-carboxy-3,3-dimethyl-1,3-dihydro-2H-indol-2-ylidene)methyl]-3

**[dicyanomethylidene]-4-oxo-cyclobut-1-en-1-olate (2b)**: A mixture of **1b** (0.5 g, 1.3 mmol), malononitrile (0.1 g, 1.49 mmol), and NEt<sub>3</sub> (0.22 mL) were dissolved in 25 mL of EtOH and stirred for 4 h at rt. The solvent was removed under reduced pressure, and the reaction mixture was subjected to column chromatography on silica gel with 1:20 (v/v) MeOH/EtOAc to afford **2b** as a red solid (0.31 g, 55% yield). Mp 222-224 °C; FT-IR (dry film, cm<sup>-1</sup>): 3422 (w), 2964-2657 (br), 2203(s), 2181 (s), 1752 (s), 1663 (m), 1614 (s), 1599 (s); <sup>1</sup>H NMR (200 MHz, DMSO-*d*<sub>6</sub>) δ: 7.86 (d, J= 1.6 Hz, 1 H), 7.82 (s, 1 H), 7.04 (d, J= 8.6 Hz, 1 H), 5.98 (s, 1 H), 3.28 (s, 3 H), 1.58 (s, 6 H); <sup>13</sup>C NMR (101MHz, DMSO-*d*<sub>6</sub>) δ: 192.7, 185.2, 178.1, 167.4, 166.8, 162.7, 147.5, 140.0, 130.3, 122.7, 119.0, 117.9, 107.2, 86.3, 72.3, 60.3, 45.8, 36.4, 29.6, 27.0, 8.6; MALDI-TOF (*m/z*): [M]<sup>+</sup> calcd for C<sub>20</sub>H<sub>15</sub>N<sub>3</sub>O<sub>4</sub>: 361.1063; found: 361.0939.

**2-[(1-Methyl-5-carboxy-3,3-dimethyl-1,3-dihydro-2H-indol-2-ylidene)methyl]-3-[cyano(ethoxycarbonyl)methylidene]-4-oxo-cyclobut-1-en-1-olate (2c):** **1b** (0.5 g, 1.3 mmol), ethyl cyanoacetate (0.28 g, 2.5 mmol), and NEt<sub>3</sub> (0.65 mL) were taken in a 50 mL round bottomed flask and 25 mL of EtOH added and stirred for 24 h at rt. The reaction mixture was concentrated under reduced pressure, and the resulting solid residue was purified by column chromatography on silica gel with 1:20 (v/v) MeOH/EtOAc to obtained as a red solid (0.27 g, 50% yield). Mp 244-246 °C; FT-IR (dry film, cm<sup>-1</sup>): 3453 (w), 2961-2856 (br), 2189 (s), 1744 (s), 1683 (m), 1610 (m), 1551 (s); <sup>1</sup>H NMR (500 MHz, DMSO-*d*<sub>6</sub>) δ: 7.82 (d, J= 7.6 Hz, 1 H), 7.7 (d, J= 6.7 Hz, 1 H), 7.1 (s, 1 H), 6.26 (s, 1 H), 4.05 (q, 12.8 Hz, 2H), 3.28 (s, 3 H), 1.58 (s, 6 H), 1.17 (t, 3H); <sup>13</sup>C NMR (126 MHz, DMSO-*d*<sub>6</sub>) δ: 192.1, 181.7,180.0, 168.5, 167.4, 166.1, 160.0, 147.7, 140.3, 130.2, 122.5, 106.5, 91.8, 58.6, 58.5, 45.1,45.5, 29.6, 29.0, 27.2, 14.7, 8.6; MALDI-TOF (*m/z*): [M]<sup>+</sup>calcd for C<sub>22</sub>H<sub>20</sub>N<sub>2</sub>O<sub>6</sub>: 408.1321; found: 408.0555.

**2-[(1-Methyl-5-carboxy-3,3-dimethyl-1,3-dihydro-2H-indol-2-ylidene)methyl]-3-[cyano(octoxycarbonyl)methylidene]-4-oxo-cyclobut-1-en-1-olate (2d):** **1b** (0.5 g 1.3 mmol), octylcyanoacetate (0.28 g, 2.5 mmol), and NEt<sub>3</sub> (0.65 mL) were mixed in a 50 mL round bottomed flask and 25 mL of EtOH was added to it and stirred for 24 h at rt. Then the solvent was removed under reduced pressure, and the solid residue was purified by column chromatography on silica gel with 1:20 (v/v) MeOH/EtOAc to obtain **2d** as a red solid (0.26 g, 40% yield). Mp 199-201 °C; FT-IR (dry film, cm<sup>-1</sup>): 3409 (w), 2961-2854 (br), 2188 (s), 1744 (s), 1683 (w), 1609 (s), 1552 (s); <sup>1</sup>H NMR (200 MHz, DMSO-*d*<sub>6</sub>) δ: 7.85 (d, J= 7.6 Hz, 1 H), 7.82 (d, J= 6.8 Hz, 1 H), 7.08 (s, 1 H), 6.3 (s, 1 H), 4.05 (q, 12.8 Hz, 2H), 3.29 (s, 3 H), 1.58 (s, 6 H), 1.36-1.15(m, 12 H), 0.85 (t, 3H); <sup>13</sup>C NMR (101 MHz, DMSO-*d*<sub>6</sub>) δ: 193.6, 187.4, 180.0, 168.6, 167.5, 165.6, 160.0, 147.7, 140.1, 137.6, 130.2, 122.5, 119.6,106.5, 91.8, 62.7, 62.6, 45.5, 31.3, 29.6, 29.0, 28.7, 27.2, 25.5, 22.1, 14.0, 8.6; MALDI-TOF (*m/z*): [M]<sup>+</sup>calcd for C<sub>28</sub>H<sub>32</sub>N<sub>2</sub>O<sub>6</sub>: 492.2260; found: 492.2196.

**General procedure for the syntheses of *cis*-configured unsymmetrical squaraine dyes, PSQ11-15** The corresponding indoium salt (**3a-3b**) and the respective dicyanovinylene, cyanoester vinylene appended semi-squaraic acid derivatives (**2a-2d**) were dissolved in 1-butanol and anhydrous PhMe(1:1, 6 mL) in a 50 mL two necked round bottom flask and then charged with Dean-Stark reflux condenser. The reaction mixture was refluxed for 24 h under

inert atmosphere, cooled to room temperature and the solvents were removed under reduced pressure. The reaction mixture was subjected to column chromatography (SiO<sub>2</sub>, 100-200 mesh, 5% MeOH and 95% CH<sub>2</sub>Cl<sub>2</sub>) to afford the required dye.

**2-[(5-Carboxy-1,3,3-trimethylindolin-2-ylidene)methyl]-4-[(3-decyl-1-hexyl-3-octyl-3H-indol-1-ium-2-yl)methylene]-3-(dicyanomethylene)cyclobut-1-en-1-olate (PSQ11):** Started with 0.15 g (0.41 mmol) of **2b** and 0.25 g (0.41 mmol) of **3a**. Product obtained: 0.23 g, Yield: 75%; Mp 268-270 °C; FT-IR (dry film, cm<sup>-1</sup>): 2964-2853 (br), 2196 (s), 2179 (s), 1721 (s), 1681 (s), 1622 (m), 1477 (s); <sup>1</sup>H NMR (400 MHz, CDCl<sub>3</sub>) δ: 7.97 (d, *J* = 7.6 Hz, 1 H), 7.93 (s, 1 H), 7.33 (d, *J* = 7.2 Hz, 2 H), 7.27-7.20 (m, 2 H), 7.16 (d, *J* = 8 Hz, 1 H), 6.54 (s, 1 H), 6.32 (s, 1 H), 4.08 (br s, 2 H), 3.49 (s, 3 H), 2.92 (br s, 2 H), 1.88 (m, 2 H), 1.64 (s, 6 H), 1.38 – 0.96 (m, 32 H), 0.796 – 0.62 (m, 11 H), 0.42 (m, 2 H); <sup>13</sup>C NMR (101MHz, MeOH-*d*<sub>4</sub>) δ: 177.8, 174.4, 174.2, 172.7, 169.5, 169.1, 166.1, 148.1, 145.1, 143.1, 140.8, 132.2, 129.7, 127.7, 127.1, 124.7, 123.7, 120.1, 120.0, 116.7, 112.5, 110.8, 91.9, 90.3, 61.0, 46.1, 40.8, 40.4, 40.3, 35.1, 33.3, 33.2, 32.9, 32.3, 32.0, 31.0, 31.0, 30.8, 30.6, 30.6, 30.5, 30.4, 30.3, 30.2, 30.2, 29.9, 29.9, 29.2, 27.7, 27.6, 26.3, 24.7, 24.5, 23.9, 23.8, 14.8, 14.7, 14.6; MALDI-TOF (*m/z*): [M]<sup>+</sup>calcd for C<sub>53</sub>H<sub>70</sub>N<sub>4</sub>O<sub>3</sub>: 810.5448; found: 810.4728.

**4-[(5-Carboxy-3-decyl-1-hexyl-3-octyl-3H-indol-1-ium-2-yl)methylene]-3-(dicyanomethylene)-2-[(1,3,3-trimethylindolin-2-ylidene)methyl]cyclobut-1-en-1-olate (PSQ12):** Started with 0.22 g (0.52 mmol) of **2a** and 0.33 g (0.52 mmol) of **3b**. Product obtained: 0.29 g, Yield: 68%; Mp 182-184 °C; FT-IR (dry film, cm<sup>-1</sup>): 2954-2854 (br), 2196 (s), 2179 (s), 1721 (w), 1682 (w), 1612 (w), 1495 (s); <sup>1</sup>H NMR (400 MHz, CDCl<sub>3</sub>) δ: 7.99 (d, *J* = 8.4 Hz, 1 H), 7.87 (s, 1 H), 7.42 (d, *J* = 7.2 Hz, 1 H), 7.34-7.16 (m, 3 H), 7.17 (d, *J* = 8.4 Hz, 1 H), 6.43 (s, 2 H), 3.98 (br s, 2 H), 3.62 (s, 3 H), 2.90 (br s, 2 H), 1.82 (m, 2 H), 1.66 (s, 6 H), 1.31 – 1 (m, 32 H), 0.81 – 0.7 (m, 11 H), 0.47 (m, 2 H); <sup>13</sup>C NMR (101MHz, MeOH-*d*<sub>4</sub>) δ: 182.3, 177.9, 176.5, 170.4, 169.4, 166.0, 165.2, 149.6, 143.9, 143.8, 132.1, 129.7, 127.1, 124.7, 123.5, 120.2, 112.6, 110.7, 90.7, 59.5, 51.5, 45.4, 40.6, 35.1, 33.3, 33.2, 33.0, 32.8, 31.0, 30.9, 30.9, 30.7, 30.6, 30.6, 30.4, 30.3, 30.2, 30.1, 30.0, 29.8, 29.7, 28.8, 27.7, 26.8, 26.2, 24.6, 24.4, 23.9, 23.9, 23.7, 14.7, 14.6, 14.5; MALDI-TOF (*m/z*): [M]<sup>+</sup>calcd for C<sub>53</sub>H<sub>70</sub>N<sub>4</sub>O<sub>3</sub>: 810.5448; found: 810.4498.

**2-[(5-Carboxy-1,3,3-trimethylindolin-2-ylidene)methyl]-4-[(5-carboxy-3-decyl-1-hexyl-3-octyl-3H-indol-1-ium-2-yl)methylene]-3-(dicyanomethylene)cyclobut-1-en-1-olate (PSQ13):**

Started with 0.22 g (0.62 mmol) of **2b** and 0.39 g (0.62 mmol) of **3b**. Product obtained: 0.26g, Yield: 50%; Mp 266-268 °C; FT-IR (dry film,  $\text{cm}^{-1}$ ): 2956-2854 (br), 2197 (s), 2179 (s), 1721 (s), 1682 (s), 1605 (s), 1474 (s);  $^1\text{H}$  NMR (200 MHz,  $\text{CDCl}_3$ )  $\delta$ : 8.35 (br s, 1 H), 8.11 (br s, 2 H), 8.03 (br s, 1 H), 7.38 (d,  $J = 9.2$  Hz, 2 H), 6.64 (br s, 1 H), 6.53 (br s, 1 H), 4.16 (br s, 2 H), 3.68 (s, 3 H), 3.01 (br s, 2 H), 2.03 (m, 2 H), 1.79 (s, 6 H), 1.37 – 1.09 (m, 32 H), 0.89 – 0.79 (m, 11 H), 0.57 (m, 2 H);  $^{13}\text{C}$  NMR (126 MHz,  $\text{CDCl}_3$ )  $\delta$ : 172.8, 172.3, 172.0, 171.9, 169.1, 168.3, 168.1, 148.1, 146.9, 142.4, 139.7, 131.3, 125.6, 125.2, 124.2, 118.5, 109.7, 109.4, 91.9, 90.8, 68.5, 66.0, 58.8, 48.9, 45.0, 41.6, 39.6, 31.9, 31.8, 31.5, 29.5, 29.4, 29.3, 29.3, 29.0, 28.9, 28.9, 27.6, 26.7, 26.5, 23.8, 22.6, 22.6, 22.4, 14.1, 13.9; MALDI-TOF ( $m/z$ ):  $[\text{M}]^+$ calcd for  $\text{C}_{54}\text{H}_{70}\text{N}_4\text{O}_5$ : 854.5346; found: 854.4550.

**2-[(5-Carboxy-1,3,3-trimethylindolin-2-ylidene)methyl]-3-(1-cyano-2-ethoxy-2-oxoethylidene)-4-[(3-decyl-1-hexyl-3-octyl-3H-indol-1-ium-2-yl)methylene]cyclobut-1-en-1-olate (PSQ13):**

Started with 0.1 g (0.19 mmol) of **2c** and 0.12 g (0.19 mmol) of **3a**. product obtained: 0.12g, Yield: 70%; Mp 255-257 °C; FT-IR (dry film,  $\text{cm}^{-1}$ ): 2954-2854 (br), 2184 (s), 1717 (w), 1678 (s), 1614 (w), 1475 (s);  $^1\text{H}$  NMR (500 MHz,  $\text{CDCl}_3$ )  $\delta$ : 8.07 (t,  $J = 13.5$  Hz, 1 H), 7.98 (br s, 1 H), 7.83 (s, 1 H), 7.38 (t,  $J = 15.5$  Hz, 1 H), 7.34-7.32 (m, 1 H), 7.28-7.26 (m, 1 H), 7.12 (t,  $J = 14.5$  Hz, 1 H), 7.08 (br s, 1 H), 6.97 (d,  $J = 8$  Hz, 1 H), 4.26 (m, 2 H), 4.19 (m, 2 H), 3.62 (br s, 3 H), 2.98 (br s, 3 H), 2.0 (t,  $J = 22$  Hz, 2 H), 1.84-1.72 (m, 6 H), 1.5 – 1.06 (m, 32 H), 0.91 – 0.78 (m, 11 H), 0.49 (m, 2 H);  $^{13}\text{C}$  NMR (126 MHz,  $\text{CDCl}_3$ )  $\delta$ : 172.8, 172.3, 172.0, 171.9, 169.1, 168.3, 168.1, 148.1, 146.9, 142.4, 139.7, 131.3, 125.6, 125.2, 124.2, 118.5, 109.7, 109.4, 91.9, 90.8, 68.5, 66.0, 58.8, 48.9, 45.0, 41.6, 39.6, 31.9, 31.8, 31.5, 29.5, 29.4, 29.3, 29.3, 29.0, 28.9, 28.9, 27.6, 26.7, 26.5, 23.8, 22.6, 22.6, 22.4, 14.1, 13.9; MALDI-TOF ( $m/z$ ):  $[\text{M}]^+$ calcd for  $\text{C}_{55}\text{H}_{75}\text{N}_3\text{O}_5$ : 857.5707; found: 857.4863.

**2-[(5-Carboxy-1,3,3-trimethylindolin-2-ylidene)methyl]-3-(1-cyano-2-octoxy-2-oxoethylidene)-4-[(3-decyl-1-hexyl-3-octyl-3H-indol-1-ium-2-yl)methylene]cyclobut-1-en-1-olate (PSQ13):**

Started with 0.1 g (0.17 mmol) of **2d** and 0.1 g (0.17 mmol) of **3a**. Product obtained: 87 mg, Yield: 55%; as green sticky gum. FT-IR (dry film,  $\text{cm}^{-1}$ ): 2954-2854 (br), 2185 (w), 1717 (w), 1679 (w), 1612 (w), 1475 (s);  $^1\text{H}$  NMR (500 MHz,  $\text{CDCl}_3$ )  $\delta$ : 8.07 (d,  $J = 8$  Hz, 1

H), 7.97 (s, 1 H), 7.83(br s, 1 H), 7.40-7.24 (m, 3 H), 7.12 (t,  $J = 14$  Hz, 1 H), 7.06 (br s, 1 H), 6.98(d,  $J = 8.4$  Hz, 1 H), 4.18 (br s, 3 H), 3.61 (br s, 2 H), 3.23 (q, 15 H), 2.97 (br s, 2 H), 2.36 (br s, 2 H), 2 (m, 2 H), 1.8-1.6(m, 6 H), 1.47 (t,  $J = 17.6$  Hz, 2 H), 1.34-1 (m, 32 H), 0.9 – 0.78 (m, 11 H), 0.48 (m, 2 H);  $^{13}\text{C}$  NMR (126 MHz,  $\text{CDCl}_3$ )  $\delta$ : 179.0, 179.0, 171.1, 170.8, 168.5, 166.7, 143.5, 143.3, 139.6, 139.4, 131.1, 130.7, 129.2, 127.9, 125.2, 125.1, 123.5, 122.3, 122.2, 110.4, 110.3, 96.3, 90.9, 66.8, 63.9, 63.8, 59.2, 46.3, 45.3, 45.0, 39.3, 39.3, 34.0, 31.7, 31.7, 31.6, 31.4, 31.2, 30.1, 29.5, 29.5, 29.4, 29.3, 29.3, 29.2, 29.1, 28.9, 28.9, 27.6, 27.4, 27.0, 26.9, 26.5, 26.4, 25.9, 25.8, 24.6, 23.7, 23.6, 22.5, 22.4, 22.4, 22.3, 13.9, 13.9, 13.8, 13.7, 13.6; MALDI-TOF ( $m/z$ ):  $[\text{M}]^+$  calcd for  $\text{C}_{61}\text{H}_{87}\text{N}_3\text{O}_5$ : 941.6646; found: 941.6144.

### 3.5 References

- (1) O'Regan, B.; Grätzel, M. A Low-Cost, High-Efficiency Solar Cell Based on Dye-Sensitized Colloidal  $\text{TiO}_2$  Films. *Nature* **1991**, *353*, 737–740.
- (2) Hagfeldt, A.; Boschloo, G.; Sun, L.; Kloo, L.; Pettersson, H. Dye-Sensitized Solar Cells. *Chem. Rev.* **2010**, *110*, 6595–6663.
- (3) Listorti, A.; O'Regan, B.; Durrant, J. R. Electron Transfer Dynamics in Dye-Sensitized Solar Cells. *Chem. Mater.* **2011**, *23*, 3381–3399.
- (4) Brennan, B. J.; Llansola Portolés, M. J.; Liddell, P. A.; Moore, T. A.; Moore, A. L.; Gust, D. Comparison of Silatrane, Phosphonic Acid, and Carboxylic Acid Functional Groups for Attachment of Porphyrin Sensitizers to  $\text{TiO}_2$  in Photoelectrochemical Cells. *Phys. Chem. Chem. Phys.* **2013**, *15*, 16605-16614.
- (5) Wiberg, J.; Marinado, T.; Hagberg, D. P.; Sun, L.; Hagfeldt, A.; Albinsson, B. Effect of Anchoring Group on Electron Injection and Recombination Dynamics in Organic Dye-Sensitized Solar Cells. *J. Phys. Chem. C* **2009**, *113*, 3881–3886.
- (6) Murakami, T. N.; Yoshida, E.; Kounura, N. Carbazole Dye with Phosphonic Acid Anchoring Groups for Long-Term Heat Stability of Dye-Sensitized Solar Cells. *Electrochim. Acta* **2014**, *131*, 174–183.
- (7) Imahori, H.; Kang, S.; Hayashi, H.; Haruta, M.; Kurata, H.; Isoda, S.; Canton, S. E.; Infahsaeng, Y.; Kathiravan, A.; Pascher, T. Photoinduced Charge Carrier Dynamics of Zn-Porphyrin- $\text{TiO}_2$  Electrodes: The Key Role of Charge Recombination for Solar Cell Performance. *J. Phys. Chem. A* **2011**, *115*, 3679–3690.



- 
- (8) Ye, S.; Kathiravan, A.; Hayashi, H.; Tong, Y.; Infahsaeng, Y.; Chabera, P.; Pascher, T.; Yartsev, A. P.; Isoda, S.; Imahori, H. Role of Adsorption Structures of Zn-Porphyrin on TiO<sub>2</sub> in Dye-Sensitized Solar Cells Studied by Sum Frequency Generation Vibrational Spectroscopy and Ultrafast Spectroscopy. *J. Phys. Chem. C* **2013**, *117*, 6066–6080.
  - (9) Mathew, S.; Yella, A.; Gao, P.; Humphry-Baker, R.; Curchod, B. F. E.; Ashari-Astani, N.; Tavernelli, I.; Rothlisberger, U.; Nazeeruddin, M. K.; Grätzel, M. Dye-Sensitized Solar Cells with 13% Efficiency Achieved through the Molecular Engineering of Porphyrin Sensitizers. *Nat. Chem.* **2014**, *6*, 242–247.
  - (10) Yao, Z.; Zhang, M.; Wu, H.; Yang, L.; Li, R.; Wang, P. Donor/Acceptor Indenoperylene Dye for Highly Efficient Organic Dye-Sensitized Solar Cells. *J. Am. Chem. Soc.* **2015**, *137*, 3799–3802.
  - (11) Würthner, F. Dipolar Dye Aggregates: A Problem for Nonlinear Optics, but a Chance for Supramolecular Chemistry. *Angew. Chem. Int. Ed.* **2000**, *39*, 1978–1981.
  - (12) Kaiser, T. E.; Wang, H.; Stepanenko, V.; Würthner, F. Supramolecular Construction of Fluorescent J-Aggregates Based on Hydrogen-Bonded Perylene Dyes. *Angew. Chemie Int. Ed.* **2007**, *46*, 5541–5544.
  - (13) Liess, A.; Lv, A.; Arjona-Esteban, A.; Bialas, D.; Krause, A.-M.; Stepanenko, V.; Stolte, M.; Würthner, F. Exciton Coupling of Merocyanine Dyes from H- to J-Type in the Solid State by Crystal Engineering. *Nano Lett.* **2017**, *17*, 1719–1726.
  - (14) Treat, N. A.; Knorr, F. J.; McHale, J. L. Templated Assembly of Betanin Chromophore on TiO<sub>2</sub>: Aggregation-Enhanced Light-Harvesting and Efficient Electron Injection in a Natural Dye-Sensitized Solar Cell. *J. Phys. Chem. C* **2016**, *120*, 9122–9131.
  - (15) Kryman, M. W.; Nasca, J. N.; Watson, D. F.; Detty, M. R. Selenorhodamine Dye-Sensitized Solar Cells: Influence of Structure and Surface-Anchoring Mode on Aggregation, Persistence, and Photoelectrochemical Performance. *Langmuir* **2016**, *32*, 1521–1532.
  - (16) Nüesch, F.; Moser, J. E.; Shklover, V.; Grätzel, M. Merocyanine Aggregation in Mesoporous Networks. *J. Am. Chem. Soc.* **1996**, *118*, 5420–5431.
  - (17) Khazraji, A. C.; Hotchandani, S.; Das, S.; V. Kamat, P. V. Controlling Dye (Merocyanine-540) Aggregation on Nanostructured TiO<sub>2</sub> Films. An Organized Assembly Approach for Enhancing the Efficiency of Photosensitization. *J. Phys. Chem. B*, **1999**, *103*, 4693–4700.

- 
- (18) Nasr, C.; Liu, D.; Hotchandani, S.; Kamat, P. V. Dye-Capped Semiconductor Nanoclusters. Excited State and Photosensitization Aspects of Rhodamine 6G H-Aggregates Bound to SiO<sub>2</sub> and SnO<sub>2</sub> Colloids. *J. Phys. Chem.*, **1996**, *100*, 11054–11061.
- (19) Liu, D.; Fessenden, R. W.; Hug, G. L.; Kamat, P. V. Dye Capped Semiconductor Nanoclusters. Role of Back Electron Transfer in the Photosensitization of SnO<sub>2</sub> Nanocrystallites with Cresyl Violet Aggregates. *J. Phys. Chem. B*, **1997**, *101*, 2583–2590.
- (20) Zhang, L.; Cole, J. M. Dye Aggregation in Dye-Sensitized Solar Cells. *J. Mater. Chem. A* **2017**, *5*, 19541–19559.
- (21) Law, K. Y. Organic Photoconductive Materials: Recent Trends and Developments. *Chem. Rev.* **1993**, *93*, 449–486.
- (22) Ajayaghosh, A. Chemistry of Squaraine-Derived Materials: Near-IR Dyes, Low Band Gap Systems, and Cation Sensors. *Acc. Chem. Res.* **2005**, *38*, 449–459.
- (23) Saccone, D.; Galliano, S.; Barbero, N.; Quagliotto, P.; Viscardi, G.; Barolo, C. Polymethine Dyes in Hybrid Photovoltaics: Structure-Properties Relationships. *Eur. J. Org. Chem.* **2016**, *2016*, 2244–2259.
- (24) Qin, C.; Wong, W.Y.; Han, L. Squaraine Dyes for Dye-Sensitized Solar Cells: Recent Advances and Future Challenges. *Chem. - An Asian J.* **2013**, *8*, 1706–1719.
- (25) Chen, G.; Sasabe, H.; Sasaki, Y.; Katagiri, H.; Wang, X.-F.; Sano, T.; Hong, Z.; Yang, Y.; Kido, J. A Series of Squaraine Dyes: Effects of Side Chain and the Number of Hydroxyl Groups on Material Properties and Photovoltaic Performance. *Chem. Mater.* **2014**, *26*, 1356–1364.
- (26) Deing, K. C.; Mayerhöffer, U.; Würthner, F.; Meerholz, K. Aggregation-Dependent Photovoltaic Properties of squaraine/PC61BM Bulk Heterojunctions. *Phys. Chem. Chem. Phys.* **2012**, *14*, 8328–8334.
- (27) Gsänger, M.; Kirchner, E.; Stolte, M.; Burschka, C.; Stepanenko, V.; Pflaum, J.; Würthner, F. High-Performance Organic Thin-Film Transistors of J-Stacked Squaraine Dyes. *J. Am. Chem. Soc.* **2014**, *136*, 2351–2362.
- (28) Urbani, M.; Grätzel, M.; Nazeeruddin, M. K.; Torres, T. Meso-Substituted Porphyrins for Dye-Sensitized Solar Cells. *Chem. Rev.* **2014**, *114*, 12330–12396.
- (29) Higashino, T.; Imahori, H. Porphyrins as Excellent Dyes for Dye-Sensitized Solar Cells: Recent Developments and Insights. *Dalt. Trans.* **2015**, *44*, 448–463.
-

- (30) García-Iglesias, M.; Cid, J.-J.; Yum, J.-H.; Forneli, A.; Vázquez, P.; Nazeeruddin, M. K.; Palomares, E.; Grätzel, M.; Torres, T. Increasing the Efficiency of Zinc-Phthalocyanine Based Solar Cells through Modification of the Anchoring Ligand. *Energy Environ. Sci.* **2011**, *4*, 189–194.
- (31) Martín-Gomis, L.; Fernández-Lázaro, F.; Sastre-Santos, Á. Advances in Phthalocyanine-Sensitized Solar Cells (PcSSCs). *J. Mater. Chem. A* **2014**, *2*, 15672–15682.
- (32) Yum, J. H.; Walter, P.; Huber, S.; Rentsch, D.; Geiger, T.; Nüesch, F.; Angelis, F. D.; Grätzel, M.; Nazeeruddin, M. K.; Efficient Far Red Sensitization of Nanocrystalline TiO<sub>2</sub> Films by an Unsymmetrical Squaraine Dye. *J. Am. Chem. Soc.*, **2007**, *129*, 10320–10321.
- (33) Shi, Y.; Hill, R. B. M.; Yum, J.-H.; Dualeh, A.; Barlow, S.; Grätzel, M.; Marder, S. R.; Nazeeruddin, M. K. A High-Efficiency Panchromatic Squaraine Sensitizer for Dye-Sensitized Solar Cells. *Angew. Chemie Int. Ed.* **2011**, *50*, 6619–6621.
- (34) Delcamp, J. H.; Shi, Y.; Yum, J.-H.; Sajoto, T.; Dell’Orto, E.; Barlow, S.; Nazeeruddin, M. K.; Marder, S. R.; Grätzel, M. The Role of  $\pi$  Bridges in High-Efficiency DSCs Based on Unsymmetrical Squaraines. *Chem. - A Eur. J.* **2013**, *19*, 1819–1827.
- (35) Jradi, F. M.; Kang, X.; O’Neil, D.; Pajares, G.; Getmanenko, Y. A.; Szymanski, P.; Parker, T. C.; El-Sayed, M. A.; Marder, S. R. Near-Infrared Asymmetrical Squaraine Sensitizers for Highly Efficient Dye Sensitized Solar Cells: The Effect of  $\pi$ -Bridges and Anchoring Groups on Solar Cell Performance. *Chem. Mater.* **2015**, *27*, 2480–2487.
- (36) Alagumalai, A.; Kavungathodi, M. F. M.; Vellimalai, P.; Sil, M. C.; Nithyanandhan, J. Effect of Out-of-Plane Alkyl Group’s Position in Dye-Sensitized Solar Cell Efficiency: A Structure–Property Relationship Utilizing Indoline-Based Unsymmetrical Squaraine Dyes. *ACS Appl. Mater. Interfaces* **2016**, *8*, 35353–35367.
- (37) Punitharasu, V.; Kavungathodi, M. F. M.; Nithyanandhan, J. Interplay between  $\pi$ -Bridges and Positions of Branched Alkyl Groups of Unsymmetrical D–A–D– $\pi$ –A Squaraines in Dye-Sensitized Solar Cells: Mode of Dye Anchoring and the Charge Transfer Process at the TiO<sub>2</sub>/Dye/Electrolyte Interface. *ACS Appl. Mater. Interfaces* **2017**, *9*, 32698–32712.
- (38) Beverina, L.; Ruffo, R.; Mari, C. M.; Pagani, G. A.; Sassi, M.; De Angelis, F.; Fantacci, S.; Yum, J.-H.; Grätzel, M.; Nazeeruddin, M. K. Panchromatic Cross-Substituted Squaraines for Dye-Sensitized Solar Cell Applications. *ChemSusChem* **2009**, *2*, 621–624.
- (39) Maeda, T.; Mineta, S.; Fujiwara, H.; Nakao, H.; Yagi, S.; Nakazumi, H. Conformational

- Effect of Symmetrical Squaraine Dyes on the Performance of Dye-Sensitized Solar Cells. *J. Mater. Chem. A* **2013**, *1*, 1303–1309.
- (40) Qin, C.; Numata, Y.; Zhang, S.; Islam, A.; Yang, X.; Sodeyama, K.; Tateyama, Y.; Han, L. A Near-Infrared *Cis*-configured Squaraine Co-Sensitizer for High-Efficiency Dye-Sensitized Solar Cells. *Adv. Funct. Mater.* **2013**, *23*, 3782–3789.
- (41) Qin, C.; Numata, Y.; Zhang, S.; Yang, X.; Islam, A.; Zhang, K.; Chen, H.; Han, L. Novel Near-Infrared Squaraine Sensitizers for Stable and Efficient Dye-Sensitized Solar Cells. *Adv. Funct. Mater.* **2014**, *24*, 3059–3066.
- (42) Islam, A.; Akhtaruzzaman, M.; Chowdhury, T. H.; Qin, C.; Han, L.; Bedja, I. M.; Stalder, R.; Schanze, K. S.; Reynolds, J. R. Enhanced Photovoltaic Performances of Dye-Sensitized Solar Cells by Co-Sensitization of Benzothiadiazole and Squaraine-Based Dyes. *ACS Appl. Mater. Interfaces* **2016**, *8*, 4616–4623.
- (43) Matsui, M.; Shibata, T.; Fukushima, M.; Kubota, Y.; Funabiki, K. Fluorescence Properties of Indolenine Semi-Squarylium Dyes. *Tetrahedron* **2012**, *68*, 9936–9941.
- (44) Volkova, K. D.; Kovalska, V. B.; Tatarets, A. L.; Patsenker, L. D.; Kryvorotenko, D. V.; Yarmoluk, S. M. Spectroscopic Study of Squaraines as Protein-Sensitive Fluorescent Dyes. *Dye. Pigment.* **2007**, *72*, 285–292.
- (45) Hagberg, D. P.; Yum, J.-H.; Lee, H.; De Angelis, F.; Marinado, T.; Karlsson, K. M.; Humphry-Baker, R.; Sun, L.; Hagfeldt, A.; Grätzel, M.; Nazeeruddin, M. K. Molecular Engineering of Organic Sensitizers for Dye-Sensitized Solar Cell Applications. *J. Am. Chem. Soc.* **2008**, *130*, 6259–6266.
- (46) Thomas, K. R. J.; Hsu, Y.-C.; Lin, J. T.; Lee, K.-M.; Ho, K.-C.; Lai, C.-H.; Cheng, Y.-M.; Chou, P.-T. 2,3-Disubstituted Thiophene-Based Organic Dyes for Solar Cells. *Chem. Mater.* **2008**, *20*, 1830–1840.
- (47) Agrawal, S.; Dev, P.; English, N. J.; Thampi, K. R.; MacElroy, J. M. D. First-Principles Study of the Excited-State Properties of Coumarin-Derived Dyes in Dye-Sensitized Solar Cells. *J. Mater. Chem.* **2011**, *21*, 11101–11108.
- (48) Würthner, F.; Kaiser, T. E.; Saha-Möller, C. R. J-Aggregates: From Serendipitous Discovery to Supramolecular Engineering of Functional Dye Materials. *Angew. Chemie Int. Ed.* **2011**, *50*, 3376–3410.
- (49) Ghosh, S.; Li, X.-Q.; Stepanenko, V.; Würthner, F. Control of H- and J-Type  $\pi$  Stacking

by Peripheral Alkyl Chains and Self-Sorting Phenomena in Perylene Bisimide Homo- and Heteroaggregates. *Chem. - A Eur. J.* **2008**, *14*, 11343–11357.

## Chapter 4

**$\pi$ -Extended *cis*-Configured Unsymmetrical Squaraine Dyes  
for Dye-sensitized Solar Cells: Panchromatic Light  
Absorption**

## 4.1 Introduction

Among the various components in dye-sensitized solar cells, dye plays an important role in increasing the light harvesting efficiencies of the device, as other components help in separating and transporting the charges and regenerating the dyes.<sup>1,2</sup> Hence convergence of synergistic effects from all the components is important for the higher device performance.<sup>3</sup> The photophysical properties of organic dyes can be dwelled judiciously due to the careful choice of electronic nature of dye components. D- $\pi$ -A,<sup>4</sup> D-A- $\pi$ -A<sup>5</sup> dyes have been designed and showed the device performance in the visible and far-red region. Further to enhance the photocurrent, NIR absorbing dyes are desirable and development of such NIR absorbing dyes is challenging owing to their photostability and aggregation properties. Aggregation of dyes facilitates the charge hopping between the photoexcited and ground state molecules rather injecting to the conduction band of TiO<sub>2</sub> surface, which reduces the device performance. Phorphyrin,<sup>6-8</sup> phthalocyanine<sup>9,10</sup> and squaraine dyes have been utilized to absorb the NIR region of the solar spectrum, the device performances were drastically reduced due to the dye-aggregation on the TiO<sub>2</sub> surface.<sup>11</sup> Hence tremendous efforts have been pursued to overcome the dye aggregate issue, and the high efficiency phorphyrin and phthalocyanine dyes have reached the device efficiencies of 12.7%, 6.4% by judicious design principles that avoids aggregation of dyes by invoking alkyl groups as an integral part of the dye. Unsymmetrical SQ dyes showed the DSSC device efficiency of 4.5%<sup>12</sup> which can be improved further by extending the conjugation by  $\pi$ -spacer. In this way YR6,<sup>13</sup> JD10,<sup>14</sup> DTS-CA<sup>14,15</sup> dyes showed the device performance of 6.7%, 7.6% and 8.9% respectively.

As a structural variance, highly electron withdrawing barbiturate,<sup>16</sup> dicyanovinyl and cyanoestervinyl units appended squaraine units provides a *cis*-configured squaraine dyes with extended absorption in the NIR region along with enhanced visible transition. Suitably functionalized *cis*-configured squaraine dyes, such as SMSQ1a,<sup>17</sup> SMSQ1b,<sup>17</sup> HSQ1-5<sup>17-19</sup> showed the device performance between 3.6-5.66%. Similar effects have been observed in extended squaraine dyes, dye YR6, unsymmetrical squaraine dyes with thiophene  $\pi$ -spacer, and cyano acetic acid as anchoring unit showed IPCE responses from visible to NIR regions. Introducing of out-of-plane branched alkyl group containing unsymmetrical squaraine dyes showed the importance of controlled aggregation of dyes on TiO<sub>2</sub> for a better device performance.<sup>20</sup>

From the previous chapters, systematic structure-property relationship analyses of unsymmetrical squaraine dyes inferred the following for a better device performance. (i) DSSC device performance can be modulated by positioning the out-of-plane alkyl groups and the nature of  $\pi$ -spacer, (ii) *Cis*-configured squaraine dyes suitably functionalized out-of-plane alkyl groups has also showed better device performances. Hence, the present chapter discusses the dye design that combine effects of both (i) extending the  $\pi$ -conjugation and (ii) *cis*-configured dyes with suitable branched alkyl groups to control the aggregation of dyes on the TiO<sub>2</sub> surface. The present dye design helps to enhance the absorption property of the dye from visible to NIR regions (**Figure 4.1**). Further to understand the dye orientation, a direct acid and cyanoacetic acid anchoring groups were incorporated in **PSQ21** and **PSQ22** dyes. This chapter will discuss the importance of *cis*-configured squaraine unit and the effect of extended conjugation and anchoring group.

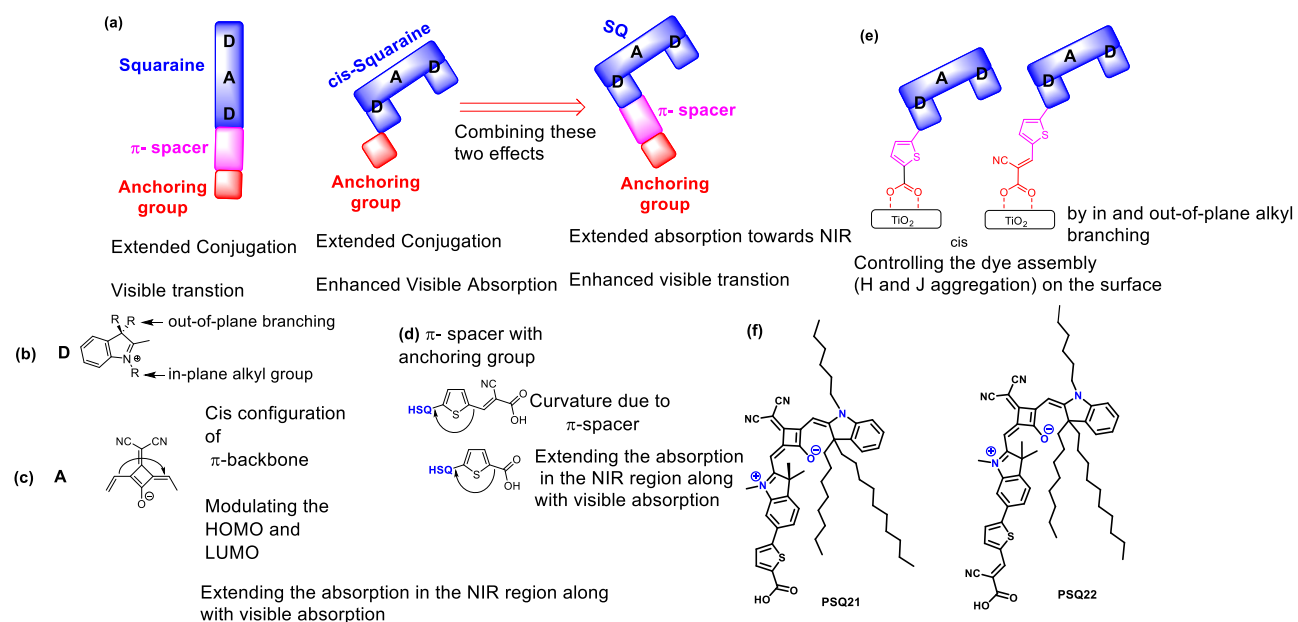


**Figure 4.1** D-A-D- $\pi$ -Anchoring group dyes based on *cis*-configured unsymmetrical squaraine dyes, b) in-plane and out-of-plane branching on indoline, (c) *cis*-configuration of substituted squaraine backbone (d) curvature due to  $\pi$ -spacer, (e) schematic representation of mode of anchoring on TiO<sub>2</sub> surface, and (f)  $\pi$ -extended of alkyl functionalized unsymmetrical squaraine dyes, **PSQ21-22**.

## 4.2 Results and Discussions



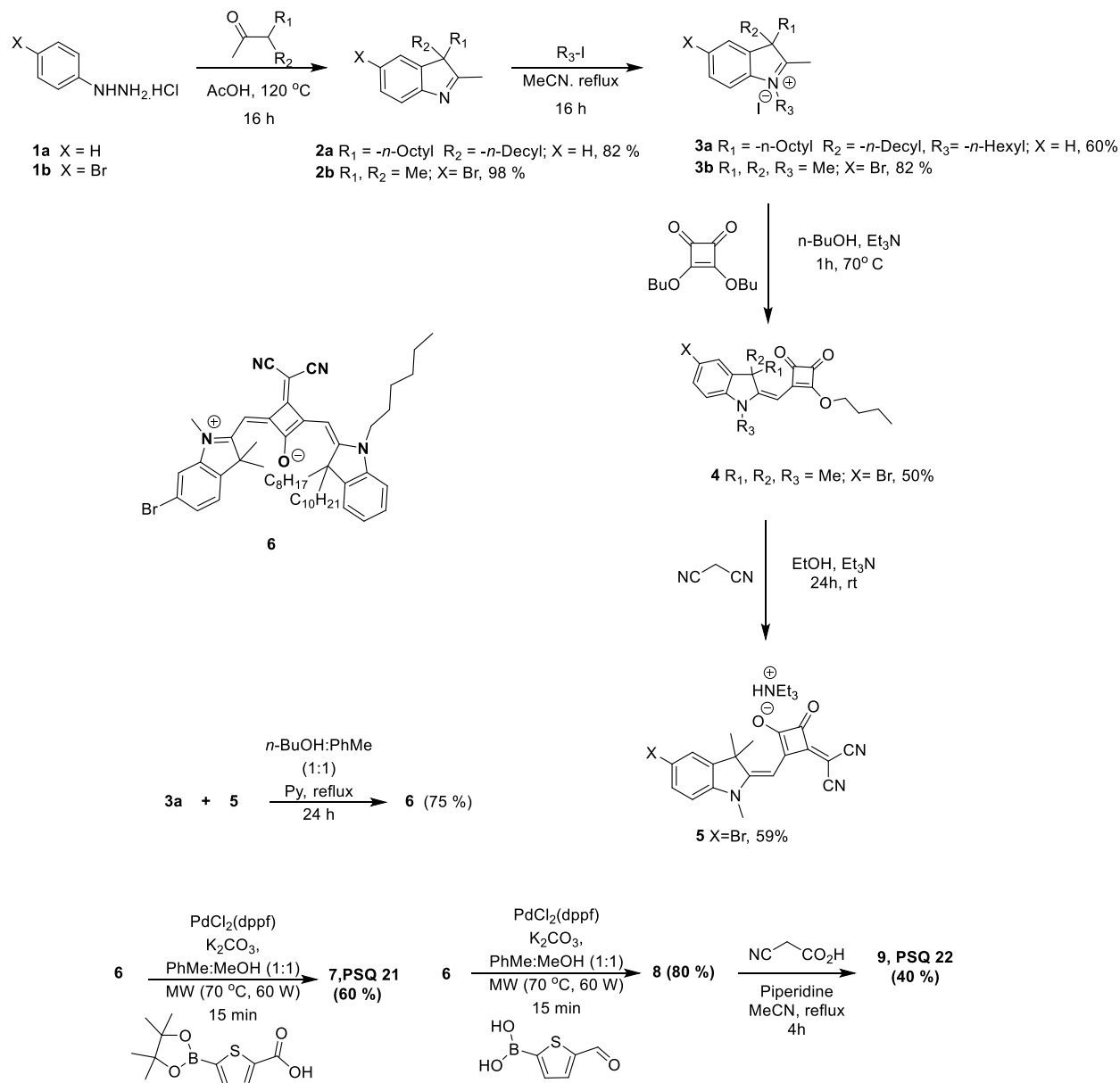
### 4.2.1 Synthesis of *cis*-configured Squaraine Sensitizers

The following three general synthetic transformations were carried out for the synthesis of **PSQ21-PSQ22** dyes.

- (i) Synthesis of bromo derivatives of the unsymmetrical *cis*-configured squaraine dye.
- (ii) Microwave mediated Suzuki coupling of bromo functionalized squaraine derivative and boronic acid containing thiophene spacer and
- (iii) Finally installing the anchoring group by Knoevenagel condensation for **PSQ22**.

Indolenine functionalized with branched alkyl group, **2a** has been synthesized by a Fisher-indole synthesis. The indolenine derivative was converted into indolium salt, **3a** by reacting with hexyl iodide. Further the corresponding bromo indolium salt, **3b** was converted into semisquaraine derivative, **4** which was then condensed with malanonitrile to provide the semisquaric acid derivative appended with dicyanovinylene unit, **5** in the presence of EtOH and NEt<sub>3</sub>. The branched alkyl group containing indolium salt, **3a** and the semisquaraine derivative, **5** were condensed under Dean-Stark experimental reaction conditions to afford the bromo derivative of *cis*-squaraine derivative, **6**. Under the microwave reaction condition the *cis*-squaraine derivative, **6** was coupled with 5-carboxylthiophene-2-boronic acid pinacol ester in the presence of Pd(dppf)Cl<sub>2</sub>, K<sub>2</sub>CO<sub>3</sub> in PhMe: MeOH (1:1) to afford the final dye **PSQ21** in moderate yield.

On the other hand, in order to install the cyanoacetic acid anchoring groups, the squaraine derivative, **6** was coupled with 5-formyl-thiophene-2-boronic acid in the presence of Pd(dppf)Cl<sub>2</sub>, K<sub>2</sub>CO<sub>3</sub> in PhMe: MeOH (1:1) to afford the aldehyde derivative, **8** in good yield in 15 min. Further, the aldehyde precursor was condensed with cyano acetic acid in the presence of piperidine provided the **PSQ22** in moderate yield (**Scheme 4.1**). These molecules were characterised by <sup>1</sup>H, <sup>13</sup>C NMR spectroscopy and mass spectrometric analyses.



**Scheme 4.1** Synthesis of branched alkyl group containing  $\pi$ -extended *cis*-configured D-A-D- $\pi$ -A squaraine dyes, **PSQ21-22**

#### 4.2.2 Photophysical Properties

The optical properties of **PSQ21-22** were analyzed through UV-Vis absorption spectra in CH<sub>2</sub>Cl<sub>2</sub> which showed in **Figure 4.2a** and summarized in **Table 4.1**. Dye **PSQ21** with carboxylic acid anchoring group possesses a strong ICT absorption at 705 nm ( $\epsilon \sim 1.5 \times 10^5 \text{ M}^{-1} \text{ cm}^{-1}$ ) with a visible transition at 390 nm ( $\epsilon \sim 3.4 \times 10^4 \text{ M}^{-1} \text{ cm}^{-1}$ ). Dye **PSQ22** with cyanoacetic acid anchoring group

exhibited intense absorption at 715 nm ( $\epsilon \sim 2.3 \times 10^5 \text{M}^{-1} \text{cm}^{-1}$ ) and a visible absorption at 450 nm ( $\epsilon \sim 4.5 \times 10^4 \text{M}^{-1} \text{cm}^{-1}$ ) and 396 nm ( $\epsilon \sim 5.4 \times 10^4 \text{M}^{-1} \text{cm}^{-1}$ ). The ICT band at 715 nm which was about 72 nm red shifted from the parent squaraine dye (SQ1) along with enhanced transition at 450 nm.

The emission spectra of **PSQ21-22** dyes are illustrated in **Figure 4.2b**, upon excitation at 670nm, **PSQ21** showed an emission maximum at 719 nm and **PSQ22** showed an emission maximum at 730 nm. The Stokes shift of  $\sim 14$ -15 nm has been observed for PSQ dyes. It showed that there may be significant change in dipole moment in the excited states.

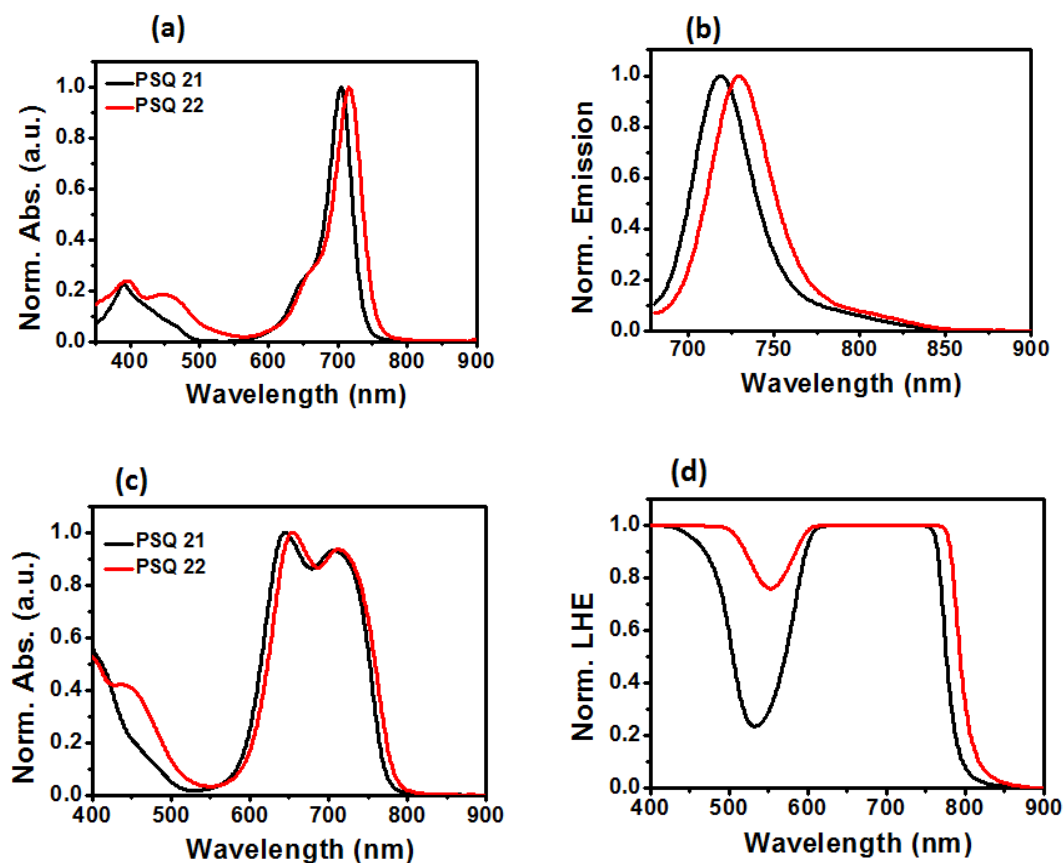


**Figure 4.2** Optical properties of **PSQ21-22** dyes. a) UV-vis absorption spectra in  $\text{CHCl}_3$ , (b) Normalized emission spectra in  $\text{CHCl}_3$  (excitation wavelength: 670 nm) (c) Normalized absorption spectra on thin film of  $\text{TiO}_2$ , thickness = 6  $\mu\text{m}$ , dipping time = 30 min, and  $[\text{PSQ}] = 0.1 \text{ mM}$  in  $\text{CH}_2\text{Cl}_2$ , (d) LHE (%) on  $\text{TiO}_2$  thin film recorded after 12 h dipping in 0.1 mM solution in  $\text{CH}_2\text{Cl}_2$ .

The optical band gap ( $E_g$ , opt) of these dyes were calculated from the intersection of UV-vis absorption and fluorescence curves using the formula  $E_{g, \text{opt}} = 1240/\lambda$ .  $E_{g, \text{opt}}$  for **PSQ21-22**

were between 1.74 -1.71 eV. Fluorescence quantum yield ( $\phi$ ) was measured in dichloromethane via relative method and it shows the decreasing order of [PSQ21] (0.61) > [PSQ22] (0.59). To understand the self-assembly of dyes on the TiO<sub>2</sub> surface, UV-vis absorption studies of PSQ21-22 chemisorbed on thin TiO<sub>2</sub> surface was carried out (Figure 4.2c). Dye PSQ21 on TiO<sub>2</sub> showed a broad peak centered around 709 nm (monomer) along with the appended blue shifted peak at 646 nm (H-aggregation). However for PSQ22 along with monomer (715 nm), H-aggregate (654 nm), a moderate intense peak was appended at 455 nm. Further, the absorbance profile indicated that PSQ22 possess better harvesting nature than the PSQ21 and it is due to the presence of different anchoring groups which enhances the dye-dye interaction on the TiO<sub>2</sub> surface.

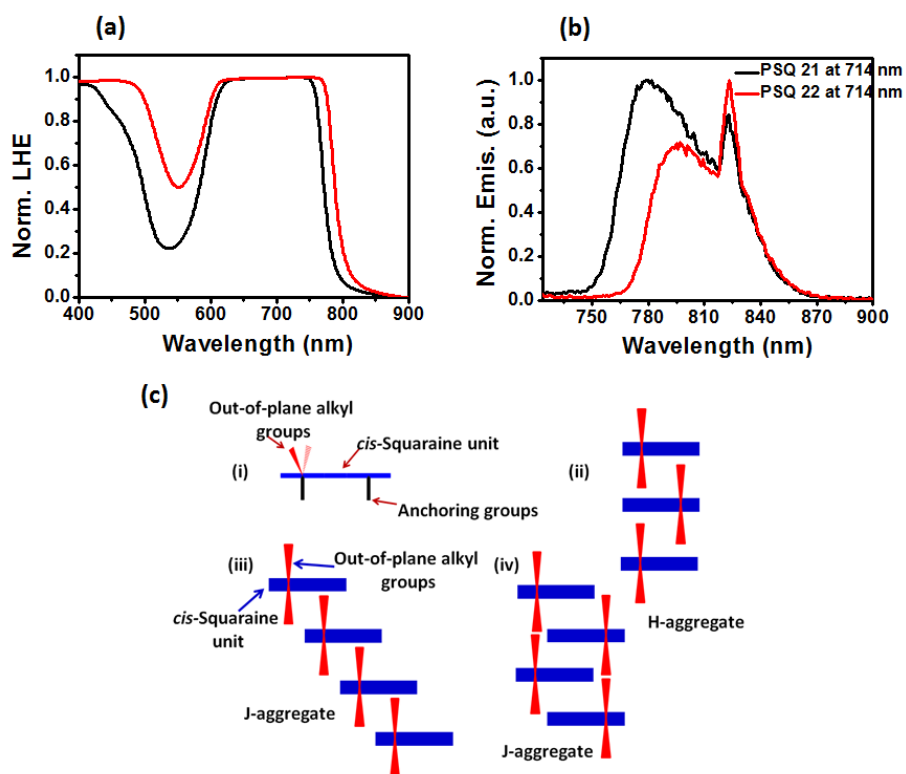


**Figure 4.3** Optical properties of PSQ21-22 dyes on Al<sub>2</sub>O<sub>3</sub> surface. (a) Normalized LHE on Al<sub>2</sub>O<sub>3</sub> thin film recorded after 12 h dipping in 0.1 mM solution in CH<sub>2</sub>Cl<sub>2</sub>. (b) Normalized emission spectra on thin film of Al<sub>2</sub>O<sub>3</sub>, excitation wavelength: 714 nm, thickness = 6  $\mu$ m, dipping time = 12 h and [PSQ] = 0.1 mM in CH<sub>2</sub>Cl<sub>2</sub>. (c) Possible arrangements of PSQ dyes on the surface for the observed H and J- type aggregations.

Further, emission studies on  $\text{Al}_2\text{O}_3$  surfaces have been carried out to understand the emission properties of **PSQ21-22** dyes. Since,  $\text{Al}_2\text{O}_3$  is an insulator, carrying out the emission study on the  $\text{Al}_2\text{O}_3$  provides the information about the organization of dyes. There were two emission peaks appeared at 780 and 823 nm by exciting wavelength at 714 nm for the squaraine dyes **PSQ21-22**. Short discussion on the sharp emission peak at 823 nm is note worthy, as it may arise from the J-aggregate due to the structural features of **PSQ21-22**, the unsymmetrical nature and heavily alkylated on the one side of the dye helps to form a stable monolayer of dyes on the anatase {101} facet by forming a slipped structure. The intensity of J-aggregate emission for **PSQ22** is more for **PSQ21** due to the presence of different anchoring group which is showed in **Figure 4.3**.

On the other hand the ratio of  $I_{\text{monomer}}/I_{\text{J-aggregate}}$  was showed the different arrangement which exploited on the surface for these PSQ dyes. Emission spectrum for **PSQ21** on  $\text{Al}_2\text{O}_3$  showed the monomer emission at 780 nm and the sharp J-aggregate emission at 823 nm. **PSQ22** dye, showed the  $I_{\text{monomer}}/I_{\text{J-aggregate}}$  ratio of 0.72 which exhibited less monomer formation compared to **PSQ21** that possess the  $I_{\text{monomer}}/I_{\text{J-aggregate}}$  ratio of 1.20 (**Table 4.1**).

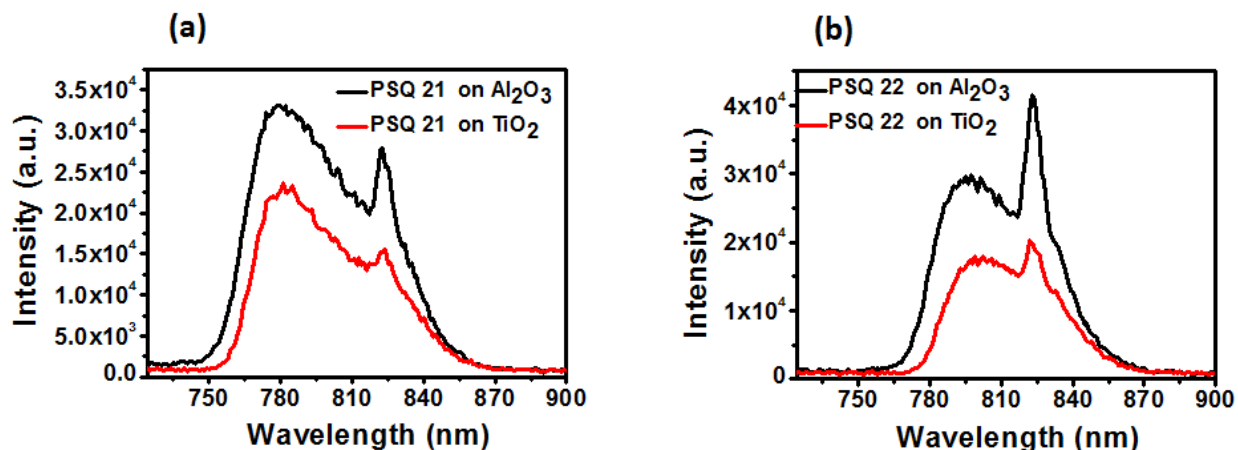


**Figure 4.4** Emission spectra of **PSQ21-PSQ22** dyes (a-b) on  $\text{Al}_2\text{O}_3$  (black line) and  $\text{TiO}_2$  (redline), excitation wavelength: 714 nm.

Furthermore the emission from J-aggregate formation is more predominant compared to monomer formation in case of **PSQ22**. The  $I_{\text{monomer}}/I_{\text{J-aggregate}}$  ratio for **PSQ21** and **PSQ122** were comparable as both the dyes are functionalized with N- and  $\text{sp}^3\text{-C}$  out-of-plane alkyl groups,  $\pi$ -

spacer on the indoline moiety including different anchoring units. In addition to emission study on Al<sub>2</sub>O<sub>3</sub>, emission from dye adsorbed TiO<sub>2</sub> also monitored and the changes in radiative emission of dyes were compiled in **Figure 4.4**. The reduced fluorescence intensity on TiO<sub>2</sub> indicates the facile charge injection from LUMO of the dyes **PSQ21-22** to conduction band of TiO<sub>2</sub>.

**Table 4.1** Emission properties of **PSQ21-22** on Al<sub>2</sub>O<sub>3</sub> at excitation wavelength of 714 nm

Dye	Maximum $\lambda_{\max}$ of monomer on Al <sub>2</sub> O <sub>3</sub> (nm)	Maximum $\lambda_{\max}$ of J-aggregate on Al <sub>2</sub> O <sub>3</sub> (nm)	Fluorescence Intensity of monomer on Al <sub>2</sub> O <sub>3</sub>	Fluorescence Intensity of J-aggregate on Al <sub>2</sub> O <sub>3</sub>	I <sub>monomer</sub> /I <sub>J-aggregate</sub>
<b>PSQ21</b>	780	823	1	0.83	1.20
<b>PSQ22</b>	796	823	0.72	1	0.72

### 4.2.3 Electrochemical Characterization

The electrochemical properties for **PSQ21-22** sensitizers were characterized by differential pulse voltammetric analysis (DPV) to understand the feasibility of charge injection from the excited dye into conduction band of the TiO<sub>2</sub> and the dye regeneration by the electrolyte (**Figure 4.5** and **Table 4.2**). The HOMO energy level of **PSQ21** and **PSQ22** were 0.81 V and 0.82 V vs NHE, respectively. The more oxidation potential of **PSQ21-22** than the electrochemical potential of I<sup>-</sup>/I<sub>3</sub><sup>-</sup> redox couple (0.4 V vs NHE) which supports for the feasible regeneration of oxidized dye (400-410 mV). **PSQ21-PSQ22** dyes the  $E_{\text{ox}}$  was around 0.81-0.82 V vs NHE, suggests that the changes in different anchoring group do not make significant difference. The optical energy gaps ( $E_{0-0}$ ) was calculated from the intersection of absorption and emission spectra and **PSQ21-PSQ22** dyes showed optical band gap between 1.74-1.71 eV. The LUMO energy level of **PSQ21** and **PSQ22** was found at -0.93 V and -0.89 V vs NHE, respectively. The LUMO energy level of **PSQ21-PSQ22** series were calculated by subtracting  $E_{0-0}$  from  $E_{\text{HOMO}}$  and that results showed more negative than  $E_{\text{CB}}$  of TiO<sub>2</sub> (-0.5 V vs NHE), which helps efficient electron injection (392-430 mV) from the excited state of the sensitizer to the TiO<sub>2</sub> conduction band.

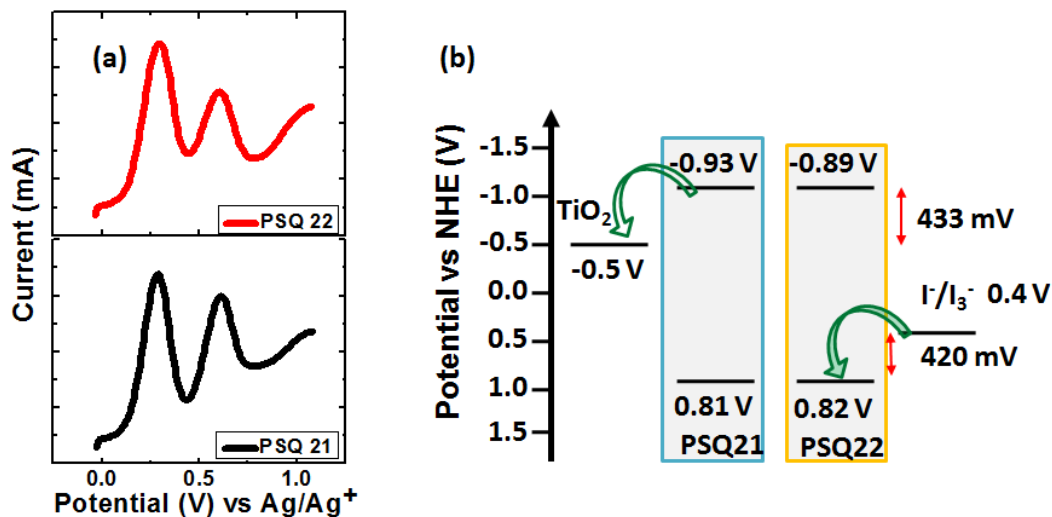


**Figure 4.5** Electrochemical properties of PSQ21-22 dyes. (a) Differential pulse voltammetry for PSQ21-PSQ22 dyes and (b) Energy level diagram of PSQ dyes (V vs NHE) with  $\text{TiO}_2$ , and electrolyte ( $\text{I}^-/\text{I}_3^-$ ).

**Table 4.2** Photophysical and electrochemical properties of PSQ21-22

Dye	$\lambda_{\text{max}}$ /nm <sup>a</sup>	$\epsilon \times 10^5 (\text{M}^-1 \text{cm}^{-1})^b$	$\lambda_{\text{max, emission}}$ /nm <sup>c</sup>	$\lambda_{\text{max}}$ /nm <sup>d</sup> TiO <sub>2</sub>	$E_{\text{HOMO}}$ (V vs NHE) <sup>e</sup>	$E_{\text{LUMO}}$ (V vs NHE) <sup>f</sup>	$E_{\text{g}}^{\text{opt}}$ <sup>g</sup> (V)
PSQ21	705	1.5	719	709	0.812	-0.930	1.74
	390	0.34		646			
PSQ22	715	2.3	730	715	0.818	-0.892	1.71
	450	0.42		654			
	396	0.54		455			

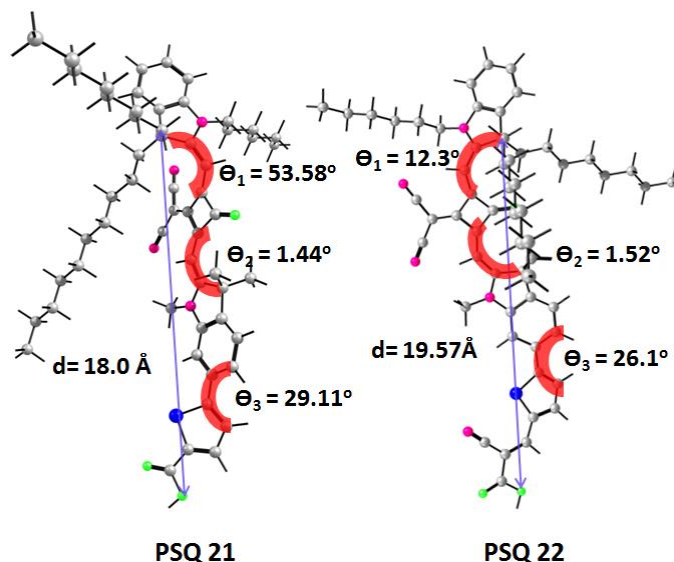
<sup>a</sup>UV-vis absorption in  $\text{CH}_2\text{Cl}_2$ . <sup>b</sup>Molar extinction coefficients of far-red and visible absorptions.

<sup>c</sup>Emission studies in  $\text{CH}_2\text{Cl}_2$ . <sup>d</sup>On thin film of  $\text{TiO}_2$ , thickness = 6  $\mu\text{m}$ , dipping time = 30 min, and  $[\text{PSQ}] = 0.1 \text{ mM}$  in  $\text{CHCl}_3$ . <sup>e</sup> $E_{\text{HOMO}}$  of PSQ 21-22 in  $\text{CH}_2\text{Cl}_2$ ,  $\text{Fc}^+/\text{Fc}$  was used as external standard and potential measured vs  $\text{Fc}^+/\text{Fc}$  (eV) were converted to NHE (V) by addition of 0.7 V.

<sup>f</sup> $E_{\text{LUMO}}$  levels were measured by subtracting  $E_{\text{HOMO}}$  from  $E_{0-0}$ . <sup>g</sup> $E_{0-0}$  deduced at the intersection of absorption and emission spectra using the equation  $E_{0-0} (\text{eV}) = 1240/\lambda$ .

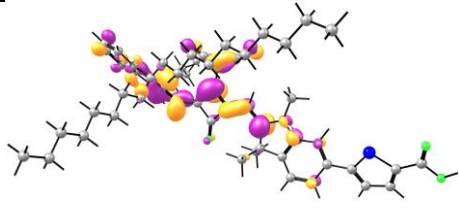
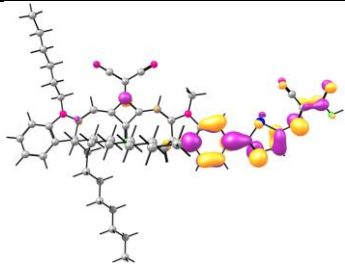
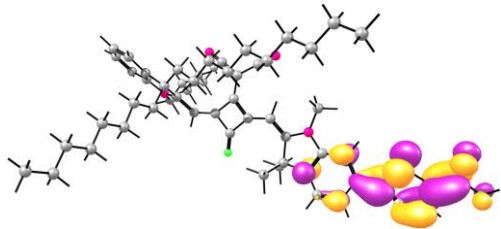
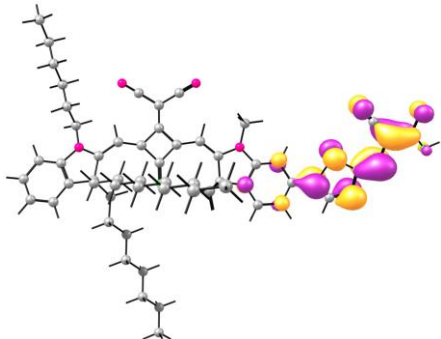
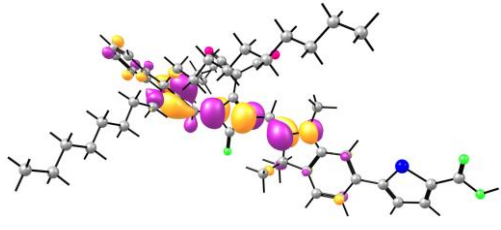
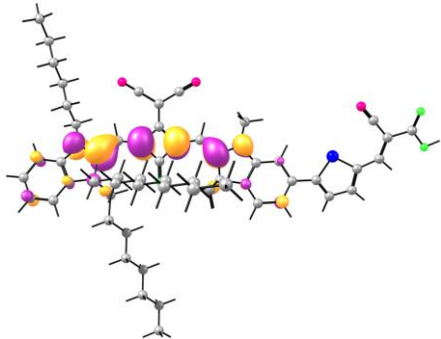
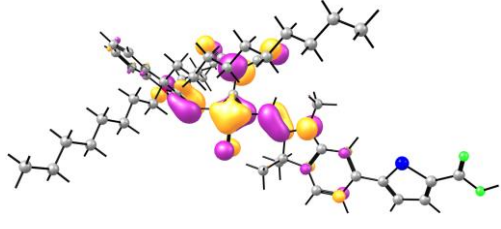
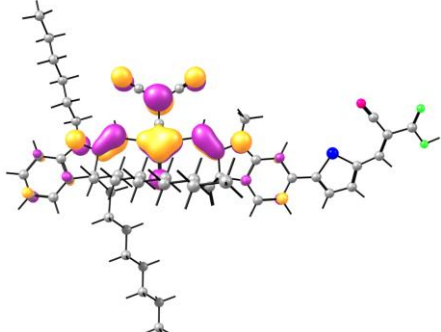
#### 4.2.4 Density Functional Theory (DFT) Calculations

To gain insight into the electronic structures of **PSQ21-PSQ22** dyes, their ground state geometries and energies were fully optimized using density functional theory (DFT) by B3LYP/6-31G\*\* level with the Gaussian 09 program. Energy minimized structures of **PSQ31** and **PSQ32** were presented in **Figure 4.6**. The isosurface plots of six selected frontier molecular orbitals and theoretical energy level of HOMO-2, HOMO-1, HOMO, LUMO, LUMO+1 and LUMO+2 were depicted in **Figure 4.7**. In **PSQ21-22** dyes, the localized electron density of HOMO was over the dicyanovinyl groups in addition to the squaraine unit, while the electron distribution of HOMO-1 and HOMO-2 were delocalized over squarate derivatives which contain electron withdrawing group, indolenine units and  $\pi$ -spacer. The LUMOs are delocalized along the backbone of the molecules, and the LUMO+1 is located on the central core with the carboxylate-substituted indolinium moieties through  $\pi$ -spacer. Such electron distribution in HOMO and LUMO or LUMO+1 suggests the effective electron transfer from donor to  $\text{TiO}_2$  through anchoring unit.



**Figure 4.6** Energy minimized structures of (a) **PSQ21**, and (c) **PSQ22**



State	PSQ21	PSQ22
$E_{\text{LUMO}+2}$	 $E_{\text{LUMO}+2} = -1.03 \text{ eV}$	 $E_{\text{LUMO}+2} = -1.12 \text{ eV}$
$E_{\text{LUMO}+1}$	 $E_{\text{LUMO}+1} = -1.89 \text{ eV}$	 $E_{\text{LUMO}+1} = -2.81 \text{ eV}$
$E_{\text{LUMO}}$	 $E_{\text{LUMO}} = -2.59 \text{ eV}$	 $E_{\text{LUMO}} = -2.81 \text{ eV}$
$E_{\text{HOMO}}$	 $E_{\text{HOMO}} = -4.66 \text{ eV}$	

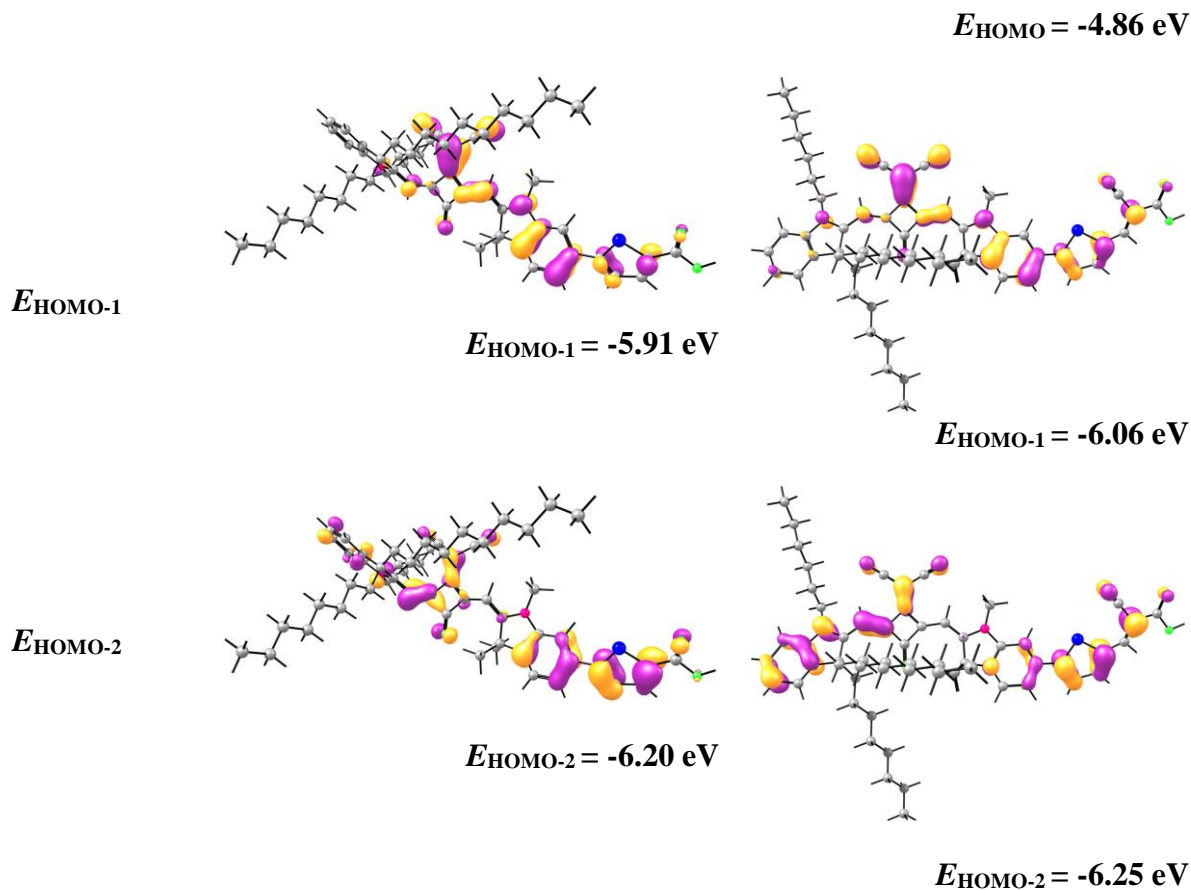


**Figure 4.7.** Isosurface plots of selected frontier orbitals (HOMO, HOMO-1, HOMO-2, LUMO, LUMO+1, LUMO+2) of **PSQ21** and **PSQ22**. Fully optimised at DFT B3LYP/6-31G\*\* level. (Isovalue set to 0.036 a.u.)

#### 4.2.5 Photovoltaic Studies of PSQ21-22

DSSC device fabrication has been carried out by utilizing  $\text{I}^-/\text{I}_3^-$  electrolyte. The current density-voltage ( $J$ - $V$ ) plot and IPCE trace of the devices for the **PSQ21-22** dyes are shown in **Figure 4.8** (**Table 4.3**). DSSC device with the dye **PSQ21** and **PSQ22** showed the device performance of 5.15% ( $V_{\text{oc}}$  0.569V, and  $J_{\text{sc}}$  13.54  $\text{mA}/\text{cm}^2$ ) and 5.15% ( $V_{\text{oc}}$  0.569V, and  $J_{\text{sc}}$  13.54  $\text{mA}/\text{cm}^2$ ) respectively. However by the addition of 10 equiv. of co-adsorbent CDCA enhanced the device performance to 7.0% for **PSQ21** and 6.93% for **PSQ22** by controlling the aggregation of dyes on  $\text{TiO}_2$  surface. The variation of device performance in the presence of CDCA indicated that the aggregation of dyes on the  $\text{TiO}_2$  surface can be minimized with the definite contribution from the aggregated state. The enhanced device performance has been observed up to 10 equivalents of

CDCA, addition of further CDCA leads to reduction in photocurrent due to reduced amount of dyes on the surface.

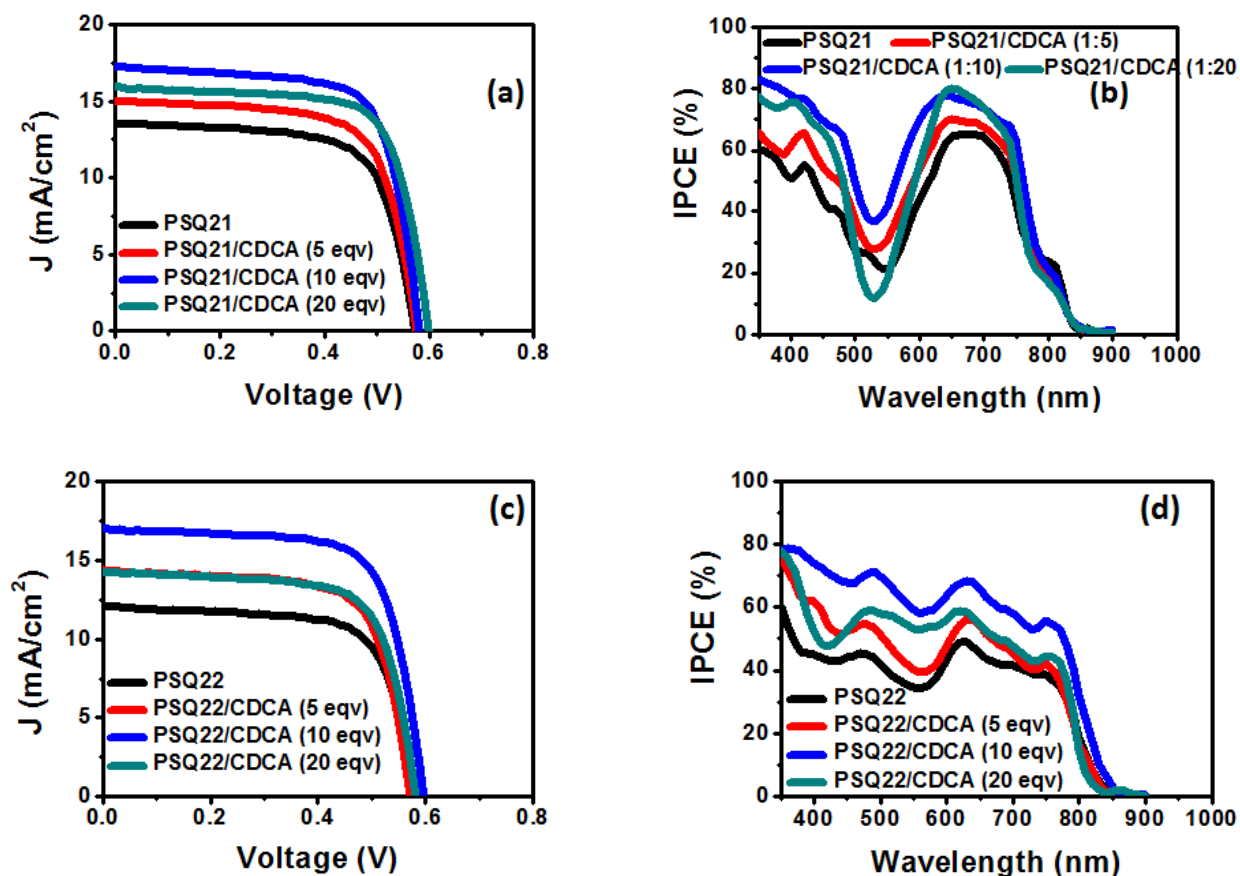


**Figure 4.8** *I-V* and IPCE characterization of **PSQ21-22** dyes. (a and c) and (b and d) *I-V* and IPCE curves for **PSQ21-22** in presence and absence of CDCA ( $\text{TiO}_2$  electrode thickness =  $8 + 4 \mu\text{m}$  (transparent+scattering layer), area =  $0.22 \text{ cm}^2$ , [Dye] =  $0.1 \text{ mM}$  in  $\text{CHCl}_3$ , dipping time 12 h at rt, electrolyte: iodolyte Z-50 from Solaronix).

IPCE profiles of **PSQ21-22** sensitized DSSCs demonstrates a panchromatic response, particularly **PSQ22** which exhibited IPCE of over 60 % throughout the solar spectrum up to 800 nm and has onset at 850 nm. **PSQ21** showed IPCE response of over 75% between 400-750 nm with a sharp dip at 540 nm, and it is interesting to note that **PSQ21** and **PSQ22** differs only the nature of anchoring group being more electron withdrawing cyanoacetic acid for **PSQ22** than the carboxylic acid anchoring group for **PSQ21**. The panchromatic response of **PSQ21-22** dyes comprises of contribution from H-aggregate (646 nm for **PSQ21** and 630 nm **PSQ22**) and J-

aggregate (741 nm for **PSQ21** and 759 nm for **PSQ22**) besides contribution from monomer and visible transition (400-550 nm).

**Table 4.3** Photovoltaic parameters for **PSQ21-22**

Dye	$J_{sc}$ (mA/cm <sup>2</sup> )	$V_{oc}$ (V)	$ff$ (%)	$\eta$ (%)
<b>PSQ21</b>	13.33±0.21	0.567±0.003	67.13±0.22	5.15±0.08
<b>PSQ21: CDCA (1:5)</b>	14.87±0.07	0.574±0.001	67.05±0.05	5.72±0.02
<b>PSQ21: CDCA (1:10)</b>	17.07±0.14	0.577±0.002	70.35±0.15	6.93±0.07
<b>PSQ21: CDCA (1:20)</b>	15.81±0.06	0.594±0.003	70.62±0.11	6.63±0.07
<b>PSQ22</b>	11.99±0.12	0.575±0.003	69.82±0.31	4.81±0.09
<b>PSQ22: CDCA (1:5)</b>	14.37±0.04	0.568±0.001	70.31±0.20	5.74±0.04
<b>PSQ22: CDCA (1:10)</b>	16.93±0.13	0.579±0.002	69.83±0.22	6.84±0.09
<b>PSQ22: CDCA (1:5)</b>	14.20±0.05	0.594±0.003	70.65±0.05	5.96±0.05

<sup>a</sup>TiO<sub>2</sub> electrode thickness = 8 + 4 μm (transparent + scattering layer), area = 0.22 cm<sup>2</sup>, [Dye] = 0.1 mM in CHCl<sub>3</sub>, dipping time was 12 h at rt, electrolyte was iodolyte Z-50 (Solaronix) and summarize the result of best six devices with deviation.

#### 4.2.6 Electrochemical Impedance Analysis

To correlate  $I$ - $V$  characteristics with charge transfer dynamics, the **PSQ21-22** device cells were characterized by various applied potential and evaluated the current through it as a function of frequency in dark conditions. For DSSC,  $V_{oc}$  is the potential difference between quasi-Fermi level of electron in the TiO<sub>2</sub> ( $E_{Fn}$ ) and the Fermi level of redox potential of electrolyte ( $E_{F, redox}$ ) (Eq 4.1). Electrochemical impedance spectroscopy (EIS) studies have been carried to understand the interfacial charge recombination dynamics between various interfaces in a DSSC device.

$$V_{oc} = E_{(F, redox)} - E_{(F, n)} \quad (4.1)$$

The Nyquist plots of two dyes are shown in **Figure 4.9a**. Herein there are three semicircles associated with the charge transfer processes in a typical DSSC Nyquist plot. The

first high frequency region represents charge transfer at the interface of the counter electrode/electrolyte, the mid frequency of large semicircle represents the charge transfer process occurs at the interface of TiO<sub>2</sub>-dye/electrolyte and the third at low frequency part represents ion diffusion resistance or Warburg diffusion coefficient in the electrolyte. The larger semicircle at lower frequencies in Nyquist plots represents the interfacial charge-transfer resistances ( $R_{ct}$ ) at the TiO<sub>2</sub>-dye/electrolyte interface (**Figure 4.9 and table 4.4**). The fitted recombination resistance ( $R_{ct}$ ) value of PSQ sensitized devices (under an applied bias of -0.47 V) increases in the order of **PSQ22** (10.2  $\Omega$ ) < **PSQ21** (11.3  $\Omega$ ). Larger the  $R_{ct}$  value, slower is the recombination of electrons from the conduction band of TiO<sub>2</sub> to the oxidized I<sub>3</sub><sup>-</sup> species in the electrolyte. The electron lifetime(s) on TiO<sub>2</sub> were calculated from  $R_{ct}$  and chemical capacitance  $C_{\mu}$  using  $\tau = R_{ct} \times C_{\mu}$ . The longer electron lifetime in **PSQ21** cell sensitized further supports the higher performance of **PSQ21** (16.95 ms) compared to **PSQ22** (13.26 ms) based cells.

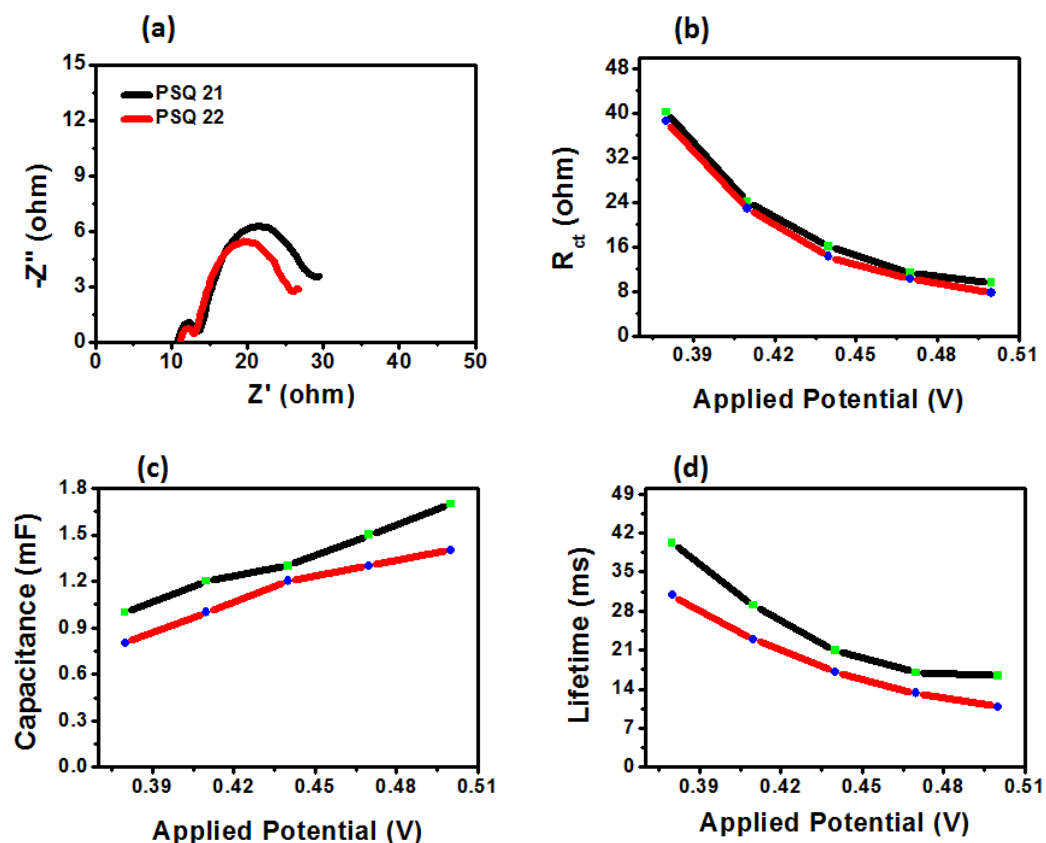


**Figure 4.9** Impedance analysis of PSQ21-22 dyes: (a) Nyquist plot, (b)  $R_{ct}$  vs applied potential, (c)  $C_{\mu}$  vs applied potential and (d)  $\tau$  vs applied potential

**Table 4.4** EIS Parameters of **PSQ21-22** dye cells at an applied potential of  $-0.47$  V in the dark

Dyes	Applied Potential (V)	$R_s$ (ohm)	$R_{ct}$ (ohm)	$C_{\mu}$ (mF)	$\tau$ (ms)
<b>PSQ21</b>	0.47	12.90	14.92	0.65	9.7
<b>PSQ22</b>	0.47	13.86	10.14	0.38	3.85

### 4.3 Summary

In summary, a series of  $\pi$ -extended and *cis*-configured unsymmetrical squaraine dyes **PSQ21-22** with two different anchoring groups have been rationally designed and synthesized. Self assemblies of these dyes have been systematically studied on  $TiO_2$  and  $Al_2O_3$  surfaces. Absorption and emission studies on the surfaces indicated that dyes of **PSQ21-22** included as both H- and J-aggregates which helped in broadening the spectral profile. The light harvesting efficiency profile exhibited **PSQ22** is better harvester than that of **PSQ21**, as both the dyes containing different anchoring group. DSSC device fabrication of **PSQ21** and **PSQ22** exhibited 7.0% and 6.93%, respectively in the presence of 10 equivalent of CDCA. Furthermore, the panchromatic power conversion efficiency profile of **PSQ22** over **PSQ21** showed the importance of choice of anchoring groups present in the sensitizers besides alkyl groups based steric factor covering around the dye which controls the dye aggregation on the surface.

## 4.4 Experimental Section

### 4.4.1 Materials and Characterization

For D-A-D dye synthesis and dye cell fabrication, all the reagents and solvents were purchased from commercial sources were used without further purification unless otherwise noted. Required precursors **1a**, **1b**, **2a**, **2b**, **3a**, **3b** and **4** were synthesized and reported according to the previous chapter 2 and 3.<sup>20,22</sup> All oxygen- and moisture-sensitive reactions were carried out under inert atmosphere.  $^1H$  NMR spectra were recorded on a 200 MHz or 400 MHz or 500 MHz spectrometers, using  $CDCl_3$ . All chemical shifts were reported in parts per million (ppm).  $^1H$  NMR chemical shifts were referenced to TMS (0 ppm).  $^{13}C$  NMR chemical shifts were

referenced to  $\text{CDCl}_3$  (77.23 ppm, and recorded on either 100 MHz or 126 MHz NMR spectrometer). HRMS and MALDI-TOF-MS were recorded on SYNAPT G2 HDM spectrometer and ABSciex 5800 MALDI TOF mass spectrometer, respectively. UV-vis absorption spectra were recorded on Analytikjena (SPECORD 210 PLUS) spectrophotometer. For differential pulse voltammetric analysis (DPV), a three electrode cell was used for and which was performed on BioLogic SP300 potentiostat. Platinum wire used as a working electrode, a thin platinum foil was used as a counter electrode, and dyes were dissolved in dry dichloromethane. Measurements were carried out at the scan rate of  $50 \text{ mVs}^{-1}$  after addition of 0.1 M of tetra butyl ammonium perchlorate (TBAP) as the supporting electrolyte and non-aqueous  $\text{Ag}/\text{Ag}^+$  (0.01 M in  $\text{CH}_3\text{CN}$ ) used as reference electrode. The reference electrode was calibrated by recording the cyclic voltammograms of ferrocene in the same electrolyte as external standard; the potential values are on the basis of the estimated value of the ferrocene redox potential in dichloromethane 0.7V versus NHE. The EIS analysis was performed under dark condition by applying external bias to dye cells using a BioLogic SP300 potentiostat equipped with frequency response analyzer. Frequency range was fixed from 1 MHz to 10 mHz with AC amplitude of 10 mV. *I-V* characteristics of the dye cells were measured under a solar simulator (PET, CT200AAA) in clean room conditions, which is controlled by a source measurement unit (Keithley 2420). A certified  $4 \text{ cm}^2$  silicon solar cell (NREL) was calibrated to an intensity of  $1000 \text{ W m}^{-2}$  (xenon lamp, 450 W, USHIO INC) of a solar simulator (AM1.5 G light). IPCE spectra measurements were conducted by Newport QE measurement kit including a xenon light source, a monochromator, and a power meter. The set-up was calibrated using a reference silicon solar cell before the device measurement.

**4.4.2 Device Fabrication Procedure** For fabricating photoanode of DSSC, FTO (F-doped  $\text{SnO}_2$  glass;  $6\text{-}8 \text{ } \Omega/\text{sq}$ ) was cleaned sequentially by mucasol (2% in water), deionized water, and isopropanol using an ultra-sonication for 15 min. A blocking layer of  $\text{TiO}_2$  was prepared by dipping cleaned FTO substrate in freshly prepared aqueous 0.05 M  $\text{TiCl}_4$  solution at  $70 \text{ }^\circ\text{C}$  for 30 min, and washed immediately with deionized water, and followed by annealing in air at  $125 \text{ }^\circ\text{C}$  for 10 min. And the mesoscopic transparent thin layer ( $6\text{-}8 \text{ } \mu\text{m}$  thickness) of  $\text{TiO}_2$  onto buffer layer modified FTO was coated using  $\text{TiO}_2$  paste ( $< 20 \text{ nm}$ , Ti-Nanoxide T/SP) by the doctor-blade technique. Then kept in air for 5 min and annealed at  $125 \text{ }^\circ\text{C}$  in air for 15 min before coating scattering layer on it. Dyesol, WER2-O paste was used to coat a  $4\text{-}6 \text{ } \mu\text{m}$  thick  $\text{TiO}_2$  layer,

kept in air for 5 min and annealed at 125 °C in air for 15 min. Resulting 0.22 cm<sup>2</sup> active area films were sintered at 325 °C for 5 min, 375 °C for 5 min, 450 °C for 15 min and 500 °C for 15 min with heating rate of 5 °C per min in air. After reaching the furnace temperature at 50 °C, sintered films were treated in TiCl<sub>4</sub> solution as described before. After sintering the layer-by-layer deposited film again at 500 °C for 30 min, allowed to reach 50 °C and were immediately immersed in 0.1 mM **PSQ21-22** dye solution in chloroform at room temperature for 12 h. The dye loaded electrodes are washed thoroughly with chloroform, to remove physisorbed molecules. Successive addition of co-adsorbent 3 $\alpha$ ,7 $\alpha$ -dihydroxy-5 $\beta$ -cholanolic acid (CDCA) was varied the concentration of de-aggregating agent in the dye solution and studied the device performance at 2, 5 and 10 equivalents of CDCA. Finally the dye cell was assembled by joining the electrolyte (Iodolyte Z50) filled photoanode and platinum cathode using a 25  $\mu$ m thick spacer. The photovoltaic parameters have been evaluated without masking the device.

#### 4.4.3 Synthetic Procedures and Characterization Data

Required precursors **1a**, **1b**, **2a**, **2b**, **3a**, **3b** and **4** were synthesized and reported according to the previous chapter 2 and 3.

##### **Triethylammonium(E)-2-((5-bromo-1,3,3-trimethylindolin-2-ylidene)methyl)-3-**

**(dicyanomethylene)-4-oxocyclobut-1-en-1-olate (5):** Reaction mixture of 0.55 g (1.36 mmol) of 3-butoxy-4-[[5-carboxy-(1-methyl-1,3-dihydro-3,3-dimethyl-2Hindol-2-ylidene)]methyl]-3-cyclobutene-1,2-dione and dicyanomethane (**4**) (0.1 g, 1.49 mmol), and triethylamine (0.22 mL) in 10 mL of ethanol were taken in 50 mL round bottomed flask and then reaction mixture was allowed to stir for 8 h at room temperature. Then the solvent was removed under reduced pressure, and the solid residue was purified by column chromatography on silica gel with 1:20 (v/v) methanol/dichloromethane to obtain **2** as a red solid (0.4 g, 59% yield). <sup>1</sup>H NMR (200 MHz, DMSO-*d*<sub>6</sub>)  $\delta$ : 8.91 (br. s., 1 H), 7.54 (d, *J* = 2.0 Hz, 1 H), 7.36 (dd, *J* = 2.1, 8.4 Hz, 1 H), 6.95 (d, *J* = 8.5 Hz, 1 H), 5.89 (s, 1 H), 3.34 (s, 3 H), 3.22 (s, 3 H), 3.18 - 2.98 (m, 6 H), 1.57 (s, 6 H), 1.25 - 1.06 (m, 9 H).

**(Z)-4-((5-Bromo-1,3,3-trimethyl-3H-indol-1-ium-2-yl)methylene)-2-(((Z)-3-decyl-1-hexyl-3-octylindolin-2-ylidene)methyl)-3-(dicyanomethylene)cyclobut-1-en-1-olate (6):** Reaction mixture of 0.67 g (1.35 mmol) triethylammonium (E)-2-((5-bromo-1,3,3-trimethylindolin-2-ylidene)methyl)-3 (dicyanomethylene)-4-oxocyclobut-1-en-1-olate (**5**) and 1.0 g (1.62 mmol) 5-



bromo-3-decyl-1-hexyl-2-methyl-3-octyl-3H-indol-1-ium iodide (**3a**) were dissolved in 1-butanol and dry toluene (1:1, 3 mL each) in a 50 mL two necked round bottom flask, dry pyridine (1.5 equiv.) was added to it and charged with Dean-Stark apparatus. The reaction mixture was refluxed for 24 h under inert atmosphere. The reaction mixture was cooled to room temperature and the solvents were removed under reduced pressure. The reaction mixture was subjected to column chromatography (SiO<sub>2</sub>, 100-200 mesh, 5% MeOH and 95% CH<sub>2</sub>Cl<sub>2</sub>) to afford the required dye as green colored compound. Yield: 0.85 g, 75%. <sup>1</sup>H NMR (400 MHz, CDCl<sub>3</sub>) δ: 7.47 - 7.42 (m, 2 H), 7.41 - 7.32 (m, 2 H), 7.29 (d, *J* = 7.3 Hz, 1 H), 7.12 (d, *J* = 7.9 Hz, 1 H), 6.91 (d, *J* = 7.9 Hz, 1 H), 6.67 (s, 1 H), 6.43 (br. s., 1 H), 4.11 (t, *J* = 7.3 Hz, 2 H), 3.57 (br. s., 3 H), 3.08 - 2.80 (m, 2 H), 2.01 (m, 2 H), 1.87 - 1.70 (m, 6 H), 1.53 - 1.08 (m, 30 H), 0.97 - 0.68 (m, 11 H), 0.51 (m, 2 H); <sup>13</sup>C NMR (101 MHz, CDCl<sub>3</sub>) δ: 173.0, 171.9, 170.4, 168.0, 167.8, 165.4, 143.6, 141.9, 139.3, 139.259, 130.8, 128.0, 125.5, 125.1, 122.3, 119.0, 118.9, 116.8, 114.0, 110.7, 110.2, 90.5, 88.7, 59.2, 49.0, 44.8, 40.8, 39.5, 33.8, 31.9, 31.8, 31.7, 31.5, 31.4, 29.6, 29.6, 29.5, 29.4, 29.2, 29.1, 29.0, 28.9, 28.8, 27.6, 26.7, 26.5, 23.7, 22.6, 22.5, 22.4, 14.0, 13.9; MALDI-TOF (*m/z*): [M]<sup>+</sup> calcd for C<sub>52</sub>H<sub>69</sub>BrN<sub>4</sub>O: 844.4655; found: 844.2513.

**(Z)-2-(((Z)-3-Decyl-1-hexyl-3-octylindolin-2-ylidene)methyl)-3-(dicyanomethylene)-4-((5-(5-formylthiophen-2-yl)-1,3,3-trimethyl-3H-indol-1-ium-2-yl)methylene)cyclobut-1-en-1-olate (7):** Started with 0.13 g (0.157 mmol) (Z)-4-((5-bromo-1,3,3-trimethyl-3H-indol-1-ium-2-yl)methylene)-2-(((Z)-3-decyl-1-hexyl-3-octylindolin-2-ylidene)methyl)-3-(dicyanomethylene)cyclobut-1-en-1-olate (**6**) was dissolved in 1:1 ratio of toluene and methanol (total volume 5 mL) in 50 mL microwave reactor vessel and 0.073 g (0.471 mmol) 5-formylthiopheneboronic acid and 0.22 g (1.57 mmol) K<sub>2</sub>CO<sub>3</sub> were added to it under N<sub>2</sub> atmosphere. The solution was purged with nitrogen for 20 min and then 0.013 g (0.0157 mmol) PdCl<sub>2</sub>(dppf) (0.1 equiv.) was added and the reaction was carried out under microwave condition at 60 W, 70 °C for 15 min. The reaction mixture cooled to room temperature, and the solvents were removed under reduced pressure. The reaction mixture was purified by column chromatography (SiO<sub>2</sub>, 100-200 mesh 5% methanol and 95% dichloromethane to afford the required compound. Yield: 0.11 g, Yield: 80%. <sup>1</sup>H NMR (400 MHz, CDCl<sub>3</sub>) δ: 9.89 (s, 1 H), 7.76 (d, *J* = 3.7 Hz, 1 H), 7.66 (d, *J* = 7.9 Hz, 1 H), 7.57 (s, 1 H), 7.44 - 7.31 (m, 3 H), 7.29 (d, *J* = 7.3 Hz, 1 H), 7.12 (d, *J* = 7.9 Hz, 1 H), 7.06 (d, *J* = 8.5 Hz, 1 H), 6.68 (s, 1 H), 6.47 (br. s., 1

H), 4.11 (t,  $J = 7.6$  Hz, 2 H), 3.59 (br. s., 3 H), 3.07 - 2.82 (m, 2 H), 2.01 (m, 2 H), 1.90 - 1.70 (m, 8 H), 1.52 - 1.05 (m, 30 H), 0.95 - 0.66 (m, 11 H), 0.56 (m, 2 H);  $^{13}\text{C}$  NMR (101 MHz,  $\text{CDCl}_3$ )  $\delta$ : 182.5, 182.4, 173.0, 172.2, 170.1, 168.3, 167.9, 165.0, 153.8, 143.9, 143.5, 142.7, 142.0, 139.4, 137.5, 128.8, 128.1, 126.7, 126.4, 125.3, 123.7, 122.3, 120.1, 119.0, 118.9, 110.3, 109.8, 90.7, 89.2, 59.3, 48.7, 44.9, 40.9, 39.4, 31.8, 31.7, 31.6, 31.5, 31.4, 29.6, 29.6, 29.5, 29.3, 29.2, 29.0, 28.9, 28.8, 27.6, 26.9, 26.5, 24.3, 23.7, 22.6, 22.5, 22.4, 14.0, 13.9; MALDI-TOF ( $m/z$ ):  $[\text{M}]^+$  calcd for  $\text{C}_{57}\text{H}_{72}\text{N}_4\text{O}_2\text{S}$ : 876.5376; found: 876.3058.

**(Z)-4-((5-(5-Carboxythiophen-2-yl)-1,3,3-trimethyl-3H-indol-1-ium-2-yl)methylene)-2-(((Z)-3-decyl-1-hexyl-3-octylindolin-2-ylidene)methyl)-3-(dicyanomethylene)cyclobut-1-en-1-olate (PSQ21):** Started with 0.12 g (0.144 mmol) (Z)-4-((5-bromo-1,3,3-trimethyl-3H-indol-1-ium-2-yl)methylene)-2-(((Z)-3-decyl-1-hexyl-3-octylindolin-2-ylidene)methyl)-3-(dicyanomethylene)cyclobut-1-en-1-olate, 6 (1 equiv.) was dissolved in 1:1 ratio of toluene and methanol (total volume 5 mL) in 50 mL microwave reactor vessel and 0.11 g (0.432 mmol) 5-carboxylthiophene-2-boronic acid pinacol ester and 0.2 g (0.144 mmol)  $\text{K}_2\text{CO}_3$  were added to it under  $\text{N}_2$  atmosphere. The solution was purged with nitrogen for 20 min and then 0.012 g (0.014 mmol)  $\text{PdCl}_2(\text{dppf})$  was added and the reaction was carried out under microwave condition at 60 W, 70  $^\circ\text{C}$  for 15 min. The reaction mixture cooled to room temperature, and the solvents were removed under reduced pressure. The reaction mixture was purified by column chromatography ( $\text{SiO}_2$ , 100-200 mesh 5% methanol and 95% dichloromethane to afford the required compound. Yield: 77 mg, Yield: 60%;  $^1\text{H}$  NMR (400 MHz,  $\text{CDCl}_3$ )  $\delta$ : 7.96 - 7.72 (br. s., 1 H), 7.70 - 7.49 (m, 4 H), 7.49 - 7.19 (m, 4 H), 7.18 - 6.94 (m, 2 H), 6.67 (br. s., 1 H), 6.47 (br. s., 1 H), 4.11 (t,  $J = 7.9$  Hz, 2 H), 3.61 (br. s., 3 H), 3.11 - 2.82 (m, 2 H), 2.16 - 1.92 (m, 2 H), 1.92 - 1.74 (m, 6 H), 1.50 - 1.17 (m, 32 H), 1.15 - 0.69 (m, 11 H), 0.64 - 0.42 (m, 2 H);  $^{13}\text{C}$  NMR (101 MHz,  $\text{CDCl}_3$ )  $\delta$ : 173.1, 171.8, 167.9, 167.8, 165.4, 143.7, 139.4, 139.2, 135.6, 130.9, 129.8, 129.0, 128.0, 126.4, 126.1, 125.1, 123.9, 123.5, 123.4, 122.4, 119.9, 119.1, 119.0, 115.9, 114.0, 110.2, 109.9, 90.6, 89.1, 59.2, 48.9, 44.8, 39.5, 33.8, 31.9, 31.8, 31.8, 31.6, 31.5, 29.7, 29.5, 29.5, 29.4, 29.3, 29.3, 29.1, 29.0, 29.0, 28.9, 27.6, 26.8, 26.5, 23.8, 22.7, 22.6, 22.4, 14.1; MALDI-TOF ( $m/z$ ):  $[\text{M}]^+$  calcd for  $\text{C}_{57}\text{H}_{72}\text{N}_4\text{O}_3\text{S}$ : 892.5325; found: 892.3264.

**(Z)-4-((5-(5-((E)-2-carboxy-2-cyanovinyl)thiophen-2-yl)-1,3,3-trimethyl-3H-indol-1-ium-2-yl)methylene)-2-(((Z)-3-decyl-1-hexyl-3-octylindolin-2-ylidene)methyl)-3-**

**(dicyanomethylene)cyclobut-1-en-1-olate (PSQ 22):** Reaction of 0.15 g (0.172 mmol) (Z)-2-(((Z)-3-decyl-1-hexyl-3-octylindolin-2-ylidene)methyl)-3-(dicyanomethylene)-4-((5-(5-formylthiophen-2-yl)-1,3,3-trimethyl-3H-indol-1-ium-2-yl)methylene)cyclobut-1-en-1-olate (**6**) was dissolved in dry CH<sub>3</sub>CN (6 mL) in a 50 mL single necked round bottomed flask, 0.044 g (0.518 mmol) cyano acetic acid was added and then finally 0.026 g (0.310 mmol) piperidine was added into it. The reaction mixture was allowed to reflux for 6 h. After the reaction completion, the solvent was removed and work up with dil. acetic acid and then it was purified by column chromatography. Yield: 57 mg, 40%; <sup>1</sup>H NMR (400 MHz, CDCl<sub>3</sub>) δ: 8.25 (br. s., 1 H), 7.86 - 7.62 (m, 2 H), 7.56 (br. s., 1 H), 7.48 - 7.22 (m, 4 H), 7.20 - 7.06 (m, 2 H), 6.66 (br. s., 1 H), 6.38 (br. s., 1 H), 4.12 (t, *J* = 7.6 Hz, 2 H), 3.62 (br. s., 3 H), 2.92 (br. s., 2 H), 2.17 - 1.93 (m, 2 H), 1.91 - 1.67 (m, 6 H), 1.49 - 1.12 (m, 32 H), 1.08 - 0.68 (m, 11 H), 0.62 - 0.34 (m, 2 H); <sup>13</sup>C NMR (101 MHz, CDCl<sub>3</sub>) δ: 172.5, 167.8, 164.7, 147.1, 143.5, 139.7, 139.4, 139.2, 134.5, 128.5, 128.1, 127.0, 125.4, 124.0, 123.9, 123.4, 122.4, 119.9, 118.7, 116.1, 115.9, 114.0, 110.4, 90.8, 88.9, 59.4, 48.9, 45.0, 39.4, 34.7, 33.8, 31.9, 31.8, 31.7, 31.6, 31.5, 31.4, 30.3, 30.1, 29.6, 29.6, 29.5, 29.4, 29.4, 29.3, 29.2, 29.1, 29.0, 29.0, 28.9, 27.7, 26.9, 26.5, 23.8, 22.6, 22.6, 22.5, 22.4, 14.1, 13.9; MALDI-TOF (*m/z*): [M]<sup>+</sup>calcd for C<sub>60</sub>H<sub>73</sub>N<sub>5</sub>O<sub>3</sub>S: 943.5434; found: 943.3452.

#### 4.5 References

- (1) Hagfeldt, A.; Boschloo, G.; Sun, L.; Kloo, L.; Pettersson, H. Dye-Sensitized Solar Cells. *Chemical Reviews* **2010**, *110*, 6595–6663.
- (2) Martinson, A. B. F.; Hamann, T. W.; Pellin, M. J.; Hupp, J. T. New Architectures for Dye-Sensitized Solar Cells. *Chemistry - A European Journal* **2008**, *14*, 4458–4467.
- (3) Listorti, A.; O'Regan, B.; Durrant, J. R. Electron Transfer Dynamics in Dye-Sensitized Solar Cells. *Chem. Mater.* **2011**, *23*, 3381–3399.
- (4) Liang, M.; Chen, J. Arylamine Organic Dyes for Dye-Sensitized Solar Cells. *Chem. Soc. Rev.* **2013**, *42*, 3453–3488.
- (5) Wu, Y.; Zhu, W. Organic Sensitizers from D-π-A to D-A-π-A: Effect of the Internal Electron-Withdrawing Units on Molecular Absorption, Energy Levels and Photovoltaic Performances. *Chem. Soc. Rev.* **2013**, *42*, 2039–2058.
- (6) Yella, A.; Lee, H.-W.; Tsao, H. N.; Yi, C.; Chandiran, A. K.; Nazeeruddin, M. K.; Diao, E. W.-G.; Yeh, C.-Y.; Zakeeruddin, S. M.; Grätzel, M. Porphyrin-Sensitized Solar Cells with

- Cobalt (II/III)-Based Redox Electrolyte Exceed 12 Percent Efficiency. *Science* **2011**, *334*, 629–634.
- (7) Urbani, M.; Grätzel, M.; Nazeeruddin, M. K.; Torres, T. Meso-Substituted Porphyrins for Dye-Sensitized Solar Cells. *Chem. Rev.* **2014**, *114*, 12330–12396.
- (8) Tang, Y.; Wang, Y.; Li, X.; Ågren, H.; Zhu, W.-H.; Xie, Y. Porphyrins Containing a Triphenylamine Donor and up to Eight Alkoxy Chains for Dye-Sensitized Solar Cells: A High Efficiency of 10.9%. *ACS Appl. Mater. Interfaces* **2015**, *7*, 27976–27985.
- (9) Martín, -G. L.; Fernández, -L. F.; Sastre, -S. Á. Advances in Phthalocyanine-Sensitized Solar Cells (PcSSCs). *J. Mater. Chem. A* **2014**, *2*, 15672–15682.
- (10) García, -I. M.; Cid, J.-J.; Yum, J.-H.; Forneli, A.; Vázquez, P.; Nazeeruddin, M. K.; Palomares, E.; Grätzel, M.; Torres, T. Increasing the Efficiency of Zinc-Phthalocyanine Based Solar Cells through Modification of the Anchoring Ligand. *Energy Environ. Sci.* **2010**, *4*, 189–194.
- (11) Kasha, M.; Rawls, H. R.; Ashraf, E.-B. M. The Exciton Model in Molecular Spectroscopy. *Pure and Applied Chemistry* **1965**, *11*, 371–392.
- (12) Yum, J.-H.; Walter, P.; Huber, S.; Rentsch, D.; Geiger, T.; Nüesch, F.; De Angelis, F.; Grätzel, M.; Nazeeruddin, M. K. Efficient Far Red Sensitization of Nanocrystalline TiO<sub>2</sub> Films by an Unsymmetrical Squaraine Dye. *J. Am. Chem. Soc.* **2007**, *129*, 10320–10321.
- (13) Shi, Y.; Hill, R. B. M.; Yum, J. H.; Dualeh, A.; Barlow, S.; Grätzel, M.; Marder, S. R.; Nazeeruddin, M. K. A High-Efficiency Panchromatic Squaraine Sensitizer for Dye-Sensitized Solar Cells. *Angewandte Chemie* **2011**, *123*, 6749–6751.
- (14) Delcamp, J. H.; Shi, Y.; Yum, J. H.; Sajoto, T.; Dell’Orto, E.; Barlow, S.; Nazeeruddin, M. K.; Marder, S. R.; Grätzel, M. The Role of  $\pi$  Bridges in High-Efficiency DSCs Based on Unsymmetrical Squaraines. *Chemistry – A European Journal* **2012**, *19*, 1819–1827.
- (15) Jradi, F. M.; Kang, X.; O’Neil, D.; Pajares, G.; Getmanenko, Y. A.; Szymanski, P.; Parker, T. C.; El-Sayed, M. A.; Marder, S. R. Near-Infrared Asymmetrical Squaraine Sensitizers for Highly Efficient Dye Sensitized Solar Cells: The Effect of  $\pi$ -Bridges and Anchoring Groups on Solar Cell Performance. *Chem. Mater.* **2015**, *27*, 2480–2487.
- (16) Beverina, L.; Ruffo, R.; Mari, C. M.; Pagani, G. A.; Sassi, M.; De, A. F.; Fantacci, S.; Yum, J. H.; Grätzel, M.; Nazeeruddin, M. K. Panchromatic Cross-Substituted Squaraines for Dye-Sensitized Solar Cell Applications. *ChemSusChem* **2009**, *2*, 621–624.

- 
- (17) Maeda, T.; Mineta, S.; Fujiwara, H.; Nakao, H.; Yagi, S.; Nakazumi, H. Conformational Effect of Symmetrical Squaraine Dyes on the Performance of Dye-Sensitized Solar Cells. *J. Mater. Chem. A* **2012**, *1*, 1303–1309.
- (18) Qin, C.; Numata, Y.; Zhang, S.; Yang, X.; Islam, A.; Zhang, K.; Chen, H.; Han, L. Novel Near-Infrared Squaraine Sensitizers for Stable and Efficient Dye-Sensitized Solar Cells. *Advanced Functional Materials* **2014**, *24*, 3059–3066.
- (19) Qin, C.; Numata, Y.; Zhang, S.; Islam, A.; Yang, X.; Sodeyama, K.; Tateyama, Y.; Han, L. A Near-Infrared *Cis*-configured Squaraine Co-Sensitizer for High-Efficiency Dye-Sensitized Solar Cells. *Advanced Functional Materials* **2013**, *23*, 3782–3789.
- (20) Alagumalai, A.; M. K., M. F.; Vellimalai, P.; Sil, M. C.; Nithyanandhan, J. Effect of Out-of-Plane Alkyl Group's Position in Dye-Sensitized Solar Cell Efficiency: A Structure–Property Relationship Utilizing Indoline-Based Unsymmetrical Squaraine Dyes. *ACS Appl. Mater. Interfaces* **2016**, *8*, 35353–35367.
- (21) Punitharasu, V.; Kavungathodi, M. F. M.; Nithyanandhan, J. Interplay between  $\pi$ -Bridges and Positions of Branched Alkyl Groups of Unsymmetrical D–A–D– $\pi$ –A Squaraines in Dye-Sensitized Solar Cells: Mode of Dye Anchoring and the Charge Transfer Process at the TiO<sub>2</sub>-dye/Electrolyte Interface. *ACS Appl. Mater. Interfaces* **2017**, *9*, 32698–32712.
- (22) Schulz, -S. M.; Gates, P. J.; Sönnichsen, F. D.; Staubitz, A. Diversely Halogenated Spiropyrans - Useful Synthetic Building Blocks for a Versatile Class of Molecular Switches. *Dyes and Pigments* **2017**, *136*, 292–301.

## Chapter 5



**Effect of  $\pi$ -Spacer and Anchoring Groups in Squaraine  
Based Dyes in the Dye Sensitized Solar Cells**

## 5.1 Introduction

The previous chapters discuss the importance of TiO<sub>2</sub>-dye interface which controls the charge injection and dye regeneration processes. Further, dye-TiO<sub>2</sub> interface has been established by the interaction of anchoring groups present in the dye with TiO<sub>2</sub> surface. Along the line dyes with multiple anchoring groups performed well compared to the dyes with one anchoring group.<sup>1-3</sup> Apart from establishing the communication between the dye and TiO<sub>2</sub>, dye orientation on the surface plays an important role in the charge injection process.<sup>4-6</sup> Dye orientation on TiO<sub>2</sub> surface also indicated the possibility of through space electron transfer from dye to TiO<sub>2</sub>.<sup>7</sup> The previous chapters have discussed the importance of  $\pi$ -spacer, (**Chapter 2**) number of anchoring group in *cis*-configured squaraine, (**Chapter 3**) and  $\pi$ -spacer appended squaraine dyes with type of anchoring group (**Chapter 4**) besides controlling the aggregation of dyes by properly functionalized out-of-plane alkyl groups for the device performance (**Figure 5.1**).

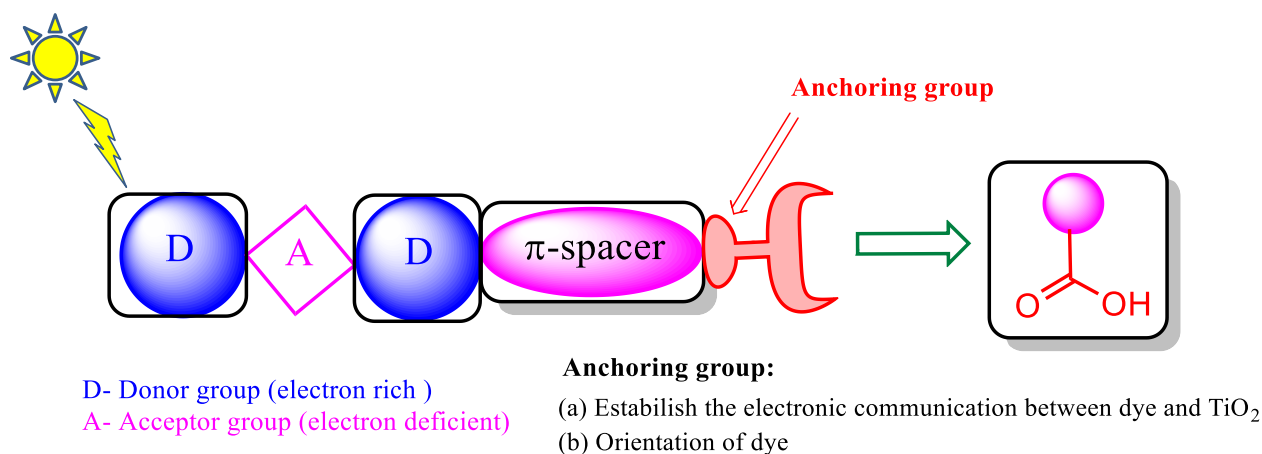


**Figure 5.1** D-A-D- $\pi$ -Anchoring group based on unsymmetrical squaraine dyes.

A comprehensive report on the structure and device performance of squaraine dyes, indicates the importance of alkyl groups and the anchoring groups present in the symmetrical and unsymmetrical squaraine dyes. Squaraine dyes are versatile as the manipulation of electronic structure has been realized by having either *cis*- or *trans*-conformation by suitable functionalisation on dyes. Though there have been several derivatives of unsymmetrical squaraine dyes with improved device performance, the importance of effects of anchoring group on the squaraine dyes and their device performance is rarely studied. Initially unsymmetrical squaraine dyes showed the device cell performance in the range of 4 to 5%. For example, dye MSQ, squaraine dye with carboxylic acid anchoring group showed the device efficiency of

2.2%,<sup>8</sup> and the device performance further enhanced to 5.03% upon exchanging anchoring group to cyanoacetic acid (SQ-B).<sup>9,10</sup> However, introducing  $\pi$ -spacer such as thiophene unit between squaraine unit and cyanoacetic acid group lead to diminish the device performance to 2.67% (SQ-C).<sup>10</sup> Further judicious incorporation of  $-C_{12}H_{25}$  group to SQ-C instead of  $-C_4H_9$  group enhances the DSSC device efficiency to 6.74% (YR6).<sup>11,12</sup> Hence the choice of selecting anchoring group and alkyl groups present in an unsymmetrical squaraine is very important for the light efficient dyes for DSSC.<sup>12,13</sup> Further we have been utilized the out-of-plane branched alkyl group and extending the conjugation of  $\pi$ -spacer in D-A-D based far red active unsymmetrical squaraine dyes which favored very important role to enhance the light harvesting efficiency of PSQ dyes.<sup>14,15</sup>

From the previous chapters, systematic studies were carried out to understand the structure-property relationship of unsymmetrical squaraine dyes to afford the better device performance. This significant studies are more favored the following factors such as (i) DSSC device performance can be varied by functionalisation of branched alkyl groups at  $sp^3C$  and N-alkyl position of indolenine units with different  $\pi$ -spacer, (ii) *cis*-configured squaraine dyes afforded better device performance with suitably functionalized branched alkyl groups and extended conjugation of  $\pi$ -spacer with different anchoring groups such as carboxylic acid vs cyano acetic acid. The present chapter discusses the dye design and systematic investigation of dye orientation and their aggregation on the  $TiO_2$  surface to understand the effect of anchoring groups with suitably functionalized branched alkyl groups and different  $\pi$ -spacer groups on unsymmetrical squaraine dyes. Herein, a series of unsymmetrical D-A-D- $\pi$ -A *trans*-squaraine PSQ dyes (**PSQ31-33**) (**Figure 5.2**) has been designed and synthesised. This chapter discuss specifically about the effect of anchoring group and the extended conjugation of  $\pi$ -spacer on unsymmetrical squaraine unit. The following dyes **PSQ31-33** were designed with *trans*-SQ frame work, which can be further functionalized with  $\pi$ -spacer and anchoring groups.



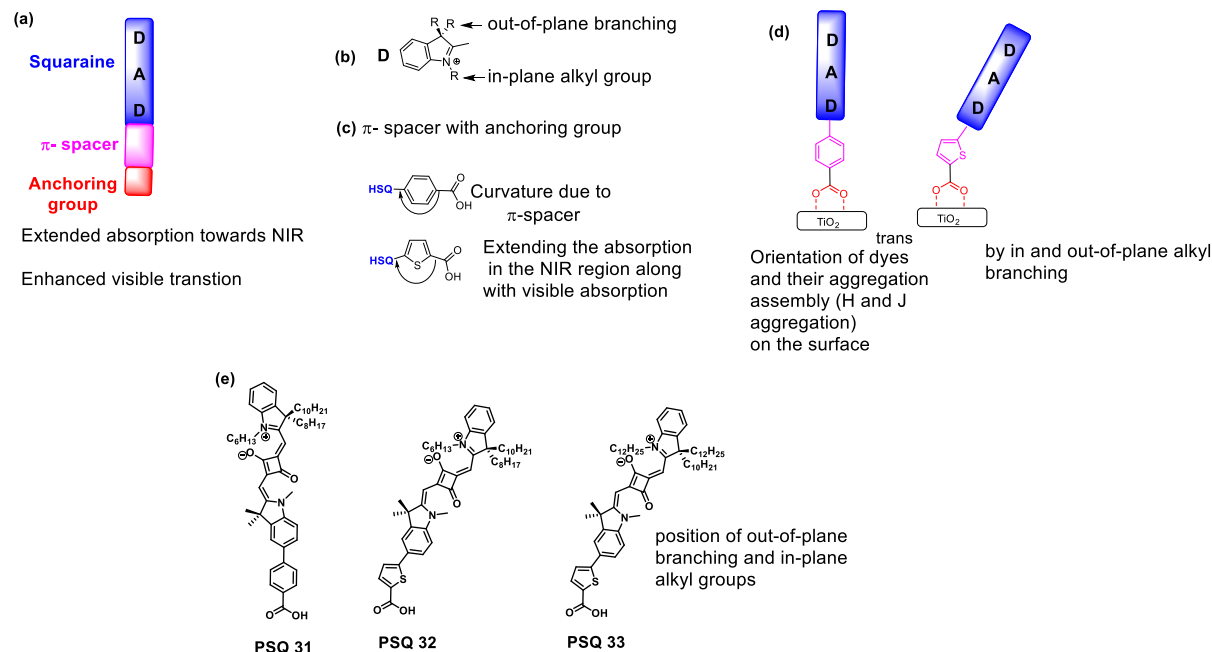


**Figure 5.2** (a) D-A-D- $\pi$ -Anchoring group based on unsymmetrical *trans*-configured squaraine dyes, (b) in-plane and out-of-plane branching on indoline, (c)  $\pi$ -spacer with anchoring group, (d) schematic representation of mode of anchoring on TiO<sub>2</sub> surface, and (e)  $\pi$ -extended of alkyl functionalized unsymmetrical squaraine dyes, **PSQ31-33**.

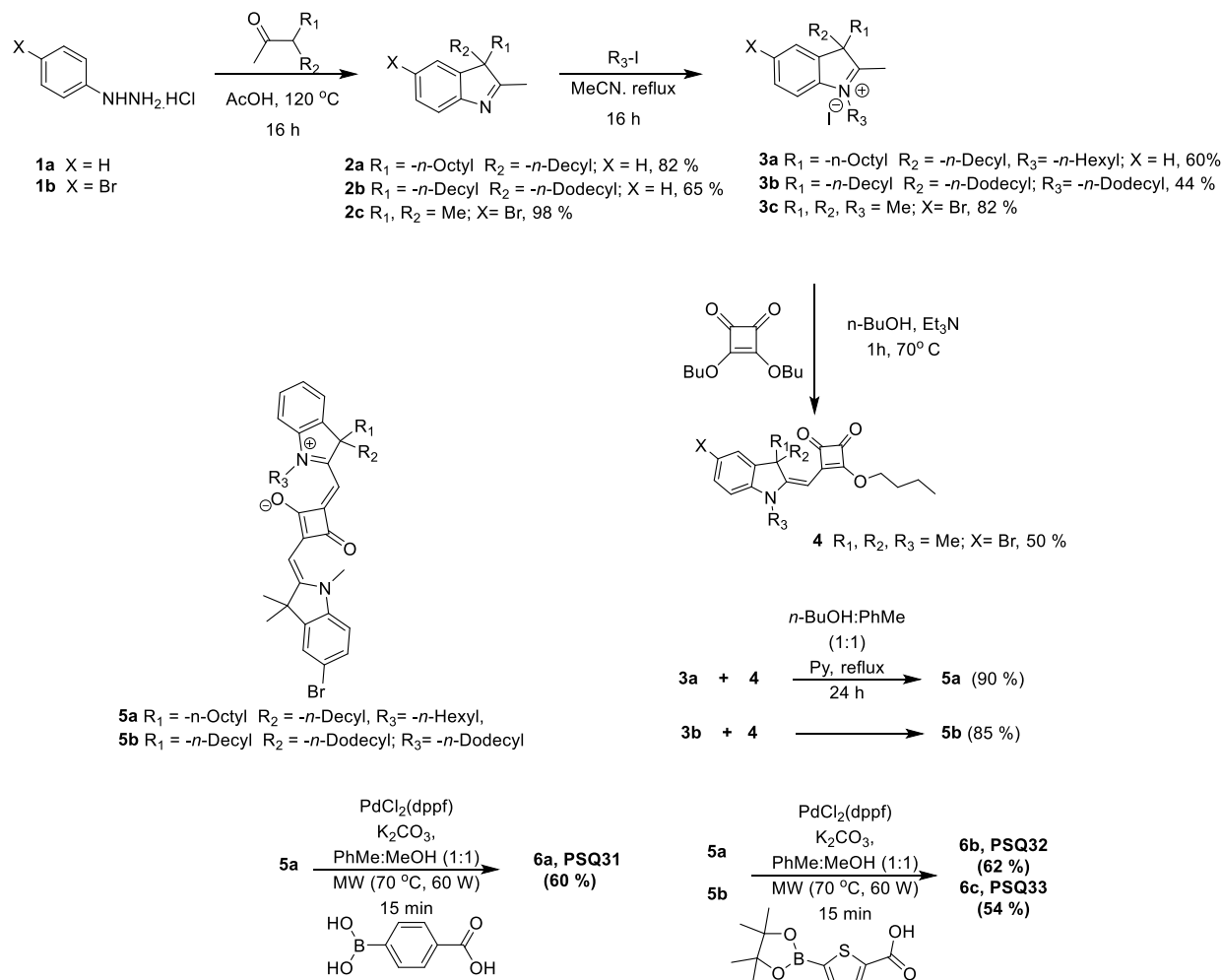
## 5.2 Results and Discussions

### 5.2.1 Synthesis of PSQ Sensitizers

The following three general synthetic transformations takes place for the synthesis of **PSQ31-PSQ33** dyes.

- Synthesis of bromo derivatives of the unsymmetrical semi-squaraine dye.
- Synthesis of bromo derivatives of the unsymmetrical squaraine dye.
- Microwave mediated Suzuki coupling of bromo functionalized squaraine derivative and boronic acid containing thiophene spacer with anchoring group.

The branched methyl ketone was synthesized via the reported procedure from our group. The indolenine derivatives, **2a-c** were synthesized using branched methyl ketone with phenyl hydrazine through Fischer-indole synthetic route. The indolenine derivatives, **2a-2c** were



**Scheme 5.1.** Synthesis of branched alkyl group containing  $\pi$ -extended D-A-D-A squaraine dyes, PSQ31-33.

converted into corresponding indolium salt, **3a-c** via N-alkylation with methyl/hexyl/dodecyl iodide. The bromo functionalized semi-squaraine, **4** was synthesized by bromo functionalized indolium salt, **3c** treated with squaric acid in presence of NEt<sub>3</sub>. Further the branched indolium salt, **3a-3b** were condensed in presence of pyridine base with bromo functionalized semi-squaraine, **4** to provide the unsymmetrical squaraines, **5a-b**. After microwave-assisted Suzuki coupling between the bromo functionalized unsymmetrical squaraines with 4-carboxylphenylboronic acid and 5-carboxylthiophene-2-boronic acid pinacol ester in presence of PdCl<sub>2</sub>(dppf) was used as catalyst and K<sub>2</sub>CO<sub>3</sub> as a base, afforded required final PSQ31-33 dyes (**scheme 5.1**). Generally microwave mediated Pd catalyzed Suzuki coupling reaction helps to

reduce the reaction time (10-15 min) with moderate yield. These dye molecules were characterised by  $^1\text{H}$ ,  $^{13}\text{C}$  NMR spectroscopy and mass spectrometric analyses.

### 5.2.2 Photophysical Properties

The optical properties of **PSQ31-33** were studied by UV–Vis absorption and emission spectra both in solution ( $\text{CH}_2\text{Cl}_2$ ) as well as in transparent thin film of  $\text{TiO}_2$  (6  $\mu\text{m}$ ), and the results were showed in **Figure 5.3**, (**Table 5.1**). **PSQ31-33** dyes that showed an intense charge transfer peak with the molar extinction coefficient of  $\epsilon \sim 1.4\text{-}3.3 \times 10^5 \text{ M}^{-1} \text{ cm}^{-1}$  in the range of at 650 nm and 657 nm and a narrow absorption peak with extinction coefficient of  $\epsilon \sim 0.05\text{-}0.18 \times 10^5 \text{ M}^{-1} \text{ cm}^{-1}$  in the range of at 381 nm, respectively. Such high energy transitions were observed by extending the squaraine dye conjugation with  $\pi$  spacer or appending dicyanovinyl groups in squaraine unit. **PSQ31-PSQ33** dyes were having maximum absorption wavelength ( $\lambda_{\text{max}}$ ) around 650 to 657 nm. For **PSQ31** and **PSQ32** substituting phenyl group with thiophene causes red shifted absorption band (7 nm). In case of **PSQ32** and **PSQ33**, both showed close similarity in their  $\lambda_{\text{max}}$  with same  $\pi$  spacer and anchoring unit but there was small changes in  $\epsilon$  values, after extending the length of top indoline  $\text{sp}^3$ -alkyl chain in **PSQ33**.

Emission  $\lambda_{\text{max}}$  of **PSQ31-33** exhibits intense peak at 659 nm (**PSQ31**), 666nm (**PSQ32-33**) upon exciting at 610nm. The Stokes shift of  $\sim 9\text{-}10$  nm for PSQ dyes showed that there may be significant change in dipole moment in the excited states. Fluorescence quantum yield ( $\phi$ ) was measured in dichloromethane via relative method and it shows an increasing order of [**PSQ32**] < [**PSQ31=PSQ33**]. The optical band gap ( $E_{0-0}$ ) was calculated from the intersection of absorption and emission spectra and **PSQ31-PSQ33** dyes exhibited between 1.87-1.89 eV.

The optical densities of the **PSQ31-PSQ33** dyes adsorbed on  $\text{TiO}_2$  surface were determined and are showed in **Figure 5.3c**. A transparent, 6  $\mu\text{m}$  thick,  $\text{TiO}_2$  film dipped in 0.1 mM dye solution for 30 min; **PSQ31-PSQ33** dyes showed a broadened absorption spectrum on the  $\text{TiO}_2$  thin film due to the dye-dye interaction of PSQ dyes on the  $\text{TiO}_2$  surface besides interaction of dyes with polar  $\text{TiO}_2$  surface. For **PSQ31** and **PSQ32** dyes, both having phenyl with thiophene spacer and the top alkylated squaraine moiety, showed a strong aggregation peak around 609 nm, which is usually assigned to the H-aggregate for **PSQ32** dye. Compared to **PSQ32** and **PSQ33** dye, the dimeric peak was reduced after increasing the length of top indoline  $\text{sp}^3$ -alkyl chain in **PSQ33**. It was found that **PSQ32** dyes are more aggregated with respect to

both hypsochromic and bathochromic region compared to **PSQ31** and **PSQ33** dye. The bare TiO<sub>2</sub> electrode was dipped in 0.1 mM dye solution for 12 h and **PSQ31-PSQ33** dyes have shown broad LHE profile for harvesting the NIR photons.

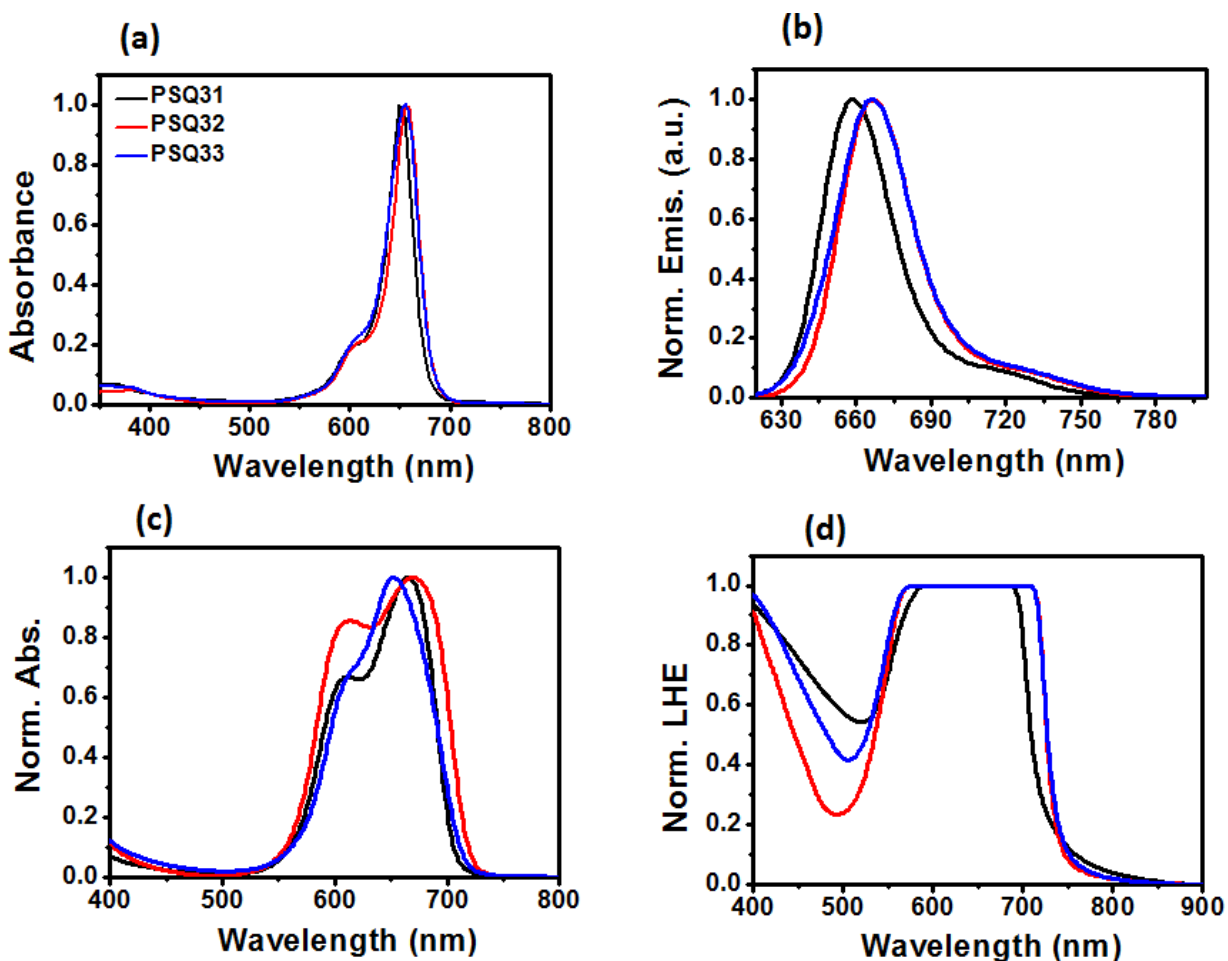


**Figure 5.3** Optical properties of **PSQ31-33** dyes. (a) UV-vis absorption spectra in CH<sub>2</sub>Cl<sub>2</sub>, (b) Normalized emission spectra in CH<sub>2</sub>Cl<sub>2</sub> (excitation wavelength: 610 nm), (c) Normalized absorption spectra on thin film of TiO<sub>2</sub>, thickness = 6 μm, dipping time = 30 min, and [PSQ] = 0.1 mM in CH<sub>2</sub>Cl<sub>2</sub>, (d) LHE (%) on TiO<sub>2</sub> thin film recorded after 12 h dipping in 0.1 mM solution in CH<sub>2</sub>Cl<sub>2</sub>.

The emission profiles of **PSQ31-33** indicated that there was no additional peak in the red-shifted region which indicates the possibility of existence of only H-aggregates (**Figure 5.4**).

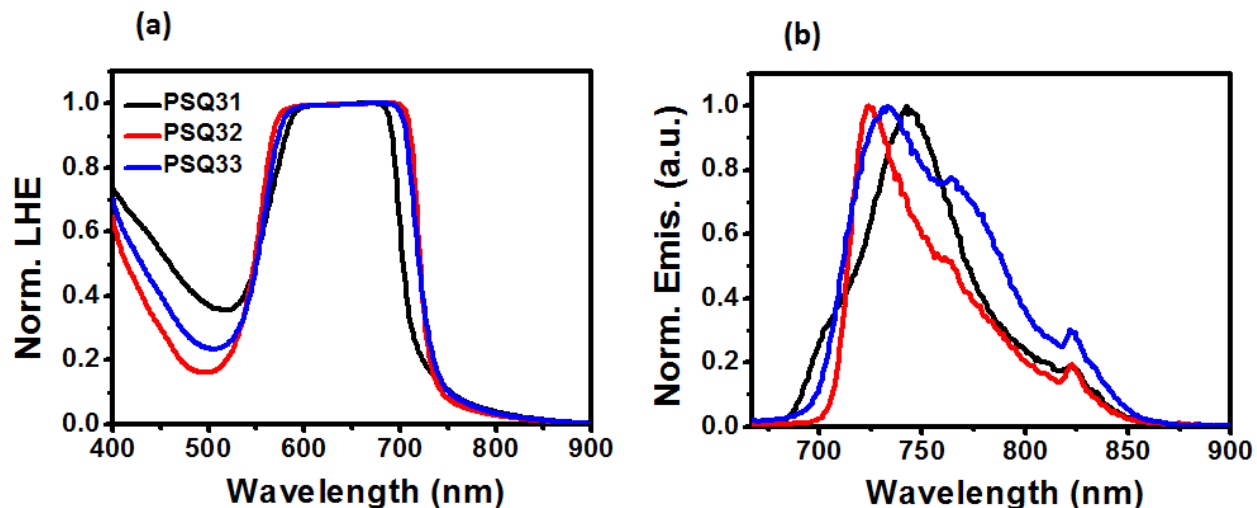


**Figure 5.4** Optical properties of **PSQ31-33** dyes. (a) Normalized LHE on  $\text{Al}_2\text{O}_3$  thin film recorded after 12 h dipping in 0.1 mM solution in  $\text{CH}_2\text{Cl}_2$ . (b) Normalized emission spectra on thin film of  $\text{Al}_2\text{O}_3$ , excitation wavelength: 657 nm, thickness = 6 nm, dipping time = 12 h and  $[\text{PSQ}] = 0.1 \text{ mM}$  in  $\text{CH}_2\text{Cl}_2$ .

### 5.2.3 Electrochemical Characterization

Differential pulse voltammetry (DPV) was carried out to understand the feasibility of electron injection from the excited dye to conduction band of  $\text{TiO}_2$  and the dye regeneration by redox electrolyte, which is performed in  $\text{CH}_2\text{Cl}_2$  by using 0.1 M tetra butyl ammonium perchlorate as supporting electrolyte (**Figure 5.5**). Redox potentials of **PSQ31-PSQ33** dyes were measured using DPV and the results were listed in **Table 5.1**. The HOMO energy level of **PSQ31**, **PSQ32** and **PSQ33** was found at 0.71V, 0.73V and 0.72V vs NHE, respectively. The more positive potential of **PSQ31-PSQ33** than redox electrolyte making the feasible regeneration of oxidized dye. In addition, there is no a significant potential difference in PSQ dyes, by extending the alkyl chain at  $\text{sp}^3$  carbon of indoline unit in **PSQ33**. The optical energy gaps ( $E_{0-0}$ ) was calculated from the intersection of absorption and emission spectra and **PSQ31-PSQ33** dyes exhibited optical band gap between 1.87-1.89 eV. The LUMO energy level of **PSQ31-33** was found at -1.2 V, -1.14V and -1.16V vs NHE, respectively. The more negative potential of **PSQ31-PSQ33** which helps a larger driving force for electron injection from the photo-excited state to the conduction band of  $\text{TiO}_2$ .

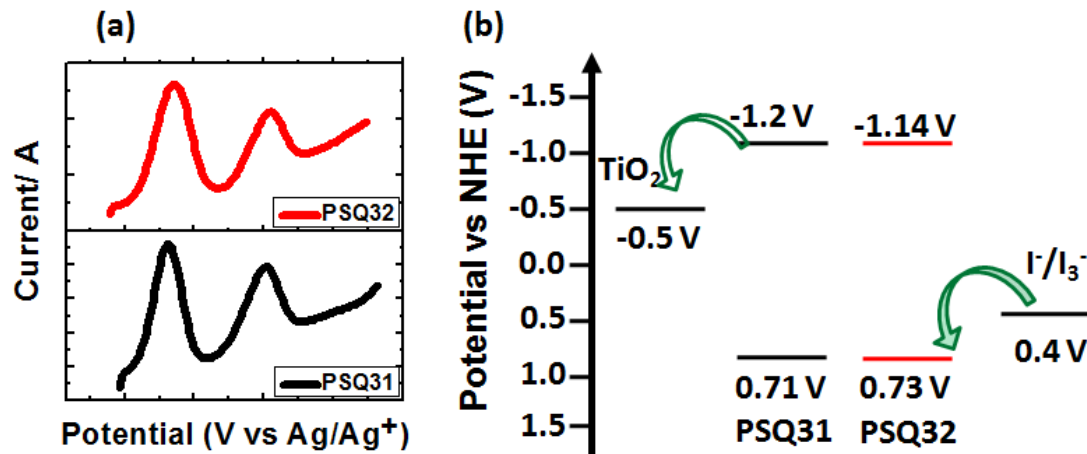


**Figure 5.5** Electrochemical properties of PSQ31-33 dyes. (a) Differential pulse voltammetry for PSQ31-33 dyes and (b) Energy level diagram of PSQ dyes (V vs NHE) with TiO<sub>2</sub>, and electrolyte (iodide/triiodide).

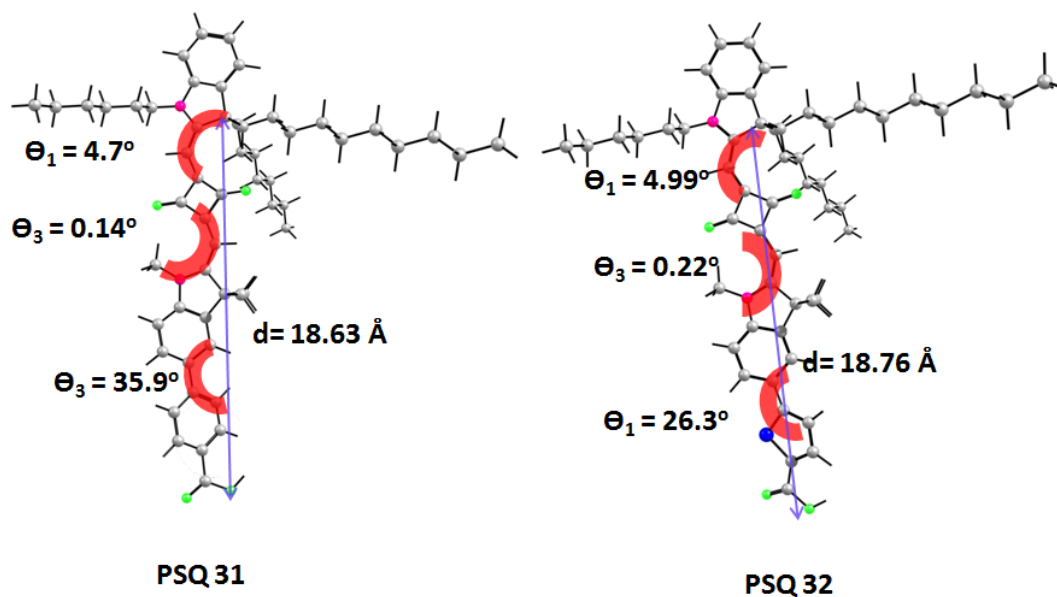
**Table 5.1** Photophysical and electrochemical properties of PSQ31-33 at room temperature

Dye	$\lambda_{\max}/\text{abs}$ (nm) <sup>a</sup>	$\epsilon_a, \epsilon_b$ $10^5(\text{M}^{-1}\text{cm}^{-1})^b$	$\lambda_{\max}/\text{emis}$ (nm) ) <sup>c</sup>	$\phi_{\text{emis}}$ <sup>d</sup>	$\lambda_{\max}/\text{abs}/\text{TiO}_2$ (nm) <sup>e</sup>	$A_{\text{dimer}}/A_{\text{monomer}}$ (%)	$E_{\text{HOMO}}^f$ (V)	$\Delta E_{0-0}^g$ (eV)	$E_{\text{LUMO}}$ (V) <sup>h</sup>
PSQ31	381,650	0.05, 1.4	659	0.61	605,667	66	0.71	1.89	-1.2
PSQ32	381,657	0.11, 2.5	666	0.59	609,671	85	0.73	1.87	-1.14
PSQ33	381,656	0.18, 3.3	666	0.61	608,652	65	0.72	1.88	-1.16

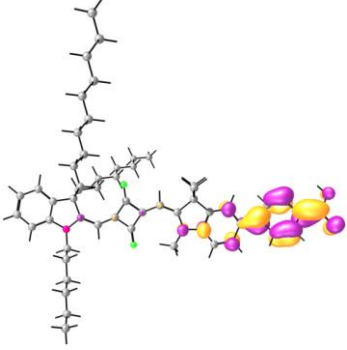
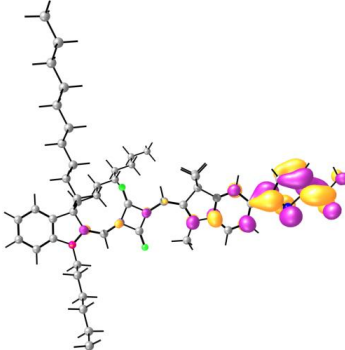
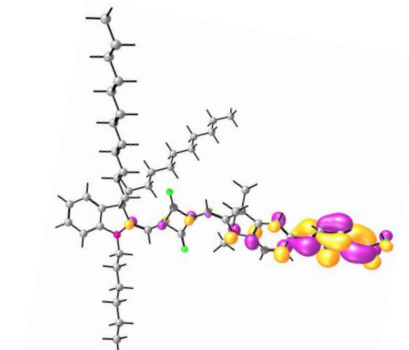
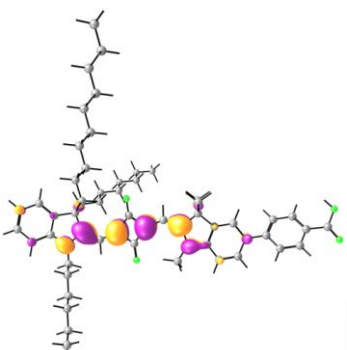
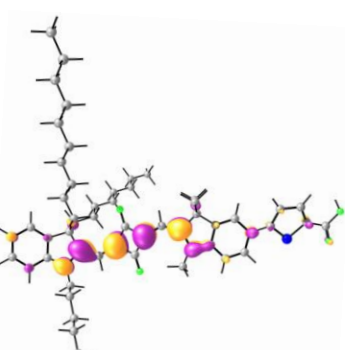
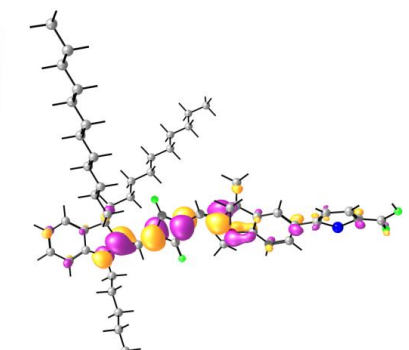
<sup>a</sup>UV-vis absorption in CH<sub>2</sub>Cl<sub>2</sub>. <sup>b</sup>Molar extinction coefficient in visible region peak  $\epsilon_a$ , and charge transfer peak  $\epsilon_b$ . <sup>c</sup>Emission studies at excitation wavelength at 610nm. <sup>d</sup>Quantum yield by relative method in CH<sub>2</sub>Cl<sub>2</sub>. <sup>e</sup>On thin film of TiO<sub>2</sub>, thickness = 6  $\mu\text{m}$ , dipping time = 30 min, and [PSQ] = 0.1 mM in CHCl<sub>3</sub>. <sup>f</sup> $E_{\text{HOMO}}$  of PSQ31-33 in CH<sub>2</sub>Cl<sub>2</sub>, Fc<sup>+</sup>/Fc was used as external standard and potential measured vs Fc/Fc<sup>+</sup> (eV) were converted to NHE (V) by addition of 0.7 V. <sup>g</sup> $E_{0-0}$  deduced at the intersection of absorption and emission spectra using the eq,  $E_{0-0}$  (eV) =  $1240/\lambda_{\max}$ . <sup>h</sup> $E_{\text{LUMO}}$  levels were measured by subtracting  $E_{\text{HOMO}}$  from  $E_{0-0}$ .

### 5.2.4 Density Functional Theory (DFT) Calculations and Energy Levels

To understand the electronic distribution of **PSQ31-33** dyes, their ground state geometries and energies were fully optimized using density functional theory (DFT) by B3LYP/6-31G\*\* level with the Gaussian 09 program. Energy minimized structures of **PSQ31** and **PSQ32** were presented in **Figure 5.6**. The isosurface plots of four selected frontier molecular orbitals of **PSQ31-PSQ33** (HOMO+1, HOMO, LUMO and LUMO-1) were showed in **Figure 5.7**. The intramolecular charge transfer (ICT) transition takes place from HOMO to LUMO on the central squaric unit, and partial distribution of electron density toward carboxylic acid. Furthermore, LUMO+1 of **PSQ31-33** dyes are localized on the anchoring group containing indoline moiety which ensures the strong coupling between PSQ dyes and TiO<sub>2</sub> surface for the efficient charge injections. The distance between the oxygen atom of carboxylic acid and the out-of-plane alkyl groups at top and down indoline units were found to be 18.63 Å and 18.76 Å for **PSQ31** and **PSQ32**, respectively (**Figure 5.6**). Further, it is interesting to note that the dihedral angle between *trans*-squaraine unit and  $\pi$ -spacer have significant changes with respect to the type of  $\pi$ -spacer. **PSQ31** dye with phenyl  $\pi$ -spacer have 35.9 Å of dihedral angles which is higher than thiophene  $\pi$ -spacer containing **PSQ32** dye with 26.3 Å.



**Figure 5.6** Energy minimized structures of (a) **PSQ31**, and (c) **PSQ32**

State	PSQ31	PSQ32	PSQ33
$E_{LUMO+1}$ 1	 $E_{LUMO+1} = -1.37$ eV	 $E_{LUMO+1} = -1.27$ eV	 $E_{LUMO+1} = -1.55$ eV
$E_{LUMO}$	 $E_{LUMO} = -2.85$ eV	 $E_{LUMO} = -2.79$ eV	 $E_{LUMO} = -3.01$ eV



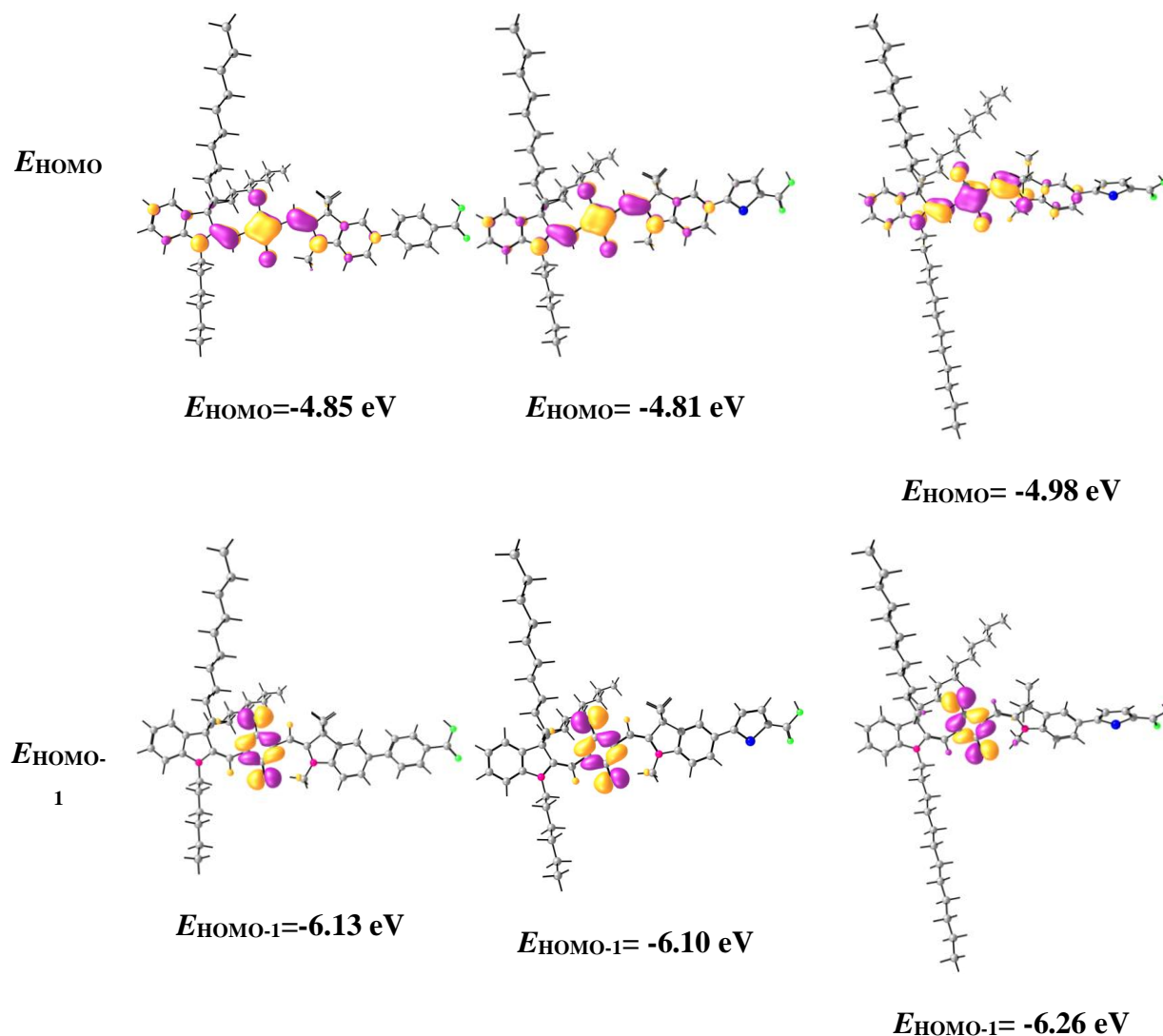


**Figure 5.7** Isosurface plots of selected frontier orbitals (HOMO, HOMO-1, LUMO, LUMO+1) of **PSQ 31** and **PSQ33**. Fully optimised at DFT B3LYP/6-31G\*\* level. (Isovalue set to 0.036 a.u.)

### 5.2.5 Photovoltaic Studies of PSQ31-33

The photovoltaic device performances of **PSQ31–PSQ33** dyes under standard conditions (AM 1.5 G, 100 mW/cm<sup>2</sup>) were measured using iodine/triiodide (I<sup>-</sup>/I<sub>3</sub><sup>-</sup>) liquid and the current-voltage (*I-V*) spectra of **PSQ31-33** dyes were shown in **Figure 5.8**. The device performance with and without co-adsorbent 3 $\alpha$ ,7 $\alpha$ -dihydroxy-5 $\beta$ -cholanic acid (CDCA) are given in **Table 5.2**. The **PSQ31** having  $\pi$ -spacer of phenyl with in-plane and out of plane alkylated groups present at indoline unit which is away from TiO<sub>2</sub> surface which afforded a short-circuit photocurrent density ( $J_{\text{sc}}$ ) of 3.08 mA/cm<sup>2</sup>, an open-circuit photovoltage ( $V_{\text{oc}}$ ) of 0.573 V, a fill factor (*ff*) of

67.3%, and achieved PCE of 1.18%. Furthermore addition of 2 equiv. of CDCA, was increased to 2.14% with a  $J_{sc}$  of 5.42 mA cm<sup>-2</sup>,  $V_{oc}$  of 0.586V and  $ff$  of 67.5(%). Further addition PCE of CDCA reduced the photocurrent drastically which infers that CDCA is competing with the dye anchoring on the TiO<sub>2</sub> surface (**Figure 5.8 and Table 5.2**). On the other hand, the insertion of thiophene  $\pi$ -spacer instead of phenyl in upper branched indoline moiety as in **PSQ32**, a notable reduction in  $J_{sc}$ ,  $V_{oc}$  and  $ff$  which provided PCE of 0.57% without CDCA. But after the addition of 2 equiv. of CDCA which afford the device performance up to 1.59%. Further addition of CDCA showed poor photovoltaic performance due to the decrease of dye amount on TiO<sub>2</sub> (**Figure 5.8 and Table 5.3**). By varying the design of dye structure with different anchoring groups, the photovoltaic performance of **PSQ32** which was reduced 34.6% comparing to **PSQ31** having phenyl  $\pi$  spacer. This is due to the different mode of dye orientation and their dye aggregation abilities on TiO<sub>2</sub> surface which influence more in the electron injection as well as overall power conversion efficiency. Further it is also shed the light on the mode of electron transfer to TiO<sub>2</sub> surface through the bond and through space, which will be focused in the future. On the other hand **PSQ33 dye** shows that there is no significant notable difference in photovoltaic performance with and without CDCA even after extending the length of alkyl chain at indoline unit compared to **PSQ31** and **PSQ32**. To further improve the DSSCs device performance, **PSQ 5** was utilized as the co-sensitizer for **PSQ31**, which gave PCE of 2.10% with a  $J_{sc}$  of 5.1 mA cm<sup>-2</sup>,  $V_{oc}$  of 0.566V and  $ff$  of 69.8%, respectively.

The IPCE response of **PSQ31-PSQ33** dyes is displayed in **Figure 5.8** and studied thoroughly in the presence and absence of coadsorbent to clarify the impact of mode of dye anchoring as well as their aggregation on the photocurrent efficiency for DSSC. Broadening response of **PSQ31-PSQ33** dyes are reflected in the IPCE spectra in which **PSQ31** dye showed greater IPCE response in the region of 540–750 nm, which corresponds to the absorption by monomers and aggregates. In addition, **PSQ31** showed IPCE response between 400 and 523 nm, which corresponds to the absorption from the result of the substitution with  $\pi$ -spacer groups. Furthermore in the absence of CDCA **PSQ31** showed IPCE with maximum of 9.7% and 25.7% at 476 and 642 nm, respectively. On the other hand, **PSQ32** and **PSQ33** dye showed IPCE response with maximum of 12% at 651 nm and 648nm, respectively even after extending the branched sp<sup>3</sup>alkyl chain. After the addition of CDCA, **PSQ31**, **PSQ32** and **PSQ33** showed a good response in IPCE at a higher wavelength region, and at 614 nm of **PSQ31**, **PSQ32** and

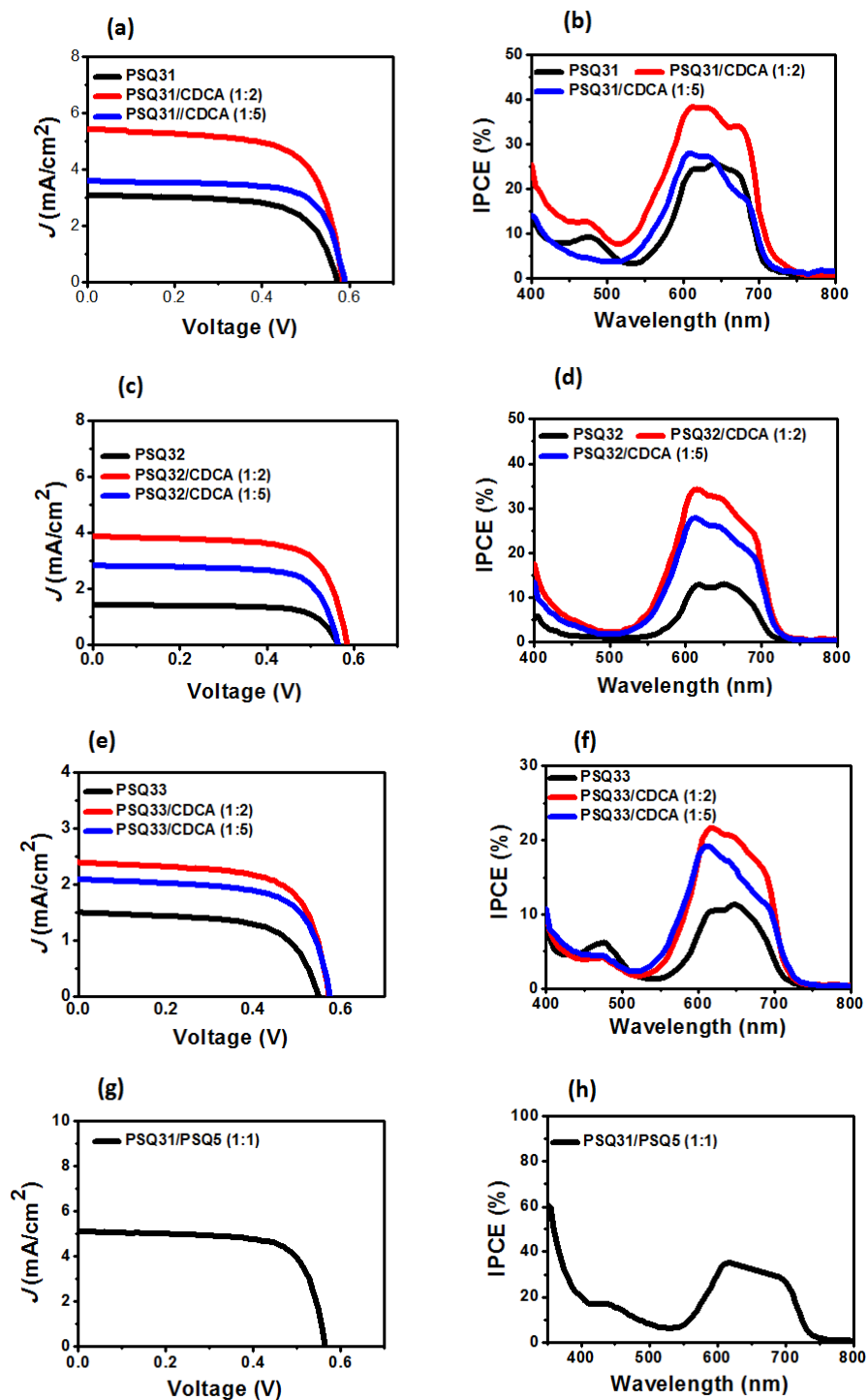


**Figure 5.8** *I-V* and IPCE characterization of **PSQ31-33** dyes. (a, c, e and g) and (b, d, f and h) *I-V* and IPCE curves for **PSQ31-33** in absence and presence of CDCA ( $\text{TiO}_2$  electrode thickness =  $8 + 4 \mu\text{m}$  (transparent+scattering layer), area =  $0.22 \text{ cm}^2$ , [Dye] =  $0.1 \text{ mM}$  in  $\text{CHCl}_3$ , dipping time 12 h at rt, electrolyte: iodolyte Z-50 from Solaronix).

**Table 5.2** *I-V* characteristics of **PSQ31-33** dyes devices with and without CDCA<sup>a</sup>

Dyes	$J_{sc}$ mA/cm <sup>2</sup>	$V_{oc}$ (V)	ff (%)	PCE (%)
<b>PSQ31</b>	3.08	0.573	67.3	1.18
<b>PSQ31/CDCA (1:2)</b>	5.42	0.586	67.5	2.14
<b>PSQ31/CDCA (1:5)</b>	3.59	0.590	72	1.52
<b>PSQ32</b>	1.42	0.563	71.8	0.57
<b>PSQ32/CDCA (1:2)</b>	3.86	0.586	70.7	1.59
<b>PSQ32/CDCA (1:5)</b>	2.83	0.564	71.9	1.14
<b>PSQ33</b>	1.50	0.550	64.3	0.53
<b>PSQ33/CDCA (1:2)</b>	2.39	0.574	67.7	0.92
<b>PSQ33/CDCA (1:5)</b>	2.10	0.576	67.1	0.81
<b>PSQ31/ PSQ5 (1:1)</b>	5.11	0.566	69.8	2.10

<sup>a</sup>TiO<sub>2</sub> electrode thickness = 8 + 4 μm (transparent+scattering layer), area = 0.22 cm<sup>2</sup>, [Dye] = 0.1 mM in CHCl<sub>3</sub>, dipping time was 12 h at rt, electrolyte was iodolyte Z-50 (Solaronix) and summarize the result of best six devices with deviation.

**PSQ33** exhibit an IPCE of 39%, 35% and 21%, respectively. It was observed from the IPCE profile that even in presence of 5 equiv. of CDCA, the response from aggregated structure dominated over monomer which indicates that either some of the aggregated structure not injecting the charges, or also it may be effect of tilted π-spacer as supported by DFT studies.

### 5.2.6 Electrochemical Impedance Analysis

Electrochemical impedance spectroscopy (EIS) studies were carried out under dark conditions to understand the interfacial charge recombination dynamics between the injected electrons in TiO<sub>2</sub>

conduction band ( $CB_{TiO_2}$ ) and  $I_3^-$  in electrolyte at interfaces of  $TiO_2$ -dye/electrolyte. Generally,  $V_{oc}$  is measured from the potential difference between shift of quasi- Fermi level of electron in the  $TiO_2$  ( $E_{Fn}$ ) and the fermi level of redox potential of electrolyte ( $E_{F, redox}$ ) in the electrolyte in eq 5.1. Thus, either the conduction band edge shift or the change in the chemical capacitance of  $TiO_2$  infers the cell potential (**Table 5.3**).

$$V_{oc} = E_{(F,redox)} - E_{(F,n)} \quad (5.1)$$

The Nyquist plots of the DSSC based **PSQ31-33** dye cells were obtained in the dark with applied bias of -0.49 V in **Figure 5.9**, whereas the bias voltage is applied in the opposite direction of the photovoltage generated under illumination. The smaller semicircle at high frequency with respect to the impedance due to the electron transfer take place at the interface of Pt/electrolyte interface, whereas the larger semicircle at mid frequency range represents charge recombination resistance owing to charge transfer processes takes place at the interfaces of  $TiO_2$ -dye/electrolyte.

The fitted recombination resistance ( $R_{ct}$ ) value of PSQ sensitized devices (under an applied bias of -0.49 V) were in the order of **PSQ31** (18.56  $\Omega$ ) > **PSQ32** (13.93  $\Omega$ ) > **PSQ33** (9.57  $\Omega$ ). Larger the  $R_{ct}$  value, slower is the recombination of electrons from the conduction band of  $TiO_2$  to the oxidized  $I_3^-$  species in the electrolyte. The similar trend of  $R_{ct}$  was observed in  $V_{oc}$  of PSQs dyes as **PSQ31** (573 mV) > **PSQ32** (563 mV) > **PSQ33** (550 mV) which is due to the good passivation of **PSQ31** dye on the  $TiO_2$  surface by suppressing the charge recombination process compared to other dyes. The electron lifetime(s) on  $TiO_2$  were calculated from  $R_{ct}$  and chemical capacitance  $C_{\mu}$  using  $\tau = R_{ct} \times C_{\mu}$ . The longer electron lifetime in PSQ device cell further supports the higher performance in the order of **PSQ31** (8.35 ms) > **PSQ32** (3.48 ms) > **PSQ33** (0.86 ms) based cells. Therefore, **PSQ31** can suppress the charge recombination reaction more efficiently than **PSQ32** or **PSQ33**, and the larger electron lifetime represents slower charge recombination rate at the interface of dye- $TiO_2$ /electrolyte, which enhance the photovoltaics performance in both  $J_{sc}$  and  $V_{oc}$ .

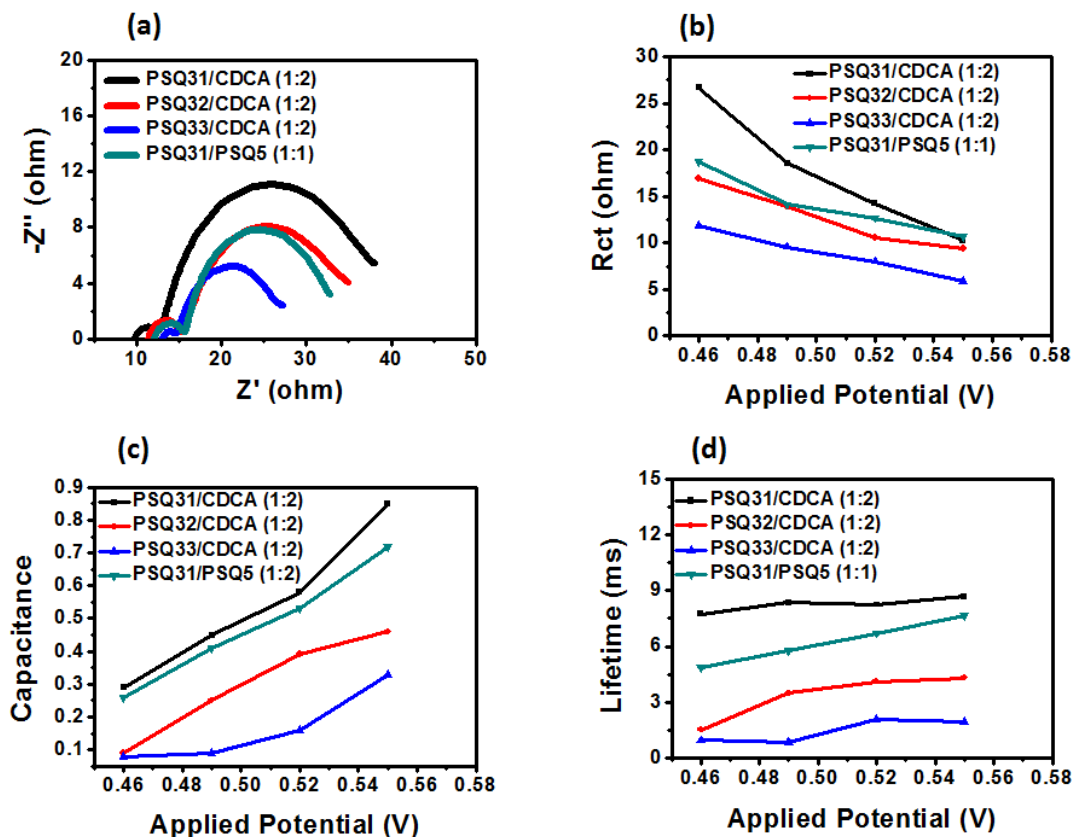


**Figure 5.9** Impedance analysis of PSQ31-33 and PSQ33/PSQ5 dyes: (a) Nyquist plot, (b) log  $R_{ct}$  vs applied potential, (c) log  $C_{\mu}$  vs applied potential and (d) log  $\tau$  vs applied potential

**Table 5.3** EIS Parameters of PSQ31-33 dye cells at an applied potential of  $-0.49$  V in the dark

Dyes	Applied potential (V)	$R_s$ (ohm)	$R_{ct}$ (ohm)	$C_{\mu}$ (mF)	$\tau$ (ms)
PSQ31	0.49	9.98	18.56	0.45	8.35
PSQ32	0.49	11.74	13.93	0.25	3.48
PSQ33	0.49	13.19	9.57	0.09	0.86
PSQ31/PSQ5	10.49	12.45	14.12	0.41	5.79

### 5.3 Summary

In summary, a series of unsymmetrical *trans*-configured squaraine system **PSQ31-33** have been systematically designed with in-plane and out-of plane branched alkyl group on the  $sp^3$ -carbon and nitrogen atoms, different  $\pi$ -bridge (phenyl and thiophene) and carboxylic anchoring group. In order to ascertain we have synthesized **PSQ31-33** dyes to understand the effect of anchoring groups such as carboxylic acid. The DSSC devices were fabricated using **PSQ31-33** respectively as the sensitizers and the photovoltaic behavior was investigated. Pheny-based **PSQ31** showed PCE of 2.14% which was comparatively high  $J_{sc}$  than thiophene based **PSQ32**. **PSQ33** showed PCE of 0.92% and exhibited less significant improvement in  $J_{sc}$  and  $V_{oc}$  after extending the length of alkylated chain of **PSQ32** with and without of CDCA. Orientation of dyes and chemisorbs on  $TiO_2$  surface is effectively depending on the sensitizer's structure as well as suitable anchoring group. To further enhance the cell performance, **PSQ 5** was used as the co-sensitizer for **PSQ31**, which exhibited a moderate efficiency of 2.10% with the  $J_{sc}$  and  $V_{oc}$  of 5.1  $mA\ cm^{-2}$  and 566 mV, respectively. This chapter suggests that the importance of cyano acetic acid over carboxylic acid as a good anchoring group for this class of NIR active PSQ dyes.

### 5.4 Experimental Section

#### 5.4.1 Materials and Characterization

For dye synthesis and DSSC fabrication, all reagents and solvents were purchased from commercial sources were used without further purification unless otherwise noted. Required precursors **1a**, **1b**, **2a**, **2b**, **2c**, **3a**, **3b**, **3c**, **4**, **5a** and **5b** were synthesized and reported according to the previous chapter 2.<sup>14,15</sup> Tetrahydrofuran and toluene were dried by standard procedure prior to use. All oxygen- and moisture-sensitive reactions were performed under nitrogen atmosphere.  $^1H$  NMR spectra were recorded on a 200 MHz or 400 MHz or 500 MHz spectrometers, using  $CDCl_3$ . All chemical shifts were reported in parts per million (ppm).  $^1H$  NMR chemical shifts were referenced to TMS (0 ppm).  $^{13}C$  NMR chemical shifts were referenced to  $CDCl_3$  (77.23 ppm, and recorded on either 100 MHz or 125 MHz NMR spectrometer). HRMS and MALDI-TOF-MS were recorded on SYNAPT G2 HDM spectrometer and ABSciex 5800 MALDI TOF mass spectrometer, respectively. UV-vis absorption spectra were recorded on Analytikjena (SPECORD 210 PLUS) spectrophotometer. A three electrode cell was used for DPV analysis and which was performed on BioLogic SP300 potentiostat. Platinum

wire used as a working electrode, a thin platinum foil was used as a counter electrode, and dyes were dissolved in dry dichloromethane. Measurements were carried out at the scan rate of 50 mVs<sup>-1</sup> after addition of 0.1 M of tetra butyl ammonium perchlorate (TBAP) as the supporting electrolyte and non-aqueous Ag/Ag<sup>+</sup> (0.01M in CH<sub>3</sub>CN) used as reference electrode. The reference electrode was calibrated by recording the cyclic voltammograms of ferrocene in the same electrolyte as external standard; the potential values are on the basis of the estimated value of the ferrocene redox potential in dichloromethane 0.7V versus NHE.<sup>64</sup>EIS analysis was performed under dark condition by applying external bias to dye cells using a BioLogic SP300 potentiostat equipped with frequency response analyzer. Frequency range was fixed from 1 MHz to 10 mHz with AC amplitude of 10 mV. *I-V* characteristics of the dye cells were measured under a solar simulator (PET, CT200AAA) in clean room conditions, which is controlled by a source measurement unit (Keithley 2420). A certified 4 cm<sup>2</sup> silicon solar cell (NREL) was calibrated to an intensity of 1000 W m<sup>-2</sup> (xenon lamp, 450 W, USHIO INC) of a solar simulator (AM1.5 G light). IPCE spectra measurements were conducted by Newport QE measurement kit including a xenon light source, a monochromator, and a power meter. The set-up was calibrated using a reference silicon solar cell before the device measurement.

**5.4.2 Device Fabrication Procedure** For fabricating photoanode of DSSC, FTO (F-doped SnO<sub>2</sub> glass; 6-8 Ω/sq) was cleaned sequentially by mucasol (2% in water), deionized water, and isopropanol using an ultra-sonication for 15 min. A blocking layer of TiO<sub>2</sub> was prepared by dipping cleaned FTO substrate in freshly prepared aqueous 0.05 M TiCl<sub>4</sub> solution at 70 °C for 30 min, and washed immediately with deionized water, and followed by annealing in air at 125 °C for 10 min. And the mesoscopic transparent thin layer (6-8 μm thickness) of TiO<sub>2</sub> onto buffer layer modified FTO was coated using TiO<sub>2</sub> paste (< 20 nm, Ti-Nanoxide T/SP) by the doctor-blade technique. Then kept in air for 5 min and annealed at 125 °C in air for 15 min before coating scattering layer on it. Dyesol, WER2-O paste was used to coat a 4-6 μm thick TiO<sub>2</sub> layer, kept in air for 5 min and annealed at 125 °C in air for 15 min. Resulting 0.22 cm<sup>2</sup> active area films were sintered at 325 °C for 5 min, 375 °C for 5 min, 450 °C for 15 min and 500 °C for 15 min with heating rate of 5 °C per min in air. After reaching the furnace temperature at 50 °C, sintered films were treated in TiCl<sub>4</sub> solution as described before. After sintering the layer-by-layer deposited film again at 500 °C for 30 min, allowed to reach 50 °C and were immediately



immersed in 0.1 mM **PSQ31-33** dye solution in chloroform at room temperature for 12 h. The dye loaded electrodes are washed thoroughly with chloroform, to remove physisorbed molecules. Successive addition of co-adsorbent 3 $\alpha$ ,7 $\alpha$ -dihydroxy-5 $\beta$ -cholanic acid (CDCA) was varied the concentration of de-aggregating agent in the dye solution and studied the device performance at 2, 5 and 10 equivalents of CDCA. Finally the dye cell was assembled by joining the electrolyte (Iodolyte Z50) filled photoanode and platinum cathode using a 25  $\mu$ m thick spacer. The photovoltaic parameters have been evaluated without masking the device.

#### 5.4.3 Synthetic Procedures and Characterization Data

Required precursors **1a**, **1b**, **2a**, **2b**, **2c**, **3a**, **3b**, **3c**, **4**, **5a** and **5b** were synthesized and reported according to the previous chapter 2.<sup>15, 16</sup>

**(E)-2-(((Z)-5-(4-Carboxyphenyl)-1,3,3-trimethylindolin-2-ylidene)methyl)-4-((-3-decyl-1-hexyl-3-octyl-3H-indol-1-ium-2-yl)methylene)-3-oxocyclobut-1-en-1-olate (PSQ31):**

Reaction mixture of 0.1 g (0.133 mmol) (E)-2-(((Z)-5-bromo-1,3,3-trimethylindolin-2-ylidene)methyl)-4-((-3-decyl-1-hexyl-3-octyl-3H-indol-1-ium-2-yl)methylene)-3-oxocyclobut-1-en-1-olate (**7a**) (1 equiv.) was taken and dissolved in 1:1 ratio of toluene and methanol (total volume 5 mL) in 50 mL microwave reactor vessel and 0.062 g (0.4 mmol) 4-carboxylphenylboronic acid and 0.1 g (0.665 mmol) K<sub>2</sub>CO<sub>3</sub> were added to it under N<sub>2</sub> atmosphere. The solution was purged with nitrogen for 20 min and then 0.011 g (0.013 mmol) PdCl<sub>2</sub>(dppf) was added and the reaction was carried out under microwave condition at 60 W, 70 °C for 15 min. The reaction mixture cooled to room temperature, and the solvents were removed under reduced pressure. The reaction mixture was purified by column chromatography (SiO<sub>2</sub>, 100-200 mesh 5% methanol and 95% dichloromethane to afford the required compound. Yield: 63 mg, Yield: 60%; <sup>1</sup>H NMR (500 MHz, CDCl<sub>3</sub>)  $\delta$ : 8.12 (br, s., 2 H), 7.70 (br. s., 2 H), 7.55 (br. S., 2 H), 7.30 (m, 2 H), 7.18 (t, 1 H), 7.03 (m, 2 H), 6.14 (br. s., 1 H), 6.01 (br. s., 1 H), 4.04 (br. s., 2 H), 3.54 (br. s., 3 H), 3.01 (br. s., 2 H), 2.36 (t, *J* = 7.8 Hz, 2 H), 2.07 - 1.64 (m, 8 H), 1.48 - 1.03 (m, 30 H), 0.94 - 0.70 (m, 11 H), 0.47 (m, 2 H); <sup>13</sup>C NMR (126 MHz, CDCl<sub>3</sub>)  $\delta$ : 178.6, 176.3, 170.3, 169.8, 169.4, 152.1, 144.0, 143.3, 142.8, 139.2, 135.3, 131.2, 130.7, 130.0, 128.3, 127.7, 127.2, 126.9, 124.1, 122.3, 121.0, 109.4, 87.9, 87.3, 74.3, 73.4, 58.9, 48.8, 43.9, 39.9, 34.2, 31.8, 31.8, 31.7, 31.5, 30.5, 30.2, 29.6, 29.6, 29.5, 29.5, 29.4, 29.3, 29.2, 29.1, 29.0, 27.3,

27.2, 26.8, 26.3, , 24.0, 22.6, 22.5, 22.5, 14.0, 13.9; MALDI-TOF ( $m/z$ ):  $[M]^+$  calcd for  $C_{56}H_{74}N_2O_4$ : 838.5649; found: 838.4293.

**(E)-2-(((Z)-5-(5-Carboxythiophen-2-yl)-1,3,3-trimethylindolin-2-ylidene)methyl)-4-((-3-decyl-1-hexyl-3-octyl-3H-indol-1-ium-2-yl)methylene)-3-oxocyclobut-1-en-1-olate (PSQ32):**

Reaction mixture of 0.1 g (0.133 mmol) (E)-2-(((Z)-5-bromo-1,3,3-trimethylindolin-2-ylidene)methyl)-4-((-3-decyl-1-hexyl-3-octyl-3H-indol-1-ium-2-yl)methylene)-3-oxocyclobut-1-en-1-olate (**7a**) (1 equiv.) was dissolved in 1:1 ratio of toluene and methanol (total volume 5 mL) in 50 mL microwave reactor vessel and 0.098 g (0.4 mmol) 5-carboxylthiophene-2-boronic acid pinacol ester and 0.1 g (0.665 mmol)  $K_2CO_3$  were added to it under  $N_2$  atmosphere. The solution was purged with nitrogen for 20 min and then 0.01 g (0.013 mmol)  $PdCl_2(dppf)$  was added and the reaction was carried out under microwave condition at 60 W, 70 °C for 15 min. The reaction mixture cooled to room temperature, and the solvents were removed under reduced pressure. The reaction mixture was purified by column chromatography ( $SiO_2$ , 100-200 mesh 5% methanol and 95% dichloromethane) to afford the required compound. Yield: 65 mg, Yield: 62%;  $^1H$  NMR (400MHz,  $CDCl_3$ )  $\delta$  = 8.44 (br. s., 1 H), 7.94 - 7.64 (m, 2 H), 7.63 - 7.40 (br. s., 2 H), 7.39 - 7.13 (m, 4 H), 7.10 - 6.96 (m, 2 H), 6.17 (br. s., 1 H), 6.02 (br. s., 1 H), 4.07 (br. s., 2 H), 3.50 (br. s., 3 H), 3.01 (br. s., 2 H), 2.13 - 1.89 (m, 2 H), 1.82 (m, 8 H), 1.54 - 1.00 (m, 30 H), 0.93 - 0.66 (m, 11 H), 0.56 - 0.35 (m, 2 H);  $^{13}C$  NMR (101 MHz,  $CDCl_3$ )  $\delta$  = 178.7, 175.2, 170.2, 169.1, 151.1, 144.0, 143.5, 142.8, 139.2, 134.8, 133.7, 132.3, 128.9, 127.7, 126.1, 124.3, 123.6, 123.0, 122.3, 119.8, 116.0, 114.0, 109.5, 109.2, 88.0, 87.5, 59.0, 48.7, 44.0, 39.9, 31.8, 31.7, 31.6, 31.5, 30.5, 29.6, 29.6, 29.5, 29.4, 29.3, 29.2, 29.1, 29.0, 27.3, 27.2, 26.8, 24.0, 23.9, 22.6, 22.5, 22.5, 22.4, 14.0, 13.9; MALDI-TOF ( $m/z$ ):  $[M+K]^+$  calcd for  $C_{54}H_{72}N_2O_4S$ : 844.5213; found: 844.3781.

**(E)-2-(((Z)-5-(5-Carboxythiophen-2-yl)-1,3,3-trimethylindolin-2-ylidene)methyl)-4-((-3-decyl-1,3-didodecyl-3H-indol-1-ium-2-yl)methylene)-3-oxocyclobut-1-en-1-olate (PSQ33):**

Reaction mixture of 0.11 g (0.122 mmol) (E)-2-(((Z)-5-bromo-1,3,3-trimethylindolin-2-ylidene)methyl)-4-((-3-decyl-1,3-didodecyl-3H-indol-1-ium-2-yl)methylene)-3-oxocyclobut-1-en-1-olate (**7b**) (1 equiv.) was dissolved in 1:1 ratio of toluene and methanol (total volume 5 mL) in 50 mL microwave reactor vessel and 0.093 g (0.367 mmol) 5-carboxylthiophene-2-boronic acid pinacol ester and 0.17 g (1.22 mmol)  $K_2CO_3$  were added to it under  $N_2$  atmosphere. The

solution was purged with nitrogen for 20 min and then 0.01 g (0.012 mmol) PdCl<sub>2</sub>(dppf) was added and the reaction was carried out under microwave condition at 60 W, 70 °C for 15 min. The reaction mixture cooled to room temperature, and the solvents were removed under reduced pressure. The reaction mixture was purified by column chromatography (SiO<sub>2</sub>, 100-200 mesh 5% methanol and 95% dichloromethane to afford the required compound. Yield: 65 mg, Yield: 54%; <sup>1</sup>H NMR (500 MHz, CDCl<sub>3</sub>) δ: 8.39 (br. s, 1H), 7.77 - 7.62 (m, 2 H), 7.45-7.38 (m, 3 H), 7.23 (br. s., 2 H), 6.95 (br. s., 2 H), 6.74 (br. s., 1 H), 6.07 (br. s., 1 H), 5.9 (br. s., 1 H), 3.97 (br. s., 2 H), 3.40 (br. s., 3 H), 2.94 (br. s., 2 H), 1.96 (br. s., 2 H), 1.82-1.50 (m, 8H), 1.35-0.97 (m, 50H), 0.80-0.74 (m, 11H), 0.45- 0.4 (m, 2 H); <sup>13</sup>C NMR (126 MHz, CDCl<sub>3</sub>) δ: 180, 179.6, 177.9, 176.0, 169.9, 166.7, 155.4, 152.7, 144.0, 141.9, 139.2, 135, 128.3, 127.6, 126.1, 123.7, 123.3, 122.9, 122.3, 119.8, 119, 115.9, 114, 109.4, 109, 88.1, 87.5, 58.9, 48.7, 44, 41.8, 39.9, 37.39, 36.9, 34.7, 34.4, 33.7, 33.2, 31.8, 31.6, 31.3, 29.6, 29.5, 29.5, 29.4, 29.3, 29.27, 29.1, 28.8, 27.3, 27.1, 26.7, 26.6, 24.8, 24.0, 22.6, 14.1; MALDI-TOF (*m/z*): [M+1]<sup>+</sup> calcd for C<sub>64</sub>H<sub>92</sub>N<sub>2</sub>O<sub>4</sub>S: 984.6778; found: 984.5620.

## 5.5 References

- (1) Galoppini, E.; Guo, W.; Qu, P.; Meyer, G. J. Long-Distance Electron Transfer Across Molecule–Nanocrystalline Semiconductor Interfaces. *J. Am. Chem. Soc.* **2001**, *123*, 4342–4343.
- (2) Galoppini, E.; Guo, W.; Zhang, W.; Hoertz, P. G.; Qu, P.; Meyer, G. J. Long-Range Electron Transfer across Molecule–Nanocrystalline Semiconductor Interfaces Using Tripodal Sensitizers. *J. Am. Chem. Soc.* **2002**, *124*, 7801–7811.
- (3) Piotrowiak, P.; Galoppini, E.; Wei, Q.; Meyer, G. J.; Wiewiór, P. Subpicosecond Photoinduced Charge Injection from “Molecular Tripods” into Mesoporous TiO<sub>2</sub> Over the Distance of 24 Angstroms. *J. Am. Chem. Soc.* **2003**, *125*, 5278–5279.
- (4) Ye, S.; Kathiravan, A.; Hayashi, H.; Tong, Y.; Infahsaeng, Y.; Chabera, P.; Pascher, T.; Yartsev, A. P.; Isoda, S.; Imahori, H.; et al. Role of Adsorption Structures of Zn-Porphyrin on TiO<sub>2</sub> in Dye-Sensitized Solar Cells Studied by Sum Frequency Generation Vibrational Spectroscopy and Ultrafast Spectroscopy. *J. Phys. Chem. C* **2013**, *117*, 6066–6080.

- 
- (5) Mulhern, K. R.; Detty, M. R.; Watson, D. F. Aggregation-Induced Increase of the Quantum Yield of Electron Injection from Chalcogenorhodamine Dyes to TiO<sub>2</sub>. *J. Phys. Chem. C* **2011**, *115*, 6010–6018.
  - (6) Luo, P.; Karsenti, P.-L.; Brisard, G.; Marsan, B.; Harvey, P. D. Are the Orientation and Bond Strength of the RCO<sub>2</sub>–M Link Key Factors for Ultrafast Electron Transfers? *Chem. Commun.* **2015**, *51*, 17305–17308.
  - (7) Imahori, H.; Kang, S.; Hayashi, H.; Haruta, M.; Kurata, H.; Isoda, S.; Canton, S. E.; Infahsaeng, Y.; Kathiravan, A.; Pascher, T.; et al. Photoinduced Charge Carrier Dynamics of Zn–Porphyrin–TiO<sub>2</sub> Electrodes: The Key Role of Charge Recombination for Solar Cell Performance. *J. Phys. Chem. A* **2011**, *115*, 3679–3690.
  - (8) Maeda, T.; Mineta, S.; Fujiwara, H.; Nakao, H.; Yagi, S.; Nakazumi, H. Conformational Effect of Symmetrical Squaraine Dyes on the Performance of Dye-Sensitized Solar Cells. *J. Mater. Chem. A* **2012**, *1*, 1303–1309.
  - (9) Shivashimpi, G. M.; Pandey, S. S.; Watanabe, R.; Fujikawa, N.; Ogomi, Y.; Yamaguchi, Y.; Hayase, S. Novel Unsymmetrical Squaraine Dye Bearing Cyanoacrylic Acid Anchoring Group and Its Photosensitization Behavior. *Tetrahedron Letters* **2012**, *53*, 5437–5440.
  - (10) Shivashimpi, G. M.; Pandey, S. S.; Watanabe, R.; Fujikawa, N.; Ogomi, Y.; Yamaguchi, Y.; Hayase, S. Effect of Nature of Anchoring Groups on Photosensitization Behavior in Unsymmetrical Squaraine Dyes. *Journal of Photochemistry and Photobiology A: Chemistry* **2014**, *273*, 1–7.
  - (11) Shi, Y.; Hill, R. B. M.; Yum, J. H.; Dualeh, A.; Barlow, S.; Grätzel, M.; Marder, S. R.; Nazeeruddin, M. K. A High-Efficiency Panchromatic Squaraine Sensitizer for Dye Sensitized Solar Cells. *Angewandte Chemie International Edition* **2011**, *50*, 6619–6621.
  - (12) Delcamp, J. H.; Shi, Y.; Yum, J. Ho; Sajoto, T.; Dell, O. E.; Barlow, S.; Nazeeruddin, M. K.; Marder, S. R.; Grätzel, M. The Role of  $\pi$  Bridges in High-Efficiency DSCs Based on Unsymmetrical Squaraines. *Chemistry – A European Journal* **2012**, *19*, 1819–1827.
  - (13) Saccone, D.; Galliano, S.; Barbero, N.; Quagliotto, P.; Viscardi, G.; Barolo, C. Polymethine Dyes in Hybrid Photovoltaics: Structure–Properties Relationships. *European Journal of Organic Chemistry* **2016**, *2016*, 2244–2259.
  - (14) Punitharasu, V.; Kavungathodi, M. F. M.; Nithyanandhan, J. Interplay between  $\pi$ -Bridges and Positions of Branched Alkyl Groups of Unsymmetrical D–A–D– $\pi$ –A Squaraines in

Dye-Sensitized Solar Cells: Mode of Dye Anchoring and the Charge Transfer Process at the TiO<sub>2</sub>/Dye/Electrolyte Interface. *ACS Appl. Mater. Interfaces* **2017**, *9*, 32698–32712.

- (15) Alagumalai, A.; M. K., M. F.; Vellimalai, P.; Sil, M. C.; Nithyanandhan, J. Effect of Out-of-Plane Alkyl Group's Position in Dye-Sensitized Solar Cell Efficiency: A Structure–Property Relationship Utilizing Indoline-Based Unsymmetrical Squaraine Dyes. *ACS Appl. Mater. Interfaces* **2016**, *8*, 35353–35367.

## Chapter 6



**Summary and Future Perspective**

---

## 6.1 Summary

Energy demand and global warming have become one of the major scientific challenges for the current and future generation and it is due to the fast urbanization and growth of population. Photovoltaic technology is considered as one of the important tools to address the abundant contribution and environmental friendliness of solar energy to make the efficient conversion of solar radiation into electricity. Dye-sensitized solar cells (DSSCs) are described as one of the third generation photovoltaic technologies in which dye is one of the important light harvesting components for photon-to-current conversion process besides other components such as anode, electrolyte and cathode. D- $\pi$ -A and D-A- $\pi$ -A dyes have systematically designed and synthesized and it was showed the highest device efficiency of 13% and 12.5%, respectively. Among the phthalocyanine, porphyrin and squaraine dyes that absorb both far-red and NIR regions of the solar spectrum, squaraine dyes shows the high molar extinction coefficient in the far-red, and NIR regions ( $10^5 \text{ M}^{-1} \text{ cm}^{-1}$ ). Further, both porphyrin and phthalocyanine dyes have afforded the device efficiency of 13% and 6.4%, respectively by modulating the steric and electronic effect. Squaraines dyes as promising class of metal free dyes which can convert far-red photons to electrons in DSSC by taking the advantage of its unique aggregation property. Even though of squaraine dyes are exploited in dye sensitized solar cell research, controlling the aggregation of squaraine dyes on  $\text{TiO}_2$  surface which helps achieving high device efficiency is a challenging task. Hence, the Thesis describes the strategies to control the aggregation of dyes on  $\text{TiO}_2$  surface and suitable modification of dyes structure for extending the conjugation for the better DSSC device performance. Further, this Thesis describes i) the importance of  $\pi$ -spacer, (**Chapter 2**), ii) number of anchoring group in *cis*-configured squaraine, (**Chapter 3**) and iii)  $\pi$ -spacer appended *cis* and *trans* squaraine dyes with different types of anchoring group (**Chapter 4 and Chapter 5**) besides controlling the aggregation of dyes by properly functionalized out-of-plane alkyl groups for the improved device performance.

Design and synthesis of series of D-A-D- $\pi$ -Anchoring group unsymmetrical squaraine based dyes (**PSQ1-5**) were carried out (**Chapter 2**) in which appending in-plane and out-of-plane alkyl groups at the indoline units helped to control the self-assembly of dyes. The  $\pi$ -spacers such as phenyl and thiophene units imparts certain degree of curvature in the SQ unit which may be further helped to extending the light harvesting in the NIR region as well as enhancing visible absorption. In addition, these systematic varied branched alkyl group

positions were investigated in solution as well as TiO<sub>2</sub> surface to understand the controlled self-assembly of dyes. In general photovoltaic properties enhanced in case these positional units are far away from the dye anchoring TiO<sub>2</sub> surface. Thiophene-based **PSQ3** showed PCE of 7.21% which was comparatively high  $J_{sc}$  than phenyl based **PSQ1**. **PSQ5** showed a significant improvement in  $J_{sc}$  and  $V_{oc}$  after extending the length of alkyl group in compared to **PSQ3** in absence of optically transparent co-adsorbent. A DSSC sensitized with **PSQ5** showed better  $J_{sc}$  and  $V_{oc}$  which leads to the efficiency of 8.15%.

Apart from extending the conjugation, introduction of electron withdrawing groups at the SQ unit has been also tested to extend the absorption. Hence a series of *cis*-configured unsymmetrical PSQ dye (**PSQ11-15**) were designed and synthesized (**Chapter 3**) which possess following features systematically with (i) in-plane and out-of-plane alkyl groups, which modulated to control the self-assembly of dye and orientation of dyes on the TiO<sub>2</sub> surface (ii) appending electron withdrawing groups such as dicyano and cyanoester to the squaric unit to maintain the *cis*-configuration besides extend the light harvesting in NIR region as well as visible regions and (iii) number of anchoring group which helps strengthening the interaction between dye and TiO<sub>2</sub> surface. **PSQ13** possess inbuilt steric factor in one side of the molecule, which helps organizing the dyes on the TiO<sub>2</sub> surface that helps to the formation of prominent J-type aggregate. **PSQ13** dyes showed superior performance of 7.58% with significant improvement in both  $J_{sc}$  and  $V_{oc}$  in presence of CDCA co-adsorbent molecules than that of **PSQ11** and **PSQ12**.

To extend the response of squaraine dyes in NIR region, we have designed and synthesized a series of  $\pi$ -extended *cis*-configured unsymmetrical squaraine dyes **PSQ21-22** with two different anchoring groups. **Chapter 4** presents dye design which helps to enhance the absorption property of the dye from visible to NIR regions. Further to understand the effect of anchoring group, a direct carboxylic acid and cyanoacetic acid anchoring groups were incorporated in **PSQ21** and **PSQ22** dyes, respectively. The IPCE profile exhibited that **PSQ22** was better harvester than that of **PSQ21**, as both the dyes containing different anchoring group. DSSC device fabrication of **PSQ21** and **PSQ22** exhibited 7.0% and 6.93%, respectively in the presence of CDCA co-adsorbent molecules.

**Chapter 5** presents dye design and systematic investigation of dye orientation and their aggregation on the TiO<sub>2</sub> surface to understand the effect of anchoring groups with suitably functionalized branched alkyl groups and different  $\pi$ -spacer groups on



unsymmetrical squaraine dyes. A series of unsymmetrical D-A-D- $\pi$ -Anchoring group *trans*-squaraine PSQ dyes (**PSQ31-33**) were synthesized and the DSSC devices were fabricated and investigated the photovoltaic behaviors. Orientation of dyes and chemisorbs on TiO<sub>2</sub> surface which is effectively depending on the sensitizer's structure as well as suitable anchoring group. **PSQ31** showed PCE of 2.14% which was comparatively high  $J_{sc}$  than thiophene based **PSQ32** and **PSQ33** dyes. This study described the importance of cyano acetic acid over carboxylic acid as a good anchoring group for this class of NIR active PSQ dyes.

### Future Perspective

Considering the factors that include, the in-plane and out-of-plane alkyl groups,  $\pi$ -spacer, nature of squaraine dye back bone (*cis*- or *trans*-) and type of anchoring groups play an important role in achieving better device performance. Judicious choice of donor moieties in D-A-D based squaraine dyes are important. Such a integrated approach of functionalizing a donor unit which helps both extending the light absorption also to avoid the aggregation induced quenching is required to obtain a dye with better device performance with good shelf life.

**Erratum**





